THE PORE SYSTEM AND ENGINEERING PROPERTIES OF HARDENED CEMENT PASTE

By

FLOROS PANTELI

Doctor of Philosophy

THE UNIVERSITY OF ASTON IN BIRMINGHAM

October 1988

To my son Pantelis Christos

THE UNIVERSITY OF ASTON IN BIRMINGHAM

"THE PORE SYSTEM AND ENGINEERING PROPERTIES OF HARDENED CEMENT PASTE"

Floros PANTELI Doctor of Philosophy 1988

SUMMARY

The work described in this thesis is an attemt to elucidate the relationships between the pore system and a number of engineering properties of hardened cement paste, particularly tensile strength and resistances to carbonation and ionic penetration.

By examining aspects such as the rate of carbonation, the pore size distribution, the concentration of ions in the pore solution and the phase composition of cement pastes, relationships between the pore system (pores and pore solution) and the resistance to carbonation were investigated. The study was carried out in two parts. First, cement pastes with different pore systems were compared, whilst secondly comparisons were made between the pore systems of cement pastes with different degrees of carbonation.

Relationships between the pore structure and ionic penetration were studied by comparing kinetic data relating to the diffusion of various ions in cement pastes with different pore systems. Diffusion coefficients and activation energies for the diffusion process of Cl^- and Na^+ ions in carbonated and non-carbonated cement pastes were determined by a quasi-steady state technique. The effect of the geometry of pores on ionic diffusion was studied by comparing the mechanisms of ionic diffusion for ions with different radii.

In order to investigate the possible relationship between tensile strength and macroporosity, cement paste specimens with cross sectional areas less than $1mm^2$ were produced so that the chance of a macropore existing within them was low. The tensile strengths of such specimens were then compared with those of larger specimens.

KEY WORDS : cements, pore system, carbonation, diffusion, strength.

ACKNOWLEDGEMENTS

I am deeply indebted to Dr C. L. Page, my supervisor, for the guidance, advice and all the help he has given.

I am grateful also to my cousin and friend Dr George Sergi for his generous help and encouragement throughout the period of the research.

Thanks are also due to Mr S. W. Yu for the development of the method of analysis for quaternary ammonium ions which has been used many times during the research.

I wish to thank the Committee of Vice-Chancellors and Principals who provided part of my tuition fees by means of an ORS award. I would like also to thank the Department of Civil Engineering for supplementing my tuition fees.

I owe my deep gratitude and appreciation to my parents and parents in-law for their encouragement and financial support during my student years.

Finally, I am very grateful to my wife Maria for her typing, but above all, her understanding and endless patience.

Page no.

LIST OF CONTENTS

LIST OF FIGURES

LIST OF TABLES

LIST OF APPENDICES

ABBREVIATIONS

Cement compounds nomenclature:

$CaO = C$; $SiO_2 = S$; $Al_2O_3 = A$; $Fe_2O_3 = F$; $H_2O = H$.

OPC = ordinary portland cement

BFS = blast furnance slag

R.H. = relative humidity

DTA = differential thermal analysis

XRD = X-ray diffraction

MIP = mercury intrusion porosimetry

CHAPTER 1: Introduction

Neat cement paste, the product of the chemical reactions of cement with water, is not an important material in civil engineering constructions. Except for special cases it is not normally used alone, for economic and practical reasons. It is too expensive, it evolves too much heat by chemical reaction with the water if used in bulk and when it hardens undergoes undesirably large volume changes [1]. Its significance arises from the fact that it is a component of the most widely spread constructional material, concrete.

Concrete is a composite material produced by using cement paste to bind fine and coarse aggregate into a dense coherent mass. In most cases in practice, in order to improve its low tensile strength, it is reinforced with steel bars. The properties of reinforced concrete, are an integration of the properties of the individual constituents and their interactions with one another. In order to improve its properties and hence its performance in practical applications, it is therefore essential to understand first the systems which constitute it, i.e. the aggregates, the cement matrix and the steel, and secondly the interactions between them.

Unlike aggregates and steel, which bring into reinforced concrete their own already defined characteristics, cement

paste develops its microstructure and therefore its properties in situ. As a result, its properties are affected by time and by the curing conditions. Such influences, together with an intrinsic complexity of cement paste, resulting from the fact that it consists of chemically and physically different phases, make the study of the properties of the cement matrix most difficult. Although more than 40 years ago Powers [2] and his co-workers started with serious investigations into the microstructure of hardened cement paste, we are still far from fully understanding the cement paste system. It is generally accepted [3-6], however, that most of its properties are influenced by its pore structure.

The significance of the cement matrix in reinforced concrete is not limited to its role as a binder. It has also the ability to protect from corrosion any type of steel reinforcement. Lack of such protection may cause the concrete to crack or spall, or could even lead to structural weakening and failure [7].

The protection of steel reinforcement offerred by the cement matrix is twofold [7,8]. First, it maintains a highly alkaline environment which induces the formation of a thin continuous passive film of ferric oxide on the surface of the steel, and secondly it protects the steel reinforcement from the ingress of aggresive ions present in the external environment. The most aggressive ion with regards to steel corrosion is the chloride ion. When present in sufficient quantities in the pore

solution it destroys the passive film on the surface of the steel causing localised corrosion even in highly alkaline environments [7].

Both aspects of the protection of steel reinforcement provided by the cement matrix can be eliminated by aggressive environmental conditions. Atmospheric CO_2, especially in the cases of urban or industrial atmospheres in which the concentration of CO_2 is enhanced by atmospheric polution, can neutralize the alkaline environment of the cement matrix (carbonation) [9,10]. In addition, concrete used in marine environments, or concrete exposed to de-icing salts in highway structures can be penetrated by chloride ions through the cement matrix [9,10], causing corrosion even in the alkaline environment around steel. Hence in addition to strength, which is the characteristic most obviously required for structural use and related to the role of cement paste as a binder in concrete, the resistances to carbonation and to ionic penetration are crucial properties of the cement matrix which affect the performance of reinforced concrete.

The aim of this work is to contribute to the understanding of cement paste and its role in reinforced concrete, by investigating a common feature of the above-mentioned properties, viz. their dependence on the pore system of the paste.

1.1 STRUCTURE OF HARDENED CEMENT PASTE

A portland cement consists basically of the following compounds:

$3CaO.SiO_2$	(C_3S)
$2CaO.SiO_2$	(C_2S)
$3CaO.Al_2O_3$	(C_3A)
$4CaO.Al_2O_3.Fe_2O_3$	(C_4AF)
$CaSO_4.2H_2O$	(Gypsum)

From the moment of mixing with water to form the cement paste, chemical reactions between these compounds and water start, producing new solid phases (see Table 1.1). The hydration products are produced in a variety of states . The crystalline compounds include calcium hydroxide, ettringite, calcium aluminate monosulphate hydrate, C_4AH_{13}, and residual C_3S, ß-C_2S and C_4AF. The phases of lesser crystallinity are primarily calcium-silicate-hydrate gel and amorphous calcium hydroxide [12]. Diamond [13] estimated that the C-S-H gel forms 70% (by weight) of an almost fully hydrated cement paste and portlandite about 20%. Calcium aluminate trisulphate hydrate (ettrngite) and calcium aluminate monosulphate form another 7%, while minor constituents such as tricalcium aluminate hydrate and unhydrated clinker make up the remainder. More recently, Taylor[15] calculated from experimental measurements, that

TABLE 1.1: Principal hydration products of cement

Unhydrated phase	Hydration product
$3CaO.SiO_2$ (Tricalcium Silicate)	$3CaO.2SiO_2.3H_2O$ (Calcium Silicate Hydrate) + $Ca(OH)_2$ (portlandite)
$2CaO.SiO_2$ (Dicalcium Silicate)	$3CaO.2SiO_2.3H_2O$ (Calcium Silicate Hydrate) + $Ca(OH)_2$ (portlandite)
$4CaO.Al_2O_3.Fe_2O_3$ (Tetracalcium Aluminoferrite) {+$Ca(OH)_2$}	$3CaO.Al_2O_3.6H_2O$ (Tricalcium Aluminate Hydrate)+$3CaO.Fe_2O_3.6H_2O$ (Tricalcium Ferrite Hydrate)
$3CaO.Al_2O_3$ (Tricalcium Aluminate) {+$Ca(OH)_2$}	$3CaO.Al_2O_3.6H_2O$ $4CaO.Al_2O_3.13H_2O$ (Calcium Aluminate Hydrates)
$3CaO.Al_2O_3$ + Gypsum	$3CaO.Al_2O_3.3CaSO_4.32H_2O$ (ettringite) $3CaO.Al_2O_3.CaSO_4.14H_2O$ (calcium monosulphoaluminate hydrate)

a three month old portland cement paste with 0.5 w/c ratio, in its saturated state, consists of 40% C-S-H gel, 16% AFm product, 12% calcium hydroxide, a total of 8% of residual unhydrated cement and a total of 24% pore space (all percentages by volume).

Fresh cement paste is a dispersion of particles of cement in water. It is plastic and in normal conditions remains thus for one to two hours. After this period (the dormant period) the plastic mass sets and hardens and thereafter the apparent volume of the paste remains almost constant, except for variations caused by changes of temperature or moisture content or by reactions with atmospheric CO_2.

The hardening of the paste is due to the formation of C-S-H gel and portlandite crystals. Unlike portlandite, the chemical composition of C-S-H gel is mutable. Although it is often quoted as $C_{1.5}SH_{1.5}$ or $C_3S_2H_3$, the mole ratios are variable (12,13). Morphologically, it can be found in different types (6,16,17). Diamond (13,14) classified four types of C-S-H gel found in "conventional cement paste". According to Wittmann (6,16), however, there is a large range of different morphological details in hardened cement paste which are not covered by these four types of C-S-H gel.

In order to describe the structure of C-S-H gel, various simplifying models have been proposed (12,15). Of these, the

most frequently discussed in the literature are those suggested by Powers and Brunauer [12,18], Feldman and Sereda [12], Kondo and Daimon [19] and the Munich model [6,12].

The classical Powers-Brunauer model [12,18] assumes that the gel is composed of gel particles, which are mainly held together by van der Waals' forces, and interstices among these particles, which are the gel pores. The gel is considered to have a high specific surface area and a layered structure. The water in the gel is distinguished as chemically bound or as physically adsorbed at the surfaces of the gel particles.

Feldman and Sereda [12] developed a model which also assumes a layered structure of the gel. It proposes, however, that the role of water is much more complex than is recognised by the Powers-Brunauer model. According to Feldman and Sereda, the water that enters the interlayer spaces is a part of the structure and is more organised, contributing to the rigidity of the system. Gel pores, as interlayer spaces, do not exist and total porosity can only be obtained by fluids that do not cause interlayer penetration. The gel is assumed to derive its strength from a combination of van der Waals' forces and siloxane, hydrogen and calcium-silica bonds.

Another proposed model is that developed by Kondo and Daimon [19]. It is essentially a geometrical model and suggests that gel consists of clusters of crystallites which are separated by inter gel particle pores. In each gel particle there are intercrystallite pores, while intra crystallite pores are found in individual crystallites.

Finally, the Munich model [6,12] is primarily concerned with the explanation of the mechanical properties of the hydrated portland cement gel. It does not take into consideration the morphology of individual gel particles and replaces the heterogeneity of elements within the gel by a statistical average. It suggests that the influence of water content on the properties of hardened cement paste can be explained by means of two different phenomena; the surface energy of the colloidal particles and disjoining pressure of water.

With the progress of cement hydration, products grow in random directions. A natural consequence of this is the development of a system of pores. Under normal conditions, the pores are partly filled with a concentrated solution of sodium and potassium hydroxides. The release of the alkali ions into the pore solution is caused by the reaction of sodium and potassium sulphates present in the cement to form mainly ettringite [20,21]. The balancing of the alkali ions in the pore solution by hydroxyl ions maintains a highly alkaline environment which as mentioned earlier protects the

steel reinforcement from corrosion. Thus an investigation of the relation between the pore system and properties of cement paste governing the protection of steel reinforcement, must not ignore the role of the pore solution. It must take into account the pores and the pore solution as a whole. In this case, the structure of hardened cement paste can be divided into two major components: the solid phase which consists mainly of the gel and portlandite crystals and the pore system which includes the pores and the pore solution.

1.2 THE PORE SYSTEM

The classical model of the structure of hardened cement paste developed by Powers and his co-workers [22,23], assumes that the pore system consists of two kinds of pore, the gel pores and the capillary pores.

Gel pores are interconnected, interstitial spaces between the gel particles. They occupy about 28 per cent of the total volume of the gel and this value is independent of the progress of hydration as well as the water/cement ratio of the mix. It is a characteristic of the gel whenever it is formed. This means that as the total volume of gel increases with the progress of hydration, the total volume of gel pores also increases[24].

Capillary pores represent that part of the gross volume of the cement paste which has not been filled by the products of hydration. At the first stages of hydration solid products form an interconnected system randomly distributed throughout the cement paste. Hydration, however, increases the solid content of the paste and in mature and dense pastes the capillary pores may become blocked by gel and segmented, so that they are interconnected solely by the gel pores (24).

Powers's model provides a simple representation of the pore system of hardened cement paste. The subdivision of the pore system into gel and capillary pores, however, gives the impression of two size ranges of pores which is not real. Measurements of pore sizes have shown a continuous distribution. Pores with diameter up to 20 nm were measured by sorption methods, while pores with diameter between 10 nm to 10 μm were measured by mercury intrusion techniques (6).

As reported by Wittmann (6) larger pores than the above-mentioned can by measured using optical methods. This kind of pore can be created by entrapped or entrained air during manufacture, or as packing defects during casting of the cement paste (185). They are underestimated by mercury intrusion techniques either because they are closed pores or because they have small entrances and so are registered as

pores of smaller size [181].

Pores in cement paste can be classified as closed, continuous or dead ended pores [127]. Uchikawa [4] suggested that there is a high probability that pores with an inlet diameter larger than 100 nm are continuous and that many of the smaller pores, less than 100 nm, are closed. Although total porosity and closed pores are important in relation to mechanical property results [44] they are less critical with regard to properties such as the resistance to ionic penetration or the resistance to carbonation. Such properties, which are associated with mass transport phenomena, are controlled especially by the continuous pores [53].

Cement pastes with more compact pore systems can be obtained by partial replacement of the portland cement in the original mix with other cementing materials [25,146]. Supplementary cementing materials such as slags (section 2.1), react with the calcium hydroxide liberated during the hydration of portland cement and form additional hydration products which fill the pores [156,134]. Smolczyk [25] reported that hardened pastes of portland cement develop more capillary pores (>30 nm) than blast furnance slag cement pastes, which develop more gel pores. An increase in slag content from 0% to 76% by weight, resulted in a relative reduction of the capillary porosity of about 25 to 30%. Gjorv and Vennesland [146] similarly showed that for an 80% slag

cement paste, 79% of the total porosity was made up of pores smaller than 20 nm, while for an equivalent portland cement paste the proportion was only 29%. This means that in the paste of slag cements the average pore size is smaller than in portland cement pastes.

The ability of slag to increase the compactness of the pore system of cement paste was used extensively in the present work. In cases where, for comparative reasons, cement pastes with different pore systems were needed the portland cement in the original mix was partially replaced, up to 65% by weight, by slag.

1.3 PLAN OF PRESENTATION AND GENERAL OBJECTIVES OF THE WORK

The thesis is divided into seven chapters. Following the introductory chapter, chapter 2 describes the materials and experimental techniques used thoughout the investigation. The next four chapters (3 to 6) present the experimental work carried out, while the last chapter (chapter 7) contains a general discussion of the investigation and suggestions for future work.

More specifically, chapter 3 is concerned with the resistance of cement paste to carbonation. Carbonation, i.e. the neutralization of the basic constituents of cement paste by

atmospheric CO_2, changes the pore system and phase composition of cement paste [51,74]. As a result characteristics such as strength, deformations and durability are affected [91]. It is important therefore to be able to predict carbonation depths in concrete structures and to develop materials with improved resistance to carbonation. For this reason, the study of carbonation is essential. Since atmospheric CO_2 penetrates hardened cement paste through the pores, the relation between the pore system and carbonation is of particular interest. The aim of this chapter was to examine aspects of this relationship.

In the literature it is accepted [62,63] that the resistance of cement paste to carbonation is controlled by two parameters; the pore structure and the amount of carbonatable material present in the paste. Although this has been shown experimentally [67], no criteria have been established which provide a firm basis for accelerated laboratory tests aimed at the characterization of cement pastes or concretes according to this property. This is partly due to the fact that there is no specific theory which describes the carbonation process, taking into account all the parametres influencing it. The various reported formulae [59,7,52,53,63,68-70] which describe carbonation can be divided into two groups: (i) general formulae obtained from curve fitting and (ii) theoretical formulae which, however, cannot necessarily be applied in practice.

Chapter 3 attempts to fill the gap between theory and practice by supporting a theoretical equation with experimental results. Furthermore, in part I of the chapter, cement pastes with different pore systems were compared in terms of their resistance to carbonation. The intention was to find criteria which can characterize cement pastes according to this property.

Part II of the chapter compares the pore systems of cement pastes with different degrees of carbonation. The aim was to provide information on the effect of carbonation on the pore system (pores and pore solution) of cement paste. Although in the literature there are a number of published studies [51,89,90] examining the effect of carbonation on the pore structure, there is a lack of published work on the effect of carbonation on the pore solution. As mentioned earlier, the pore solution of the cement matrix in concrete is responsible for the protection of steel reinforcement. Any changes in the pore solution therefore are of particular interest. Information on changes in the pore solution caused by carbonation can also contribute to the better understanding of the carbonation process.

There are indications [37] that chloride contamination affects the resistance of cement paste to carbonation. This necessitated the study of the effect of chloride ions on the

relationship between the pore system and the resistance to carbonation. For this reason in both parts of the chapter, chloride contaminated specimens were used in parallel with the non-contaminated ones.

Chapters 4 and 5 are concerned with the resistance of cement paste to ionic penetration. The most usual way for aggressive ions to penetrate cement paste, which has been made and placed in accordance with the proper rules and specifications (112), is by diffusion through the pore system (11). The penetration of aggressive ions into such cement pastes, therefore, is primarily controlled by their resistance to ionic diffusion. As a result of the importance of this property of cement paste in terms of the durability of concrete, a substantial amount of experimental work concerned with ionic diffusion has been carried out (see section 4.2). The controlling mechanisms of ionic diffusion, however, have not yet been clearly understood (136). There is a need for a general ionic diffusion theory in cement pastes which can be useful to the design of cementitious materials of improved resistance to ionic penetration. Such materials are important not only in the construction industry, but also in other diverse areas, as in the nuclear industry for the construction of such structures as trenches for low-level waste disposal (119).

The aim of chapter 4 was to contribute to the understanding

of the mechanism of ionic diffusion in cement paste. It describes work involving the determination of effective diffusion coefficients of chloride and sodium ions in cement pastes with different pore systems, at various temperatures.

More specifically, part I of the chapter examines the changes in the mechanism of ionic diffusion caused by partial replacement of portland cement in the original mix by BFS. It is generally accepted that BFS-blended pastes cause a significant retardation of ionic diffusion, provided they are used under conditions that allow adequate moist curing to be undertaken [116,128-130]. It is uncertain, however, whether the low diffusivities found in these pastes are ascribable simply to physical differences between their pore structures and those of portland cement pastes of the same w/c ratio or to differences in chemical pore surface characteristics of the materials.

Part II of the chapter, examines the changes in the mechanism of ionic diffusion caused by carbonation which, as already mentioned, affects the pore system of cement paste. There are indications [37,142] that carbonation causes a reduction in the cement paste's resistance to ionic diffusion. It is perhaps surprising, however, that no serious investigations on the subject have as yet been published. As carbonation is in practice a common phenomenon, such investigations could provide useful information on the true

mechanism of ionic ingress in practical applications.

In order to understand the mechanism of ionic diffusion it is essential to study the factors which govern it. The most important of these factors are the pore structure and the interactions of the diffusing ions with the pore walls (116,122,123). Although in the literature there are a number of published studies (122,123,125,126) examining the latter, there is a lack of experimental data concerning the effect of the geometry of pores on ionic diffusion. Chapter 5 attempts to fill this gap by comparing the mechanisms of ionic diffusion for ions with different radii.

The last experimental chapter (chapter 6) is concerned with the strength of hardened cement paste. Although it is generally accepted that strength is related to the pore structure of cement paste, there are two essentially different theories concerning this relationship. The first considers that the volume porosity is the major determinant of strength (169), while the second suggests that strength is governed less by the total porosity than by the large pores or flaws present in cement paste (182). This chapter investigates the possible relationship between strength and macropores. Cement paste specimens with cross sectional areas less than 1 mm^2 were carefully produced so that the chance of a macropore existing within them was low. Useful information could then be obtained by testing these

specimens in tension and comparing the results with those of larger specimens tested with the same technique.

CHAPTER 2 : Materials and experimental techniques

2.1 MATERIALS

For the investigation of the relationships between the pore system and engineering properties of hardened cement paste it was essential to prepare specimens with different pore systems. In order to achieve this using the conventional processes different types of hardened cement pastes were prepared from mixtures of ordinary portland cement (OPC) and ground granulated blast furnace slag (BFS). The oxide compositions of OPC and BFS used are shown in Table 2.1.

Blast furnace slag is a waste product obtained in the manufacture of pig-iron in the blast furnace. It is formed from the gangue derived from the iron ore, the combustion residue of the coke, the limestone and other materials present in the furnance [26,151]. It has essentially the same main oxides as a portland cement but in different proportions. A slowly cooled crystalline slag has good mechanical properties and can be used as aggregate. If however the slag is cooled rapidly so that no crystallisation can take place and the slag is in a glassy state it can become reactive and thus suitable for the manufacture of slag cements. This product, known as granulated blast furnace slag, in the presence of an activator (lime, alkali or alkali sulphate) reacts with water to form a cementitious material. It is not considered a pozzolana because it needs only very small

TABLE 2.1: Oxide compositions of cement and ground granulated blast furnace slag (% by weight).

Material	CaO	SiO_2	Al_2O_3	Fe_2O_3	SO_3	MgO	Na_2O	K_2O
OPC	64.5	20.0	5.3	3.4	3.0	1.2	0.10	0.78
BFS	39.4	36.7	11.5	0.70	1.3*	7.8	0.43	0.82

*Total S

amounts of activators to make it hydraulic [26].

Portland blast furnace slag cement is produced either by simultaneously griding portland cement clinker and granulated blastfurnace slag [25] or, as in the present work, by mixing on site portland cement and ground granulated blast furnace slag.

2.2 EXPRESSION OF PORE SOLUTIONS

The pore system of hardened cement paste as defined in the present work (chapter 1) includes the pores as well as the solution in them. It was important therefore to be able to observe changes in the pore solution, especially changes in ionic concentrations and alkalinity. This necessitated sampling of pore solutions by means of a technique developed by Longuet et al [20], in which the pore solution is expressed from pastes, mortars or concretes at high pressure.

The pore solution expression device is a cylindrical pressure vessel, consisting of four main sections as shown in figure 2.1. Hardened cement paste, in the form of a cylinder or, in the case of the present work as a series of discs stacked together, was positioned on the platten encased by the die body. A slowly increasing pressure was then applied to the piston, reaching a maximum of 310 MPa. The PTFE disc inserted between the specimen and the piston , spread to seal the whole diameter of the die body, preventing liquid from escaping other than through

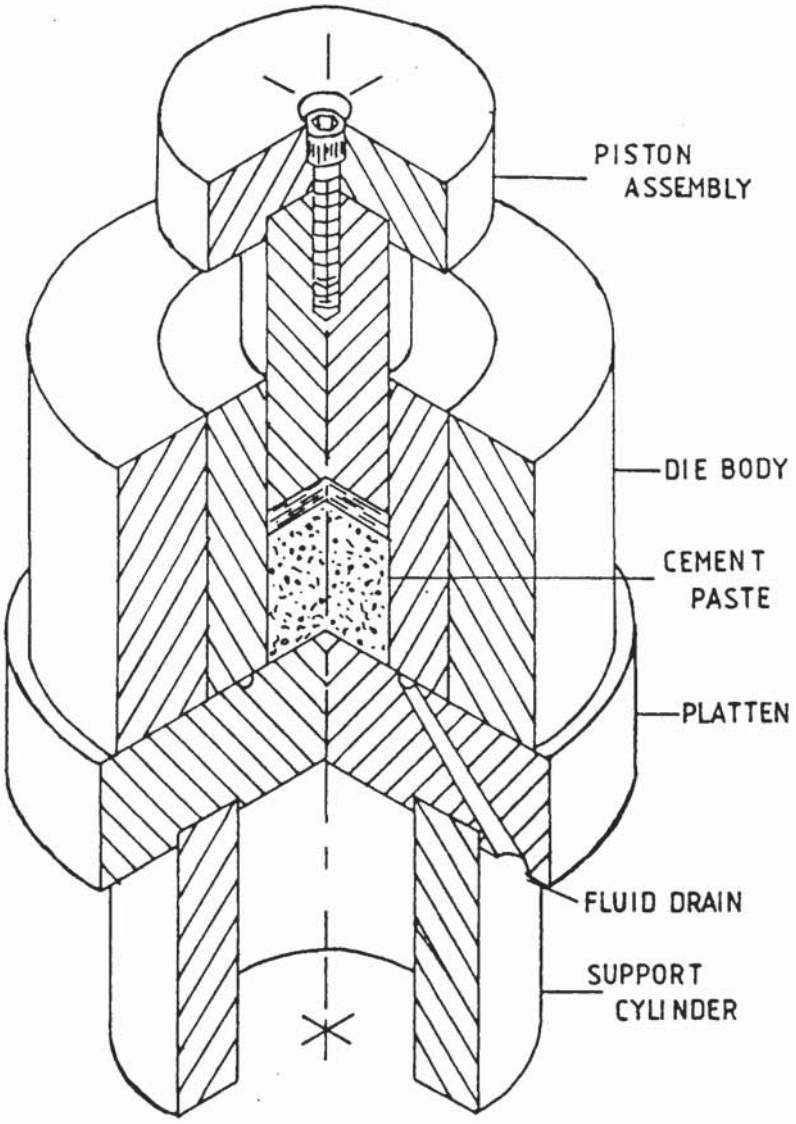

FIGURE 2.1 : The Pore Solution Expression Device.

the fluid drain via a circular groove on the platten. The solution was then drawn into a syringe through a drain hole lined with PTFE and stored in sealed plastic vials to prevent unnecessary exposure to air. Normally around 4 ml of solution was extracted from the paste.

As the rate of increase of the applied pressure and the post-expression handling of the pore solutions may affect the results [27] care was taken that these factors were the same for all the specimens.

After each run, the separate parts of the press were thoroughly cleaned with water and acetone and the connecting surfaces were sprayed with PTFE non-stick spray for lubrication and protection ready for the next specimen.

2.3 SOLUTION ANALYSIS

The expressed pore solutions as well as any other solutions were analysed using standard methods. Usually 100µl aliquots taken with a standard micropipette were sufficient for the analysis. On occasions, however, where the concentrations were very small or where the accuracy of a method was satisfactory only at relatively high concentrations, larger aliquots were taken for analysis. For all the ions analysed, at least duplicate tests were perfomed and an average was taken.

2.3.1 HYDROXYL ION

The 100 µl aliquots were made up to 1 ml with deionized water and then were titrated against standard 0.01 M nitric acid solution with phenolphthalein as the indicator. The acid was dispensed from a 10 µl graduated microburnette.

The pH of the solution was calculated from the hydroxyl concentration as follows:

$$pH = - Log_{10} [H^+]$$

$$pOH = - Log_{10} [OH^-]$$

$$[H^+].[OH^-] = 10^{-14} \text{ , (at 25 } ^oC)$$

$$pH + pOH = 14$$

$$pH = 14 + Log_{10} [OH^-].$$

2.3.2 pH METER

In cases where the pH value of the solution was about 10 or less, a Pye Unicam pH electrode in conjuction with a Philips digital pH meter was used instead of titration. The pH meter was first calibrated with buffers at pH 4, 7, and 9. The readings obtained for the sample solutions were, at intermediate values, accurate to within 0.01 of a pH unit.

2.3.3 CARBONATES AND BICARBONATES

When titrating a carbonate solution with acid, two inflections

are established at around pH 9 and pH 4 [28]. The first coincides with the point of conversion to bicarbonate:

$$CO_3^- + 2H^+ \longrightarrow 2HCO_3^-$$

and the second with the complete neutralisation:

$$HCO_3^- + H^+ \longrightarrow H_2CO_3$$

By measuring the volumes of the acid corresponding to the two inflections, it is possible to calculate the carbonates and bicarbonates present in the solution.

In the present work, the sample solution was titrated against 1mM nitric acid and a pH electrode in conjuction with a pH meter (2.3.2) was used to obtain the changes of the pH of the solution. A worked example can be found in appendix 1.

2.3.4 SODIUM POTASSIUM AND CALCIUM IONS

Analysis of Na^+, K^+ and Ca^{++} ions was carried out with a flame photometer. Depending on the expected concentration, the sample solution was first diluted by 500 or 1000 in deionized water. It was then drawn through a thin tube into the flame photometer which atomized and sprayed the liquid over a flame.

When an ionic species is burned in a flame, it glows transmitting a light of a specific set of wavelenths. A filter placed in front of the flame, which allowed only light of the required wavelength to pass through, enabled the estimation of the concentration of each ionic species by relating the intensity

of the light to the ionic concentration.

2.3.5 CHLORIDE ION

When added to mercury (II) thiocyanate solution, chloride ions displace thiocynate ions which in the presence of iron (III) ions form a highly coloured complex [29]:

$$2Cl^- + Hg(SCN)_2 + 2Fe^{3+} \longrightarrow HgCl_2 + 2Fe(SCN)^{2+}$$

The colour intensity of the complex is related to the original chloride ion concentration. By measuring therefore, the intensity of the colour it is possible to determine the original chloride concentration. Colour intensity can be determined by a spectrometer which measures the absorption of light at a specific wavelength.

A technique based on the above principles was used in the present work by employing a Beckman, model 24, spectrophotometer. Using deionised water, each 100 µl aliquot of sample solution was first diluted to 10 ml. Two millilitres of 0.25 M ferric ammonium sulphate [$Fe(NH_4)(SO_4)_2 .12H_2O$] in 9 M nitric acid and 2 ml of saturated mercuric thiocyanate in ethanol were then added to it. Finally the obtained solution was lightly shaken and left undisturbed for ten minutes.

Two glass cells, one containing the coloured solution and the other water, were placed next to each other inside the spectrophotometer. A beam of monochromatic light whose

wavelength was selected by a prism (460 nm for this analysis) was passed through the cells onto a photoelectric device. The difference in absorption between the two cells was related to the concentration of chloride by the Beer - Lambert law (30) which states that the intensity of a beam of monochromatic light varies as function of the concentration of the absorbing substance it passes through:

$$I_t = I_o \cdot 10^{-ect}$$

where:

I_t = intensity of trasmitted light

I_o = intensity of incident light

e = molecular extinction coefficient

c = concentration of solution

t = thickness of solution.

Chloride concentrations were estimated from a calibration curve constructed by plotting a curve of concentration of standard chloride solutions against absorption (appendix 2).

2.3.6 QUATERNARY AMMONIUM IONS

The quaternary ammonium ions used in the present work were:

(1) tetraethylammonium ion, $(C_2H_5)_4N^+$,

(2) tetrapropylammonium ion, $(C_3H_7)_4N^+$,

(3) tetrabutylammonium ion, $(C_4H_9)_4N^+$,

(4) tetrapentylammonium ion, $(C_5H_{11})_4N^+$.

The method of analysis used was a development of the methods described by Crompton [31] and Thomas and Chamberlin [32].

Methyl orange or bromo cresol green react with quaternary ammonium ions to form a chloroform-soluble coloured complex. The colour intensity of the complex is proportional to the concentration of the quaternary ammonium ion and can be measured by making spectrophotometric readings of the chloroform solution at the optimum wavelength.

(i) Analysis of $(C_3H_7)_4N^+$, $(C_4H_9)_4N^+$, $(C_5H_{11})_4N^+$:

Using a standard micropipette, a 100 µl aliquot of solution was placed into a separating funnel and diluted to 37 ml with deionised water. To the separating funnel was added 1 ml of methyl orange (0.1% by weight), 2 ml of a buffer solution (a mixture of 0.5 M citric acid and 0.2 M disodium hydrogen orthophosphate in equal proportions), and 10 ml of chloroform. The separating funnel was then stoppered and shaken vigorously for 30 seconds. After shaking the solution was allowed to stand undisturbed for 20 minutes, so that the chloroform could settle as a lower layer. The chloroform layer was then filtered through a small plug of glass wool wedged in the stem of a filtering funnel, to remove the water. The filtered solution was collected in a glass cell and placed in a Beckman, model 24, spectrophotometer. The difference in absorption at 415 nm wavelength between this cell and another cell placed next to it containing chloroform, was an indication of the concentration of

the quaternary ammonium ions (as shown in par. 2.3.5). The actual concentrations were estimated from calibration curves constructed by plotting the concentrations of standard quaternary ammonium ion solutions against absorption (appendix 3).

(ii) Analysis of $(C_2H_5)_4N^+$:

The principle and procedure of the method used were the same as those described above for the rest of the quaternary ammonium ions. The preparation of the chloroform solution, however, was slightly different. In particular, higher ionic concentration was needed in the solution. So, instead of 100 µl, a one ml aliquot of sample solution was pipetted into the separating funnel and diluted to 37 ml with deionized water. The reagents added to it were the same as above except for the methyl orange. In its place a solution of bromo cresol green was used (0.1% by weight bromo cresol green + 7 ml 0.1N NaOH / 500ml solution).

2.4 ION CHROMATOGRAPHIC ANALYSIS

Ion chromatography is an analytical technique which basically involves separation due to differences in the equilibrium distribution of sample components between a mobile phase and a stationary phase [33]. There are multiple modes of separation, each based on different separation mechanisms. The one employed in the present work is "high performance ion chromatography" (HPIC). Its essential principle is an ion

exchange process between the mobile phase or eluant and the exchange groups covalently bound to the stationary phase. For hydrophobic ions in particular adsorption processes are also involved. The stationary phase is typically a polystyrene based resin which has been cross linked with divinyl benzene. For the analysis of anions, the exchange function is usually served by a quaternary ammonium group, whereas for the analysis of cations a sulphonate group is most often employed (33).

The ion chromatograph used was the Dionex model 2000i/SP with conductivity detection. Its components and simplified configuration are shown schematically in figure 2.2. The mobile phase or eluant (Table 2.2) is constantly pumped through the system by a double reciprocating pump. The sample solution is first injected through a 0.2 μm syringe filter in the sample loop and then is introduced into the system via a loop injector which is shown schematically in figure 2.3 (a+b). The two outlets of the sample loop are joined by a three-way valve. After the valve is swithed the sample is transported on to the separator column by the eluant. The separator column, which is the stationary phase, is operated at room temperature. The columns used in the present work are shown in Table 2.2.

The effluent from the separator column flows into the detection system. This system consists of a suppressor device, which is an ion exchange membrane, and a conductivity detector (fig. 2.2).

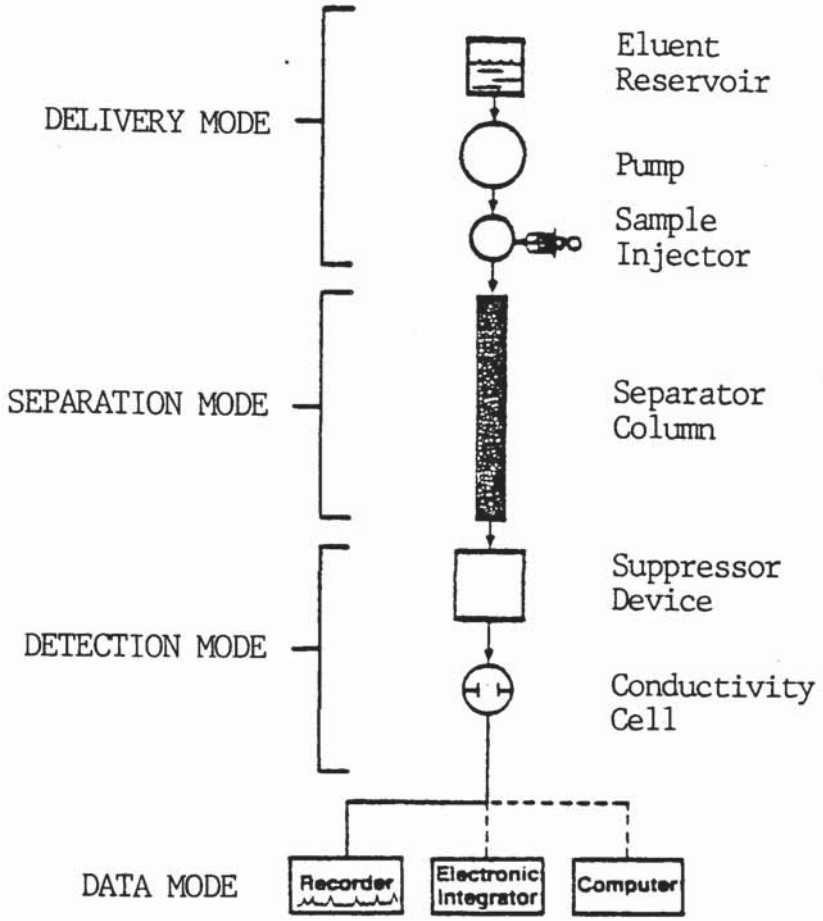

FIGURE 2.2 : The Dionex Ion Chromatograph configuration.

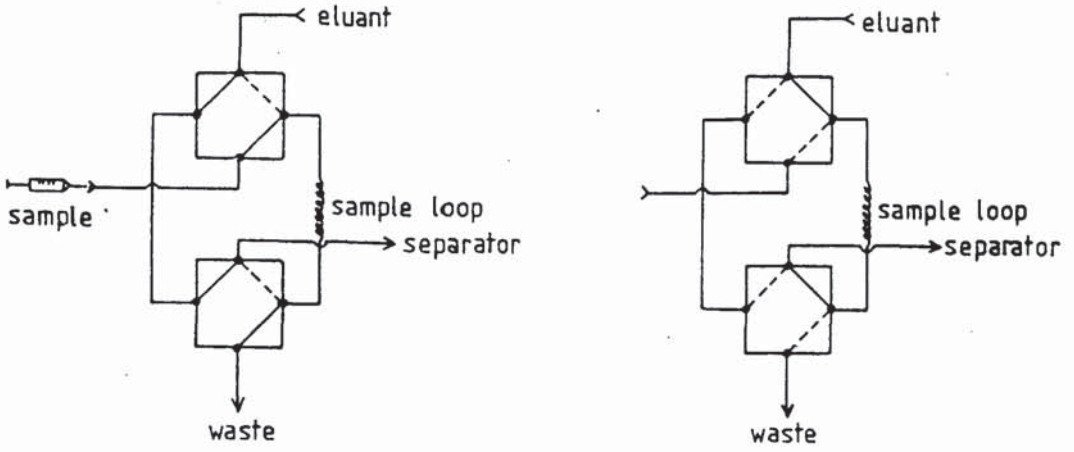

FIGURE 2.3 : The loop injector of the ion chromatograph.
(a): Flow path during sample loading;
(b): Flow path during sample injection.

TABLE 2.2 : Reagents used for ion chromatography

a. Anions:

Column	Eluant	Regenerant
HPIC-AS5	2% v/v acetonitrile (CH_3CN) 0.0008 M 4-cyanophenol 0.0043 M $NaHCO_3$ 0.0034 M Na_2CO_3	0.025N H_2SO_4

b. Cations:

Column	Eluant	Regenerant
HPC-CS3	27.5 mM HCl 2.25 mM 2,3-diaminopropionic acid monohydrochloride (DAP) 2.25 mM L-histidine mono-hydrochloride monohydrate	70 mM tetra-methylammo-nium hydroxide (TMAOH)

The suppressor device, through which the regenerant (Table 2.2) flows at constant rate, serves to chemically reduce the background conductivity of the eluant. At the same time it converts the species of interest into a more conductive form. The results of the chromatographic separation are displayed on a strip chart recorder in the form of a series of peaks. The constituents in a sample can be identified by comparing the retention times of the obtained peaks to those of standard solutions. The area under each peak and the peak height are proportional to the concentration and can be used to obtain quantitative results. A worked example can be found in appendix 4.

2.5 EVAPORABLE AND NON-EVAPORABLE WATER

Ionic species can be expressed as free amounts present in the pore solution or as total present in the paste as a fraction of the unhydrated cement. In order for this to be possible it is necessary to determine the quantities of bound and free water present in the cement.

Various methods have been employed for the evaluation of the two types of water [34] but the dinstiction between free and bound water is always somewhat arbitrary.

The method adopted in this work assumes that the water driven off at 105°C is mainly the evaporable or free water and that the

remaining is the non-evaporable or bound water.

According to Taylor [35], bound water,which includes interlayer water in C-S-H and AFm phases, crystal water in ettringite and adsorbed water, cannot be identified with non-evaporable water. As he reported, drying to 105°C causes major loss of interlayer water and destruction of ettringite, leading to an overestimated evaporable water. By studying the dehydration behaviour of the individual hydrated phases in cement paste he concluded that bound water may defined experimentally as the amount of water retained on equilibration at 18°C and 11% R.H.

Although drying to 105°C is a controversial way of determining the evaporable or free water present in cement pastes, it is a simple method which has been widley used in the past. It enables therefore useful comparisons to be made between the present results and research carried out previously.

In order to measure the water lost at 105°C, about 2 grammes of hydrated cement paste was broken into small fragments. It was then immediately weighed in a glass crucible and heated in an oven at 105°C until a steady weight was obtained which was noted.

The remaining bound water was estimated from the amount of bound hydrogen measured by an Elemental Analyser. A small amount of the hydrated cement was ground to powder using a

pestle and mortar, passed through a 150 μm sieve and heated to 105°C until a constant weight was obtained. The sample was then placed in a lightweight tin container and dropped into a vertical quartz tube of the Elemental Analyser, model 1106, maintained at 1030°C, through which a constant flow of helium was run. The helium stream was temporarily enriched with pure oxygen after which flash combustion took place, primed by the oxidation of the container. Quantitative combustion was then achieved by passing the mixture of gases over Cr_2O_3. The mixture of combustion gases then passed over copper at 650°C to remove the excess of oxygen. The individual components were then separated and eluted as CO_2 and H_2O. They were measured by a thermal conductivity detector whose signal fed a potentiometric recorder. Calibration of the instrument was achieved by combustion of standard compounds.

From the amount of bound hydrogen found in the cement paste the non-evaporable water (N.E.W.) was calculated in grammes of water per grammes of unhydrated cement. The evaporable water (E.W.) was also calculated in grammes of water per grammes of unhydrated cement by the following equations[36]:

$$W_{950} = W_{105} \cdot (100 - i + a) / [\, N.E.W.(\%) + 100 + a]$$

$$E.W.\ (\%) = (W_o - W_{105}).(100 - i + a) / W_{950}$$

Where: W_o = weight of hydrated cement (g)

W_{105} = weight at 105°C (g)

W_{950} = weight at 950°C (g)

a = admixture content (% g/g of unh. cem.)

i = loss-on-ignition (% g/g of cements)

The derivations of the formulae and a worked example are given in appendix 5.

2.6 TOTAL CHLORIDE

The total amounts of chloride present in hardened cement pastes (as bound and free in the pore solution) were measured by a method used by Sergi [37] which is a development of Berman's technique [38].

A small amount of the cement paste was ground to powder in a pestle and mortar and passed through a 150 μm sieve. One gramme of the powder was then placed in a glass vessel and dried at 105°C to constant weight which was noted. Ten millilitres of deionised water were then added and the mixture was thoroughly shaken to "wet" all the cement powder. The glass vessel was then attached to a condenser, needed to avoid evaporation of the solution. Three millilitres of concentrated nitric acid were then added from the top of the condenser and the mixture was placed over a flame to encourage the dissolution of all the chloride by the acid (figure 2.4).

Once the solution had cooled and settled leaving a clear solution on top, a 100μl aliquot was withdrawn and analysed for chloride

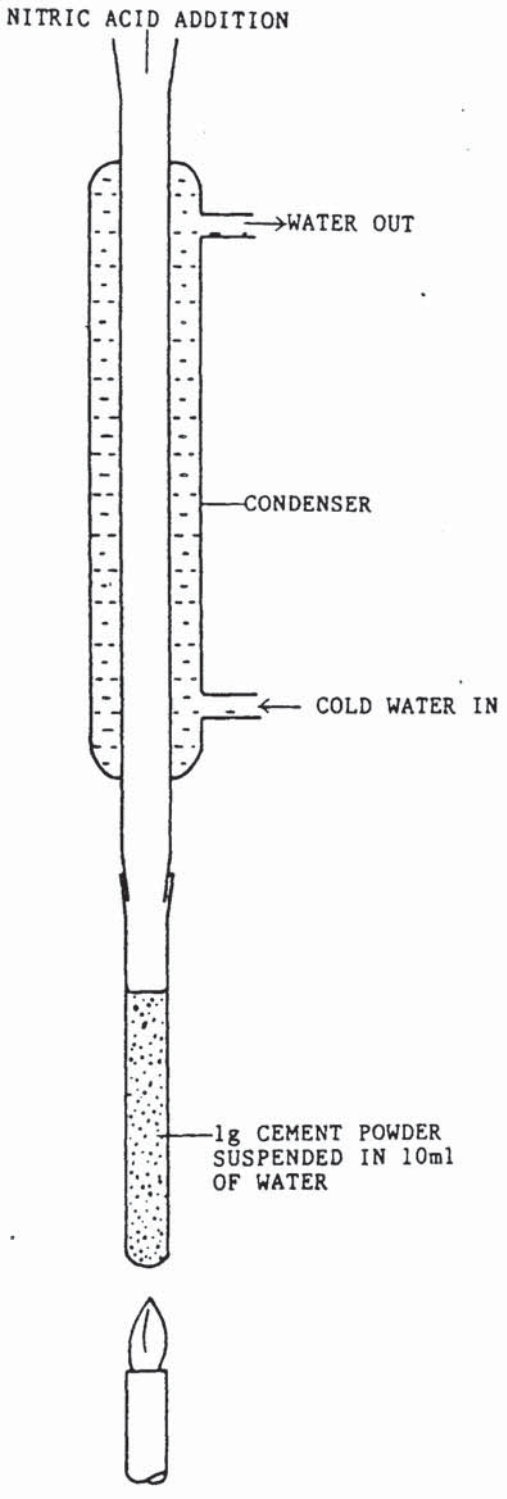

FIGURE 2.4 : Apparatus set-up for the determination of total chloride in cement pastes.

as described in section 2.3.5. On occasions where the chloride concenration was small, larger aliquots were taken for analysis. The total chloride was then calculated from the following equation:

$$\text{Total chloride (m mol } Cl^- \text{ /g cem)} = \frac{\text{Conc. of } Cl^- \text{ in solution (m mol/l) x 13}}{\text{Weight of sample at 950°C (g) x 1000}}$$

The weight of the sample at 105°C needed to be corrected to that at 950°C by means of the evaporable and non-evaporable water data as shown in section 2.5. A worked example is shown in appendix 6.

2.7 DIFFERENTIAL THERMAL ANALYSIS

The differential thermal analyser (DTA) used in the present investigation was the Stanton Redcroft model 673-4 which is shown schematically in figure 2.5. Its main components are two small Rhodium-platinum crucibles situated over two thermocouples inside a furnance. A small amount of powdered hydrated cement, dried over silica gel at ambient temperature, is placed in the one crucible and an equal amount of calcined alumina acting as an inert reference, in the other. The same packing procedure is carried out each time to ensure reproducibility between successive experiments. Both crucibles are heated at a slow rate of 20°C per minute up to a maximum of 950°C. The difference in the temperature between the sample and the reference at any time during the heating procedure is

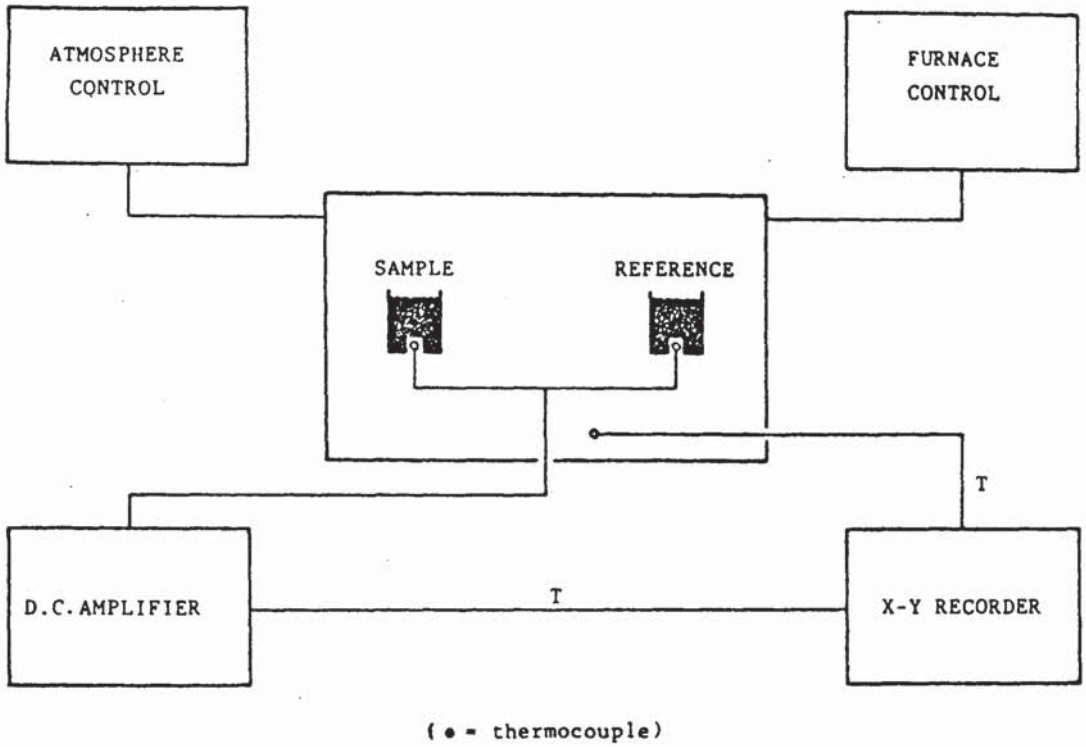

FIGURE 2.5 : Schematic representation of the Differential Thermal Analyser.

shown on a chart recorder as temperature of the furnance against the differential temperature. A thermal change in the sample, either an absorption or evolution of heat, at a particular temperature, is shown on the recorder either as a trough or a peak.

In cement pastes the dehydration of the various phases is normally accompanied by characteristic endothermic reactions at specific temperatures. By comparing the obtained peaks with standard data from the literature, it is possible to identify most of the hydrated compounds in hardened cement paste. It was convenient in this work to represent the traces as peaks rather than the troughs normally shown for endothermic reactions. Peaks found in the present work are shown diagramatically in appendix 7.

2.8 X-RAY DIFFRACTION ANALYSIS

When x-rays of a specific wavelength are diffracted by a crystal, the conditions that need to be satisfied are given by Bragg's law [39]. Its mathematical form is:

$$n\lambda = 2d \sin\theta$$

where: n = the order of reflection

λ = the wavelength of the x-rays

d = the spacing of the crystal planes

θ = the angle of incidence or reflection of the x-ray beam.

By knowing the angle of reflection, θ , of x-rays of a given wavelength it is therefore possible to calculate the atom spacings which characterize each crystal. This can be used to identify the different phases present in cement pastes.

A "Philips" x-ray spectrometer (with Cu K_α radiation) was used in the present work for the analysis of powdered specimens. The most important component of it, is an electronic counter tube to measure the intensity of the x-ray reflections. The counter tube is rotated at twice the speed of the specimens in order to receive the reflected rays (fig. 2.6) . A trace of intensity against Bragg angle is recorded on a chart recorder from which values of d can be determined. By comparing these values to standard data [40], various phases of cement paste can be identified. An example of cement phase identification can be seen in appendix 8.

2.9 PORE SIZE DISTRIBUTION DETERMINATIONS

Pore size distributions were determined by mercury intrusion porosimetry using the "Micrometrics Instrument Corporation" porosimeter, model 900/910. The experimental technique involves intrusion of mercury into oven dried specimens at pressures up to 303.5 MPa (44000 psi) and the determination of the volume of mercury intruded at each pressure. The volume of mercury intruded at the maximum pressure was considered to be the total porosity.

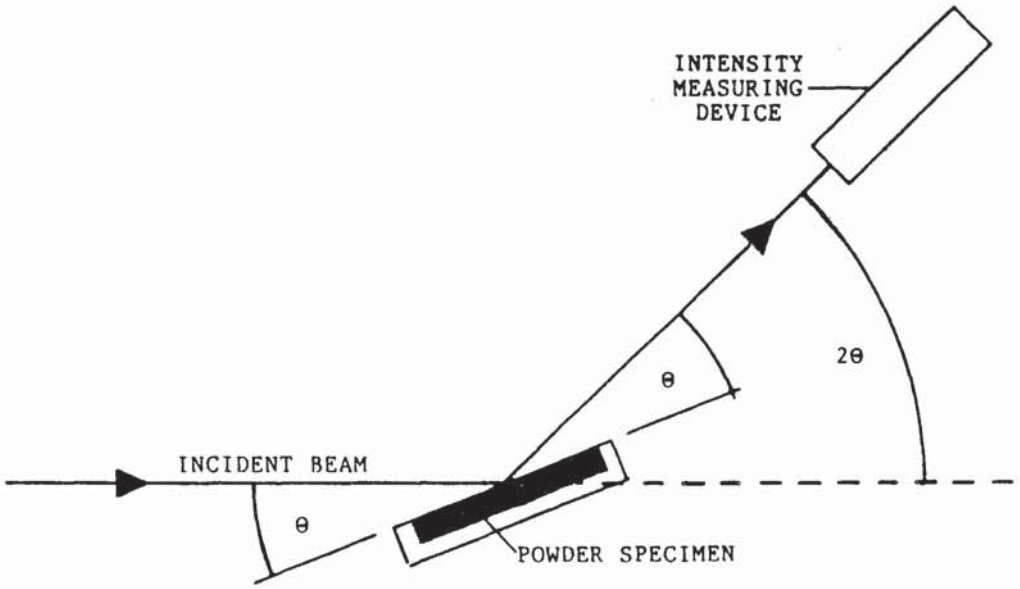

FIGURE 2.6 : Geometric arrangement of the X-ray Diffractometer.

A three millimetre thick disc of a cement paste was broken into small platelets and dried at 105°C for two days. After weighing, the sample was placed in a glass cell which was fixed into the pressure vessel of the porosimeter. The system was first evacuated, for removal of remaining moisture and gases, and then was filled with mercury, a non wetting liquid. The latter was subjected to increasing pressures, forcing it to penetrate the pores of the sample in proportion to their size and the pressure applied. The volume of mercury intruded at each pressure was taken as that which had penetrated a certain size of pores. It was determined from the level of mercury in the sample cell which was followed by a movable contact .

The pressure at which mercury enters pores of a given size may calculated from the Washburn equation [41]:

$$P = \frac{-4 \gamma \cos \theta}{d}$$

where: P = the applied pressure (Pa)

d = the pore diameter (m)

γ = the surface tension of the mercury (N/m)

θ = the contact angle between mercury and the material (degrees).

From this equation, if the value for the contact angle is known, the pressure can be translated into pore diameter. Following the work of Winslow and Diamond [42] the contact angle between mercury and cement paste was assumed to be 117°. It was therefore possible to plot the volume of the penetrated

mercury versus the pore diameter for the cement paste (appendix 9).

Results do not represent exactly the pore size distribution of the cement paste. The uncertainty in the value of the contact angle and the necessity to dry the specimens prior to the test are factors which influence the results. Since moisture content has a major effect on the microstructure of C-S-H gel, pore size distributions of saturated pastes are probably much different from those of dry specimens [43].

According to some researchers [3,44-46] in the higher pressure region, mercury intrusion creates differential pressure between the inside and outside of narrow-necked pores of blended pastes which can damage the pore structure. As a result, the estimation of the pore size distribution in the high pressure range can be misleading. It has also been reported [3,47,48] that direct oven drying does not give a paricularly accurate measure of porosity because it damages the pore structure. Midgley and Illston [49] found that different drying techniques mainly affect pores less than 100 Å radius.

Although mercury porosimetry does not measure accurately the pore size distribution of cement pastes it provides a simple way of obtaining relative data and has two important advantages when compared with alternative methods:

(a) it enables the widest range of pore sizes to be measured

(3 nm to 10 μm) [50] ,

(b) it has been widley used in the past for relevant research.

It is therefore useful as a means of comparing the present results with research carried out previously and in order to be able, in the present work, to compare different cements, or similar specimens but of varying conditions of exposure and curing. Care is needed in comparing mercury porosimetry data for Portland and blended pastes because of different degrees of damage involved [44,45].

CHAPTER 3 : Resistance to carbonation

3.1 INTRODUCTION

Atmospheric CO_2 affects hardened cement paste by reacting with the hydration products forming mainly calcium carbonate. As a result, the structure of the paste changes and its properties are altered.

The most important change in the structure of hardened cement paste, as far as its performance as a structural material is concerned, is the modification of its pore system (pore structure and pore solution). Changes in the pore structure affect properties such as strength, deformations and durability [51] whilst changes in the pore solution affect the protection of reinforcing steel in reinforced concrete .

The carbonation process, involves gradual penetration of CO_2 through the external surfaces of concrete and during the lifetime of a well made structure, the carbonated zone should be limited to a thin layer at the exterior. This requires a degree of resistance to carbonation, however, which depends on the hardened cement paste itself as well as on the surrounding environment. It is influenced by factors such as the type and amount of cement used, the degree of hydration, the water to cement ratio of the paste, and also by the

relative humitity and the CO_2 concentration in the atmosphere.

Since atmospheric CO_2 penetrates hardened cement paste through the pores, the relation between the pore system and the resistance of the paste to carbonation is of particular interest. This chapter examines aspects of the relationship. The work is presented in two parts. The first part is concerned with the effects of variation of the pore system, of the uncarbonated paste, on its resistance to carbonation. Changes in the pore system were produced by replacing parts of Portland cement in the original mix by BFS.

Part II compares the pore systems of hardened cement pastes with different degrees of carbonation , which were created by exposing specimens to atmospheres with different CO_2 contents.

As there are indications that chloride ions may affect the resistance of hardened cement paste to carbonation [37], in both parts of the chapter, chloride contaminated specimens were used in parallel with non-contaminated specimens.

3.2 INTRODUCTION TO CARBONATION AND LITERATURE REVIEW

3.2.1 General description of the carbonation process

Carbonation is the process whereby carbon dioxide from the atmosphere penetrates hardened cement paste and concrete reacting with the hydration products and lowering the alkalinity of the pore solution. Carbon dioxide first dissolves in the pore water forming carbonic acid which neutralizes the sodium and potassium hydroxides present in the pore solution. The decreasing alkali hydroxide content of the pore solution, however, is replaced by soluble $Ca(OH)_2$ derived from the solid hydration products which in turn reacts with dissolved CO_2 forming the insoluble calcium carbonate. The final result is a slow conversion of all the soluble $Ca(OH)_2$ of the paste to solid calcium carbonate and a considerable decrease of the alkalinity of the pore solution.

Atmospheric CO_2 can carbonate the surface layer of a concrete structure quite easily, but in order for the carbonation to propagate towards the interior, carbon dioxide must penetrate via the pores. The penetration of CO_2 into concrete is primarily a diffusional phenomenon and is controlled especially by the continuous pores of concrete

(7,52,53). It is important to note, however, that the diffusion of CO_2 in air is 10^4 times faster than in water (54), so the rate of penetration of CO_2 in concrete will be in the first place, determined by whether the pores are filled with water or not.

If the pores are completely saturated with water, as might be the case for a fully submerged structure, the carbonation rate would be negligible owing to the low rate of diffusion of CO_2 in water. On the other hand , if the pores are completely dry, as might be the case for oven-dried concretes, the pores would be open to easy penetration by CO_2 but carbonation would not occur because of lack of water. In any intermediate case between the above extremes, in which the pores are partly filled with water, carbonation to a certain degree can occur. This is normally the case close to a concrete surface when the surrounding atmosphere has a relative humidity lower than 100%. Part of the continuous pores would be empty for easy CO_2 penetration but enough moisture would be present to allow the carbonation reaction to proceed.

It follows from the above that an optimum amount of water in the pores would be necessary to maximize carbonation (55). This is illustrated in figure 3.1 which shows the

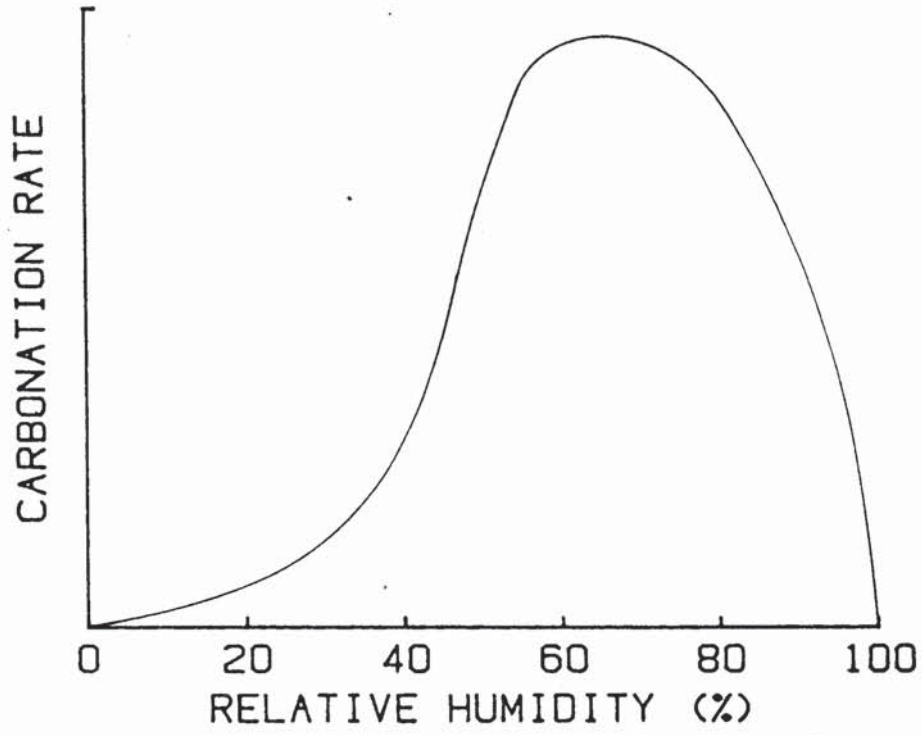

FIGURE 3.1 : Relationship between the relative humidity and the carbonation rate (from ref. 37).

probable relationship between the rate of carbonation and the relative humidity of the surrounding atmosphere [37]. The highest carbonation rate, as agreed by many researchers [37,56-60] can be achieved at relative humidities between 60% and 70%. According to figure 3.1 small changes in the relative humidity of an almost saturated environment (R.H.>90%) cause considerable changes in the moisture content of concrete and therefore to the carbonation rate. Tuutti [8] stated that even at a 99.9% R.H. there are still a substantial number of capillary pores which are not completely filled with water. This is because of the phenomenon of capillary condensation which is governed by the Kelvin equation :

$$r = \frac{-2\gamma V \cos\Theta}{R\ T\ \ln P/Po} \qquad \text{(ref. 61)}$$

where: r = the pore radius

γ = the surface tension of the liquid

V = the molar volume of the liquid

Θ = the wetting angle of the liquid

R = the gas constant

T = the temperature

P/Po = the relative vapour pressure

At any value of the relative vapour pressure,the pores of cement paste with radii smaller than the value given by the Kelvin equation will be full of condensed water. Those with radii larger than that value will carry only adsorbed layers of water on their surfaces.

3.2.2 Rate of carbonation

Theoretically, as soon as carbon dioxide comes into contact with cement paste or concrete, a certain degree of carbonation will occur, first at the surface. This carbonation front will then propagate slowly deeper into the concrete until all the alkaline components of concrete are neutralized.

In practice, however, this equilibrium situation is rarely if ever reached. The important factor is the rate of carbonation which determines the time at which the carbonation front will reach a certain depth e.g. the depth at which the reinforcement lies in reinforced concrete. The rate of carbonation depends mainly on the resistance of the cement paste to carbonation and on the environmental conditions of the surrounding atmosphere , as discussed in the previous section .

The resistance of cement paste to carbonation is controlled by two factors [62-64]:

(a) the pore structure of the paste which is determined by the w/c ratio, the compactness, the curing conditions and the degree of hydration,

(b) the amount of carbonatable material present in a unit volume of the paste which depends on the type and proportion of the cement used. Results from surveys of existing

structures which were reported by various researchers (59,62,65,66) substantiate the above.

Experimentally, the dependence of the resistance to carbonation on the above mentioned factors, has been shown clearly by Meyer (67) who carried out long-term carbonation experiments with concretes and mortars. By measuring the depth of carbonation of specimens with different W/C ratios after 2.5 years storage in air at 18°C and 50% R.H. he found a nearly linear relationship between the w/c ratio and depth of carbonation. He also showed that curing time and storage conditions affect the rate of carbonation. Concretes cured under water for longer periods showed reduced rates of carbonation. Concretes stored in a normal room atmosphere had higher rates of carbonation than concretes stored under water or concretes which were periodically moistened. To show the effect of the type and amount of cement used on the rate of carbonation, he measured the depth of carbonation of 2.5 year-old concretes made from portland cement, blast furnance cement and pozzolanic cement. Concretes made from blast furnace cement or pozzolanic cement showed greater depths of carbonation than concretes made from portland cement, all other conditions being identical. In concrete made from blast furnance cement, the depth of carbonation increased with an increasing percentage of blast furnance slag.Finally, by plotting the depth of carbonation of concretes stored in air, against the age of the concretes, he found a

parabolic relationship.

Since carbonation is primarily a diffusional phenomenon [7,52] the same parabolic relationship can be obtained theoretically by using Fick's first law for the diffusion of carbon dioxide in concrete. Page [7] by using Fick's first law suggested that for the simple unidirectional diffussion of CO_2 into a uniform concrete, the rate of advance of the carbonation front would be:

$$\frac{dx}{dt} = \frac{D \cdot C}{A \cdot x}$$

where: x = depth of carbonation

t = time

D = diffusion coefficient of CO_2

C = CO_2 concentration

A = amount of alkaline substances reacting per unit volume of concrete

On integration, assuming that there is no variation of the diffusion coefficient D with time or depth this yields a parabolic equation

$$x^2 = \frac{2 D C t}{A}$$

or $$x = K t^{1/2}$$

Where K is a constant which represents the rate of carbonation. This equation takes into account the factors

which influence the rate of carbonation. Water/cement ratio, compaction and curing are represented by the diffusion coefficient, cement content and cement composition are represented by the value of A, and the level of atmospheric pollution by the value of C. The assumptions involved with the equation however, cannot apply in reality to exposed concrete. For example, the factors which influence the diffusion coefficient of CO_2 in concrete may change with time (degree of hydration) and with depth from the surface (moisture content).

A more complicated equation was suggested by Japanese researchers [52,53,68]. It is also a parabolic relationship between the depth of carbonation and time

$$x^2 = \frac{2 D_o}{273^{1.75}} \frac{T^{0.75} \Delta P \varepsilon}{R C_o \rho f} t$$

where: x = carbonation depth (cm)

t = time (sec)

T = temperature (^oK)

ΔP = difference in pressure (atm)

ε = porosity of the specimen (cm^3/cm^3)

f = tortuosity

ρ = density of the specimen (g/cm^3)

C_o = maximum amount of fixed CO_2 or produced H_2O (mole/g specimen)

D_o = diffusion constant at 0^oC (cm^2/sec)

R = gas constant

The equation takes into consideration both physical and chemical factors involved in carbonation. It cannot, however, be applied easily in practice because some of the factors which it contains are too difficult to measure, especially tortuosity.

A simple relationship based on experimental results was obtained by Schubert and Berg [69] using cement containing fly ash and by Schubert and Efes [70] using jet cement. In their experiments they used concrete and mortar prisms stored at 20°C in 65% R.H. environments either in air or in 10% CO_2. By curve fitting they developed an empirical formula for the rate of carbonation as follows:

$$d_k = K_o + V_k t^{1/2}$$

where: d_k = depth of carbonation (mm)

t = time (days)

K_o = constant for a particular condition

V_k = carbonation rate (mm/days$^{1/2}$)

For both types of cement used they had observed a dependence of the rate of carbonation on w/c ratio for both normal and accelerated carbonation. Higher amounts of water in the original mix resulted in higher carbonation rates. In the case of the specimens that contained fly ash they found that the rate of carbonation was increased with the increase of fly

ash content. They attributed this to the higher pore content and to the reduced carbonatable material present in the mortars and concretes containing fly ash.

Alekseev and Rozental [71] had found that in short term carbonation experiments the depth of carbonation is proportional to the square root of time. For longer periods of exposure however they observed deviations from the square root relationship. They suggested that these deviations were probably caused by :

(a) a continuing hydration of cement resulting in higher density concrete and therefore in lower CO_2 penetration,

(b) an increase with time of the degree of carbonation in the neutralized layer which leads to a reduction of concrete diffusion permeability,

(c) diffusion of calcium hydroxide into the neutralized layer, in the direction opposite to CO_2 diffusion, so that when the flow of $Ca(OH)_2$ gets close in its magnitute to the CO_2 flow the displacement of the chemical reaction zone, i.e. the carbonation front, slows down or even stops completely.

The introduction of accelarators of hardening, such as $CaCl_2$, Na_2S0_4 and $Ca(NO_2)_2$ + $Ca(NO_3)_2$, in their concretes caused a considerable decrease of the carbonation rates. Supporting their theory, they attributed this to the increase of cement hydration rate and as a consequence to the

decrease of concrete permeability to CO_2.

Long term studies on carbonation undertaken in West Germany were reported by Smolczyk [63,72-74]. Based on 300 tests, he showed [72] that there is a linear relationship between the depth of carbonation after ten years of exposure and $1/B^{1/2}$, where B is the compressive strength of the mortar or concrete after 28 days of water curing , i.e. at the beginning of carbonation. From this he developed the equation:

$$x = a\,(1/B^{1/2} - 1/B_G{}^{1/2})\,t^{1/2}$$

where: x = depth of carbonation

a = rate constant

B_G = strength limit of carbonation (constant)

t = time exposure

The constants a and B_G depend on the curing conditions. Following further statistical evaluations he later reported [74,63] that the highest accuracy was found by taking into account the w/c ratio of the mix. So he proposed a new formula:

$$x = a\,\left(\frac{w/c}{N_T{}^{1/2}} - b\right)\,t^{1/2}$$

where a and b are constants depending on carbonation conditions and N_T is the compressive strength of the concrete after T days of water-curing. To a first approximation, T was the age of the concrete when the

carbonation began (in his experiments 7 days). As there was a degree of deviation from the linear relationship with some concretes, which he attributed to the continued hardening of the structure, he assumed the value of T to increase at the rate of about 1 day per year. Refering to Verbeck and Helmuth [75] who had reported that a concrete's compressive strength is inversely proportional to its capillary porosity, and to Mills [76] who had shown an increase in capillary porosity with increasing CaO/SiO_2 ratio at constant strength, he arrived at the expression:

$$\text{strength} \sim \frac{f(\text{ CaO content })}{f(\text{ capillary porosity })}$$

According to his formula, however, carbonation is inversely proportional to the square root of compressive strength. So he concluded that:

$$\text{carbonation} \sim \sqrt{\frac{f(\text{ capillary porosity })}{f(\text{ CaO content })}}$$

To support the relationship between strength and capillary porosity he determined the porosities and compressive strengths of mortars cured for various lengths of time. He showed that, in spite of the very different strengths, little differences in total porosities were observed. Great differences, however, appeared in the pore size distributions between 10 nm and 1μm, i.e. in the size range of capillary porosity.

Smolczyk's conclusion that carbonation is inversely

proportional to the CaO content of concrete agrees with the results of many researchers [51,62,65,67,69,77,37] who found that concretes, of constant w/c ratio, made with blended cements have reduced resistance to carbonation owing to the fact that they contain less carbonatable material than portland cement.

A verification of Smolczyk's formula was provided by Ho and Lewis [66] who tested concrete prisms made with cements of various fly ash content stored at 23°C and 50% R.H. in a 4% CO_2 content environment. Their results had shown that carbonation proceeded in proportion to the square root of time and that fly ash concretes had lower resistance to carbonation. For specimens which received 7 days of moist curing before carbonation, they found a linear relationship between the carbonation depth and the w/c ratio. Finally, by plotting the depth of carbonation against the reciprocal of the square root of 7-day or 28-day strengths they found linear relationships with high correlation coefficients.

Treadaway at al [65] studied carbonation of concrete in Bahrain under natural conditions. Although their results generally agree with Smolczyk's conclusions, using Smolczyk's formula they predicted lower carbonation rates than their measured values after a nine month exposure. It appears therefore that other parametres omitted from

the relationship may have a considerable effect on the rates. The large difference in the ambient temperature between Bahrain and Germany is probably one factor [37]. Krzywoblocka-Laurow [78] found that a change of curing temperature from 20°C to 32°C resulted in higher carbonation rates. Parrott[59] reported that an increase of temperature increases the rate of carbonation but it would also promote drying. Depending upon the degree of drying, elevated temperatures could increase or decrease the later rate of carbonation.

In summary, although the formula developed by Smolczyk might predict carbonation rates in Germany to a high degree of accuracy, it can not be used in countries of different climatic conditions. Generally there is a lack of a theory taking into account all the parameters influencing carbonation[59,79]. Except for the formulae obtained from Fick's law of diffusion which are based, however, on assumptions not applicable in reality, the other reported formulae [59] are empirical, i.e. based on curve fitting.

3.2.3 The structure of carbonated cement paste

Cement pastes are made up of a number of basic constituents. It is generally accepted [74,80,81] that during carbonation all of them at least partly, neutralize forming calcium carbonate. This is accompanied by the release of

bound water and obviously by the intake of CO_2.

Pihlajavaara [51] by determining the non-evaporable water and CO_2 content of carbonated and non-carbonated cement pastes with various w/c ratios showed that carbonation causes a considerable release of bound water. Taking as an example his 0.5 w/c ratio paste, the non-evaporable water had dropped after carbonation from 17% to 7%, accompanied by a 36% intake of CO_2. All percentages were expressed by weight of the original unhydrated cement. In a later publication, Pihlajavaara and Pihlman [82] showed that the relative humitity of the storage air as well as the w/c ratio affect the amount of CO_2 intake. The maximum amount of the CO_2 intake found in their 0.45 w/c ratio paste was 50% higher than that found in their 0.3 w/c ratio paste. Similarly they found that at 70% R.H. the maximum CO_2 intake was 40-50% greater than at 40% R.H. The greatest maximum CO_2 intake of the cement pastes tested was 35% by weight, measured in pastes with 0.45 w/c ratio exposed at 70% R.H. This CO_2 level, as discussed by Sergi [37], would represent about 45% carbonated CaO, assuming that all the CO_2 intake is by the CaO-bearing phases which are the majority of cement paste constituents. Since the CaO content of an OPC is about 65% by weight, there still remains 20% "unreacted"

CaO in the carbonated paste.

Smolczyk [74], reporting on the same subject, stated that the quantity of the "uncarbonatable CaO" is independent of the type of cement and the w/c ratio and has fairly constant values between 25% and 30% by weight of the cement. In another publication [72] he showed that the "uncarbonatable CaO" depends on the CO_2 concentration of the atmosphere . Cement pastes carbonated in 3% CO_2 atmospheres had 5 to 10% more carbonatable CaO than the same pastes carbonated in air.

A theoretical explanation for the uncarbonatable CaO present in cement pastes can be obtained from Powers's [83] hypothetical account of the carbonation of calcium silicate hydrate gel. He speculated that the calcium ions in the gel are between sheets of silica and at the exposed surfaces, and that these particles are generally 2-3 sheets thick, so one half to two-thirds of the calcium is immediately available to solutes in the pores. As the surface calcium ions react with dissolved CO_2 the resultant calcium carbonate remains attached to the underlying silica. A chemical reaction localized in the inner layer could still ensue, but since it would involve diffusion of atoms within the solid phase, the process might be a slow one. If the same applies for all fairly insoluble CaO bearing phases in the structure, then the

observations that a substantial amount of CaO remains uncarbonated are not unrealistic.

Since, as mentioned earlier, the greater part, if not all, of the CO_2 intake is by the CaO bearing phases of the cement paste, the main product of carbonation is calcium carbonate. All three modifications of it, vaterite, calcite and aragonite have been reported in the literature on carbonation, but aragonite is the least common. Sauman [56,57], studying the carbonation of 11Å-tobermmorite ($C_5S_6H_5$) and C-S-H gel, established that the first reaction product formed was vaterite which gradually was converted either partly or fully to the more stable modification calcite. A relative humidity of 100% resulted in the rapid and complete transformation of the vaterite into calcite. Higher CO_2 levels of 30% also faciliated a more complete transformation. Aragonite was only formed to a very small extent. He illustrated the reaction mechanism of the carbonation of 11Å-tobermorite and C-S-H gel as follows:

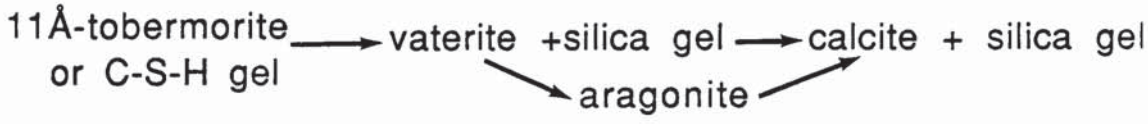

As he reported, the main difference between the carbonation of C-S-H gel and 11Å-tobermorite lies in the fact that in the case of C-S-H gel aragonite formation was substantiated only after 30 days of storage. The examination under the S.E.M. of both the C-S-H gel and 11Å-tobermorite had shown

that after carbonation they did not change in morphology even though their chemical composition had changed. A similar observation was also reported by Berger [84] who studied uncarbonated and carbonated C_3S and C_2S pastes under the S.E.M. This supports Powers's [83] speculation for the carbonation of calcium-silicate-hydrate gel which, as mentioned earlier, assumes that C-S-H gel carbonates by topochemical reactions.

By comparing the carbonation of 11Å-tobermorite ($C_5 S_6 H_5$) with the carbonation of tobermorite containing 5% Al_2O_3 in its crystalline lattice Sauman and Lach [85] found that the carbonation of the latter takes place at a substantially lower rate and results in the formation of less vaterite for the same conditions. A C_2SH paste carbonated even slower, showing that small variations in the gel structure could lead to different rates of carbonation.

In another publication [80] they reported on the carbonation of C_3AH_6 phase. Their results showed that the degree of carbonation of C_3AH_6 is increased with the period of exposure to CO_2, its concentration and the relative humidity of the environment. The reaction mechanism involves the formation of a metastable complex carbonate as follows:

$$4\,(3CaO.Al_2O_3.6H_2O) + 3\,CO_2 + (1+x)\,H_2O \longrightarrow$$

$$3\,(\,3CaO.Al_2O_3.CaCO_3\,.xH_2O\,) + 2\,Al(OH)_3$$

which is further decomposed to $CaCO_3$:

$$3\,CaO.Al_2O_3.CaCO_3.xH_2O + 3\,CO_2 + 3\,H_2O \longrightarrow$$

$$4\,CaCO_3\,(\,\text{vaterite} \longrightarrow \text{calcite}\,) + 2\,Al(OH)_3 + x\,H_2O$$

$$\text{vaterite} \searrow \text{aragonite} \nearrow \text{calcite}$$

Kondo et al [52] by carbonating mortar prisms through one surface only, showed that the modifications of calcium carbonate vary with increasing depth. According to their results, amorphous carbonate is likely to form at the deeper parts of the prisms while in intermediate depths the predominant modification is calcite. As the depth decreases the amount of calcite decreases relative to that of vaterite. Explaining their results, they claimed that at the deeper parts, at which carbonation is in the early stage, the major modification is calcite while near the surface where carbonation is in later stage, carbonation of unhydrated cement components takes place and this produces vaterite.

Similar studies by others [86,87,78,58] have shown that the formation of vaterite is favoured by high pH, higher temperatures and lower humidities. Sergi [37] by carbonating hardened cement pastes under natural and accelerated conditions, found that the ratio of vaterite to calcite increases with the rate of carbonation. As he speculated, the finer crystalline vaterite would form more readily where the reactions are faster. Depending on the existing conditions

vaterite could then slowly recrystalize to form coarser calcite.

According to Moorehead [88] who reported on the carbonation of hydrated lime, for each mole of portlandite converted to calcite there is an 11.8% increase in solids volume which is accomodated in the internal pores of the compact. Comparing the pore size distribution of lime compacts before and after carbonation he found that after carbonation, pore sizes larger than 1 μm and smaller than 0.01μm in diameter had been reduced while intermediate pore sizes had been increased.

Rozental and Alekseev [89] examined the changes of porosity during carbonation of cement-sand mortars using a mercury pressure porosimeter. Their results showed that for cement-sand mortar of 1:2 composition, with w/c ratios 0.5 and 0.6, the volume of pores in the range of 0.1-10 μm radius had decreased by half after carbonation. In general they found a displacement of the maxima of the pore volumes towards larger pores. Microscopic examination of hardened cement paste carbonated naturally at 60% R.H. indicated that pores with radius greater than 120 μm had shown no evidence of carbonation. Explaining their results they claimed that since the interaction between CO_2 and cement paste occurs in the presence of water, $Ca(OH)_2$ crystals from the larger pores dissolve in the higher moisture content smaller pores

and capillaries, in which they carbonate to $CaCO_3$; this reduces the volume of the smaller pores.

A different theory was given by Yuping et al [90]. They speculated that the drop in the percentage of small pores observed after carbonation of their autoclaved aerated concrete specimens was caused by the contraction of particles when calcium ions leave them to form calcium carbonate.

Pihlajavaara [51] carried out similar experiments using mature cement pastes with various w/c ratios. His results indicate that although there was a reduction in the total porosity of cement pastes after carbonation, the most affected pores were in the range of 20 nm to 100 nm in diameter. As he pointed out, however, before any definite conclusions could be formed more research was required, performed with different methods and pastes with different histories.

3.2.4 Affected properties

The most important engineering properties of a structural material such as concrete are the strength, the deformations and the durability. It is generally accepted [51,67,91,10] that after carbonation, all three of these characteristics are

affected owing to the change of the structure of cement paste (see previous section).

(i) Strength

Meyer [67] studied the influence of carbonation on the strength with mortar cylinders exposed to an atmosphere of 10% CO_2 and 80% R.H. His results showed that after carbonation the strength of OPC and low BFS content mortars was increased significantly. For mortars of 50% BFS content and mortars of aluminous cement, however, the increase in strength was insignificant while the strength of mortars of higher slag content remained almost unchanged. The strength of supersulphated cement mortars was substantially decreased after carbonation.

Similar results were observed by Manns and Wesche [92] who carbonated cement paste specimens under accelerated conditions (9% CO_2, 65% R.H.). They found that pastes containing over 40% OPC by weight had shown an increase in strength by up to 70%, where pastes with OPC content below 40% had shown a decrease in strength by up to 50%. In general, the higher the OPC content as opposed to BFS or trass, the higher the strength observed after carbonation. As they reported, the variation in strength was accompanied by a variation in the modulus of elasticity and in density.

Comparing the time dependence of the change in density and compressive strength they found that the variation in density was linearly related to that in strength. To explain their results they considered the carbonation reactions of the cement paste's components. When C-S-H gel and $Ca(OH)_2$ are carbonated, an increase in weight occurs because in effect, one mole of water is replaced by a heavier one mole of CO_2 according to the equation:

$$Ca(OH)_2 + CO_2 \longrightarrow CaCO_3 + H_2O$$

The carbonation of ettringite, however, causes a decrease in weight because 27 moles of water are replaced by the uptake of 3 moles CO_2 according to the equation:

$$C_3A \,.\, 3CaSO_4 \,.\, 32H_2O + 3\, CO_2 + 3\, H_2O \longrightarrow$$

$$3\, CaCO_3 + 2\, Al(OH)_3 + 3\, CaSO_4 \,.\, 2H_2O + 30\, H_2O$$

They argued that the cement pastes with the higher proportion of OPC release more $Ca(OH)_2$ during hydration and so after carbonation they would have a resultant density increase. On the other hand, specimens with cements of low $Ca(OH)_2$ content where sulphoaluminates and other poly-hydrate phases are most prominent, would suffer a net decrease in density when carbonated. As far as the link between density change and variation of strength was concerned, they were uncertain. It follows from the previous paragraphs, however, that the amount of $Ca(OH)_2$ in

the precarbonated paste determines the porosity of the carbonated paste and therefore the strength. An overall decrease in density would cause a decrease in strength because of a less compact structure.

(ii) Shrinkage and Creep

Shrinkage due to carbonation can be of the same order of magnitude as the drying shrinkage or even more. It is strongly dependent on the humidity of the ambient air, the sequence of drying and the carbonation periods[91]. According to Verbeck [93] who studied carbonation shrinkage using mortar specimens, maximum shrinkage is observed at about 50% R.H. He found that the size of the specimens as well as the concentration of the CO_2 in the exposure atmosphere influence carbonation shrinkage by affecting the internal humidity of the specimens.

Roy [86] speculated that hardened cement paste shrinks considerably at 50% R.H. during carbonation because both $Ca(OH)_2$ and C-S-H gel are affected, while at a relative humidity of 25% little carbonation shrinkage occurs because carbonation of only the $Ca(OH)_2$ is involved.

Experiments by Sauman [57], who used mortar specimens containing 27% portland cement and 6% lime, had shown that

shrinkage is proportional to the CO_2 concentration and to the storage time, whereas relative humidity exhibits a smaller influence. By measuring the length changes of his specimens exposed to air, 1%, 10% and 30% CO_2 at various relative humidities he observed that the greatest length changes were recorded for specimens exposed to 30% CO_2 at 75% R.H.

A theoretical explanation for carbonation shrinkage was given by Powers [83] who also observed that maximum shrinkage occurs at intermediate R.H.'s. According to him, the partial drying of the cement paste causes a compressive stress on the calcium hydroxide crystals. As the dissolved $Ca(OH)_2$ in the pore solution carbonates, more dissolves from the stressed crystals slowly releasing the compressive stresses. This gives rise to shrinkage which is proportional to the temporary increase of compressibility of the paste caused by the removal of calcium hydroxide from regions under stress and deposition of $CaCO_3$ in stress free regions. Even though there may be a net increase in mass, it would not necessarily prevent shrinkage, as the newly formed $CaCO_3$ can nucleate in pores thereby reducing the porosity. The other phases in the paste, such as C-S-H gel, carbonate by topochemical reaction (see section 3.2.3) and therefore shrinkage would not occur.

Parrott [94] studied the effect of carbonation on creep using prisms of hardened cement paste. He found that carbonation under load increased the creep of his specimens by more than 50%. The magnitude of any increase in creep, however, depended upon the time and upon the size of the tested specimens. Explaining his results he speculated that the calcium hydroxide which constitutes a substantial proportion of the hydrated cement forms part of the load-bearing skeleton of the hardened cement paste. During carbonation, however, it loses its load-bearing ability due to the chemical conversion to calcium carbonate, and this gives rise to additional creep.

(iii) Protection of the steel reinforcement

Cement paste and thus concrete has the ability to protect the reinforcing steel from corrosion. This property is based on the fact that cement paste maintains a highly alkaline environment in which the embended steel displays passivity under most circumstances [7,8]. As it is generally accepted [7,8,37,95,96] there are two common agencies that may cause breakdown of this passivity. These are acidic gases such as CO_2 which may carbonate concrete depressing the pH value of its pore solution towards non-passivating levels and chloride salts which may induce depassivation even at high pH values.

The effect of carbonation on the protection of steel in concrete is not limited to the lowering of the pH of the pore solution. It also causes a release of the bound chloride into the pore solution [97,37], which as mentioned above, may induce depassivation of steel even in regions of incompletely carbonated concrete where the pH is still relatively high. Sergi [37] attributed this to the carbonation of the insoluble complex calcium chloroaluminate salt which decomposes, releasing the soluble chloride ions into the pore solution according to the equation:

$$3CaO.Al_2O_3.CaCl_2.10H_2O + 3CO_2 + 3H_2O \longrightarrow$$

$$3CaCO_3 + 2Al(OH)_3 + CaCl_2 + 10H_2O.$$

By carbonating cement pastes under normal and accelerated conditions he found that normal carbonation encouraged more chloride release than accelerated carbonation. He suggested that the cause for this difference may be the entrapment of the calcium chloroaluminate, or other chloride bearing phases, within rapidly forming carbonates, which may not have had sufficient time to redistribute themselves elsewhere, as might be the case for the much slower normal carbonation .

Carbonation may initiate the corrosion process since a reduction in the pH value allows the steel to pass from the passive to the active state. The rate of attack, however,

depends on other external corrosion factors namely, a minimum atmospheric moisture content to guarantee the presence of an electrolyte in the concrete pores and free access of oxygen to the metal surface to enable the cathodic reaction to take place. This was shown experimentally by Gonzalez et al [95,96] who measured the corrosion rates of steels embeded in carbonated mortars. Their results showed a dependence of the corrosion rate on the enviromental moisture condition. In dry environments carbonation did not promote appreciable corrosion of the reinforcement. In the case of moist environments or partially immersed specimens, however, a serious corrosion rate was produced.

From the reviewed studies on carbonation (sections 3.2.1 to 3.2.4) the following general conclusions can be obtained :

(i) The resistance of cement paste or concrete to carbonation depends on the :

(a) w/c ratio of the original mix,

(b) type and proportion of cement in the mix,

(c) degree of hydration,

(d) curing conditions,

(e) compacteness of the paste which also depends in part on a,c,d,

(f) relative humidity, with maximum between 60% and 70%,

(g) CO_2 partial pressure in the atmosphere.

(ii) The various reported formulae which describe

carbonation are either general equations obtained from curve fitting or theoretical equations which cannot be applied in practice.

(iii) No criteria have been established which provide a basis for accelerated laboratory tests aimed at characterization of cement pastes or concretes according to their resistance to carbonation.

(iv) Carbonation changes the pore structure and phase composition of cement paste or concrete. There is no information, however, on the effect of carbonation on ionic concentrations in the pore solution.

(v) After carbonation characteristics of cement paste or concrete such as strength, deformations and durability are affected .

As carbonation affects most of the properies of concrete, the prediction of carbonation depths in concrete structures and the development of materials which can offer improved resistance to carbonation are particularly important. For this reason the development of a general carbonation theory is essential.

The aim of this chapter is to contribute to the understanding of the mechanisms of carbonation of hardened cement paste. More specifically, as mentioned in section 1.3, the intentions were:

(i) to fill the gap between the theoretical representation of

carbonation and practice,

(ii) to look for criteria which characterize cement pastes in terms of their resistance to carbonation,

(iii) to provide information on the effects of carbonation on the pore system (pores and pore solution),

(iv) to investigate the effects of chloride contamination on the resistance of cement paste to carbonation.

3.3 EXPERIMENTAL PROCEDURE

As mentioned in the introduction, the experiments were carried out in two parts. In the first part cement pastes with 0%, 25%, 45% and 65% BFS content were subjected to accelerated carbonation (in a 100% CO_2 atmosphere). In the second part cement pastes with 65% BFS content were subjected to carbonation in three different atmospheres: 100% CO_2, 5% CO_2 and Air. A fourth atmosphere of 100% N_2 was also used for comparison (uncarbonated paste).

In both parts of the work, the specimen preparation and the experimental set-up were the same. For all the conditions studied, the following aspects were investigated :

(1) The rate of carbonation

(2) The concentration of ions in the pore solution

(3) The proportion of free and bound chloride present in the pastes

(4) The porosity of the pastes

(5) The phase composition of the pastes

3.3.1 Specimen preparation

Ordinary portland cement (OPC) and blast-furnace-slag (BFS) were first separately sieved through a 150 μm mesh in order to produce a consistent fineness. Both materials were then weighed and mixed in the required proportions, to produce mixtures of 0%, 25%, 45% or 65% BFS content. Deionised water was then added to the mixtures to produce 0.5w/c ratio pastes.

In the case of pastes contaminated with chloride, 1% chloride ion by weight of cement, in the form of sodium chloride, was dissolved in the water prior to the addition to the mixture.

The pastes were then mixed thoroughly by hand for 5 minutes with a wooden rod. They were then poured into cylindrical PVC containers, 49 mm diameter by 75 mm in height which were vibrated for a further 3 minutes on a vibrating table.

On at least two occasions the foamy layer that had accumulated on the surface was removed and replaced by fresh cement paste. A polythene sheet was then placed on top of each of the containers to prevent the entrapment of air by the cap which was subsequently fitted on top.

In order to minimise segregation and to enable the production of uniform cement pastes, the cylinders were then rotated top to bottom at a speed of 8 rpm for 24 hours and finally stored in a high humidity room at 22°C.

After a 28 day curing period, the cylindrical specimens were demoulded and sliced into 3 mm thick discs. The discs were cut from the central part of the cylinders, by means of a Cambridge micro-slice-2 which is a high precision diamond wheel saw, working on the principle of a carefully counterbalanced "see-saw". Deionised water was used as a lubricant. After cutting, the discs were lightly ground on 600 grade carbide paper.

The effect of the preparation procedure on the w/c ratio of the specimens was found to be negligible. The difference between the amount of water originally added to the mixture and the total water content of the pastes (E.W.+N.E.W. ; see section 2.5), measured just after demoulding, was found to be less than 0.01 g/g cem.

3.3.2 Experimental set-up

For each experiment, two groups of cement paste discs, 24 chloride-free and 24 chloride-containing, were placed separately in an upright position on two specially made

perspex racks. The racks were then placed individually above a saturated $NaNO_2$ solution in air-tight containers at room temperature, thus maintaining the relative humitity at about 65%, as recommended by the RILEM permanent commitee on concrete [98].

At 24 hour intervals, a gas of known composition was passed over the discs and through a water trap for half an hour. This procedure was followed in order to avoid any changes in humidities with the continued passage of the gas. The gas was passed over the discs until 30 days after their complete carbonation was detected using phenolphthalein (see next section). The gases used were 100% N_2 (as control), 100% CO_2 and a mixture of 5% CO_2 and 95% N_2 . One container was simply exposed to the lab air for similar periods of time.

3.3.3 Rate of carbonation

To measure the rate of carbonation of the discs the depth of carbonation was recorded with time. For this purpose, discs were removed from the containers at regular intervals and broken by hand at right angles to the flat surfaces. A 1% solution of phenolphthalein in alcohol was then applied to the freshly broken surfaces in order to locate the carbonation front [98]. The latter was assumed to be the interface between the colourless and the red coloured parts of the

surface which, especially in pastes containing BFS, was not a clear straight boundary (fig.3.2). A travelling microscope was used to measure the depth of carbonation on three discs to the nearest 100 μm and the average value was recorded.

The phenolphthalein indicator method used in the present investigation is simple, is well documented [59,93,98,99,67] and can give reproducible results [59]. It indicates, however, the depth at which the pH is about 9 and this does not necessarily correspond to the true carbonation front. In reality, as can be seen from figure 3.3, carbonation can occur at depths greater than those indicated by phenolphalein.

3.3.4 Pore solution analysis

Thirty days after the complete carbonation of the chloride free discs in each condition, 16 chloride free and 16 chloride-rich discs from each condition were pressed, by means of the "pore-press" as described in chapter 2 (section 2.2) in order to extract the pore solution.

At 65% R.H. in which the discs were cured, however, there is not sufficient water to be pressed for analysis, so a saturation process before the pressing was essential. The saturation was achieved by adding on the one surface of the discs small amounts of deionised water which was quickly absorbed by the cement paste. The addition of water was

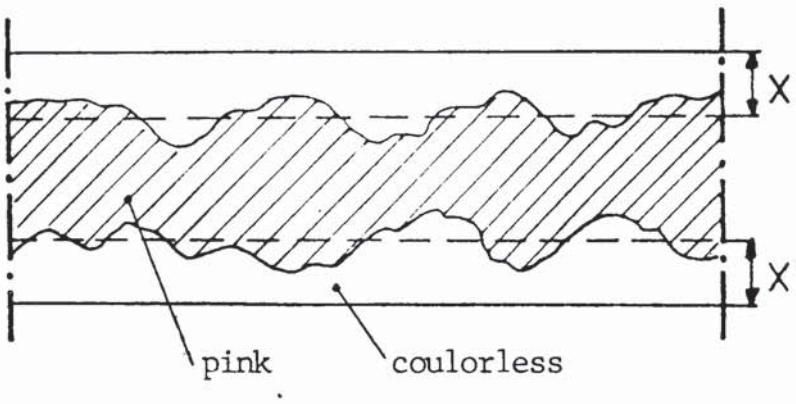

FIGURE 3.2 : Depth of carbonation, x, measured in a cement paste disc using phenolphthalein.

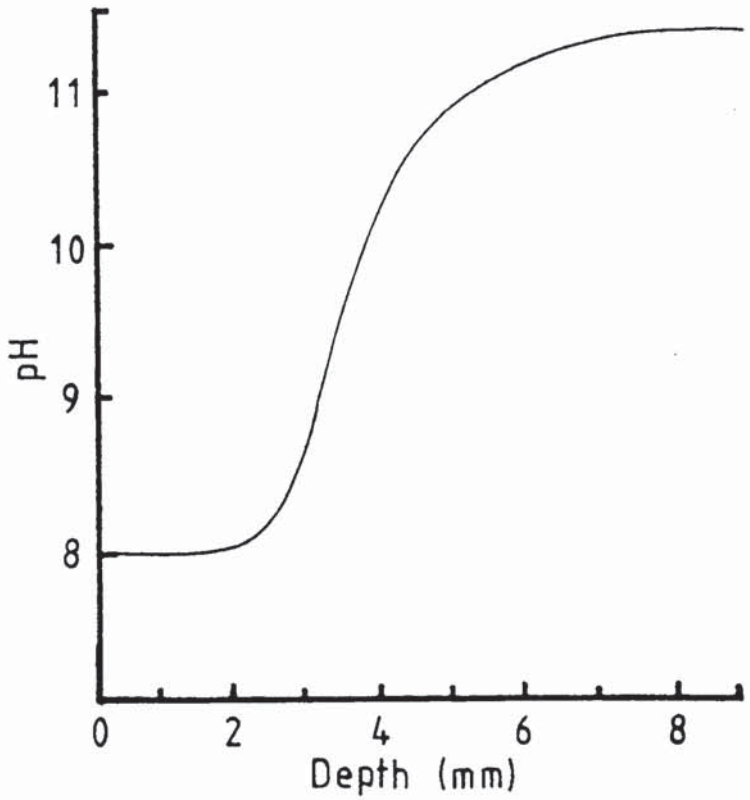

FIGURE 3.3 : pH profile induced by carbonation (from ref. 99).

repeated every day until no further absorption was observed. In order to ensure reproducibility the discs were then allowed to stand in a 100% R.H. environment for 7 days, replacing the $NaNO_2$ solution by water in the same containers.

The extracted solution was analysed for the following ions: Na^+, K^+, Ca^{++}, Cl^-, OH^-, CO_3^{--} and HCO_3^- (see section 2.3). In addition, ion chromatography was employed (see section 2.4) to verify the results obtained from the above methods and to look for any other ionic species present in the pore solution. In the case of low hydroxyl content solutions a pH electrode and a meter was used to determine the pH values (section 2.3.2).

3.3.5 Phase composition analysis and M.I.P.

Samples from discs of each condition were ground to powder, sieved through a 150 μm mesh and subjected to DTA (section 2.7) and XRD (section 2.8). Powder from the same samples was also used for the total chloride determination (section 2.6).

M.I.P. investigations and evaporable/non-evaporable water determinations (sections 2.9 and 2.5) were also carried out from similar samples which were broken into small

platelets.

3.4 RESULTS AND DISCUSSION

PART I: PARTIAL REPLACEMENTS OF CEMENT WITH BFS

3.4.1 RESULTS

3.4.1.1 Rate of carbonation

For all the conditions studied a parabolic relationship between the depth of carbonation and time was obtained. Figure 3.4 represents graphically the increase in carbonation depth with the square root of time for eight different types of discs, made of cement with 0%, 25%, 45% and 65% BFS content, with and without chloride contamination. A full table of the results can be found in appendix 10. In all the graphs, after a certain induction period, the depth of carbonation increases linearly with the square root of time, indicating that the mathematical equation representing the relationship is similar to that used by other researchers [37,69,70] of the form :

$$x = K\, t^{1/2} - K_o$$

where:

x = depth of carbonation

t = time (days)

K = constant for the rate of carbonation ($mm/day^{1/2}$)

K_o= constant, related to the induction period t_o , by :

$$K_o = K\, t_o^{1/2}$$

For each condition studied, the carbonation depth measurements fit the above equation with high correlation coefficients (see table 3.1). Calculated values of K and t_o for all the types of specimens used are tabulated in table 3.1. It should be noted, however, that the induction period t_o is the time period calculated from the extrapolation of the obtained linear relationship, to the time axis. The real induction period, i.e. the period needed for the carbonation to be observable by the phenolphthalein method, as can be seen from figure 3.4, may be somewhat lower.

Higher values of K represent faster carbonation rates i.e. lower carbonation resistance. So, as may be seen from table 3.1 the carbonation resistance reduces with the increase of the BFS content. It is also clear that the chloride contamination had a slight reducing effect on carbonation resistance.

3.4.1.2 Concentration of ions in the pore solution

Ionic concentrations and pH values of the extracted solution for each type of cement paste disc used are represented in table 3.2 . The analysis for each ion had been made as

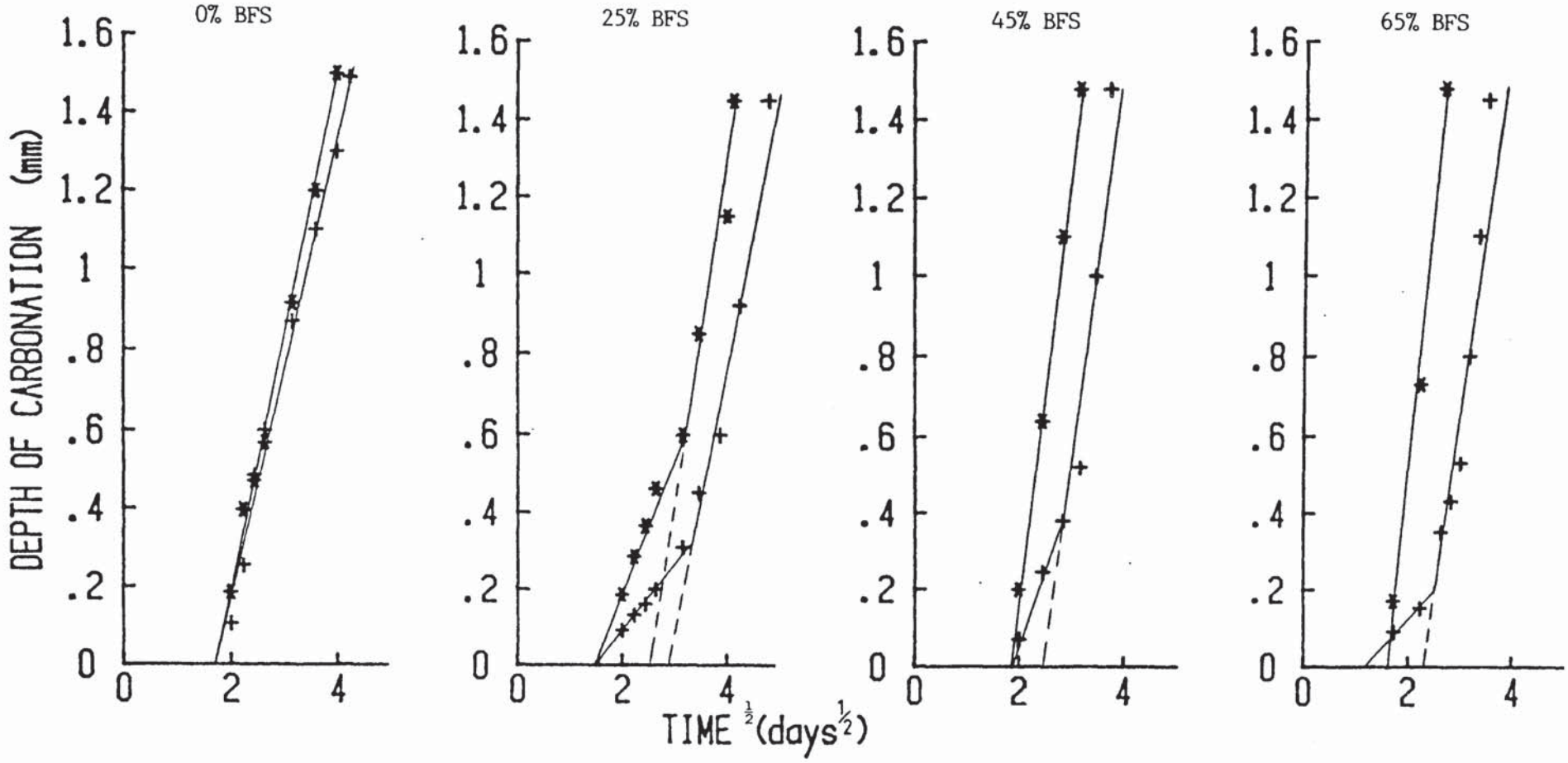

FIGURE 3.4 : The increase of carbonation depth with the square root of time for BFS blended cement pastes carbonated in a 100% CO_2 /65% R.H. atmosphere.
+, no contamination; ⁎, NaCl contamination.

Table 3.1: Rates of carbonation and induction periods of BFS blended cement pastes.

BFS content	K mm/day$^{1/2}$	t_o days	correlation coefficient
0%	0.58	2.82	0.996
25%	0.74	8.28	0.951
45%	0.94	5.56	0.941
65%	1.39	6.57	0.975
NaCl contaminated pastes			
0%	0.64	2.89	0.998
25%	0.79	5.81	0.974
45%	1.11	3.38	0.999
65%	1.44	2.72	0.989

Table 3.2: Pore solution analysis for BFS blended cement pastes carbonated in a 100% CO_2 - 65% R.H. atmosphere. (concentrations in mmol/l).

BFS content	pH	OH^- $x10^{-4}$	Cl^-	Na^+	K^+	Ca^{++}	Σ^-	Σ^+
0%	7.65	4.5	9.5	10.2	51.7	382.3	9.5	826.6
25%	7.68	4.8	32.5	9.8	26.4	239.7	32.5	515.6
45%	7.72	5.3	36.5	18.1	19.1	249.6	36.5	536.5
65%	7.57	3.7	45.5	19.4	10.2	199.7	45.5	429.0
NaCl contaminated pastes								
0%	7.53	3.4	630.0	289.5	81.1	494.9	630.0	1360.4
25%	7.28	1.9	745.0	244.1	33.3	275.3	745.0	828.0
45%	7.22	1.7	825.0	260.5	24.7	289.8	825.0	864.9
65%	7.31	2.0	720.0	211.4	12.8	262.5	720.0	749.2

described in section 2.3. As expected the pH values were nearly neutral for all the solutions. The pore solutions of the chloride - contaminated discs, however, had lower pH values than those of the non-contaminated discs, which may be connected with the reducing effect on carbonation resistance of the added sodium chloride.

Carbonates and bicarbonates were not found in the solutions in accurately measurable quantities. For discs without the addition of sodium chloride the concentrations of carbonates and bicarbonates in the pore solution were found to be respectively in the order of magnitude of 3×10^{-3} to 4×10^{-3} mmol/l and 1 to 2 mmol/l while for NaCl contaminated discs both carbonates and bicarbonates were negligible. A typical curve of the titration of the extracted solution with 1mM nitric acid (see section 2.3.3) is shown in figure 3.5 for discs without addition of sodium chloride and in figure 3.6 for discs with sodium chloride addition (for the calculation of carbonates and bicarbonates see appendix 1).

Comparing the total negative (Σ^-) and the total positive (Σ^+) charge for ions detected in each pore solution it can be seen that the total cationic charge is much higher than the total anionic charge, especially in the case of the non-contaminated discs. To explain this difference, as well as to verify the results obtained, ion chromatography was employed (see section 2.4) to produce the chromatographs

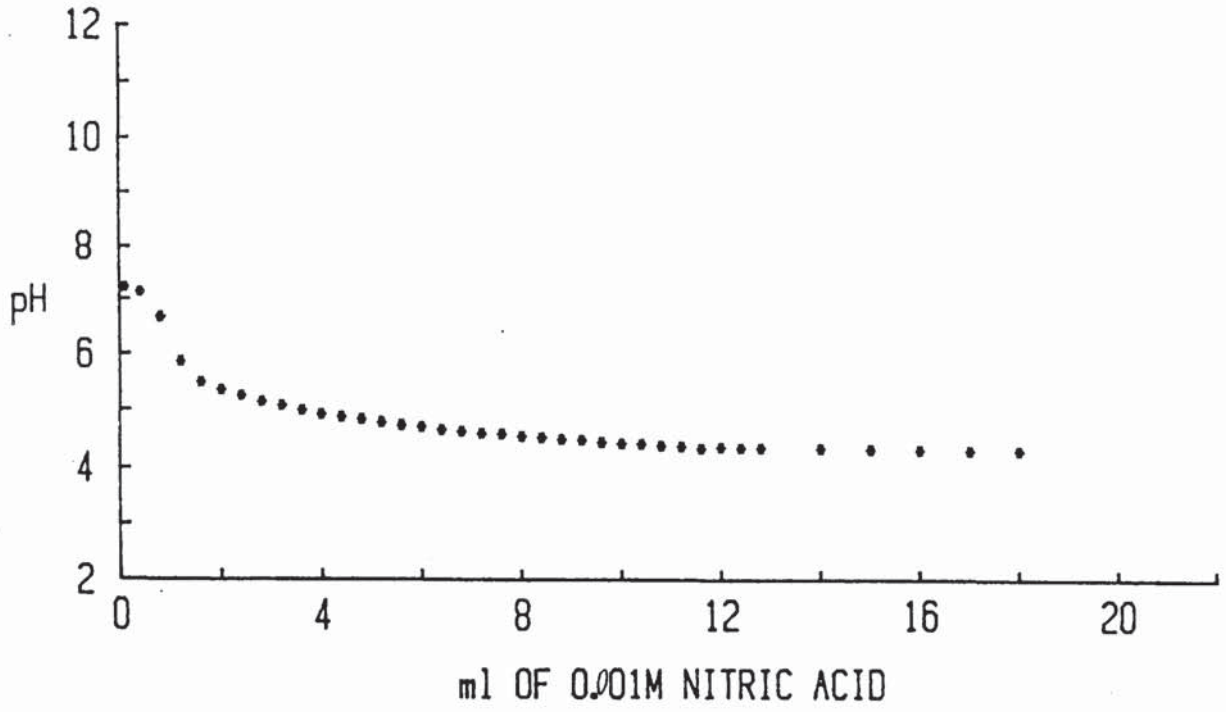

FIGURE 3.5 : Titration curve for the pore solution of OPC/65% BFS cement paste carbonated in 100% CO_2. (volume of pore solution = 6 ml).

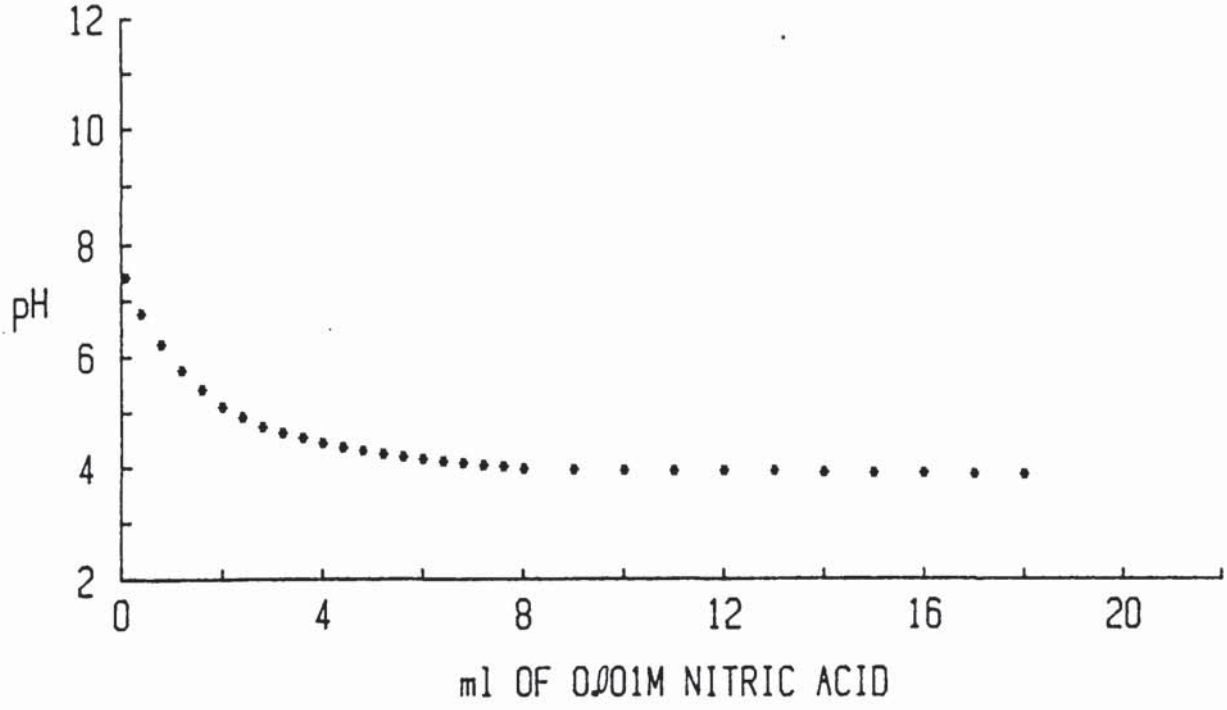

FIGURE 3.6 : Titration curve for the pore solution of OPC/65% BFS cement paste carbonated in 100% CO_2 (NaCl contaminated paste; volume of pore solution =6ml).

presented in figures 3.7(a+b) and 3.8(a+b). Examining the cation chromatographs, (fig. 3.7) it may be seen that in addition to the analysed calcium, sodium and potassium ions, magnesium ions were also present in the pore solutions in relatively high concentrations. As far as the anion chromatographs (fig 3.8) are concerned, it may be seen that in addition to the chloride ions, sulphate ions were also present in the pore solution. There is, however, a third peak which does not correspond to any common anion which was thought likely to be present in the pore solution. As will be discussed later, this may attributed to an ionic form of soluble silica. By comparing the ion chromatographs of the samples to ion chromatoghraphs of standard solutions, a quantitative analysis was performed (a worked example can be found in appendix 4). The results are tabulated in table 3.3. Comparing these results with the corresponding results obtained by other analytical methods (table 3.2) it can be seen that, except for chloride ion, the concentrations of each of the remaining ions are similar for both the methods. The concentrations of chloride ion obtained by ion chromatography are considerably higher than those obtained by the spectrophotometric method. The reason for this is that chloride ions co-elute with silicate ions. When a solution of sodium silicate and sodium chloride was passed through the chromatograph, only a single peak was obtained. The same peak was obtained when sodium chloride and sodium silicate were separately tested. This suggests that silicate ions are

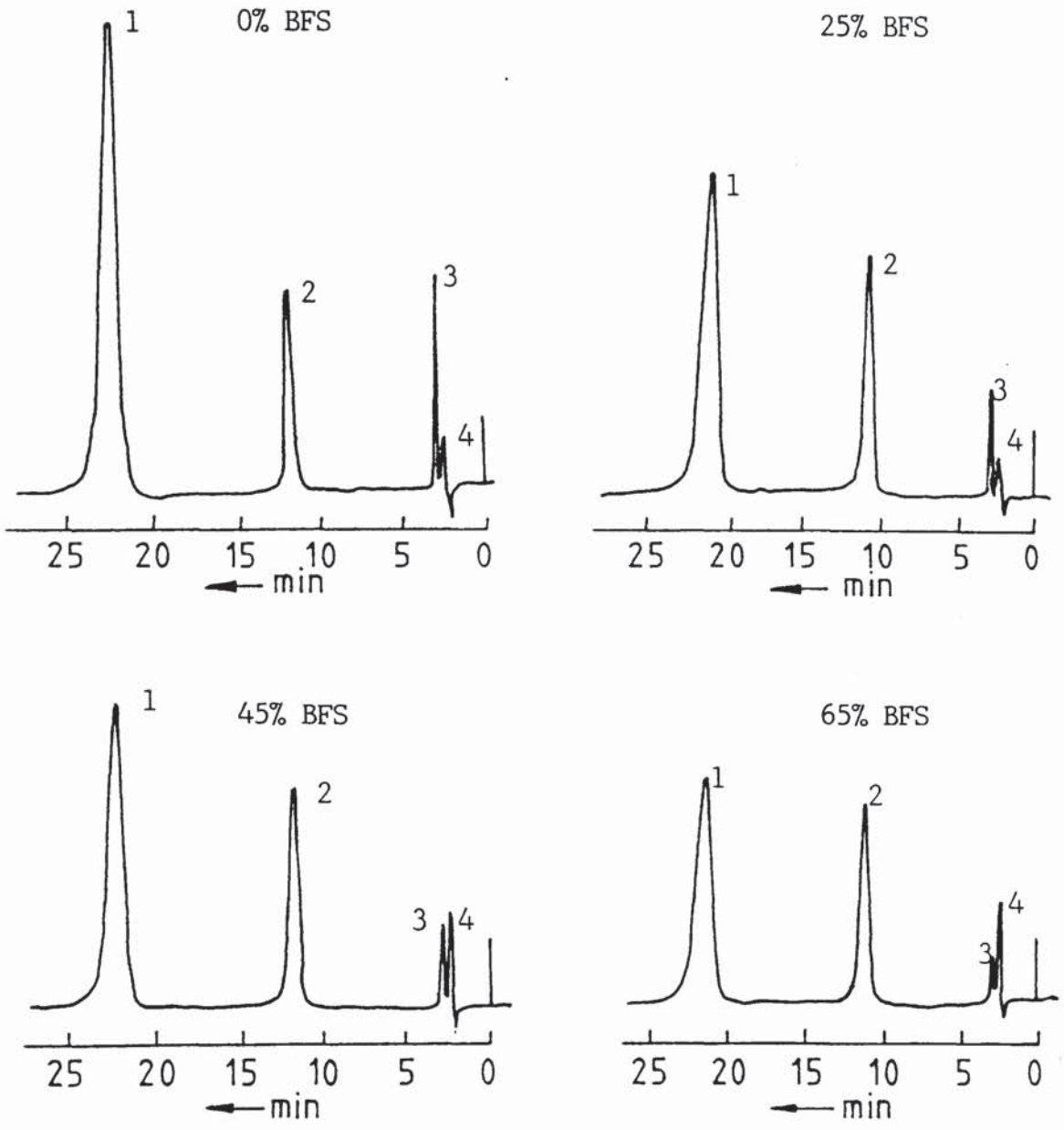

FIGURE 3.7(a) : Cation chromatographs of BFS blended cement pastes carbonated in 100% CO_2 atmosphere.
1= Ca^{++}, 2= Mg^{++}, 3= K^{+}, 4= Na^{+}.

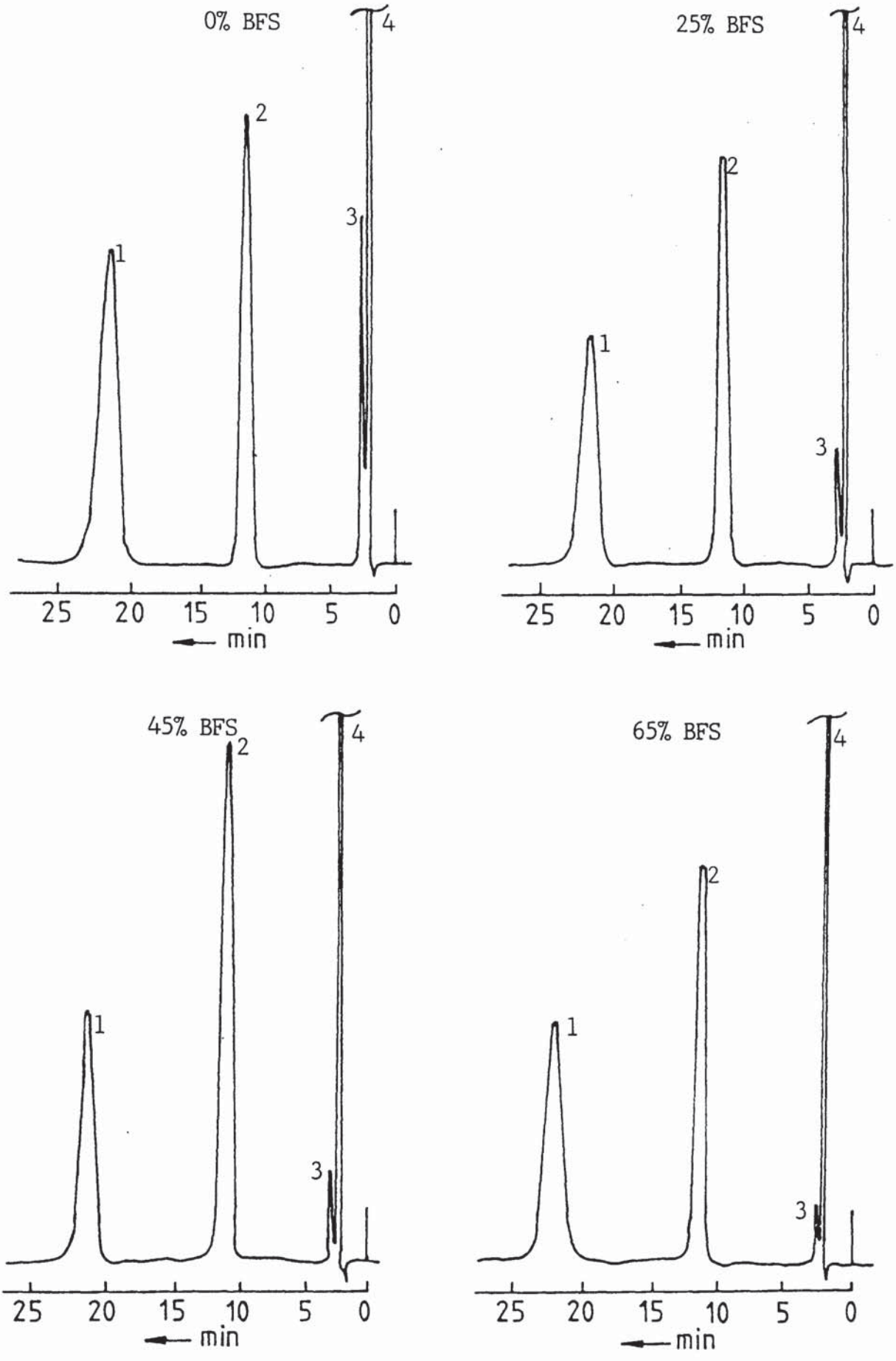

FIGURE 3.7(b) : Cation chromatographs of BFS blended cement pastes contaminated with NaCl and exposed to 100% CO_2.
1= Ca^{++}, 2= Mg^{++}, 3= K^{+}, 4= Na^{+}.

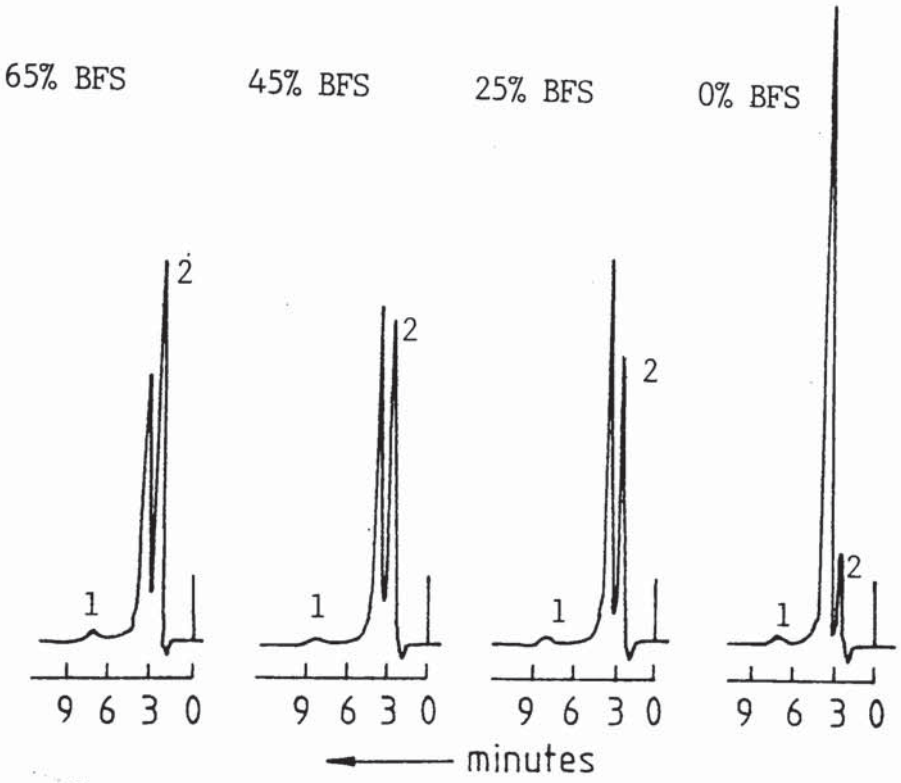

FIGURE 3.8(a) : Anion chromatographs of BFS blended cement pastes carbonated in 100% CO_2. 1= SO_4^{--}, 2= Cl^-.

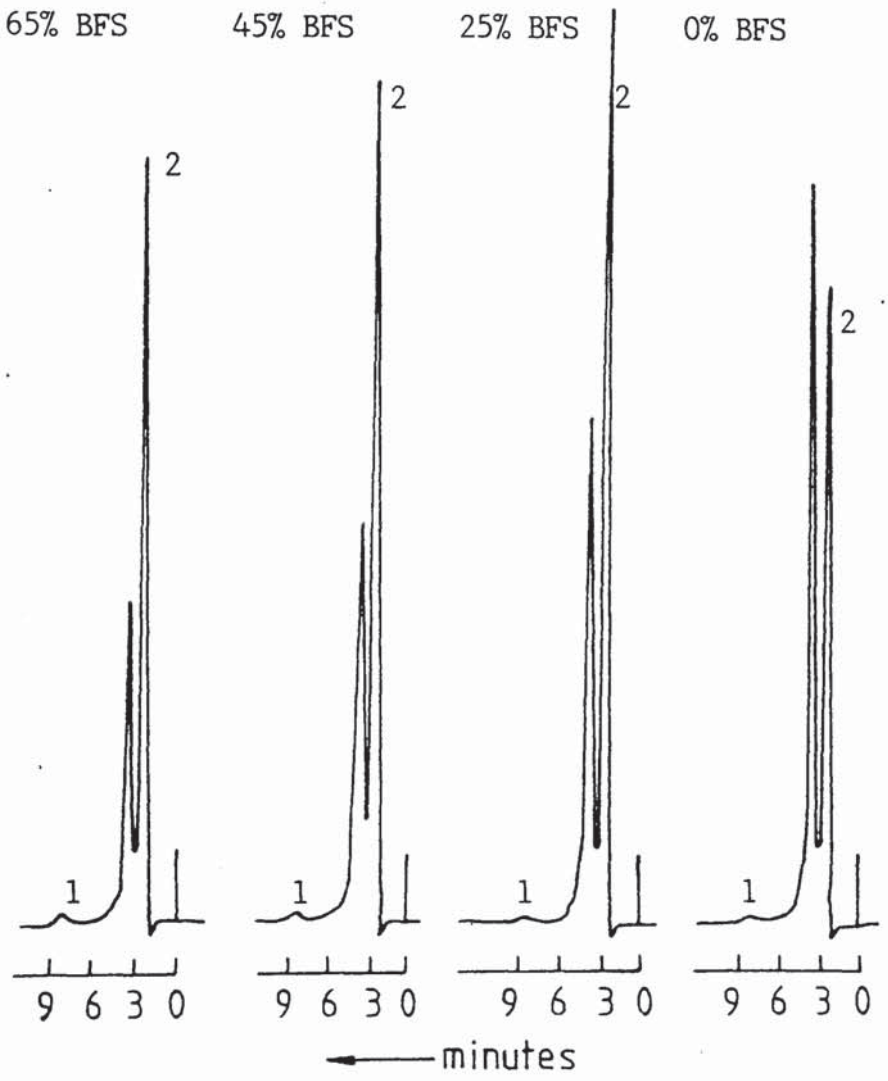

FIGURE 3.8(b) : Anion chromatographs of BFS blended cement pastes contaminated with NaCl and exposed to 100% CO_2.
1= SO_4^{--}, 2= Cl^-.

Table 3.3: Ionic concentrations found in the pore solution of carbonated BFS blended pastes using ion chromatography. (concentrations in mmol/l)

BFS content	Cl^{-*}	Na^{+}	K^{+}	Ca^{++}	Mg^{++}
0%	124.0	11.9	54.2	402.5	88.6
25%	310.0	10.0	27.9	268.5	122.0
45%	354.0	22.6	22.0	272.0	98.5
65%	398.0	23.8	11.1	205.0	82.2
NaCl contaminated pastes					
0%	829.0	293.0	90.0	520.3	341.0
25%	1085.0	251.0	36.4	278.0	255.5
45%	1010.0	265.9	27.0	293.0	392.0
65%	933.0	218.4	14.6	278.8	211.0

* As chloride ions co-elute with silicate ions, these values do not represent the true concentrations of chloride ions (see section 3.4.1.2)

also present in the pore solution and that they may account for the "missing" anions in table 3.2.

3.4.1.3 Free and total chlorides

Free and total chlorides (section 2.6) are shown in table 3.4. It can be seen that a considerable fraction of the total (free and bound) chloride present in each type of cement paste tested is free in the pore solution. The ratio of the free to the total chlorides is increased with the increase of the BFS content.

Surprisingly, the total and free chlorides in the non-contaminated pastes were significant. This is attributed to the presence of chlorides in the unhydrated materials used. Measurements of the total chloride contents of the unhydrated OPC and BFS showed them to be 0.003 mmol/g cem and 0.026 mmol/g cem respectively.

In order to determine the total chlorides and in order to convert the free chlorides from mmol/l in table 3.2 to mmol/g cem the water content of each paste was needed. Both the evaporable and non-evaporable water contents were estimated as described in section 2.5 and are tabulated in table 3.5. Both the types of water content are increased with the increase of the BFS content of the cement paste.

Table 3.4: Free and total chloride contents of carbonated BFS blended cement pastes.

BFS content	Total chloride mmol/g cem	Free chloride mmol/g cem	Free / Total
0%	0.011	0.001	0.091
25%	0.023	0.003	0.130
45%	0.027	0.004	0.148
65%	0.032	0.005	0.156
NaCl contaminated pastes			
0%	0.221	0.075	0.338
25%	0.237	0.096	0.406
45%	0.255	0.124	0.484
65%	0.282	0.086	0.304

Table 3.5: Evaporable and non evaporable water content of carbonated BFS blended cement pastes.

BFS content	N.E.W. (g/g unh.cem)	E.W. (g/g unh. cem)
0%	0.047	0.121
25%	0.059	0.130
45%	0.065	0.134
65%	0.073	0.120
NaCl contaminated pastes		
0%	0.047	0.118
25%	0.060	0.129
45%	0.065	0.150
65%	0.071	0.119

3.4.1.4 Phase composition analysis

Figure 3.9 represents the DTA thermographs obtained after the carbonation of the specimens. As it can be seen, with the increase of BFS content in the pastes, the following changes in the phase composition became more evident:

(1) The reduction of the endothermal peak at 900°C associated with the crystalline calcite.

(2) The reduction of the shallow "hump" starting at about 500°C and terminating at a peak at around 750°C (vaterite), associated with a less crystalline form of calcite, calcite II (103). The latter, according to Lach and Sauman (103) exists in a very fine form having no time to crystallize properly into larger ordered crystals.

(3) The increase of the endothermal peak at 750°C associated with vaterite.

(4) The appearance of the peaks at around 150°C and 250°C associated with the calcium sulphoaluminate and C_4AH_{13}.

Figure 3.10 represents the DTA thermographs of the NaCl contaminated specimens. Here, the more obvious changes with the increase of BFS content are:

(1) The reduction and finally the elimination of the two peaks at 850°C and 900°C assocciated with sodium chloride and calcite respectively.

(2) The decrease of the shallow "hump" starting at 500°C and

terminating at a peak around 750°C (calcite II).

(3) The increase of the peak at 750°C which is associated with vaterite.

(4) The appearance of a peak at 250°C-300°C associated with calcium chloroaluminate.

(DTA identidication peaks can be found in appendix 7).

X-Ray diffractometer traces (figures 3.11 and 3.12) show that calcite and vaterite are the only forms of calcium carbonate present in the specimens. The ratio of vaterite to calcite appears to increase with the increase of the BFS content in both the contaminated and non-contaminated specimens.

3.4.1.5 Porosimetry

Figures 3.13 and 3.14 represent the pore size distributions of the specimens before their exposure to 100% CO_2. As it can be seen, for the non-contaminated specimens (fig.3.13) the volume of pores decreases with the BFS content. For the NaCl contaminated specimens (fig. 3.14) the volume of pores is almost independent of the BFS content and is similar to that of the 100% OPC specimen. Figure 3.15 represents the pore size distributions of the carbonated specimens. In this case , the pore volume of the 100% OPC specimens is less than that of the BFS blended specimens.

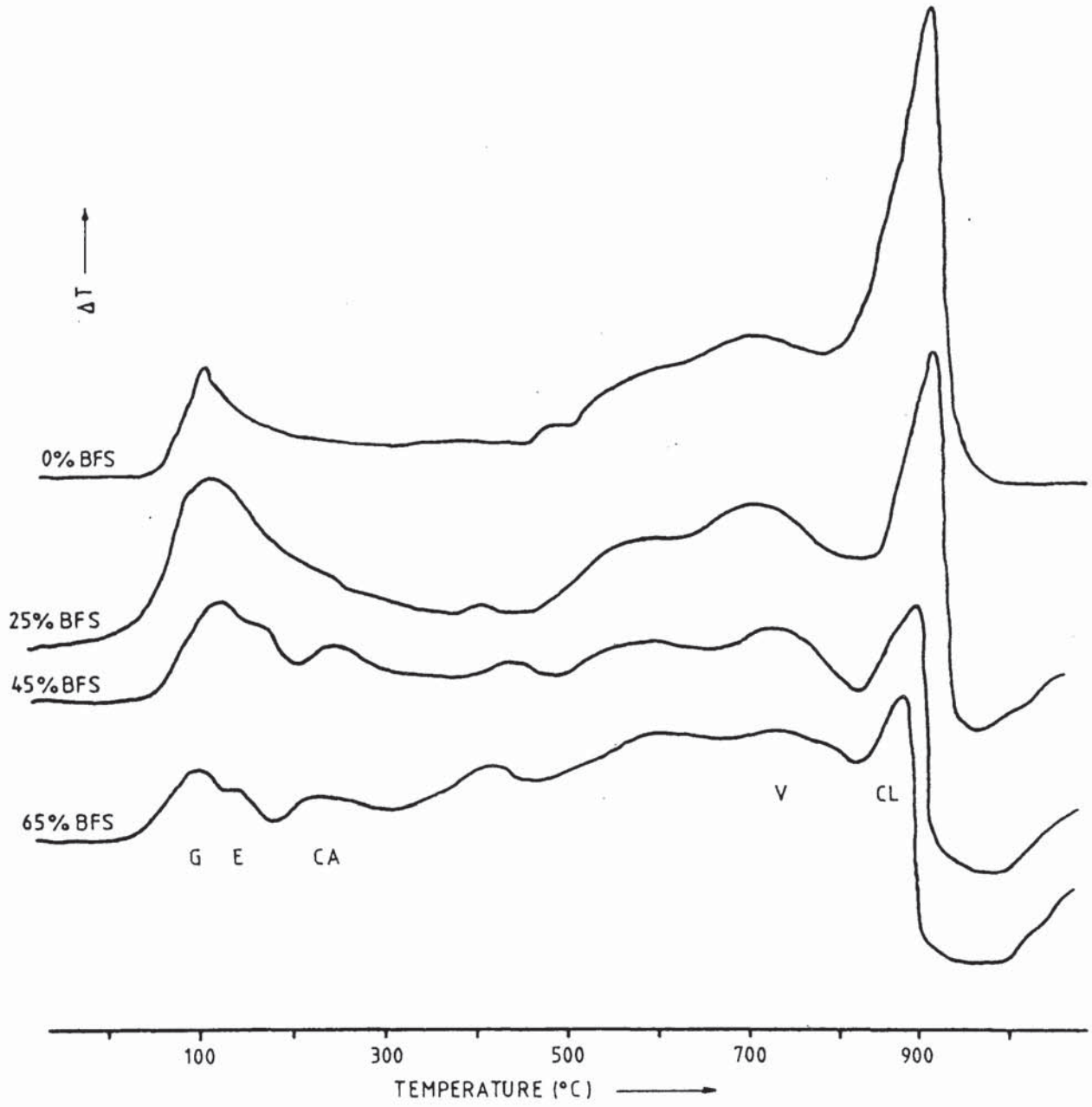

FIGURE 3.9 : DTA thermographs of BFS blended cement pastes carbonated in 100% CO_2.

G = C-S-H gel

E = Ettringite

CA = C_4AH_{13}

V = Vaterite

CL = Calcite

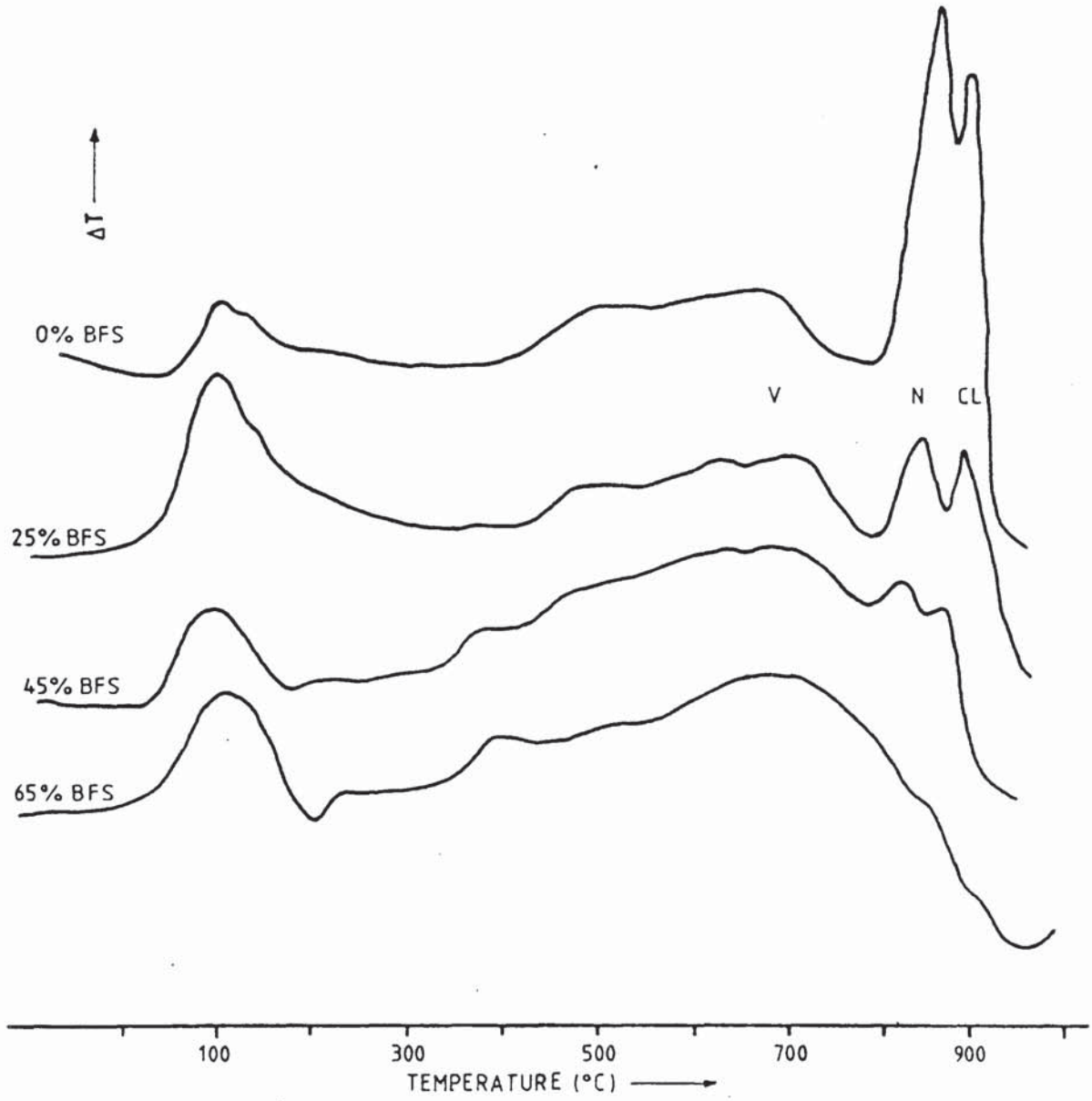

FIGURE 3.10 : DTA thermographs of BFS blended cement pastes carbonated in 100% CO_2 (NaCl contaminated pastes)
V = vaterite
CL = calcite
N = sodium chloride

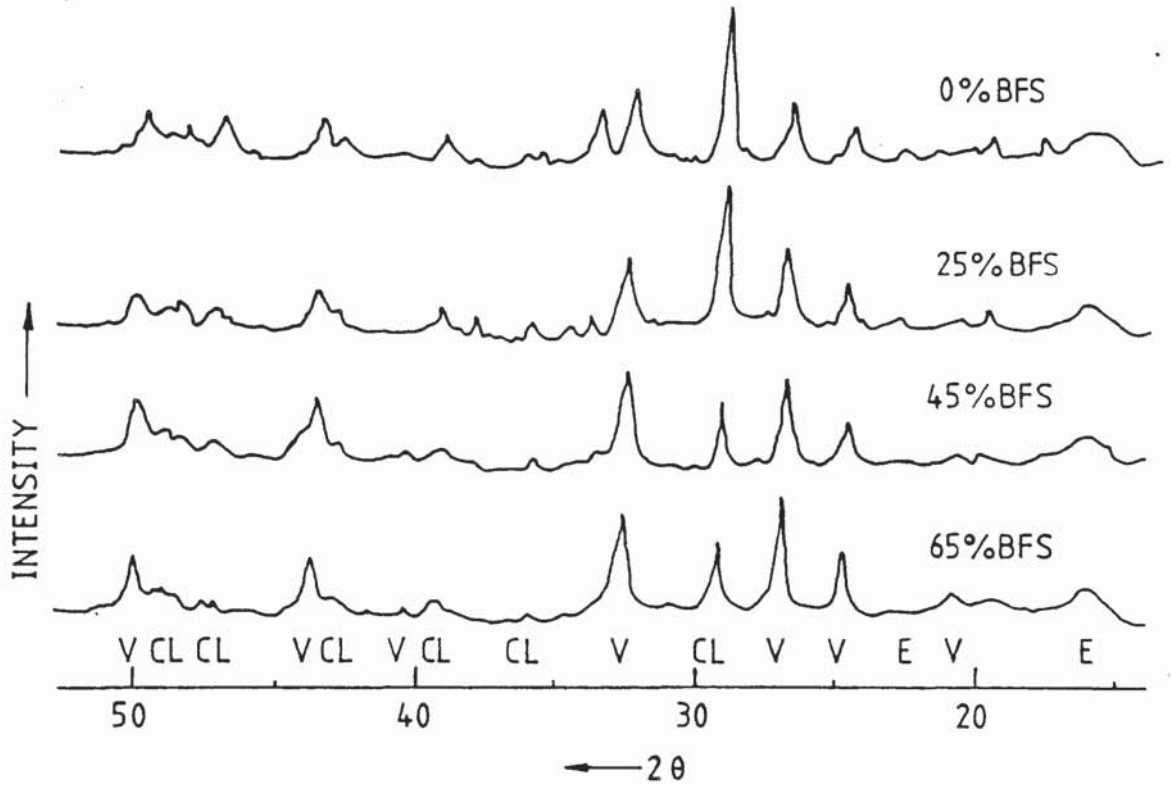

FIGURE 3.11 : X-ray diffractometer traces of BFS blended cement pastes carbonated in 100% CO_2.
V = vaterite
CL = calcite
E = ettringite

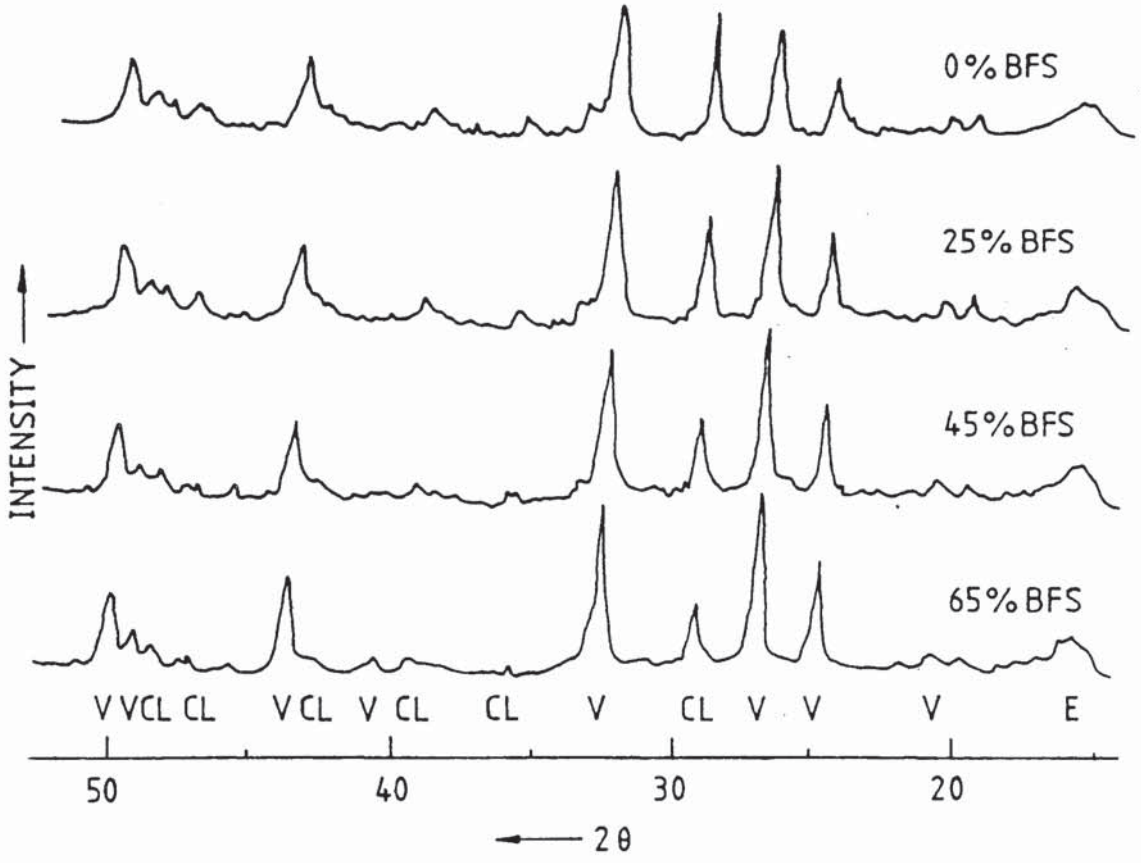

FIGURE 3.12 : X-ray diffractometer traces of BFS blended cement pastes contaminated with NaCl and carbonated in 100% CO_2.
V = vaterite
CL = calcite
E = ettringite

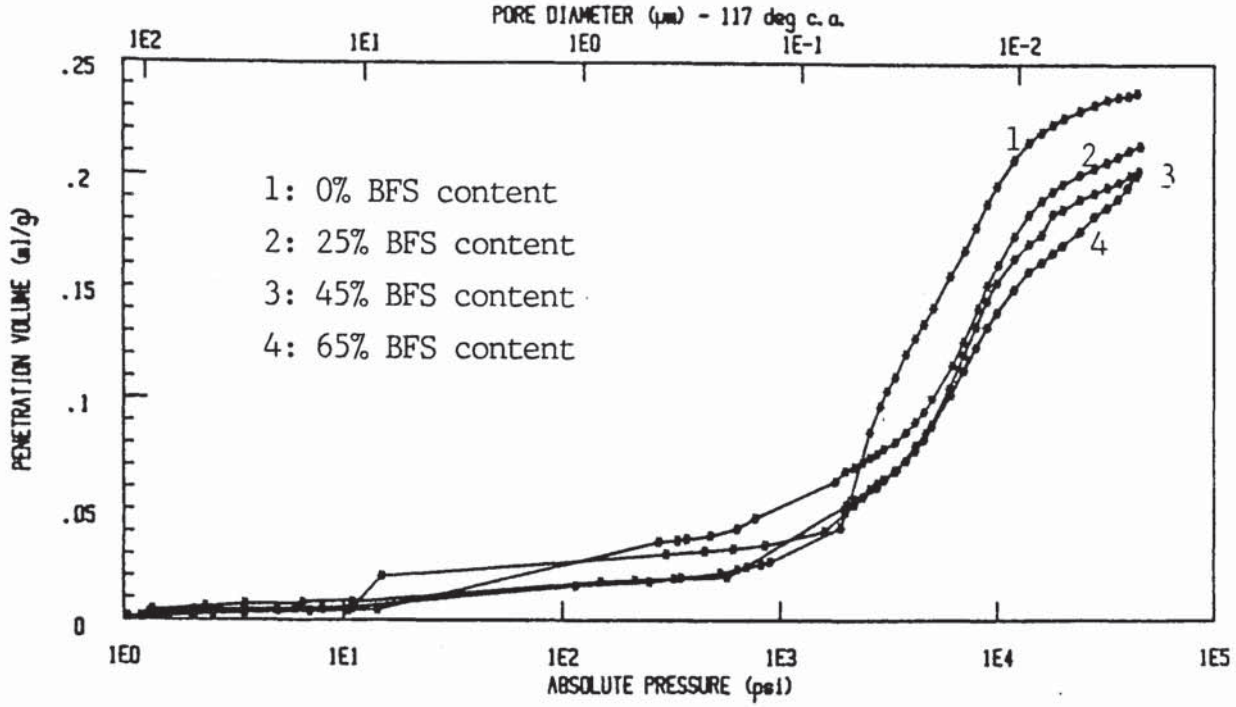

FIGURE 3.13 : Pore size distributions for uncarbonated BFS-blended cement pastes.

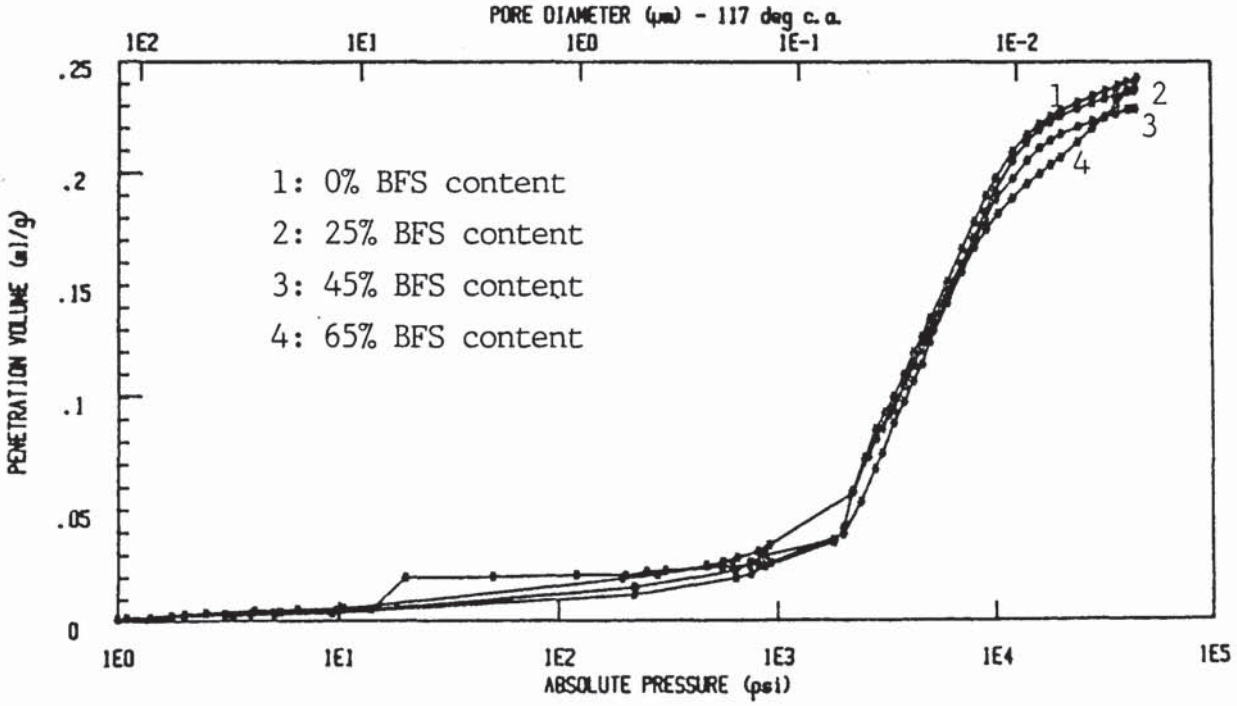

FIGURE 3.14 : Pore size distributions for uncarbonated BFS-blended cement pastes, contaminated with NaCl.

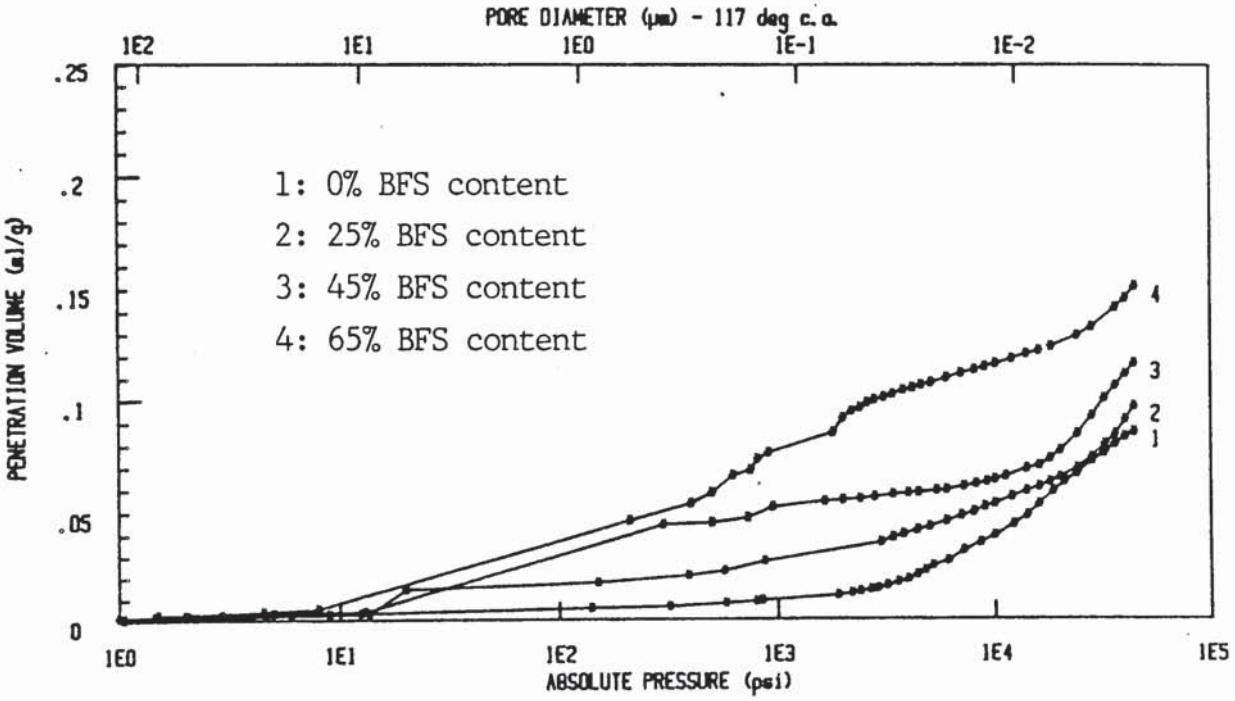

FIGURE 3.15 : Pore size distributions for carbonated BFS-blended cement pastes.

3.4.2 DISCUSSION

3.4.2.1 Pore structure

The increase of the BFS content in the specimens caused an increase of the constant for the rate of carbonation (table 3.1) and thus a reduction of the resistance to carbonation. In addition, NaCl contamination caused a further slight reduction of the carbonation resistance.

As it can be seen from figures 3.13 and 3.14 the porosity of the non-contaminated specimens, contrary to the rate of carbonation, reduces with the addition of BFS, while the porosity of the NaCl contaminated specimens remains almost unchanged. This shows that there is no simple relation between the porosity before the beginning of carbonation and the resistance to carbonation. Simple characterization of cement pastes in terms of their behaviour to carbonation using their porosities can thus be misleading.

On the other hand, DTA and X-Ray diffraction measurements after carbonation (fig. 3.9-3.12) showed that the increase of BFS content causes a reduction of the crystalline $CaCO_3$ phases (calcite and vaterite) which are the main products of carbonation. In addition, by comparing each DTA thermograph in figure 3.9 with the corresponding thermographs in figure

3.10 it can be seen that the crystalline forms of $CaCO_3$ are less in the NaCl contaminated specimens which at the same time have higher carbonation rates. So the increase of the carbonation rate is correlated with the amount of carbonation products i.e. with the carbonatable material present in the paste. Support for this conclusion is provided by the high correlation coefficients obtained when the constant for the rate of carbonation was plotted versus $1/\sqrt{A}$. "A" is a value which represents the variation of the carbonatable material with the variation of the OPC content of the cement paste (for the determination of "A" see appendix 11). The lines obtained are presented in figure 3.16. Their correlation coefficients are 0.98 and 0.99 for the non-contaminated and the NaCl-contaminated specimens respectively.

The amount of the carbonatable material present in the paste, and therefore the amount of the carbonation products, is associated with the porosity of the pastes after carbonation. Since the conversion of $Ca(OH)_2$ to $CaCO_3$ increases the solid volume, the carbonation products reduce the volume of pores. This can be seen from figure 3.15 which shows the pore size distributions of carbonated specimens. The porosity of carbonated OPC paste, with the higher amount of carbonatable material, is much less than that of the carbonated 65% BFS paste, although before carbonation this

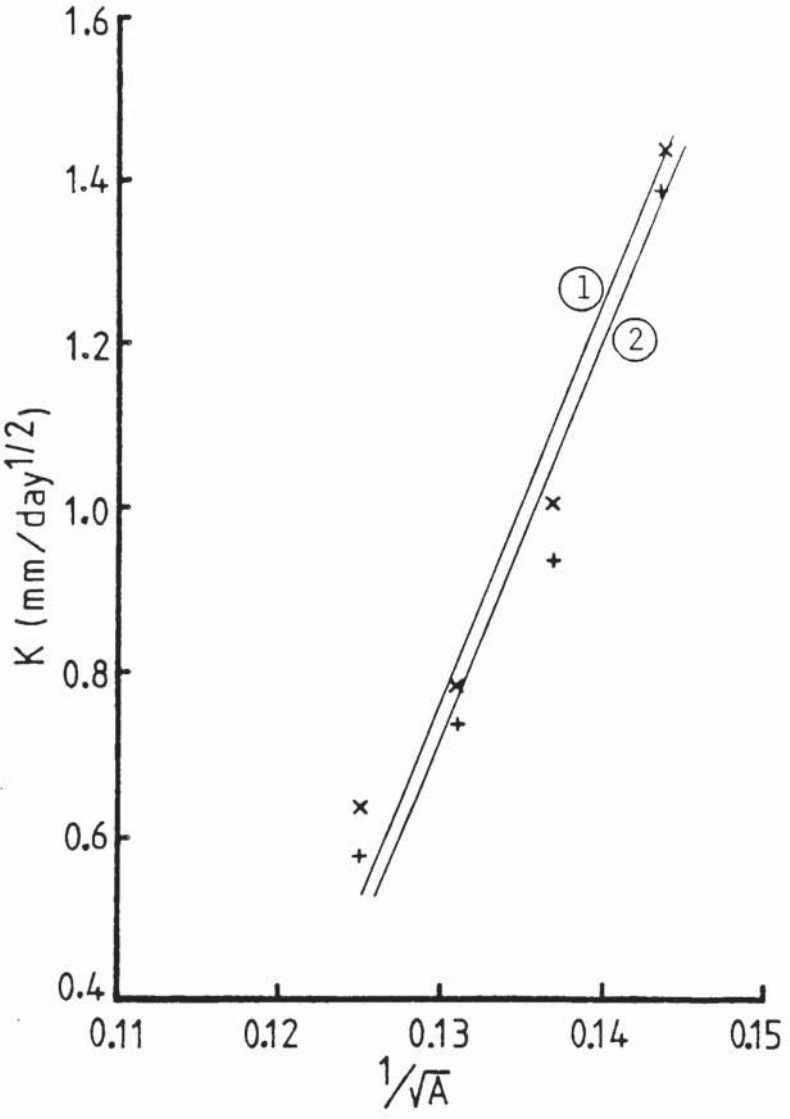

FIGURE 3.16 : The constant K for the rate of carbonation versus the reciprocal of the square root of parameter "A".

1(x): $K = 43.3\ A^{-\frac{1}{2}} - 4.8$ (NaCl contamination)

2(+): $K = 42.1\ A^{-\frac{1}{2}} - 4.7$ (no contamination).

was the opposite.

The main forms of the crystalline $CaCO_3$ present in the examined pastes are vaterite and calcite. As can be seen from figures 3.9 and 3.10 as the BFS content of the paste increased, the amount of vaterite increased at the expense of calcite. This is more apparent in the NaCl contaminated specimens. The 100% OPC specimens have a high peak at 900°C (calcite) and a low peak at 750°C (vaterite), while the 65% BFS specimens have a high peak at 750°C and no peak at 900°C. It is difficult to envisage the reason for this dependence of the amount of produced calcite on BFS content. The cause is probably not the BFS content itself but the increased speed of carbonation which is associated with it. Sergi [37] reported that the rapid formation of vaterite may force its nucleation at unfavourable sites, where the product could be under compression and hence unable to transform to the stable but more expansive form of calcite.

For each type of cement paste, NaCl contamination caused a slight reduction of the resistance to carbonation (table 3.1). The cause for this reduction cannot be deduced from the present results. It is, however, possible that the presence of NaCl in the pores may cause the increase of the relative humidity within them. At this higher R.H. the dissolution of CO_2 may be easier and hence the carbonation rate increases.

According to some researchers [104-106], curing of cement pastes in NaCl solutions for long periods of time promotes the formation of a more porous C-S-H. If it is assumed that NaCl when added at the mixing stage of the paste causes a similar effect, it may be speculated that the higher carbonation rates for the NaCl-contaminated specimens are due to the easier penetration of CO_2 in these pastes.

The increase of BFS content in the NaCl-contaminated pastes has caused the reduction of the peak associated with NaCl on the DTA thermographs (fig. 3.10). This may be related with the increase of the peak associated with calcium chloroaluminate (250-300^{o}C). As the BFS content of NaCl-contaminated pastes increases, the amount of chloride-bearing phases probably increases resulting in a decrease of the amount of remaining NaCl.

3.4.2.2 Pore solution

The most striking result in the pore solution analysis is the high concentrations of calcium ions accompanied by the presence of silicate ions. As was mentioned earlier, during carbonation, CO_2 transforms the majority, of the CaO present in the paste to calcium carbonate. Since the solubility of the latter is very low, the concentration of calcium ions in the pore solution was expected to be very

low. According to Atkinson et al [107], however, it is the gel, not the $CaCO_3$, which controls the calcium ion concentration. The addition of CO_2 to C-S-H gel removes calcium from it and the pore solution conforms to the new lower Ca/Si ratio of the gel. Based on thermodynamic data, Atkinson et al [107] were able to model the composition of the liquid and solid phases of C-S-H gels and thus to predict relationships between them. Figure 3.17 represents the relationship between the pH of the liquid phase as a function of the Ca/Si ratio in the solid phase of C-S-H gels with low calcium content, and figure 3.18 represents the $[Ca_T]/[Si_T]$ ratio in the aqueous phase as a function of the Ca/Si ratio in the solid phase (the subscript "T" denotes total concentration irrespective of ionic speciation). Although experimental results generally fit the predicted relationships, at the SiO_2-rich end (Ca/Si<0.01) of the pH vs Ca/Si in solids relationship the model tends to overestimate the experimentally measured pH (fig 3.17). According to their experimental results (fig 3.17) at a pH range of 7.2 to 7.7, which is the obtained pH range of the pore solutions in this work, the Ca/Si ratio in solids is between 0.002 and 0.005. The $[Ca_T]/[Si_T]$ ratio in the aqueous phase is therefore less than 0.2 (fig3.18). This indicates that the high concentrations of calcium ions obtained in the pore solutions are accompanied by even higher total concentrations of silica

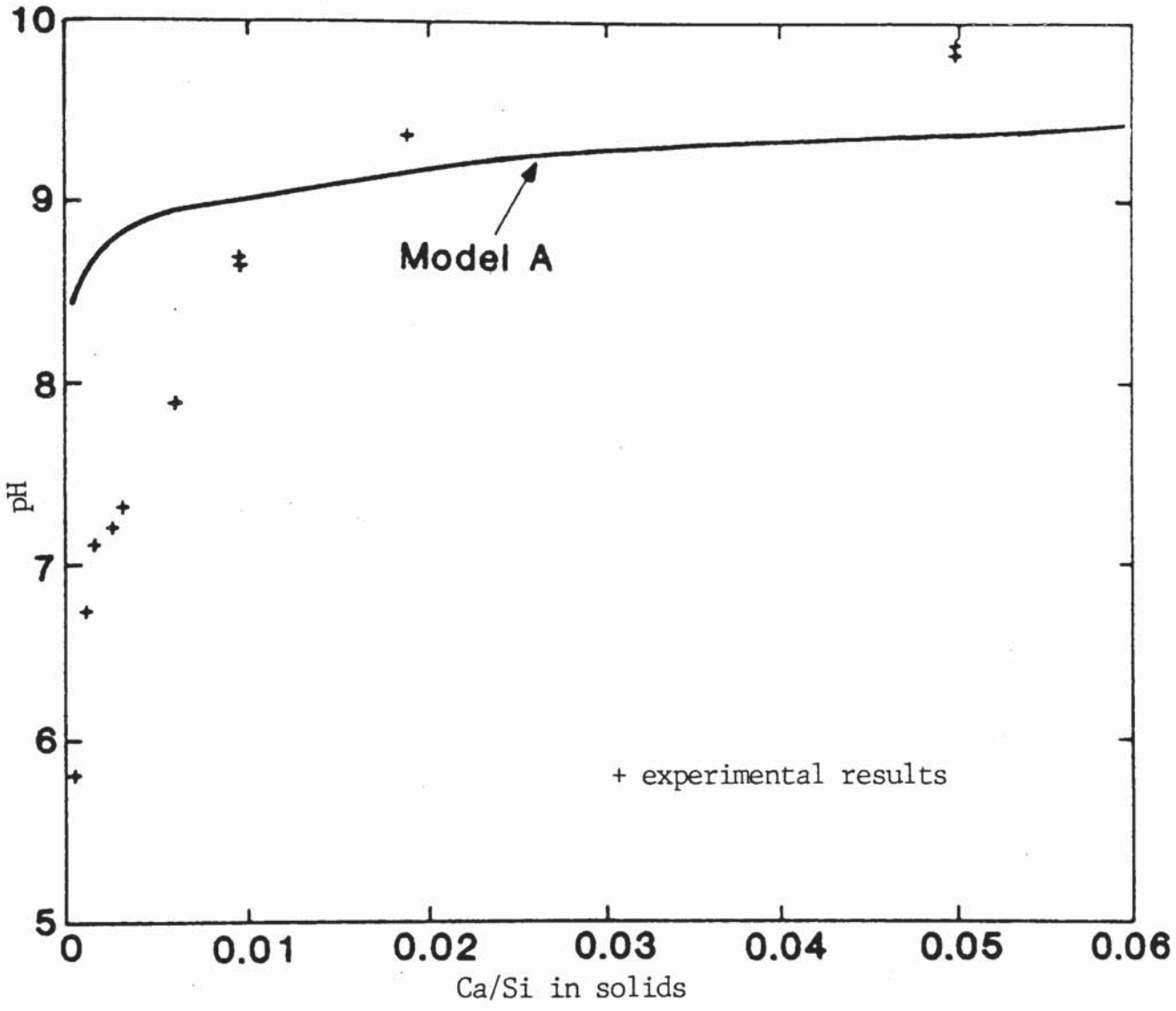

FIGURE 3.17 : The pH of aqueous solution in equilibrium with reacted C-S-H gels containing low concentrations of Ca (from ref. 107).

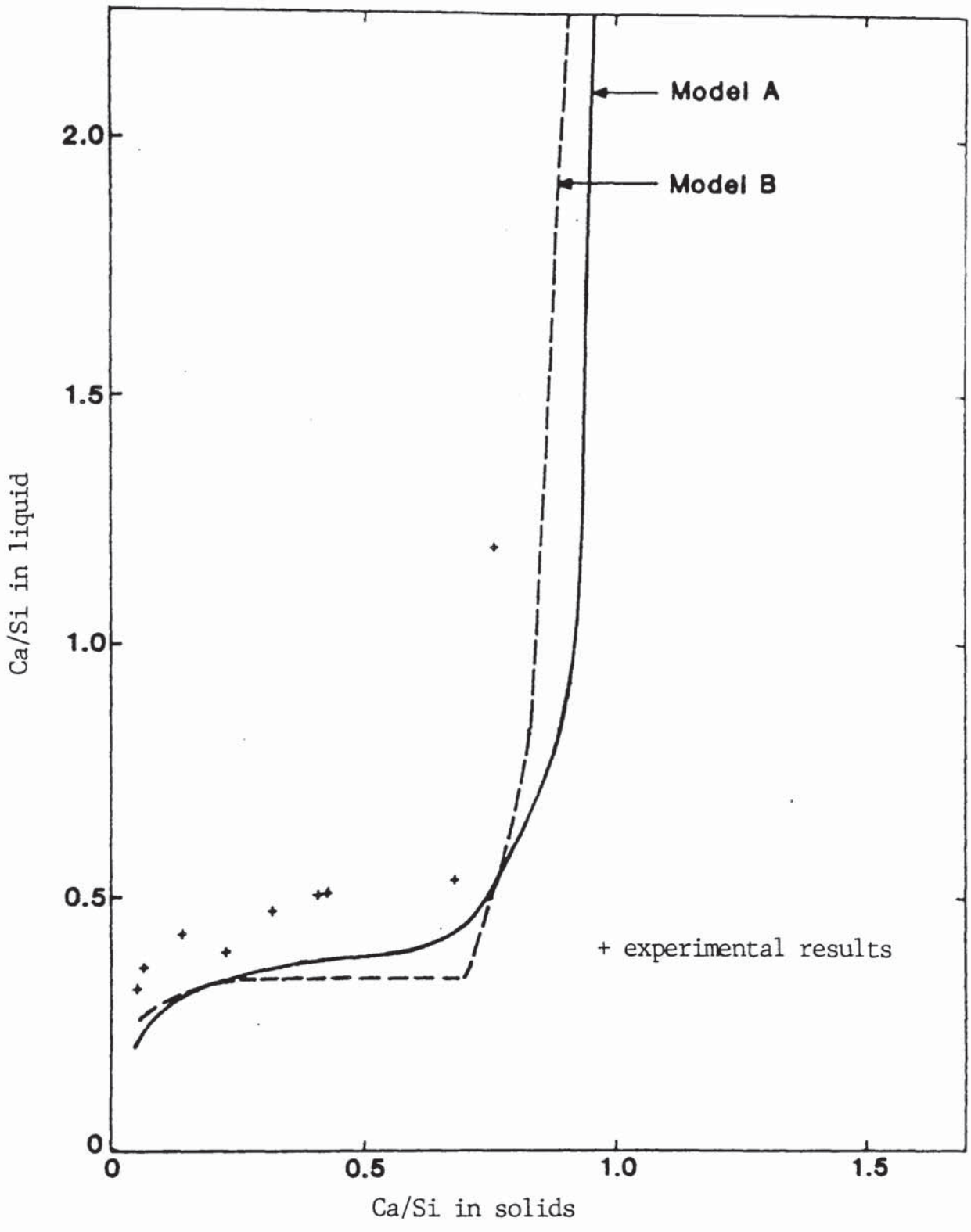

FIGURE 3.18 : The Ca/Si ratio in the aqueous phase as a function of the Ca/Si ratio in the solid phase for C-S-H gels equilibrated in water. The curves are predicted from the thermodynamic models. (from ref. 107).

$[Si_T]$. In addition to the silicate ions, another form of soluble silica may be present in the pore solutions, associated with the third unidentified peak of the anion chromatographs (fig 3.8). The exact ionic speciation of the soluble silica present in the pore solutions is unknown. The various methods of analysis existing in the literature [100,101] determine the total silica concentration irrespective of ionic speciation. The chemical identity of soluble silica, often called silicic acid, is not constant. According to Kolthoff and Elving [100] silicic acid can be found in aqueous solutions in various arrangements. Some of them are: $(SiO_4)^{-4}$, $[Si(OH)_6]^{-2}$, $Si(OH)_4$ or even a hydrate $Si(OH)_4 .2H_2O$. Generally, as reported by Iller [101], the chemistry of silicate and polysilicate ions is still not fully understood.

The most aggressive of all the ions present in the pore solution is the chloride ion. As mentioned earlier, the presence of free chlorides in the pore solution of reinforced concrete can cause corrosion of the reinforcing steel. Carbonation causes the release of the bound chloride into the pore solution by the dissolution of the insoluble complex calcium chloroaluminate salt [37]. The amount of the released chloride depends on the extent of the CO_2 attack. In other words it depends on the resistance of cement paste to carbonation. This can be substantiated by examining the ratio of free to total chlorides present in the cement pastes

tested, which is a characteristic parameter representing the degree of chloride liberation. As was expected, for both the contaminated and non-contaminated pastes (table 3.4) the "free/total" ratio increases with the increase of BFS content, i.e. with the decrease of the resistance of the paste to carbonation. The sodium chloride contaminated, 65% BFS cement paste, however, appears to be an exception. It is difficult to envisage the reason for this inconsistency. It may be related to the fact that the rate of carbonation of this paste was the highest of all the pastes tested. Sergi[37] suggested that at high carbonation rates the chloride-bearing phases may be entrapped within rapidly forming carbonates which may not have had sufficient time to redistribute themselves elsewhere . In this case the release of the chloride ions might be difficult.

PART II : SPECIMENS EXPOSED TO ATMOSPHERES WITH DIFFERENT CO_2 CONTENT

3.4.3 RESULTS

3.4.3.1 Rate of carbonation

The increase in carbonation depth with the square root of time is represented graphically in figure 3.19 for six conditions, namely for discs with or without sodium chloride

contamination, exposed to 100% CO_2, 5% CO_2 and Air (a full table of the results can be found in appendix 10). In all the conditions, after an induction period the depth of carbonation increases linearly with the square root of time. The equation which represents each condition is the same as that used in part I:

$$x = K\ t^{1/2} - K_o$$

where x = depth of carbonation

t = time (days)

K =constant for the rate of carbonation ($mm/day^{1/2}$)

K_o= constant, related to the induction period t_o by:

$$K_o = K\ t_o^{1/2}$$

For each condition the carbonation depth measurements fit the above equation with high correlation coefficients (see table 3.6). Values of K and t_o are also tabulated in table 3.6. As was expected, the rate of carbonation increases with the increase of the CO_2 concentration. It is also evident that a condition leading to a higher carbonation rate also leads to a shorter induction period t_o. The contamination of the specimens with NaCl promotes slightly faster carbonation.

Useful information can be obtained by comparing the results from this work with the results of Sergi [37] who exposed OPC paste discs to 5% CO_2 and Air (fig 3.20 and table 3.7).

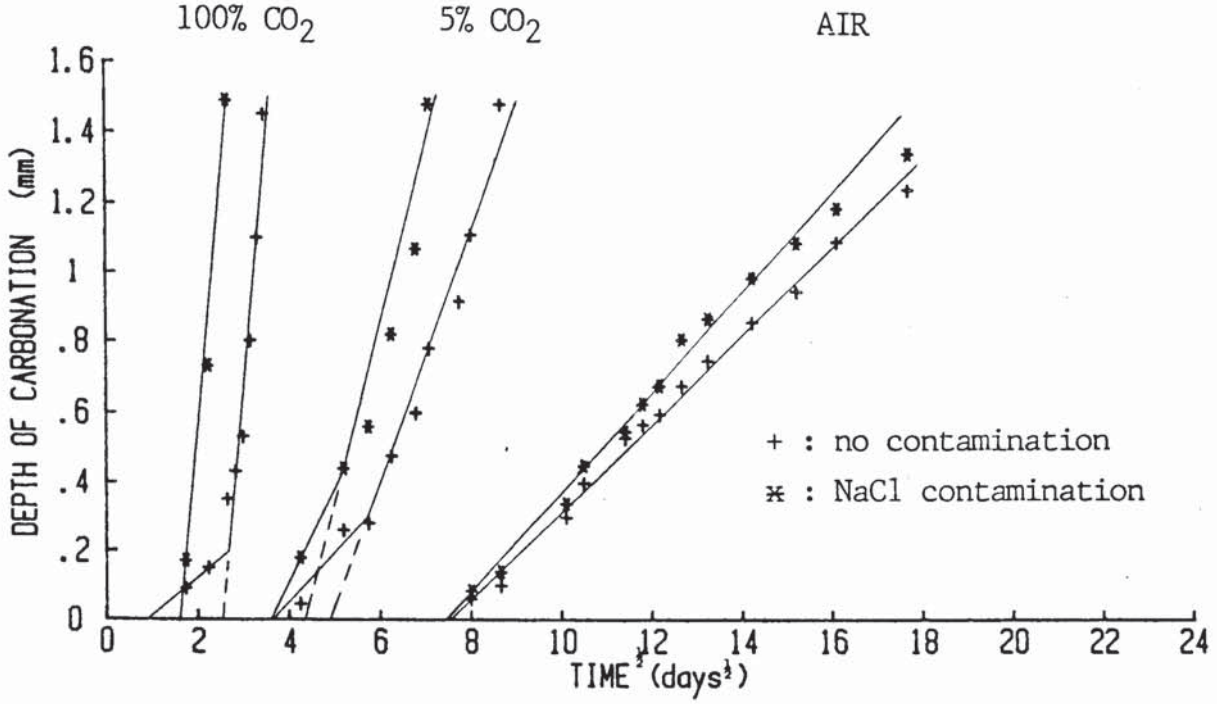

FIGURE 3.19 : The increase of carbonation depth with the square root of time for 65% BFS cement pastes exposed to various atmospheres.

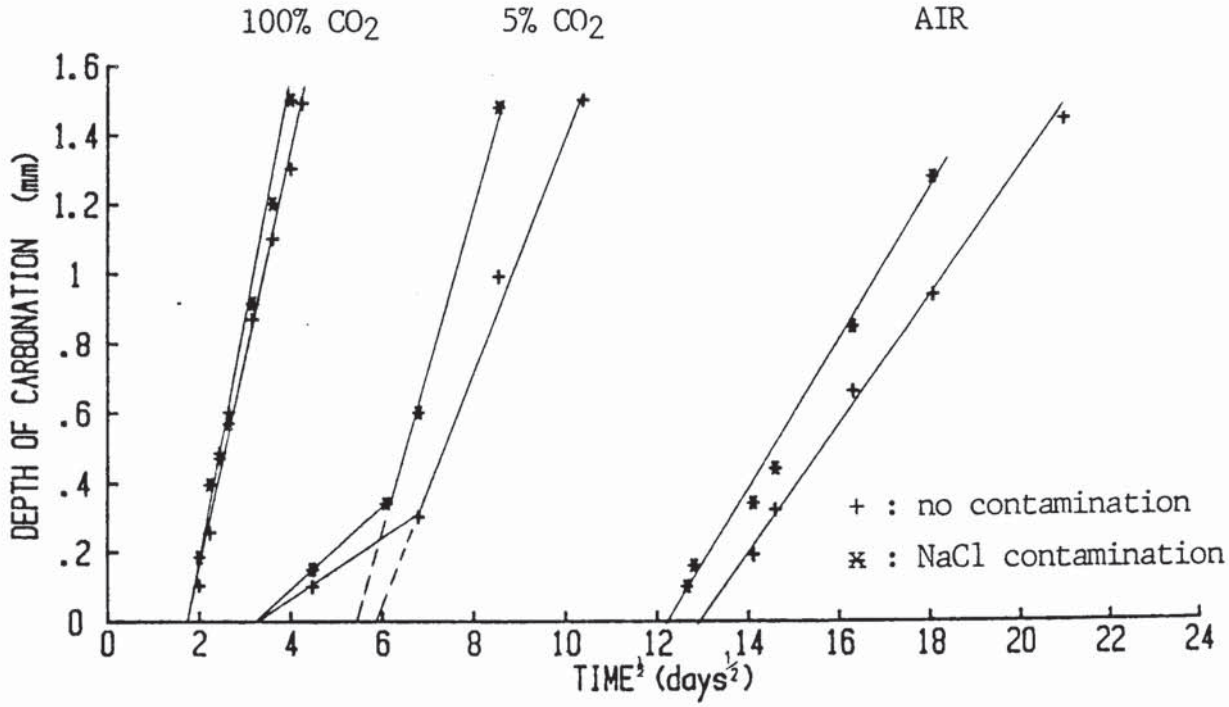

FIGURE 3.20 : The increase of carbonation depth with the square root of time for OPC pastes exposed to various atmospheres (100% CO_2 from part I, 5% CO_2 and Air from ref. 37).

Tables 3.6: Rates of carbonation and induction periods of 65% BFS pastes exposed to various atmospheres.

Exposed atmosphere	K mm/day$^{1/2}$	t_o days	correlation coefficient
Air	0.13	55.52	0.99
5% CO_2	0.40	26.36	0.984
100%CO_2	1.39	6.57	0.975
NaCl contaminated specimens			
Air	0.14	52.91	0.993
5% CO_2	0.53	20.82	0.957
100%CO_2	1.44	2.72	0.989

Table 3.7: Rates of carbonation and induction periods of OPC pastes exposed to various atmospheres.

Exposed atmosphere	K mm/days$^{1/2}$	t_o days
Air*	0.18	165.3
5% CO_2*	0.33	33.3
100% CO_2**	0.58	2.8
NaCl contaminated pastes		
Air*	0.24	161.6
5% CO_2*	0.47	29.4
100% CO_2**	0.64	2.9

* From ref. (37).

** From part I.

Table 3.8: Rate of carbonation and induction period ratios between 65% BFS and OPC pastes exposed to various atmospheres.

Exposed Atmosphere	$\frac{K_{65\%\ BFS}}{K_{OPC}}$	$\frac{t_{o\ 65\%\ RFS}}{t_{o\ OPC}}$
Air	0.70	0.34
5% CO_2	1.19	0.79
100% CO_2	2.42	2.33
NaCl contaminated specimens		
Air	0,58	0.33
5% CO_2	1.14	0.71
100% CO_2	2.26	0.94

Table 3.8 represents the ratios of the constants for the carbonation rate and the induction periods between the 65% BFS and OPC discs. It can be seen, as will be discussed later, that both ratios decrease with the decrease in CO_2 concentration in the atmosphere.

3.4.3.2 Concentration of ions in the pore solution

Ionic concentrations and pH values of the extracted solution for each condition tested are presented in Table 3.9. For comparison, the same table shows the ionic concentration of the extracted solution of specimens exposed to 100% N_2 (uncarbonated specimens). The analysis for each ion was made by analytical methods as described in chapter 2. Carbonates and bicarbonates were not found in measurable quantities.

The degree of carbonation of the specimens in each condition is represented by the pH values of the pore solution. As can be seen, higher CO_2 containing atmospheres induced lower pH values. The addition of NaCl in the original mix of the pastes caused further reduction in pH.

As noted for the extracted solutions in part I, the total concentration of anions (Σ^-) in the pore solutions of the carbonated pastes was found to be much lower than the total

Table 3.9: Pore solution analysis for 65% BFS cement pastes exposed to various atmospheres (concentrations in mmol/l).

Exposed Atmosphere	pH	OH^-	Cl^-	Na^+	K^+	Ca^{++}	Σ^-	Σ^+
100% N_2	13.25	177.8	3.5	51.0	150.0	2.1	181.3	205.4
Air	10.60	0.4	51.5	35.6	10.5	30.4	51.5	106.8
5% CO_2	8.10	0.0	53.0	19.1	9.7	102.3	53.0	233.3
100% CO_2	7.57	0.0	45.5	19.4	10.2	199.7	45.5	429.0
NaCl contaminated pastes								
100% N_2	13.38	240.0	225.0	398.4	153.3	4.5	465.0	560.8
Air	9.73	0.05	780.0	321.2	23.5	246.7	780.0	837.9
5% CO_2	7.93	0.0	720.0	247.4	13.3	245.7	720.0	752.1
100% CO_2	7.31	0.0	720.0	211.4	12.8	262.5	720.0	749.2

concentration of cations (Σ^+). To explain the difference, as in part I, ion chromatography was employed (see section 2.4). Examining the anion chromatographs (fig 3.21, a+b) it can be seen that the heights of the peak associated with chloride ion, increase with the CO_2 content of the exposure atmosphere. In the case of specimens carbonated in 100% CO_2 an additional peak was obtained. As discussed in part I, this peak is probably associated with an ionic form of soluble silica. From the cation chromatographs (fig 3.22, a+b) it can be seen that higher CO_2 containing atmospheres induced higher concentrations for the calcium ion and lower concentrations for the alkali ions. In addition, in the case of specimens exposed to 5% CO_2 and 100% CO_2 atmospheres, a peak assosiated with magnesium ion was obtained.

Table 3.10 presents the results of the quantitative analysis of the ion chromatographs. Comparing these results with the corresponding results obtained by other analytical methods it can be seen that, except for chloride ion, the concentrations of each of the remaining ions are similar for both the methods. As far as the chloride ion is concerned, there is a difference between the concentrations measured by the two methods. As was explained in part I, this difference is associated with silicate ions which co-elute with chloride ions. Higher CO_2 containing atmospheres appear to have induced higher

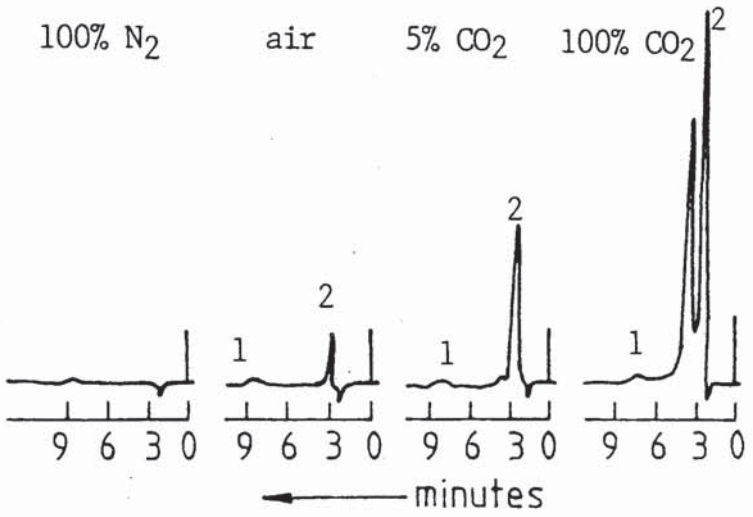

FIGURE 3.21(a) : Anion chromatographs of the pore solution of 65% BFS cement pastes exposed to various atmospheres. 1 = SO_4^{--}, 2= Cl^-.

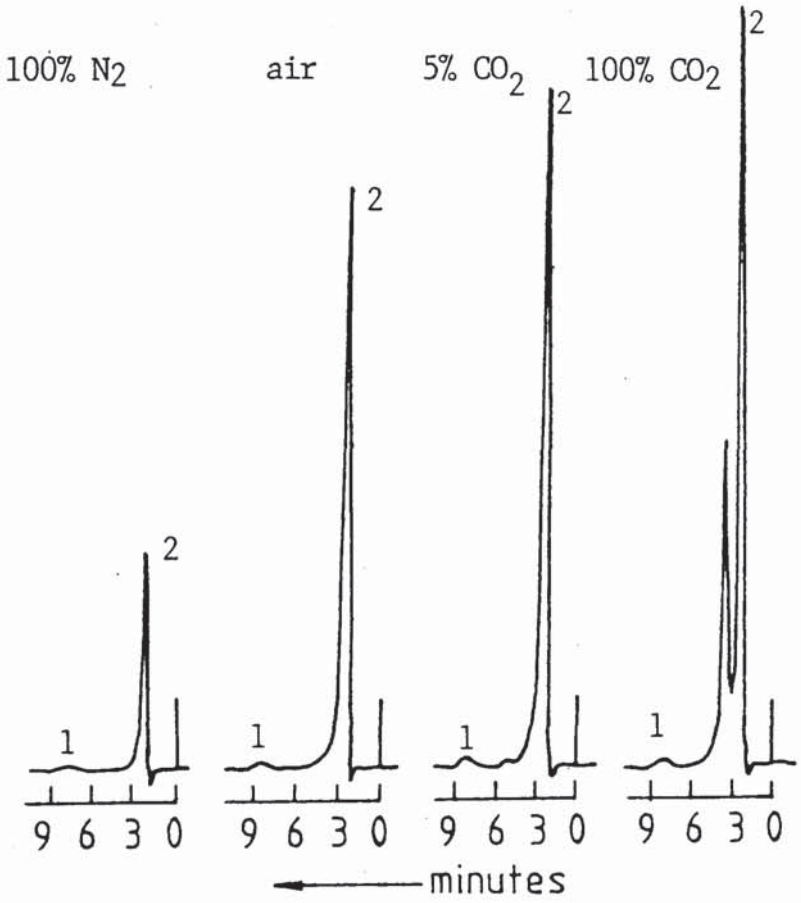

FIGURE 3.21(b) : Anion chromatographs of the pore solution of 65% BFS cement pastes exposed to various atmospheres (NaCl contaminated pastes). 1= SO_4^{--}, 2= Cl^-.

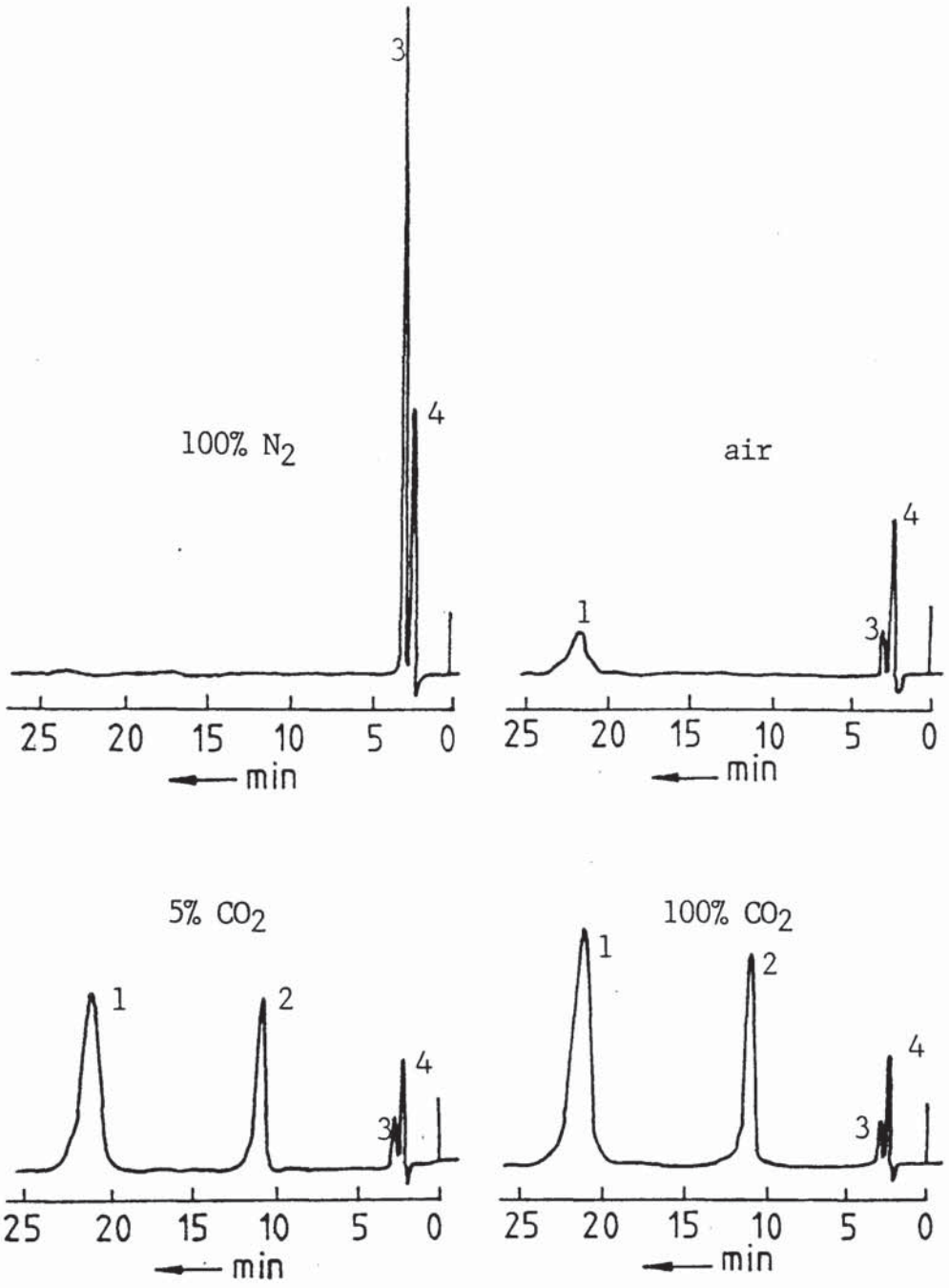

FIGURE 3.22(a) : Cation chromatoghraphs of the pore solution of 65% BFS cement pastes exposed to different atmospheres.
1= Ca^{++}, 2= Mg^{++}, 3= K^{+}, 4= Na^{+}.

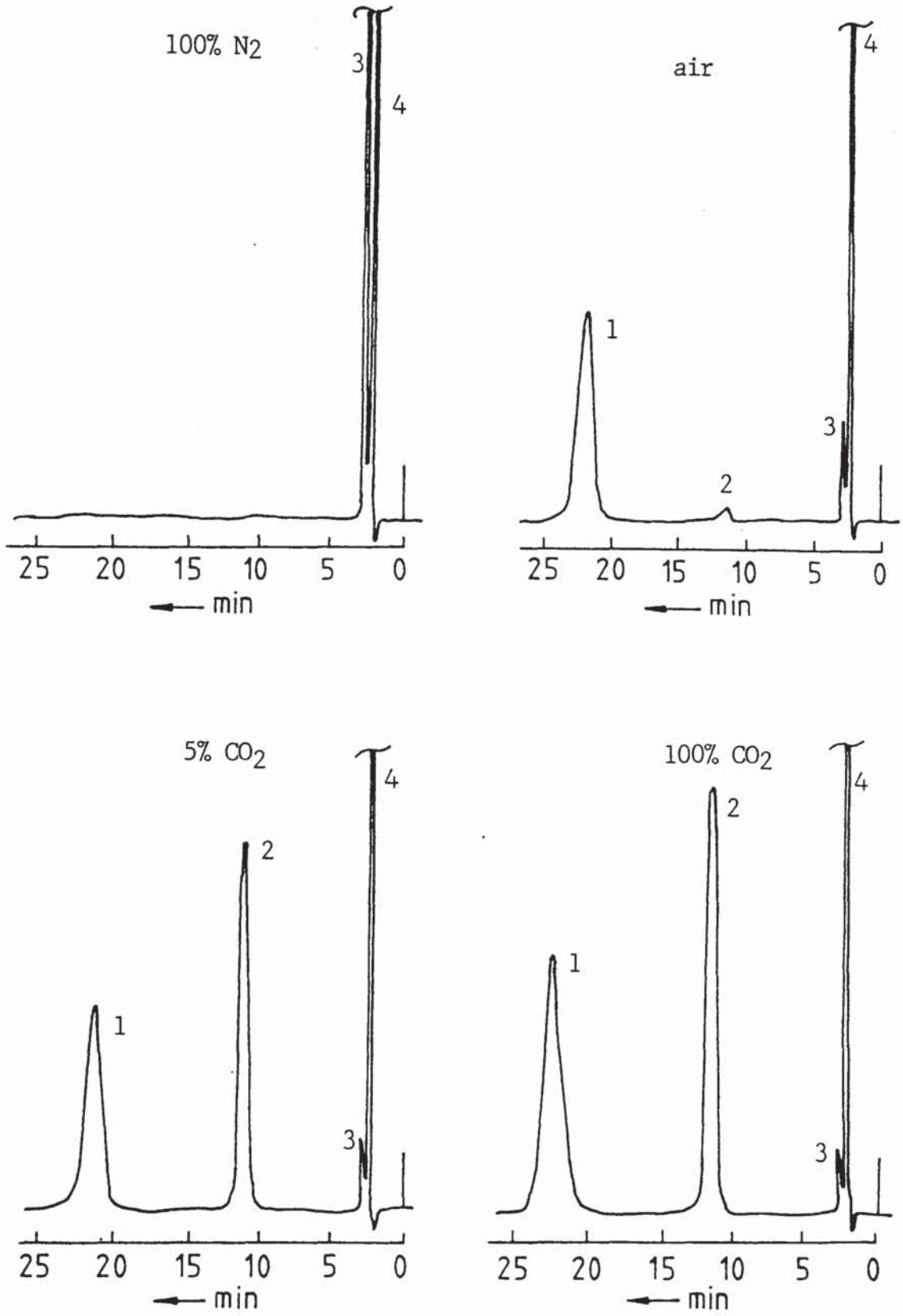

FIGURE 3.22(b) : Cation chromatographs of the pore solution of 65% BFS cement pastes exposed to various atmospheres (NaCl contaminated pastes). 1= Ca^{++}, 2= Mg^{++}, 3= K^{+}, 4= Na^{+}.

Table 3.10: Ionic concentrations found in the pore solution of 65% BFS cement pastes exposed to different atmospheres, using ion chromatography (concentrations in mmol/l).

Exposed Atmosphere	Cl^{-*}	Na^{+}	K^{+}	Ca^{++}	Mg^{++}
100% N_2	0.0	59.0	153.0	0.0	0.0
Air	70.3	37.0	11.6	33.7	0.0
5% CO_2	196.0	21.3	12.9	138.6	59.6
100% CO_2	398.0	23.8	11.1	205.0	82.2
NaCl contaminated pastes					
100% N_2	233.0	374.0	162.0	0.0	0.0
Air	745.0	325.2	24.6	247.6	8.0
5% CO_2	837.0	258.4	18.3	251.3	167.0
100% CO_2	933.0	218.0	14.6	278.8	211.0

* As chloride ions co-elute with silicate ions, these values do not represent the true concentrations of chloride ions. (see section 3.4.3.2)

concentrations of silicate ions in the pore solution.

3.4.3.3 Free and total chlorides

Free and total chlorides present in the specimens tested are shown in Table 3.11. Examining their ratio, it can be seen that, as was expected, in the case of the uncarbonated specimens it is very low. It is also apparent that carbonation under normal conditions (in air) encouraged more chloride release than accelerated carbonation.

Table 3.12 shows the non-evaporable and evaporable water content of the specimens. These values were used for the determination of free and total chlorides (see appendix 6). The drop in the non-evaporable water represents the release of bound water due to the carbonation reactions.

3.4.3.4 Phase composition analysis

Figures 3.23 and 3.24 represent the DTA thermographs for the specimens exposed to four different atmospheres. It can be seen that the endothermal peaks associated with the $Ca(OH)_2$ and C_4AH_{13} phases in the specimens exposed to 100% N_2 are no longer evident in any of the carbonated conditions and the peak associated with ettringite disappears only in the specimens exposed to 100% CO_2. These peaks are replaced by

Table 3.11: Free and Total chloride contents of 65% BFS cement pastes exposed to various atmospheres.

Exposed Atmospheres	Total chloride mmol/g cem	Free chloride mmol/g cem	Free / Total
100% N_2	0.026	0.001	0.038
Air	0.025	0.005	0.200
5% CO_2	0.035	0.005	0.143
100% CO_2	0.032	0.005	0.156
NaCl contaminated pastes			
100% N_2	0.341	0.046	0.135
Air	0.323	0.075	0.232
5% CO_2	0.300	0.063	0.210
100% CO_2	0.282	0.086	0.304

Table 3.12: Evaporable and non-evaporable water content of 65% BFS cement pastes exposed to various atmospheres.

Exposed Atmospheres	N.E.W. g/g cem	E.W. g/g cem
100% N_2	0.129	0.306
Air	0.099	0.097
5% CO_2	0.080	0.096
100% CO_2	0.073	0.120
NaCl contaminated pastes		
100% N_2	0.113	0.205
Air	0.082	0.083
5% CO_2	0.074	0.087
100% CO_2	0.071	0.119

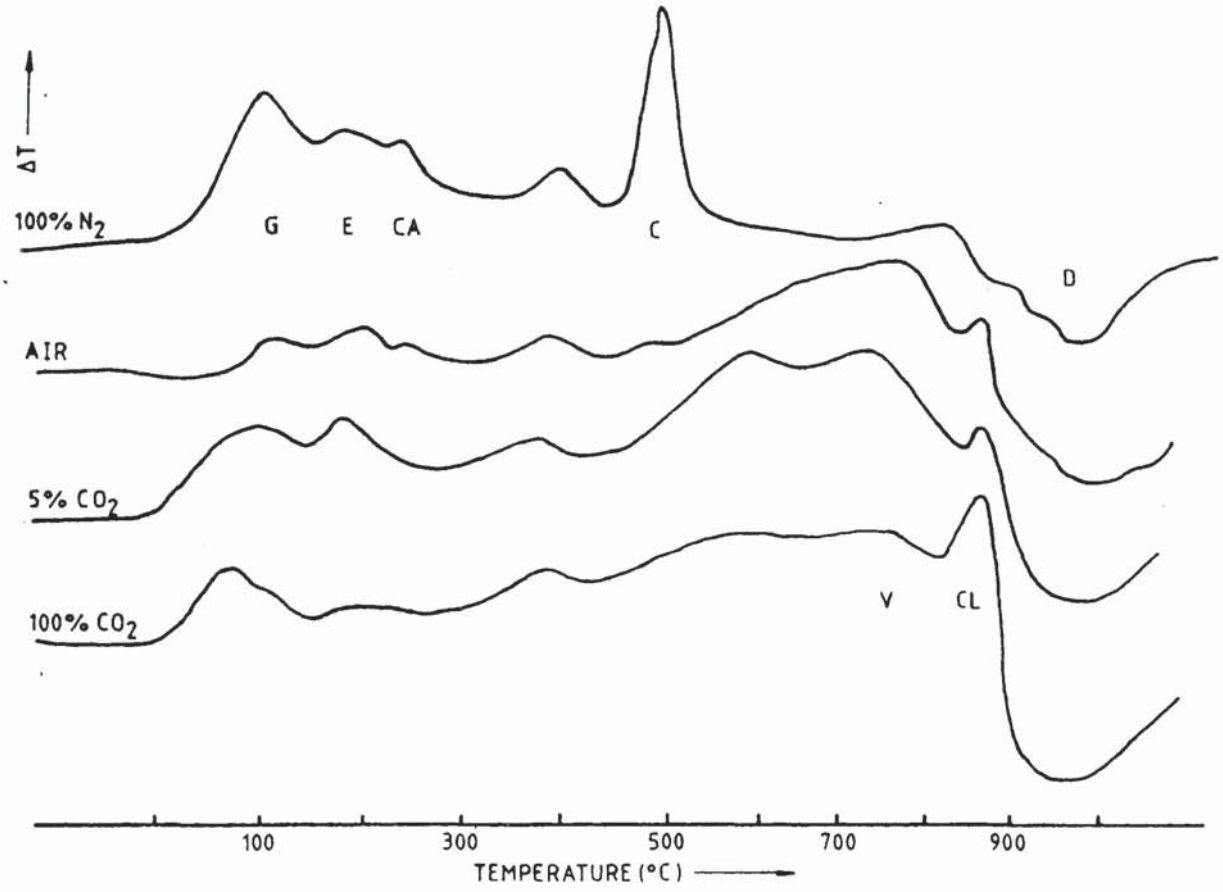

FIGURE 3.23 : DTA thermographs of 65% BFS cement pastes exposed to various atmospheres.

G = C-S-H gel

E = ettringite

CA = C_4AH_{13}

C = calcium hydroxide

V = vaterite

CL = calcite

D = devitrification of glassy phase

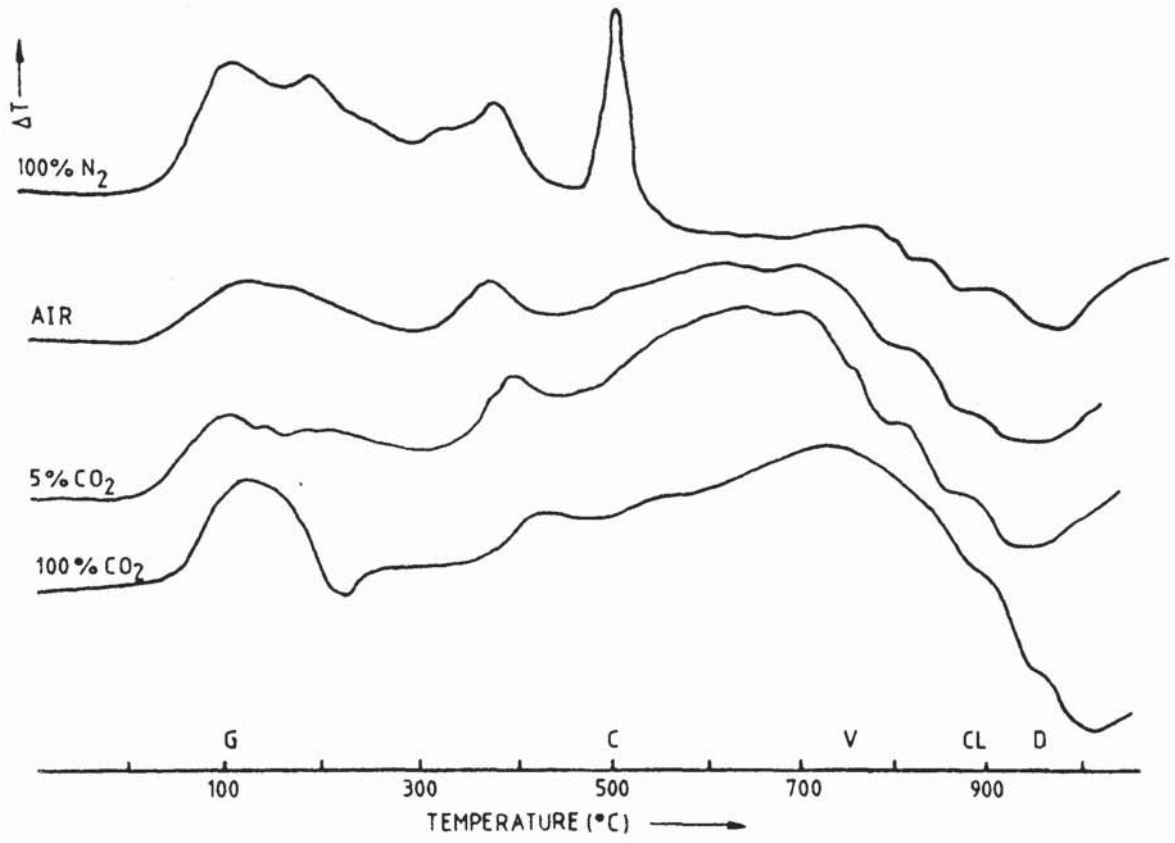

FIGURE 3.24 : DTA thermographs of 65% BFS cement pastes contaminated with NaCl and exposed to various atmospheres.

G = C-S-H gel

C = calcium hydroxide

V = vaterite

CL = calcite

D = devitrification of glassy phase

a shallow "hump" starting at about 500°C and terminating at a peak at 750°C, more apparent in the non-contaminated specimens. The shallow "hump", as mentioned in part I, is associated with a less crystalline form of calcite and the peaks at 750°C and 900°C are associated with vaterite and calcite respectively (see DTA identification peaks in appendix 7).

X-Ray diffractometer traces (figures 3.25 and 3.26) show that the main crystalline phases present in any of the carbonated conditions are vaterite and calcite. In accordance with the findings in part I, the ratio of vaterite to calcite appears to increase with the CO_2 content in the atmosphere, i.e. with the rate of carbonation. In the case of the NaCl contaminated specimens (fig 3.26) it can be seen that the calcium chloroaluminate phase disappears only in the case of specimens exposed to 100% CO_2.

3.4.3.5 Porosimetry

Figures 3.27 and 3.28 show the pore size distribution after the exposure of the specimens to 100% N_2, Air, 5% CO_2 and 100% CO_2. It can be seen that although the total porosity decreases with the increase of the CO_2 content in the atmosphere the volume of pores greater than about 40 nm

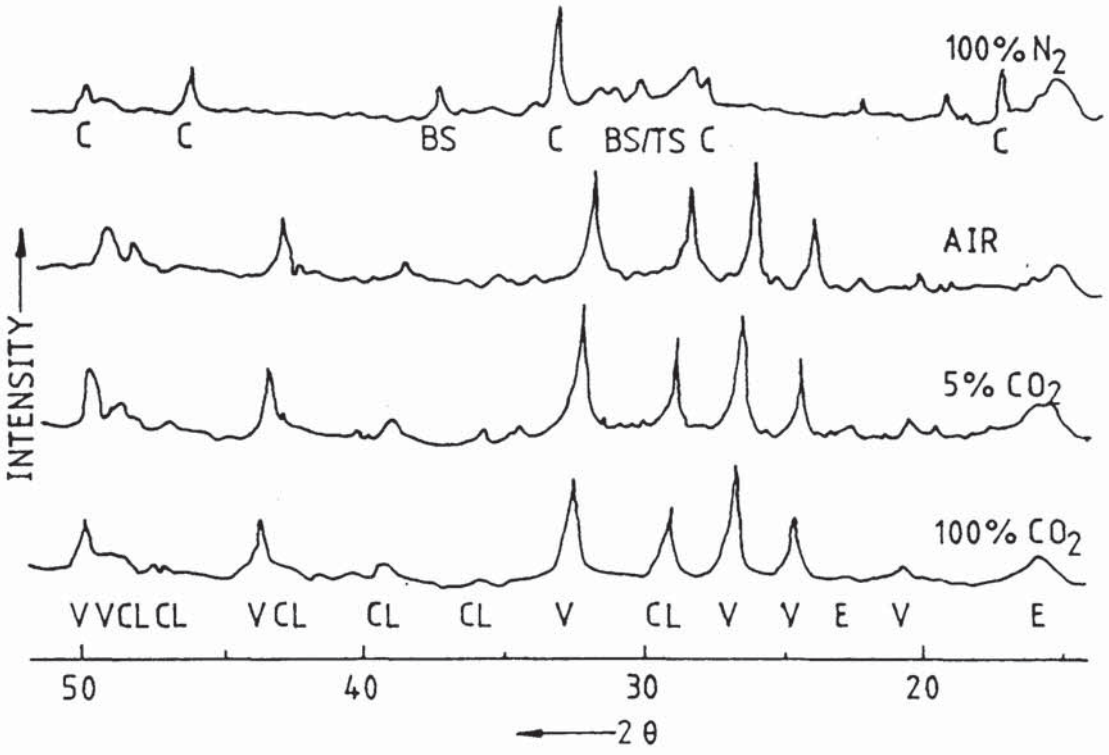

FIGURE 3.25 : X-ray diffractometer traces of 65% BFS cement pastes exposed to various atmospheres.

V = vaterite

CL = calcite

E = ettringite

C = calcium hydroxide

BS = C_2S

TS = C_3S

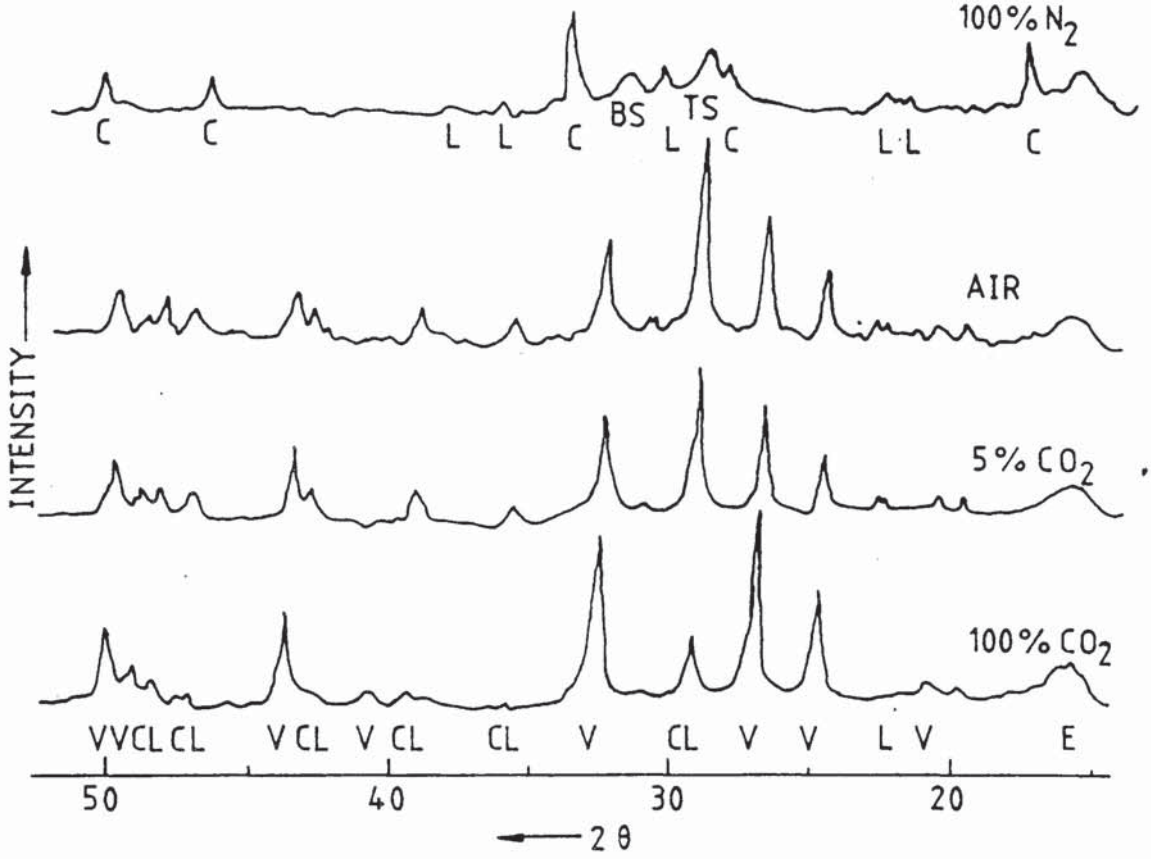

FIGURE 3.26 : X-ray diffractometer traces of 65% BFS cement pastes contaminated with NaCl and exposed to various atmospheres.

V = vaterite

CL = calcite

C = calcium hydroxide

L = calcium chloroaluminate

E = ettringite

BS = C_2S

TS = C_3S

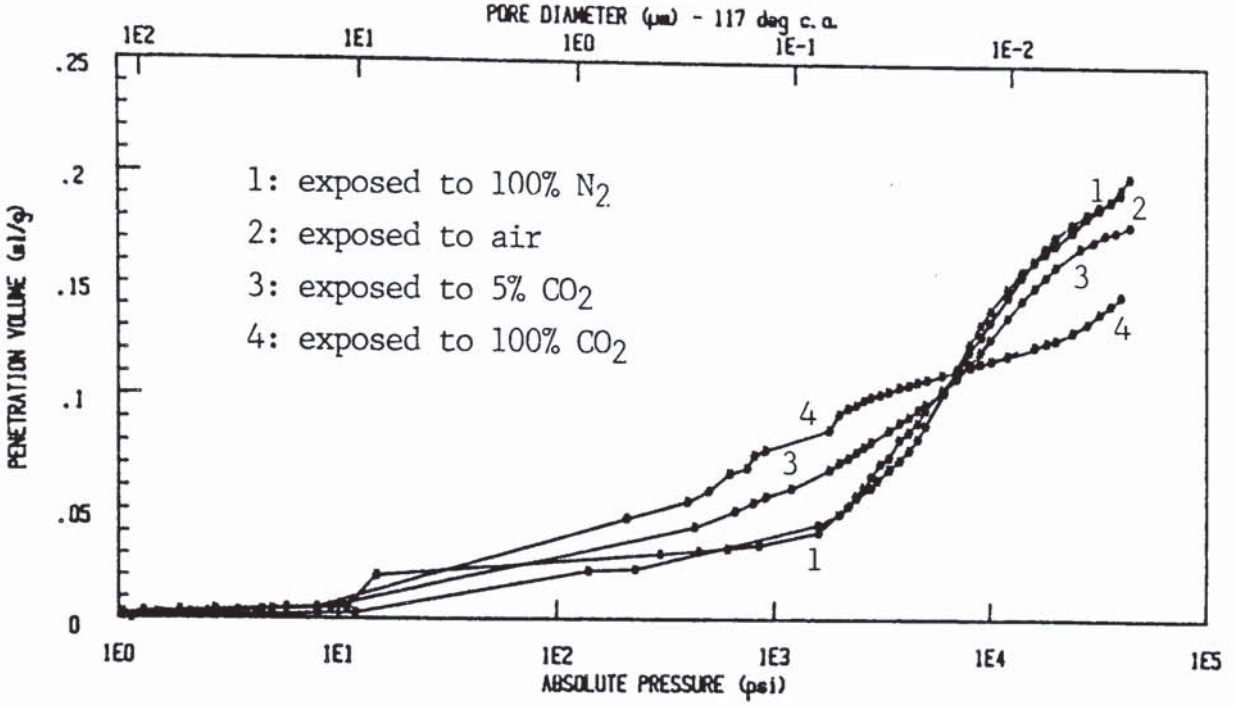

FIGURE 3.27 : Pore size distributions of 65% BFS cement pastes exposed to various atmospheres.

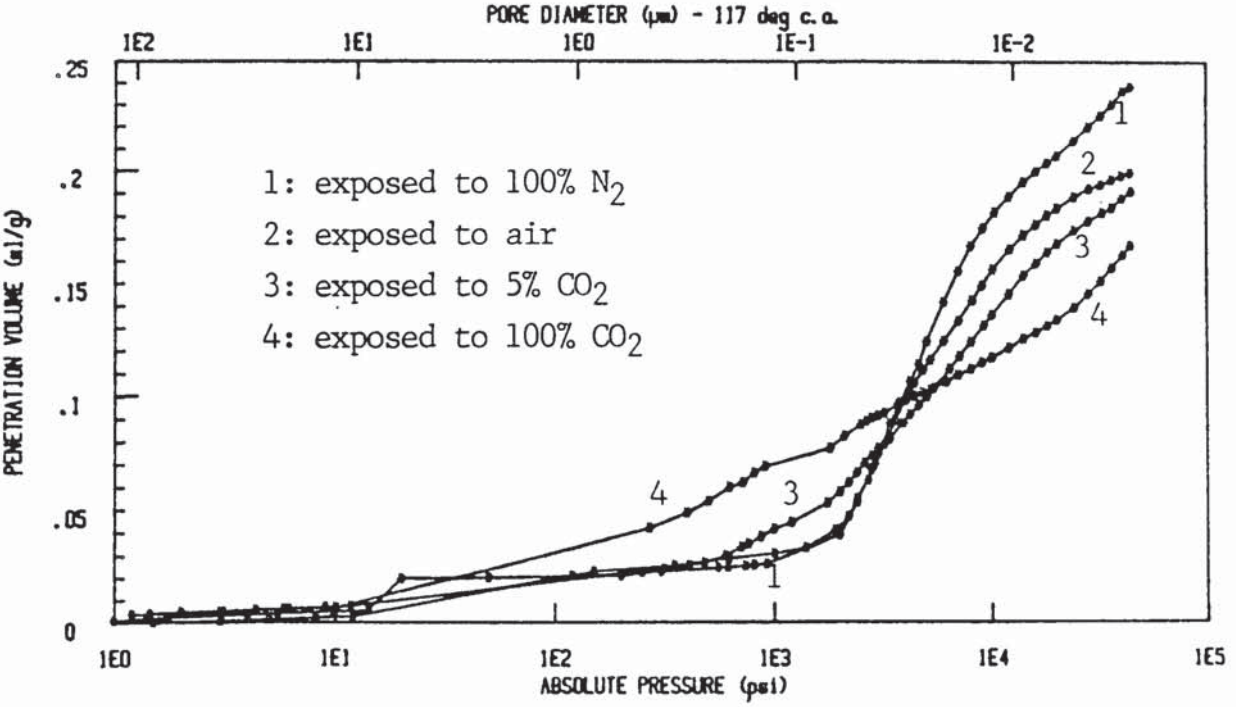

FIGURE 3.28 : Pore size distributions of 65% BFS cement pastes contaminated with NaCl and exposed to various atmospheres.

increases. This is a fact for both the contaminated and non-contaminated specimens. An exception is the non-contaminated specimens exposed to Air which appear to have almost the same pore size distribution as the uncarbonated specimens.

3.4.4 DISCUSSION

3.4.4.1 Pore structure

The increase of the CO_2 content in the atmosphere from about 0.03% in air to 5% and then 100% caused, as expected, an equivalent increase of the carbonation rate (table3.6). Using linear regresion analysis it can be seen that the relation between the square root of CO_2 content in the atmosphere, C, and the constant K for the rate of carbonation is linear (fig 3.29). The equation representing the relation is:

$$K_{65\%BFS} = 0.110 + 0.128\ C^{1/2}$$

with correlation coefficient 0.999. For the sodium chloride contaminated specimens the equivalent equation is:

$$K_{65\%BFS} = 0.173 + 0.128\ C^{1/2}$$

with correlation coefficient 0.995. Thus the above two equations have the same gradient. Examining the data for specimens made of 100% OPC exposed to equivalent conditions (table 3.7), it can be seen that, in similar manner

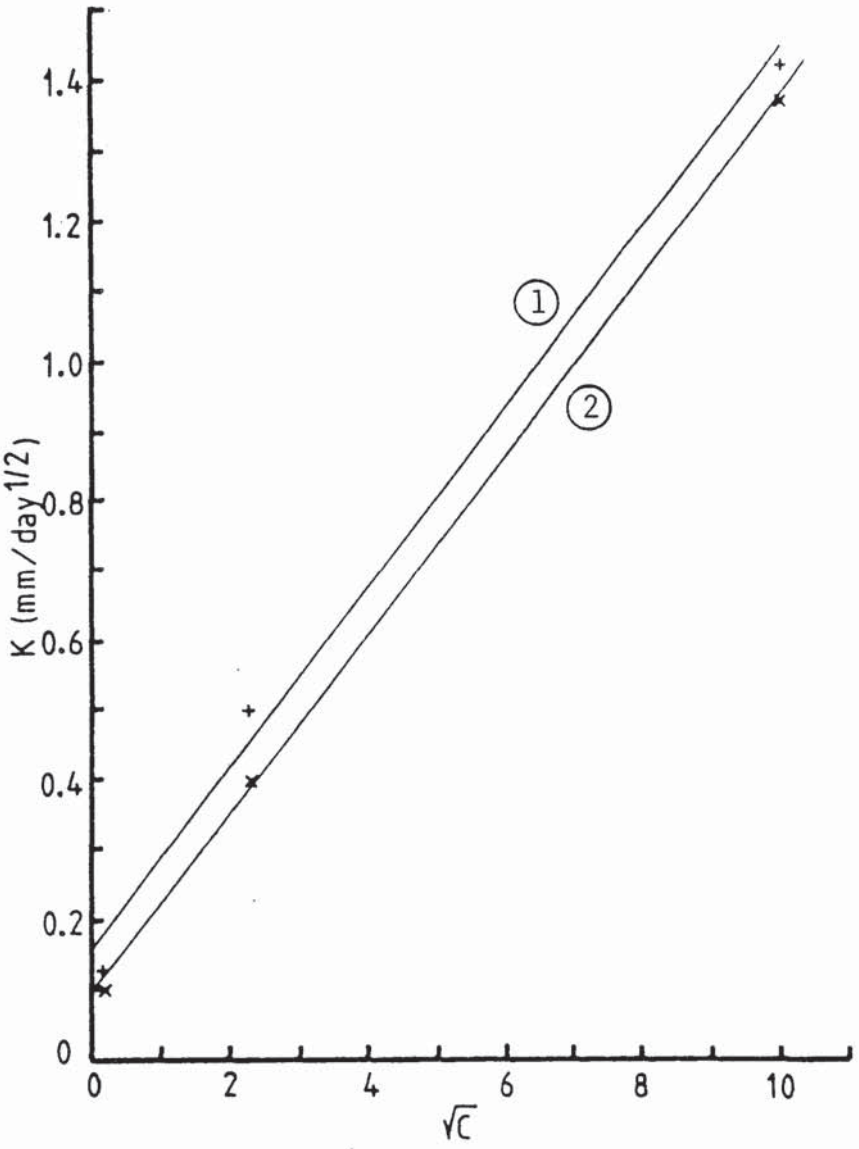

FIGURE 3.29 : The constant K for the rate of carbonation versus the square root of the CO_2 content in the atmosphere.

1(+): $K = 0.173 + 0.128\ C^{\frac{1}{2}}$ (NaCl contamination)

2(x): $K = 0.110 + 0.128\ C^{\frac{1}{2}}$ (no contamination).

to the 65% BFS specimens, the relation between the square root of CO_2 content and the constant K is linear. The corresponding equation for the non-contaminated specimens is:

$$K_{OPC} = 0.205 + 0.038\ C^{1/2}$$

with correlation coefficient 0.984 and for the NaCl contaminated specimens is:

$$K_{OPC} = 0.303 + 0.036\ C^{1/2}$$

with correlation coefficient 0.917. The lower correlation coefficients for the OPC specimens are possibly due to the fact that the specimens exposed to 100% CO_2 were made of different cement than the specimens exposed to 5% CO_2 and air (data from ref. 37). As for the case of the 65% BFS specimens, the gradients of the above two equations are practically the same.

In both the OPC and 65% BFS specimens the addition of NaCl induced higher carbonation rates. This is consistent with the results in part I. The change in the pore structure of the specimens caused by the NaCl contamination (see fig 3.27 and 3.28), however, did not affect the gradients of the K vs $C^{1/2}$ equations, i.e. the rate of increase of the constant K with the CO_2 content in the atmosphere. The affected parameter was the K-intercept which probably represents any changes in the pore structure of the pastes. The gradient of the K vs $C^{1/2}$

equations probably represents any changes in the amount of carbonatable material present in the pastes. This was shown in part I where a linear relationship was obtained between the rate of carbonation and the reciprocal of the square root of the amount of carbonatable material present in the paste.

It is apparent from the above experimental data that the constant K for the carbonation rate is generally given by the following expression:

$$K = a + b \frac{\sqrt{C}}{\sqrt{A}}$$

where a and b are constants for each particular type of cement paste. The former probably represents any variations in the pore structure of the paste. Theoretically, the constant K is given by a similar equation [7]:

$$K = \sqrt{(2D \frac{C}{A})}$$

This equation can be derived from Fick's first law for the diffusion of CO_2 in cement paste, assuming that there is no variation of the diffusion coefficient D with time or depth. In the case of this work, for each condition tested, the above assumption was realistic either because the diffusion coefficient was effectively constant or because there was no significant variation of the diffusion coefficient, due to the small thickness of the specimens (max. 3mm). The constant b of the experimentally obtained relation appears to

represent the diffusion of CO_2 in each particular cement paste. It is constant for specimens with small thickness. In the case of cement pastes with large thickness, however, there is a possibility for the diffusion coefficient to vary with depth or time, e.g. due to variations in moisture content.

The ratios between the rates of carbonation of the 65% BFS and OPC specimens are tabulated in Table 3.8. It can be seen that for the 100% CO_2 and 5% CO_2 conditions the $K_{65\%BFS}/K_{OPC}$ ratio is greater than unity, showing that the 65% BFS specimens carbonate faster. However, in the case of specimens exposed to air, the ratio is less than unity showing that the OPC specimens carbonate faster. This suggests that there exists a critical concentration of CO_2 in the atmosphere for which both OPC and 65% BFS specimens carbonate at the same rate. Knowledge of this concentration is clearly important with respect to the characterization of cement pastes according to their resistances to carbonation. The comparison of the carbonation resistances of the different cement pastes in the laboratory under accelerated conditions can otherwise be a misleading guide to their behaviour under natural conditions. It is important to know if the test conditions are above or below the critical CO_2 concentration. This "critical" concentration for the specimens tested in this work is 1.1% for the

non-contaminated specimens and 2.0% for the NaCl contaminated specimens. These values were calculated from the obtained relations between the constant K and the $C^{1/2}$.

Examining the DTA thermographs and the x-ray diffractometer traces of the tested specimens (fig. 3.23-3.26) it can be seen that in all the carbonated conditions the main products of carbonation are calcite and vaterite. As in part I, the ratio of vaterite to calcite increases with the rate of carbonation. From figures 3.27 and 3.28 which represent the pore size distributions of the specimens after their exposure to different atmospheres, it can be seen that although the total porosity decreases with the carbonation rate, the volume of pores greater than about 40 nm increases. This is in agreement with the findings of others [88-90] who found similar effects of carbonation on the pore size distributions of their specimens. According to Rozental and Alekseev [89] this effect is probably caused by the dissolution of $Ca(OH)_2$ crystals present in larger pores followed by carbonation and nucleation of $CaCO_3$ in the higher moisture content smaller pores where dissolution of CO_2 might be easier.

3.4.4.2 Pore solution

Examining the ionic concentrations in the pore solutions of

the pastes carbonated in 5% CO_2 and 100% CO_2 (Table 3.9) it can be seen that their general characteristics are low pH, low concentrations for the alkali metal ions and high concentration for the calcium ion. In addition, Table 3.10 shows the presence of magnesium and silicate ions in their pore solution. These characteristics are similar to those of the carbonated pastes tested in part I.

Conversely, specimens exposed to 100% N_2 (uncarbonated specimens) show high concentrations of alkali metal ions, small concentration of calcium ions and no magnesium or silicate ions. Finally, the specimens carbonated under natural conditions (in air) are in an intermediate situation.

The above can be seen graphically in figures 3.21 and 3.22. From the anion chromatographs (fig 3.21) it can be seen that only the 100% CO_2 condition shows the third peak which, as mentioned in part I, is probably associated with a form of soluble silica. This suggests that the latter may be produced only at later stages of carbonation or its dissolution may favoured by high carbonation speeds.

The gradual increase of the concentration of the calcium ions with the increase of the CO_2 content in the atmosphere, i.e. with the increase of the degree of carbonation, is probably caused, as explained in part I, by the gradual decrease of the

Ca/Si ratio of C-S-H gel, which also increases the concentration of the silicate ions.

The removal from the pore solution of the alkali metal ions (Na^+ and K^+) on carbonation is a fact also found by experiments carried out by Sergi [37] using 100% OPC specimens. It is probably a similar situation to that caused by partial replacements of cement with silica fume [108] slag or PFA [109]. As discused by Roy and Idorn [109], lower CaO to SiO_2 ratios in the C-S-H gel caused by slag additions increase the retention capacity of the gel for alkalis. Butler et al [110], as reported by Roy and Idorn [109], found that the overall effect of the PFA/$Ca(OH)_2$ reaction in PFA blended pastes was to reduce the C/S ratio of the reaction product as a whole and to cause the alkali metal ions to be trapped within this gelatinous material. A very low C/S ratio would exist in carbonated cement pastes, so the incorporation of the alkali metal ions in the C-S-H gel or in the newly formed silica gel, is not unrealistic.

Carbonation causes the release of chloride ions into the pore solution. In all the carbonated conditions (table3.9) the concentration of the chloride ions was increased considerably. This can also be seen from table 3.11 which shows the ratios of free to total chlorides. The reason is probably, as mentioned in part I, the dissolution of the

insoluble complex calcium chloroaluminate salt. The ratios of free/total chlorides show that the chloride release is higher for normal as opposed to accelerated carbonation conditions. It is difficult to envisage the reason for such a difference. As suggested by Sergi[37] in the case of accelerated carbonation, calcium chloroaluminate or other chloride-bearing phases might be entrapped within rapidly forming carbonates which may not have had sufficient time to redistribute themselves elsewhere. In this case, the release of the chloride ions might be difficult.

3.5 CONCLUSIONS

The conclusions obtained from this chapter can be summarized as follows:

(1) The equation which represents the progress of carbonation depth, x, with time, t, is parabolic of the form:

$$x = K\, t^{1/2} - K_o$$

where K is a constant representing the rate of carbonation.

(2) There is no simple relation between the porosity before the beginning of carbonation and the carbonation rate, i.e. the resistance to carbonation.

(3) The constant K which represents the rate of carbonation is generally given by the following expression :

$$K = a + b\,\frac{\sqrt{C}}{\sqrt{A}}$$

where "C" is the CO_2 content of the atmosphere, "A" is the amount of carbonatable material present in unit volume of the paste, "a" is a constant for each particular type of cement paste which represents any variations in the pore structure of the paste, and "b" represents the diffusion of CO_2 in each particular cement paste; "b" is a constant for specimens with small thickness, but for cement pastes with large thickness may be expected to vary.

(4) There is a certain concentration of CO_2 in the atmosphere for which OPC and 65% BFS cement pastes have the same resistance to carbonation. Knowledge of this concentration is important to the characterization of the pastes in terms of their resistance to carbonation.

(5) NaCl contamination of cement pastes causes a slight reduction of their resistance to carbonation.

(6) The main forms of crystalline $CaCO_3$ produced by carbonation are vaterite and calcite. The ratio of vaterite to calcite increases with the increase of the rate of carbonation.

(7) Carbonation reduces the total porosity of 65% BFS cement pastes and increases the volume of pores greater than about 40 nm. The extent of these effects depends on the degree of carbonation.

(8) The effects of carbonation on the pore solution of cement pastes are the removal of the alkali metal ions and the increase of the concentration of chloride, calcium,

magnesium and silicate ions. The extent of these effects increases with the degree of carbonation.

CHAPTER 4 : Resistance to ionic penetration

4.1 INTRODUCTION

The penetration of ions into hardened cement pastes and thus into concretes is of great importance in terms of durability. Aggressive ions can attack concrete causing its degradation (10). Corrosion of the reinforcement, cracking or surface deterioration by spalling or splitting are situations commonly found in concrete structures which have been attacked by such ions.

Aggressive ions can enter into concrete in various ways which Kay et al (111) classified in three main groups as primary, secondary and tertiary entry. They particularly refered to chloride ions, but their classification can be generalized.

Primary entry includes the ions which may be introduced at the mixing stage of concrete from its constituents (aggregates, water, admixtures). Secondary entry includes the ions which may be absorbed from a concrete surface sometime after the casting of the concrete, while tertiary entry includes the ions which may enter the concrete through cracks which have occurred from causes like shrinkage, thermal expansion or stress.

Primary and tertiary entry can be prevented or at least reduced to a minimum, by using materials of good quality and by good design and construction of the concrete structure (112). Therefore the most usual way for aggressive ions to enter concrete which has been made and placed in accordance with the proper rules and specifications, is by secondary entry. In this case, ions enter into concrete mainly through the pores of the cement matrix and thus the porosity and pore structure of the latter exert major control on the resistance of concrete structures to ionic attack.

Studies carried out by many researchers have shown that ionic penetration into hardened cement paste is often controlled by the laws of diffusion. This was substantiated by Sorensen and Maahn (11) who studied the penetration of chloride ions in many 15-20 years old concrete structures on the Danish coast. They found that the chloride penetration profile obeyed Fick's second law of diffusion.

This chapter examines the relation between the pore system and ionic diffusion. The aim is to contribute to the understanding of this relation by studying ionic diffusion in hardened cement pastes with different pore systems. The experiments were carried out in two parts. In the first part the pore system of hardened cement paste was altered by partial replacement of cement with BFS, while in the second part, the pore system was altered by carbonation of the

cement pastes. In both the parts, the experiments were particularly concentrated on chloride ion as this is one of the most common ions in practice which attack concrete structures. Its depassivation action on steel reinforcement [8] destroys the ability of the cement matrix to protect the reinforcing steel (see chapter 1). In parallel with chloride ion, sodium ion was also studied in the same experiments. The two ions enable useful comparisons to be made which may lead to better understanding of ionic diffusion in concrete.

4.2 LITERATURE REVIEW

For diffusion-controlled ionic migration in hardened cement paste the mobility of the ions is controlled by the Nernst-Einstein relationship [113] which states that for a given temperature, the mobility of the ions is directly proportional to the diffusion coefficient:

$$D = u K T$$

where: D = the diffusion coefficient
u = the mobility of the "particles"
K = the Boltzman constant
T = the absolute temperature.

The laws of diffusion developed by Fick [114] allow the determination of the diffusion coefficient from measurable quantities. Fick's first law states that the amount of

substance passing perpendicularly through a surface of unit area during unit time is proportional to the concentration gradient of the diffusing substance in the direction of diffusion. The factor of proportionality is the diffusion coefficient. This law is applicable to steady state conditions in which the concentration gradient is constant.

Fick's second law is applicable to non-steady state conditions, that is, it relates the time and space variations of the concentration during diffusion. It is a partial differential equation and describes the general characteristics of all diffusion problems but not the details of any one particular diffusion process. For any particular problem it must be solved with the aid of the initial and boundary conditions which characterize the problem.

As a result of the great significance of ionic penetration on concrete's durability, Fick's laws of diffusion were widely used in the past for the determination of ionic diffusion coefficients in cement pastes, mortars or concretes. A lot of relevant experimental work has been reported in the literature. The majority of it was based generally on two different experimental techniques; the "Thin disc" technique and the "Penetration profile" technique. The description and some applications of both techniques follow.

4.2.1 "Thin disc" diffusion experiments

This experimental technique was developed [116-118] on the basis of Fick's first law of diffusion which, as mentioned earlier states that:

$$J = -D \frac{dc}{dx}$$

where: J = the flux, i.e. the amount of substance passing perpendicularly through a surface of unit area during unit time,

D = the diffusion coefficient,

dc/dx = the concentration gradient of the diffusing substance in the direction of diffusion.

Since the above relationship is applicable in steady state conditions [114], by keeping the concentration gradient through a thin disc of cement paste effectively constant, it is possible to determine the diffusion coefficient by measuring the flux.

Practically this can by achieved [116-118] using specially designed cells comprising of two compartments with the cement paste disc fitted in between. The first compartment contains a solution of a high concentration of the investigated ionic species and the other a much lower concentration of the same solution, so that any small increase in the latter, although detectable, is insignificant

compared to the difference in the concentration of the two compartments.

The increase in concentration with time in the second compartment represents the amount of the diffused substance per unit area of the cement paste disc, i.e. the flux.

From a solution of Fick's first law as applied to quasi-steady state diffusion (see appendix 12), we can calculate the diffusion coefficient from the slope of the rectilinear plot of the concentration of the investigated ionic species in the low side against time.

According to Atkinson and Nickerson [120] this experimental technique leads to the determination of the "intrinsic" diffusion coefficient, because of the measurement of the average flux per unit area of the porous medium rather than per unit area of the liquid. As they pointed out, the average flux per unit area of the porous medium is influenced by the volume fraction of porosity in the medium which reduces the diffusion coefficient to :

$$D_i = D_f \frac{\varepsilon \delta}{\tau^2}$$

where: D_i = the "intrisic" diffusion coefficient

D_f = the diffusion coefficient for diffusion in the free aqueous medium

ε = the volume fraction of porosity (assuming that

all the porosity is interconnected)

δ, τ = the constrictivity and tortuosity respectively.

"Thin disc" experiments carried out by Kondo et al [117] have shown that the diffusion of ions in hardened cement pastes is influenced by the type of the diffused ion. They used plates of 0.4 w/c ratio portland cement paste, cured for 28 days in saturated lime water. From their results, as summarized in table 4.1, they showed that the diffusion coefficients of various ions are in the decreasing order of D_{Cl^-}, D_{K^+}, D_{Na^+}, D_{Li^+} and all are of the order of margnitude of 10^{-8} cm^2 sec^{-1}. They also found that the diffusion of the chloride ions was greately affected by the co-diffusing cations and decreased in the order : D_{MgCl_2}, D_{CaCl_2}, D_{LiCl}, D_{KCl}, D_{NaCl}. The faster chloride ion diffusion compared to that of the accompanying cation led them to the conclusion that hardened cement pastes behave as electropositive semi-permeable membranes.

It is evident from the above results that effective diffusion coefficients of ions in cement paste are reduced by several orders of magnidude as compared to their diffusivities in infinitely diluted bulk solutions, with values for D_{Li^+}, D_{Na^+}, D_{K^+}, D_{Cl^-}, of 1.04, 1.35, 1.98 and 2.03 x 10^{-5} cm^2 s^{-1} respectively [121]. The most interesting aspect of these results is the degree of reduction with ratios of

Table 4.1: Diffusion coefficients of various ions in OPC pastes of w/c = 0.4 (ref.117).

Thickness of disc (cm)	Solution on "high" side of the cell	D_{Cl^-}	D_{Li^+}	D_{Na^+}	D_{K^+}
0.3	0.5N LiCl	8.13	1.70		
	0.5N NaCl	6.25		1.70	
	0.5N KCl	6.73			2.95
	0.5N $MgCl_2$	18.30			
	0.5N $CaCl_2$	10.38			
0.2	0.5N LiCl	7.81	1.44		
	0.5N NaCl	6.94		1.89	
	0.5N KCl	7.35			3.78
	0.5N $MgCl_2$	23.30			
	0.5N $CaCl_2$	9.44			
0.08	Mixture of 0.5N LiCl + 0.5N NaCl + 0.5N KCl	7.72	1.45	2.22	3.30

$D_{bulk}/D_{cement\ paste}$ of 717, 608, 600 and 263 respectively (in the same order as above).

After the diffusion experiments, Kondo and his coworkers (117) found that the cement paste surface contacted with $CaCl_2$ or $MgCl_2$ suffered from chemical or physical change. As they suggested this was caused by the mutual diffusion of chloride and hydroxyl ions (counter diffusion effect). The chloride ions penetrating into the plate of cement paste, exchanged the hydroxyl ions in it. The latter reacted with the calcium and magnesium ions previously associated with the chloride ion and formed low solubility hydroxides at the surface of the plate.

In contrast with Kondo et al (117), Page et al (116) carried out "thin disc" experiments, using a constant solution, 1 M NaCl in saturated $Ca(OH)_2$, but altering the w/c ratio, the curing conditions and the cement composition of the cement paste disc. For three w/c ratios (0.4,0.5,0.6) they obtained a linear relationship between the reciprocal of the absolute temperature and the logarithm of the diffusion coefficient, enabling the calculation of the activation energies. The fact that they were able to do so suggested, as they pointed out, that for a given paste diffusion kinetics were under the control of a single dominant process over the temperature range considered. The activation energy for each of the three w/c ratios was found to be in excess of values characteristic

of the diffusion of chloride ions in normal electrolyte solutions. This led them to the conclusion that a form of surface interaction might be the rate-limiting process governing the diffusion of chloride ions in mature portland cement paste. They were unable to suggest the precise nature of this interaction, but they pointed out that it may involve desorption of the diffusing ions from binding sites on the pore walls and/or structural rearrangements necessary to accomodate ion migration through surface bound water. Diffusion coefficients of cement pastes with different w/c ratio and curing conditions had a marked effect on the transport properties of mature cement pastes. They attributed this to the different structure of hardened cement pastes of different w/c ratios or curing conditions. Additions of PFA and BFS to the OPC resulted in a considerable decrease in the mobility of the chloride ion in the pastes. They suggested that since the reductions of the diffusion coefficient could not be attributed solely to the respective pore size distributions, different mechanisms of diffusion rate control must be involved.

By calculating diffusion coefficients of I^- and Cs^+ ions in cement pastes of different w/c ratios, Atkinson and Nickerson [119] confirmed the conclusion of Page et al [116] that ionic diffusion through cement pastes is a strong function of the w/c ratio. They found that the relationship between the diffusion coefficient and the w/c ratio is

approximately exponential.

Takagi and his coworkers [122,123] calculated diffusion coefficients for Na^+ and I^- ions in a selection of cements. They concluded that the anion diffused faster than the cation and they attributed this to an electric double layer effect. According to them, the surface of the hydrates is positively charged by adsorption of calcium ions, so the resultant electric double layer attracts the anions towards the surface enabling them, by diffusing through that layer, to enter the micropores easily. On the other hand, the repelled cations could not readily diffuse through the electric double layer (see figure 4.1).

The assumption involved in the above-mentioned theory, that the surface of the hydrates is positively charged, cannot be considered as realistic. According to experimental results [124,4] the surface of calcium-silicate-hydrates can be either positively charged (e.g when high concentration of Ca^{++} is present) or negatively charged (e.g. at high pH values of the solution).

Uchikawa et al [125,126] by examining the diffusion of Na^+ and Cl^- ions in blended cement pastes found that the diffusion coefficients were reduced as the mixing ratio of fly ash or slag was increased. Contrary to Takagi et al [122,123] they attributed this partly to the increase in zeta potentials

FIGURE 4.1 : Effect of the electric double layer on the diffusion of ions in hardened cement paste (from ref. 123).

of the pore surfaces. As they pointed out, higher zeta potentials were caused by factors facilitating adsorption of sodium ions onto the C-S-H gel surfaces decreasing the mobility of the alkali ion by electric repulsion. As the Ca/Si ratio of C-S-H gel was decreased by adding fly ash or slag, the specific surface area of the gel was increased. As a result the amount of alkali ions adsorbed or incorporated was increased, preventing the movement of sodium ion by electric repulsion.

Sergi [37] using solutions of NaOH and KOH, carried out "thin-disc" experiments in order to determine activation energies and diffusion coefficients for hydroxyl ions in various types of cement paste. He found that the effect of the co-diffusing cation on the diffusion coefficient of hydroxyl ions was minimal. He also showed that, contrary to other anions [117,120,122,125], hydroxyl ions diffuse in hardened cement pastes at the same rate as sodium ions. As he suggested, this is because in the case of hydroxyl ions, no counter diffusion effect is possible, as there is no other available anionic species. So for a charge balance to be maintained across the cement paste disc and in the two compartments of the cell, OH^- ions can only diffuse at the same rate as the Na^+ ions. By adding PFA and BFS to OPC, he found that the diffusivity of OH^- ions was reduced. As he pointed out, the reduction can not be attributed only to the differences in pore size distributions, but it may be

explained by differing surface interactions caused possibly by changing zeta potentials. Comparing the activation energies obtained for OH^- ions and for Cl^- ions in similar pastes, he showed that there is no significant difference between the two. He therefore concluded that the same limiting mechanism of surface interactions may apply for chloride and hydroxyl ion diffusion.

The influence of the type of cement on ion diffusion was the subject of investigation of German researchers (127-130) who carried out "thin-disc" diffusion experiments using BFS cement pastes and concretes. Their findings agree that these concretes or hardened cement pastes display high resistance to the diffusion of ions. Brodersen (130), as reported by Smolczyk (129), derived a quantitative relationship between the BFS content of cement pastes and their diffusion coefficients with regard to chloride and sodium ions. According to it, the decrease in ionic permeability conforms to a function involving the sixth power of the slag content. Substantial decrease in ionic diffusivities of both the investigated ions was observed in hardened cement pastes with BFS content higher than about 40%.

Kumar and Roy (131-133) carried out diffusion experiments using a modification of the "thin-disc" technique as described here. By examining ionic diffusion in blended cement pastes they concluded that, although in general the addition of

mineral admixtures to portland cement leads to a significant retardation of ionic diffusion, the nature of the blending agent determines the mechanism of its action. As they pointed out, in some cases, as with BFS, the blending admixture may cause a decrease in porosity and pore size reducing the diffusion rate of ions. In other cases, as with silica fume, an electronegative surface charge or a tortuous finely porous matrix may be created, which retards the migration of ions.

Another modification of the "thin-disc" technique, which involves the application of an electric potential difference between the two sides of the diffusion cell was also used by Roy and her coworkers [118,134,135]. In the absence of a clear undersdanding of the mechanism of ionic diffusion in cement pastes, however, it is possible that this technique, which accelerates diffusion, may distort the normal diffusion mechanism and hence yield misleading information.

4.2.2 "Penetration profile" diffusion experiments

This experimental technique is based on Fick's second law of diffusion, which as mentioned earlier, is a partial differential equation. Different solutions of it, allow the determination of the diffusion coefficients for any ionic species from the concentration at increasing depths from the surface at a particular time, i.e. the penetration profile.

By assuming that cement paste or concrete may be regarded as a semi-infinite medium of constant chloride diffusivity, chloride penetration can be described by the error function solution to Fick's second law (11,136):

$$C_x = C_s - (C_s - C_o)\ \mathrm{erf}\frac{x}{2\sqrt{(Dt)}}$$

where: C_x = chloride concentration at a depth x from the surface

C_s = chloride concentration at the surface

C_o = original chloride concentration in the specimen

x = depth into the specimen

D = diffusion coefficient

t = duration of exposure

Practically the determination of the penetration profile and therefore the diffusion coefficient of an ionic species in hardened cement paste, mortar or concrete can be achieved by serial sectioning of the porous medium, after exposing one flat surface of it to a solution of the investigated ionic species for a known length of time. The concentrations of the investigated ionic species at the various depths represent the penetration profile.

As reported by Atkinson and Nickerson (120), since this technique is applicable in non-steady state conditions, it is dependent on sorption processes and therefore gives an apparent diffusion coefficient:

$$D = \frac{D_i}{a}$$

where: D_i = the "intrinsic" diffusion coefficient

a = the capacity factor, a parameter which can be regarded as a measure of the "capacity" of the medium for a particular diffusant.

Researchers have used this experimental technique extensively (137-146) as it closely resembles many real situations such as offshore structures exposed to seawater. All of them agree that penetration of ions into cement pastes follows Fick's second law of diffusion into a semi-infinite porous medium.

Penetration profile experiments were made as long ago as 1952 by Spinks at al (137) who used solutions labelled with radioactive isotopes (^{45}Ca, ^{35}S, ^{131}I, ^{22}Na). After exposing the one side of cylindrical OPC and SRPC pastes for a length of time, they measured the radiation at different depths of the pastes and translated their readings into concentrations of the particular ion under investigation. They calculated diffusion coefficients which ranged in the order of 10^{-11} to 10^{-9} cm^2s^{-1} with anions having higher values than cations. No mention was made, however, of curing conditions or w/c ratios of the cement pastes.

Collepardi et al (138-140) used cylindrical specimens of OPC and pozzolanic cement pastes of w/c ratio 0.4 to 0.6. After

exposure of one surface of the cylinders to solutions of $CaCl_2$, KCl and Na_2S, the specimens were sliced into discs at increasing depths which were then subjected to specific chemical analysis to determine the total concentrations of the ions under investigation. For chloride ions they calculated diffusion coefficients in the order of $10^{-8}cm^2sec^{-1}$ at 25^oC for both types of the cements used. The diffusion coefficients of both the anions used (Cl^-,S^{--}), however,were three times smaller in the pozzolanic cement paste than in OPC paste. They attributed this to the more intense interaction between the diffusing ions and the pore surfaces in the pozzolanic cement paste. In agreement with other researchers (116,117,141) they found that the penetration of chloride ions is influenced by the co-diffusing ion as well as by the w/c ratio of the paste.

Similar experiments by Effes (155), who used beam concrete specimens made with BFS blended cements, had shown that ionic diffusivity was decreased according to the increase of the slag content of the specimens. He explained his results in terms of the differences in pore size distribution of the specimens. By using mercury pressure porosimetry, he found an increase in gel pores and a decrease in capillary pores with increasing slag content.

Traetteberg (142) studied the effect of maturity of portland cement paste on the penetration rate of chloride, by

determining total amounts of chloride at increasing depths. She concluded that penetration depths decreased with increasing maturity of the paste. She also suggested that during penetration of chloride ions, chloroaluminate was formed, by transformation of ettringite accompanied by precipitation of calcium sulphate.

Similar studies by Midgley and Illston [143,144], however, indicated that Friedel's salt is not formed at the expense of other calcium aluminate hydrates, but only by reaction of Cl^- with anhydrous C_3A. Mehta [145] reported that C_3A for chloride complexation is available only after the C_3A corresponding to the formation of calcium monosulfo-aluminate hydrate has been used up.

Gjorv and Vennesland [146] as well as Traetteberg [142] carried out penetration profile experiments using cement pastes and mortars made with 0% to 8.6% C_3A content portland cement. By measuring total amounts of chloride ions, they concluded that C_3A content does not have any significant influence on the penetration of chloride ions. They suggested that this is because the major part of the chloride bound in hardened cement paste is held by physical adsorption to the gel surface rather than chemical binding with the aluminate compound.

Sergi [37] by determining total amounts of chloride as well as free chlorides in the pore solution at increasing depths, calculated diffusion coefficients of free and total chloride in OPC paste. He found that the ratio of free to total chloride is concentration dependent and increases as the total amount of chloride increases. As he pointed out, this is because at high chloride levels the paste approaches its saturation point in chemically bound chloride and so more chloride remains in the pore solution. He also concluded that the C_3A phase present in portland cement paste, by reacting with part of the chloride, causes some reduction in the penetration rate of free chloride as compared to total chloride.

From the reviewed studies on diffusion of ions in cement pastes or concretes (sections 4.2.1 and 4.2.2) it is obvious that there is currently no clear understanding of the mechanisms by which ionic diffusion is controlled in hydrated cement systems. As mentioned in the first chapter, however, it is particularly important to develop a general theory for ionic diffusion in cement paste which could be useful to the design of cementitous materials of improved resistance to ionic penetration. In an attempt to assist in the development of such theory, this chapter examines the effect of the type of the pore system on ionic diffusion in hardened cement paste. As mentioned in the introduction, the experiments were carried out in two parts. In each part the pore system of hardened cement paste specimens was altered

by a different method while the rest of the parameters affecting ionic diffusion were kept constant.

It is generally known (see par.1.2) that partial replacement with BFS of the portland cement in a cement paste, results in a more compact pore structure. In part I cement paste specimens with 65% BFS content were used together with specimens made with 100% OPC and their resistance to ionic diffusion was compared. Similar specimens were also used in part II, but before the diffusion experiments their pore structure was changed by carbonation (see chapter 3).

4.3 EXPERIMENTAL PROCEDURE

4.3.1 Specimen preparation

Part I: Cylindrical specimens of 0.5 w/c ratio made with 100% OPC and 35% OPC/65% BFS were prepared as described in chapter 3 (par.3.3.1). After 3 days storage in a high humidity room at 22^{o}C they were demoulded and cured under saturated $Ca(OH)_2$ solution at room temperature for 60 days. From their central part, 2.8 mm to 3.0 mm discs were then cut by means of a diamond saw, using deionized water as lubricant. Finally, the discs were lightly ground on 600 grade carbide paper and rinsed with deionized water.

Part II: Similar cylindrical specimens of 0.5 w/c ratio were

prepared as in part I. After a curing period of 28 days in a high humidity room at 22°C they were demoulded and their middle sections sliced into 2.8 mm to 3.0 mm discs as in part I. The discs were lightly ground on 600 grade carbide paper, rinsed with deionized water and finally placed over a saturated $NaNO_2$ solution in air-tight containers at room temperature, thus maintaining the relative humidity at 65% (98). At 24 hour intervals 100% CO_2 was passed over the discs and through a water trap for half an hour. The carbonation procedure terminated 30 days after the complete carbonation of the discs was detected using phenolphthalein (98).

4.3.2 Experimental set up

The experimental technique used for both parts of the experiments was that developed by Page et al (116). The cement paste discs were fitted between the two compartments of specially designed glass cells (fig 4.2). Compartment 1 of each cell was filled with a molar NaCl solution in saturated $Ca(OH)_2$ for part I experiments and a molar NaCl solution for part II experiments. Compartment 2 of each cell was filled with a known volume of either saturated $Ca(OH)_2$ solution in part I experiments or deionized water in part II experiments.

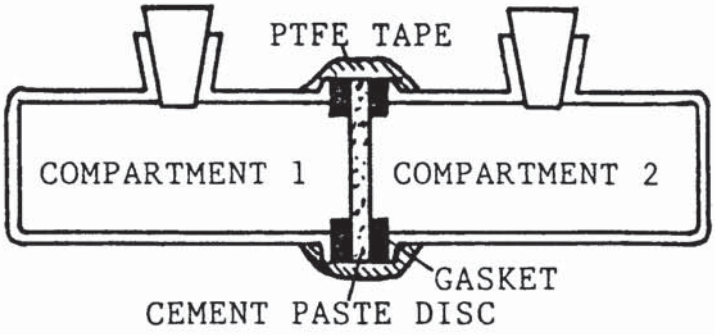

FIGURE 4.2 : The diffusion cell.

Five or six cells were set up for each type of specimen used and these were then placed in a water bath of constant temperature. On a regular basis, 100 µl aliquots of the compartment 2 solutions were withdrawn and analysed for chloride and sodium ions by the methods described in chapter 2. The withdrawn solutions were not replaced as the overall reduction in volume was negligible. The experiments were terminated before the concentration in compartment 2 had reached 0.1 molar, after at least six readings had been recorded.

On completion of each set of diffusion measurements the thicknesses of the discs were determined by means of a micrometer gauge.

Samples of all the types of specimens used were analysed by DTA and subjected to MIP.

4.4 RESULTS AND DISCUSION

PART I : ALTERATION OF THE PORE SYSTEM BY PARTIAL REPLACEMENT OF CEMENT WITH BFS

4.4.1 RESULTS

Figure 4.3 represents a typical plot of ion concentration in compartment 2 of the diffusion cell versus time of diffusion. It can be seen that after a period when diffusion becomes established across the disc, the concentration of both chloride and sodium ions in compartment 2 increases linearly with time. The concentration in compartment 1 remains effectively constant. Assuming that conditions of quasi steady state diffusion are operating across the disc and so the flux and activity of the diffusing ion remains effectively unchanged through the disc, a solution of Fick's first law (see appendix 12) can be obtained which enables the calculation of the diffusion coefficient from the following simple relation:

$$D = \frac{S\,V_2\,l}{A(C_1-C_2)}$$

where: D = the diffusion coefficient (cm^2s^{-1})

V_2 = the volume of the solution in comp. 2 (cm^3)

A = the cross-sectional area of the disc (cm^2)

l = the thickness of the disc (cm)

C_1, C_2 = the concentration of the investigated ionic species in compartment 1 and 2 respectively

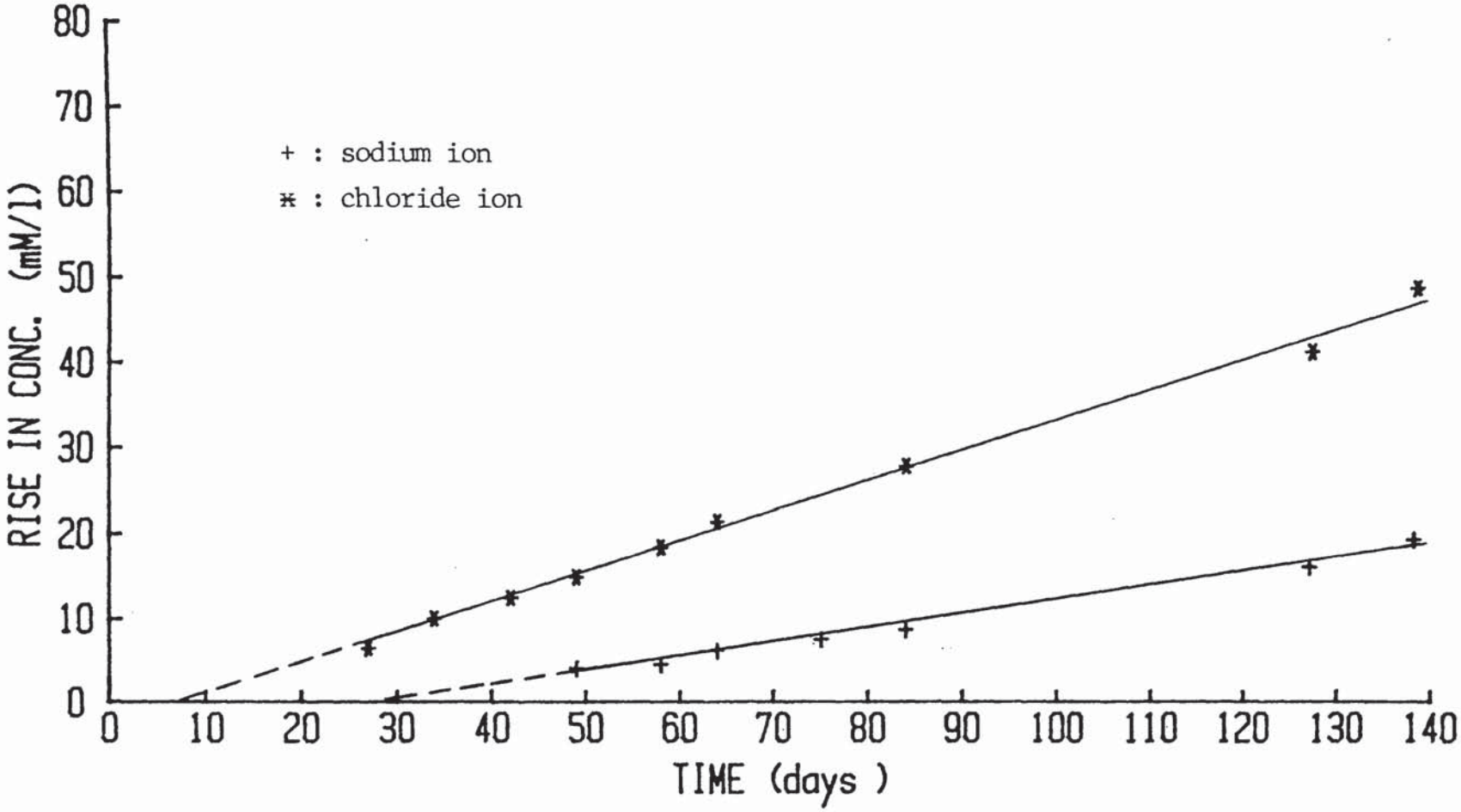

FIGURE 4.3 : Rise in concentration of chloride and sodium ions in the compartment 2 of the diffusion cell No 4 at 42 °C (uncarbonated 65% BFS cement paste).

(mole cm^{-3})

S = the gradient of the rectilinear plot of C_2 versus t.

The calculated diffusion coefficients of chloride and sodium ions in OPC and 65% BFS cement pastes are given in table 4.2 (see worked example in appendix 13). Table 4.3 shows the diffusion coefficients of chloride ion in OPC paste (0.5 w/c) at five temperatures, obtained by Page et al (116). As can be seen the value of the diffusion coefficient at 25°C is similar to that obtained in this work, indicating that the results in the two works are comparable.

From the data for the 65% BFS cement paste (table 4.2), best fit Arrhenius plots of log D versus the reciprocal of absolute temperature were constructed by means of linear regression analysis (fig. 4.4). Correlation coefficients for the lines relating to chloride and sodium ions were calculated to be -0.97 and -0.93 respectively. The slopes of the lines corresponded to activation energies which are shown with 95% confidence limits in table 4.4. The same table shows the activation energy for the diffusion of chloride ion in OPC paste calculated from the results in table 4.3 (116) (a worked example can be found in appendix 14).

Table 4.2: Effective diffusion coefficients of chloride and sodium ions in uncarbonated 65% BFS/OPC and OPC pastes ($D \times 10^9$ cm^2 s^{-1}).

65% BFS					OPC
9°C	17°C	25°C	33°C	42°C	25°C
CHLORIDE ION					
3.77	4.33	5.23	6.70	7.73	41.13
3.29	4.91	5.52	5.92	8.22	39.90
3.06	4.68	4.94	5.91	7.32	47.11
3.75	4.12	5.68	6.56	9.91	47.02
3.76	4.41	5.55	6.00	8.83	43.84
		5.61		9.08	
MEAN	MEAN	MEAN	MEAN	MEAN	MEAN
3.53	4.49	5.42	6.22	8.52	43.80
SODIUM ION					
1.44	1.92	2.41	2.69	7.01	
1.67	1.61	1.80	2.76	7.90	
1.29	1.20	2.58	3.31	10.63	
1.20	1.68	2.28	3.30	10.60	
1.47	1.86	2.77	3.35	10.74	
	1.43		2.80		
MEAN	MEAN	MEAN	MEAN	MEAN	
1.41	1.75	2.37	3.04	9.38	

Table 4.3: Effective diffusion coefficients of chloride ion in uncarbonated OPC paste (0.5w/c) from ref.116 ($D \times 10^9$ cm^2s^{-1}).

7°C	13.5°C	25°C	33.5°C	45°C
18.6	22.9	40.6	98.4	201
22.0	24.5	44.2	92.5	152
22.3	14.7	48.2	91.7	190
20.3	31.7	44.0	99.9	186
20.2	24.4	47,8	91.3	189
		43.3		
MEAN	MEAN	MEAN	MEAN	MEAN
20.7	23.6	44.7	94.8	183.6

Table 4.4 : Activation energies for diffusion of Cl^- and Na^+ in uncarbonated OPC and 65% BFS pastes. (in KJ/mole)

	Cl^-	Na^+
OPC	44.6 ± 4.3* 50.2**	83.7**
65% BFS	19.0 ± 3.3	23.9 ± 5.0

* From ref. 116 . ** From ref. 118.

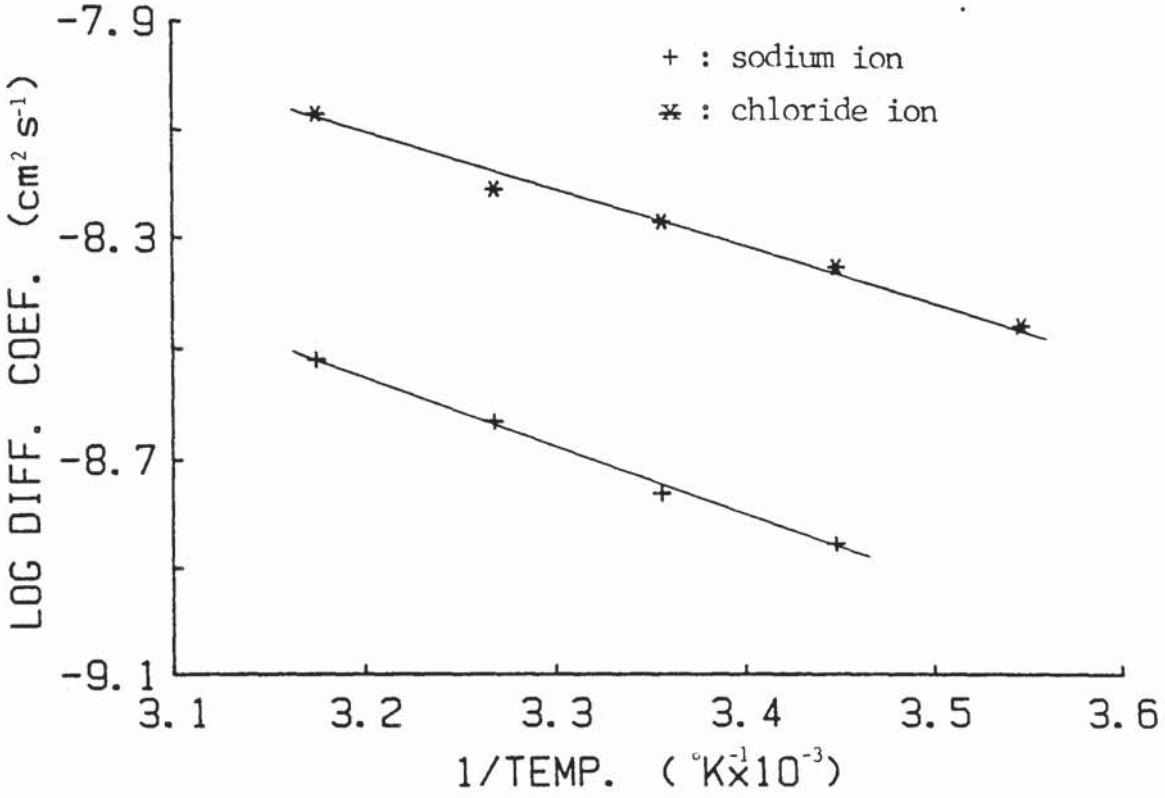

FIGURE 4.4 : Arrhenius plots for diffusion of sodium and chloride ions in uncarbonated 65% BFS cement paste.

4.4.2 DISCUSSION

According to the rate process theory [148], an ion diffusing in an aqueous solution moves randomly to the direction of diffusion and , for a particular "jump", the ion has to jump out of one site in the liquid structure into another site. For the diffusion "jump" to be accomplished, the free energy of the system (site and jumping ion) has to attain a critical value - the activation energy. This energy barrier is the sum of different amounts of energy such as the amount of energy required by the ion to push back molecules to provide space for itself and to break bonds with neighbouring molecules so that it can move into the formed space [149]. There are an infinite number of paths representing the passage of an ion from one site in the liquid structure to the other. The ion, however, moves along the easiest path which corresponds to the lowest energy barrier.

In the case of ionic diffusion in cement pastes, the diffusion process differs from that in a free aqueous solution. There are three additional factors which might influence the diffusion process in cement paste [149]:

(i) the constrained geometry of the pores, which may restrict the movement of ions in certain directions,

(ii) interactions between the diffusing ions and the pore surfaces,

(iii) structural alteration in the pore solution.

The fact that diffusion coefficients for sodium and chloride ions in 65% BFS blended cement paste could both be fitted to unique straight lines on the Arrhenius plots (fig.4.4) suggests that diffusion kinetics in this paste are under the control of a single dominant process over the temperature range considered.

The activation energies for the diffusion of chloride and sodium ions in infinitely dilute aqueous solution are 17.5 KJ/mole and 18.4 KJ/mole respectively [121]. In the case of diffusion of these ions in 65% BFS blended cement pastes the activation energies were found to approach the above values (table 4.4). On the contrary, the activation energies for diffusion in OPC pastes are much higher (table 4.4). As reported by Page et al [116] the latter indicates that the rate-limiting process governing ionic diffusion in OPC pastes may involve desorption of the diffusing ions from binding sites on the pore walls and/or structural rearrangements necessary to accomodate ion migration through surface-bound water. Since diffusion is a rate process, however, it cannot be concluded that in 65% BFS blended pastes, for which the obtained activation energies were low, the diffusion process is necessarily similar to that in a free aqueous solution. The fact that the activation energies in these pastes were found to be lower than those in OPC pastes suggests that the mechanism of surface

interactions in the slag paste is different from that in the OPC paste. The reason for this difference may be associated with the different type of C-S-H gel [150-152] in BFS blended paste. Hydrated pastes of the mineral alite (substituted $3CaO.SiO_2$) exhibit activation energies for ionic diffusion similar to those found in OPC pastes [153]. It would appear from this that the surface interactions in OPC pastes are associated with the C-S-H gel which is common to hydrated alite and hydrated OPC but different for BFS blended cement pastes.

The diffusion coefficient of sodium and chloride ions in 65% BFS blended cement pastes were found to be lower than those in the OPC paste (tables 4.2 and 4.3). This is consistent with the results of others [127-129,154,155] who generally agree that addition of BFS to portland cement leads to a significant retardation of ionic diffusion. A factor responsible for this phenomenon is probably the low porosity (fig 4.5) and discontinuous pore structure [25,44,132] of BFS blended pastes. The small amount of continuous pores in which ions can move may retard ionic diffusion. According to Bakker [156], with BFS cement pastes we have both hydration of clinker grains and slag grains, which take place, from a microscopic point of view, at a different location. The $Ca(OH)_2$ set free by the hydration of clinker, reacts with the acid components, $Al_2O_4^{--}$ and SiO_3^{--}, set free by the hydration of slag and the products of the reaction precipitate

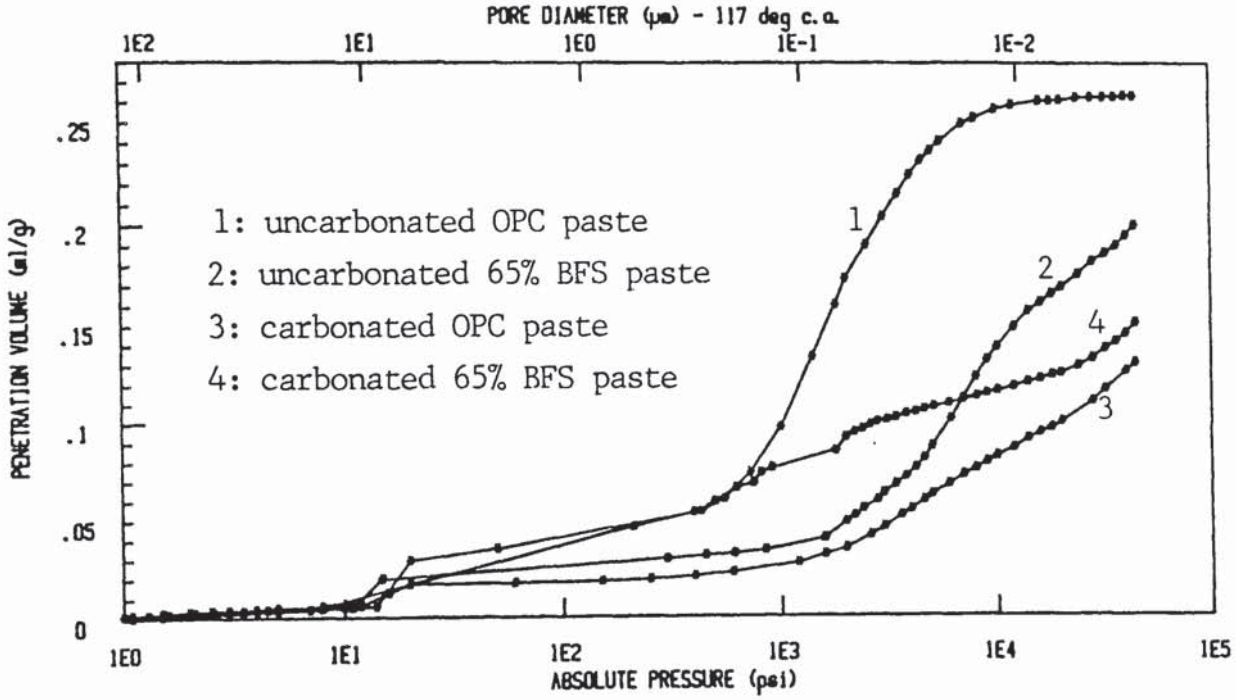

FIGURE 4.5 : Pore size distributions for the pastes studied in chapter 4.

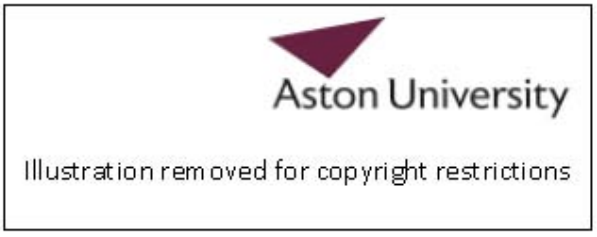

FIGURE 4.6 : Hydration of OPC and BFS-blended cement pastes (from ref. 156).

somewhere in between the clinker and the slag grains, thus blocking the pores between them (fig 4.6a). With OPC pastes there will be only precipitatiion of $Ca(OH)_2$ in the pores without the blocking effect (fig 4.6b).

In agreement with the findings of others (117,122,123,125, 126) diffusion coefficients for sodium ion were found to be about 3 times lower than those for chloride ion (table 4.2). Kondo et al (117) attributed this phenomenon to the counter - diffusion of hydroxyl ions. They suggested that the exchange of chloride and hydroxyl ions, as they counterdiffuse, results in higher diffusion rates for the chloride ion compared to those for the accompanying cation. A verification of this theory was offered by Sergi (37) who found that the excess of Cl^- compared to Na^+ ions in compartment 2 of the diffusion cell was consistent with an equivalent increase of the OH^- concentration in compartment 1, so that a charge balance could be maintained.

Others (122,123,125) have suggested that the difference between the diffusion rates of anions and the accompanying cations is caused by the different interactions between the pore surfaces and the diffusing anions or cations.

Another factor which is probably associated with the higher diffusion rates of anions compared to those of cations is the difference in the size of the hydrated ions. Cations are

usually more hydrated than anions (157) so the smaller, less hydrated, chloride ion can easily penetrate more pores than sodium ion, resulting in higher diffusion rates. This situation is probably more dominant in BFS blended pastes because of their small continuous pores. In the case of cement pastes with larger continuous pores, as probably for the carbonated pastes used in part II, the above situation may exist for ions with larger size. This will be further examined in the next chapter in which the geometrical characteristics of the pore structure are investigated.

PART II : ALTERATION OF THE PORE SYSTEM BY CARBONATION

4.4.3 RESULTS

Figure 4.7 represents a typical plot of ion concentration in compartment 2 of the diffusion cell versus time of diffusion. As in the case of the uncarbonated pastes (part I) the concentration increases linearly with time. In contrast to part I, however, the rate of increase of the concentration in compartment 2 is the same for both the chloride and sodium ions.

From the gradient of the rectilinear plots of the concentration in compartment 2 versus time, diffusion coefficients for chloride and sodium ions were calculated as described in part I. The calculated diffusion coefficients are

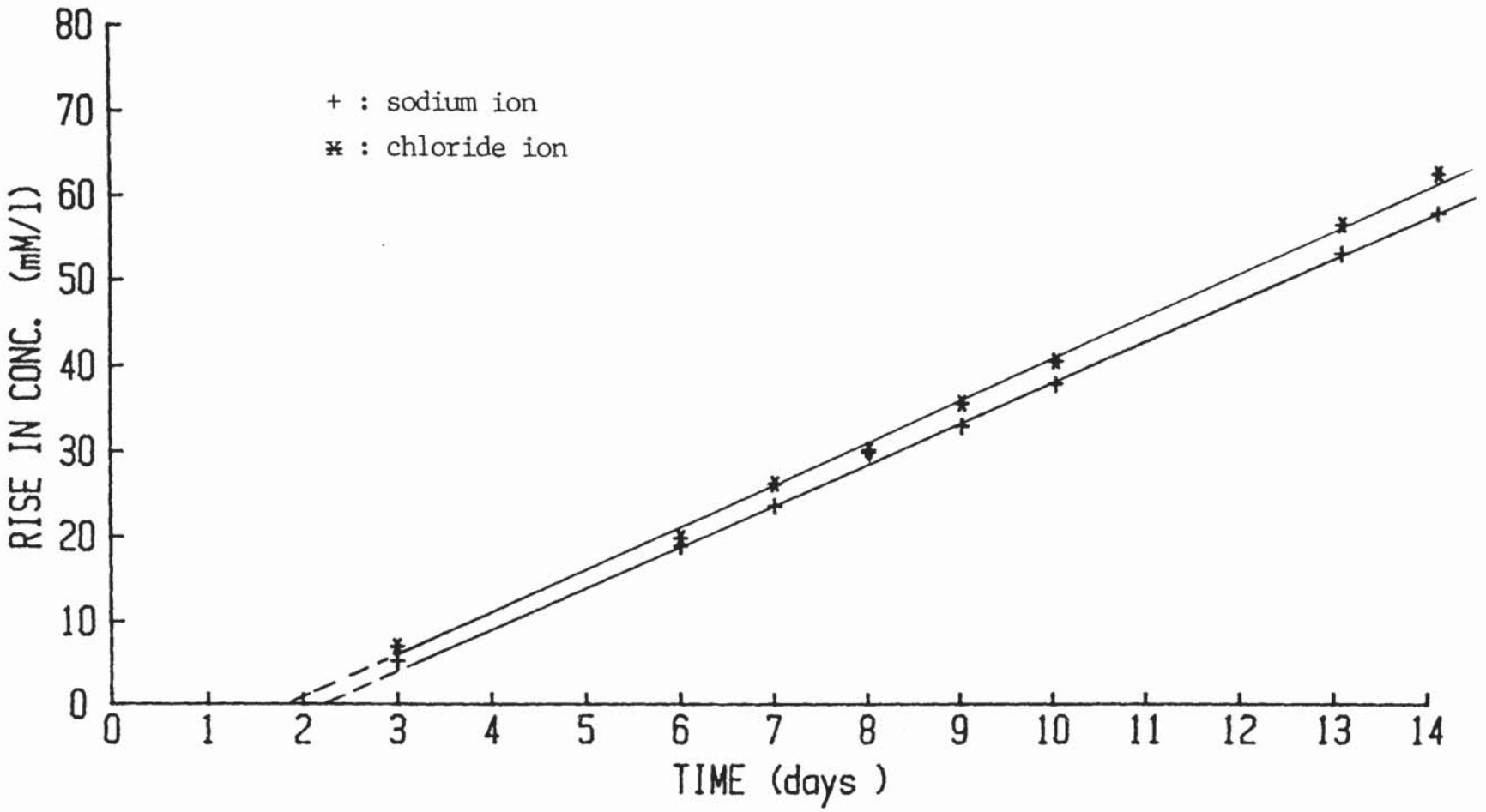

FIGURE 4.7 : Rise in concentration of chloride and sodium ions in the compartment 2 of the diffusion cell No 1 at 25 °C (OPC paste carbonated in 100% CO_2).

tabulated in table 4.5 for carbonated OPC paste and in table 4.6 for carbonated 65% BFS cement paste. From these data it is clear that at all five temperatures : (i) the diffusivities of both ions are much higher in the carbonated 65%BFS cement paste than in the carbonated OPC paste, (ii) the diffusion coefficients of sodium and chloride ions are the same for both the types of cement pastes tested, and (iii) the obtained diffusion coefficients are much higher than those for uncarbonated cement pastes obtained in part I, in which it was also shown that chloride ion diffuses faster than sodium ion.

From the data in tables 4.5 and 4.6, best fit Arrhenius plots were constructed by means of linear regression analysis (figures 4.8 and 4.9). The correlation coefficients for the obtained lines are -0.88 and -0.85 for chloride and sodium ion respectively in carbonated OPC paste and -0.97 for both chloride and sodium ions in carbonated 65% BFS blended cement paste. The activation energies corresponded to the slopes of these lines are shown with 95% confidence limits in table 4.7 (a worked example can be found in appendix 14).

Table 4.5: Effective diffusion coefficients of Cl^- and Na^+ ions in carbonated OPC paste. (D x 10^8 cm^2s^{-1})

CHLORIDE ION				
9°C	17°C	25°C	33°C	42°C
8.63	12.44	14.81	22.71	27.91
10.23	12.73	12.74	18.10	35.74
4.08	15.01	14.48	17.16	21.24
11.94	14.02	13.40	20.48	27.49
6.92	11.50	13.44	20.75	22.10
MEAN	MEAN	MEAN	MEAN	MEAN
8.36	13.14	13.77	19.84	26.90
SODIUM ION				
9.29	13.95	14.52	23.89	30.98
10.16	13.14	11.69	11.67	38.09
4.46	14.98	15.10	21.35	22.04
12.11	15.39	13.90	24.37	28.96
7.46	10.60	15.06	22.72	20.51
MEAN	MEAN	MEAN	MEAN	MEAN
8.70	13.61	14.05	20.80	28.12

Table 4.6: Effective diffusion coefficients of Cl^- and Na^+ ions in carbonated 65% BFS/OPC paste ($Dx10^8$ cm^2 s^{-1}).

9°C	17°C	25°C	33°C	42°C
CHLORIDE ION				
32.51	46.00	46.35	87.45	101.94
31.99	47.58	53.15	85.71	117.94
34.04	41.41	58.36	95.12	114.01
34.75	35.37	50.55	88.24	111.90
28.97	50.06	56.55	86.81	111.01
MEAN	MEAN	MEAN	MEAN	MEAN
32.45	44.08	52.99	88.67	111.36
SODIUM ION				
23.71	46.36	62.37	107.83	118.86
32.21	51.51	64.43	104.95	109.40
36.98	44.11	68.36	104.58	110.92
39.36	44.87	64.12	100.48	111.24
31.55	54.44	61.83	103.27	106.93
MEAN	MEAN	MEAN	MEAN	MEAN
32.76	48.26	64.22	104.22	111.42

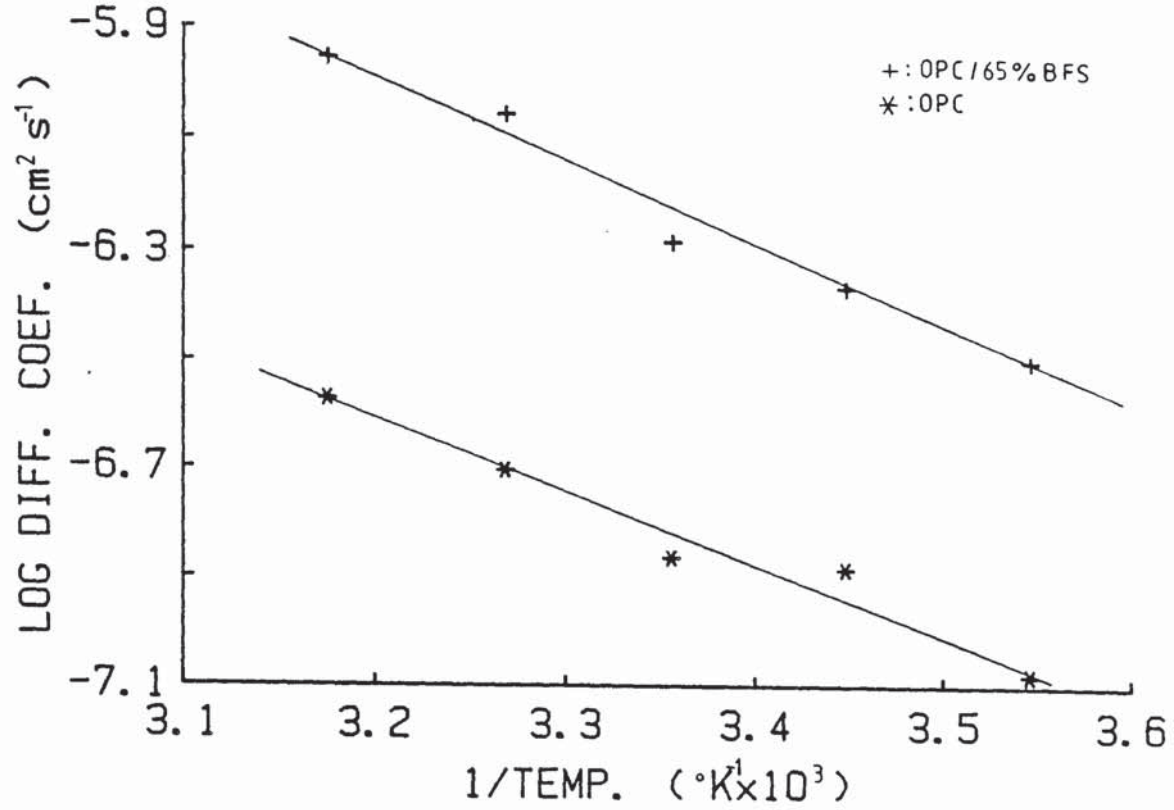

FIGURE 4.8 : Arrhenius plots for diffusion of chloride ions in OPC and OPC/65% BFS pastes carbonated in 100% CO_2.

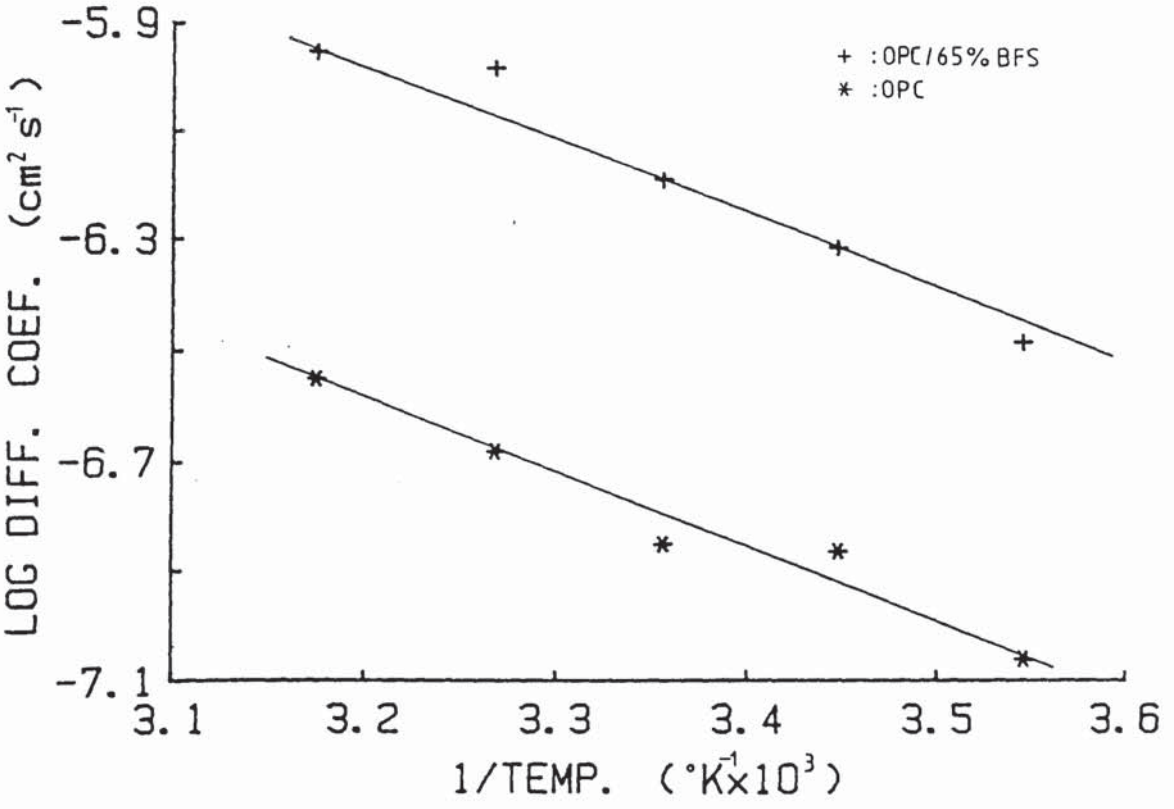

FIGURE 4.9 : Arrhenius plots for diffusion of sodium ions in OPC and OPC/65% BFS pastes carbonated in 100% CO_2.

Table 4.7: Activation energies for diffusion of Cl^- and Na^+ in carbonated OPC and 65% BFS pastes. (in KJ/mole)

	Cl^-	Na^+
OPC	25.6 ± 6.0	25.3 ± 6.6
65% BFS	28.6 ± 3.6	29.3 ± 4.1

4.4.4 DISCUSSION

As for the results obtained with the uncarbonated 65% BFS blended pastes (part I), the diffusion coefficients for sodium and chloride ions in both the carbonated pastes tested could be fitted to unique straight lines on the Arrhenius plots (fig 4.8 and 4.9). As mentioned in part I, this suggests that diffusion kinetics in these pastes are under the control of a single dominant process over the temperature range considered. The fairly low activation energies obtained for the diffusion of Na^+ and Cl^- ions in both the types of carbonated pastes used (table 4.7) suggests that the mechanism of ionic diffusion in these pastes may be similar to that in the 65% BFS paste used in part I.

Figure 4.10 shows the changes in phase composition after carbonation of OPC and 65% BFS cement pastes, in terms of their DTA thermographs. The common changes observed for the two pastes are probably one of the reasons for their similar low activation energies for ionic diffusion. These common changes, caused by carbonation, are the replacement of $Ca(OH)_2$, calcium sulphoaluminate and C_4AH_{13} mainly with calcite, and the reduction of the peak just above 100^oC which represents the C-S-H gel.

An additional factor which may affect the diffusion mechanism in the carbonated pastes is their different pore

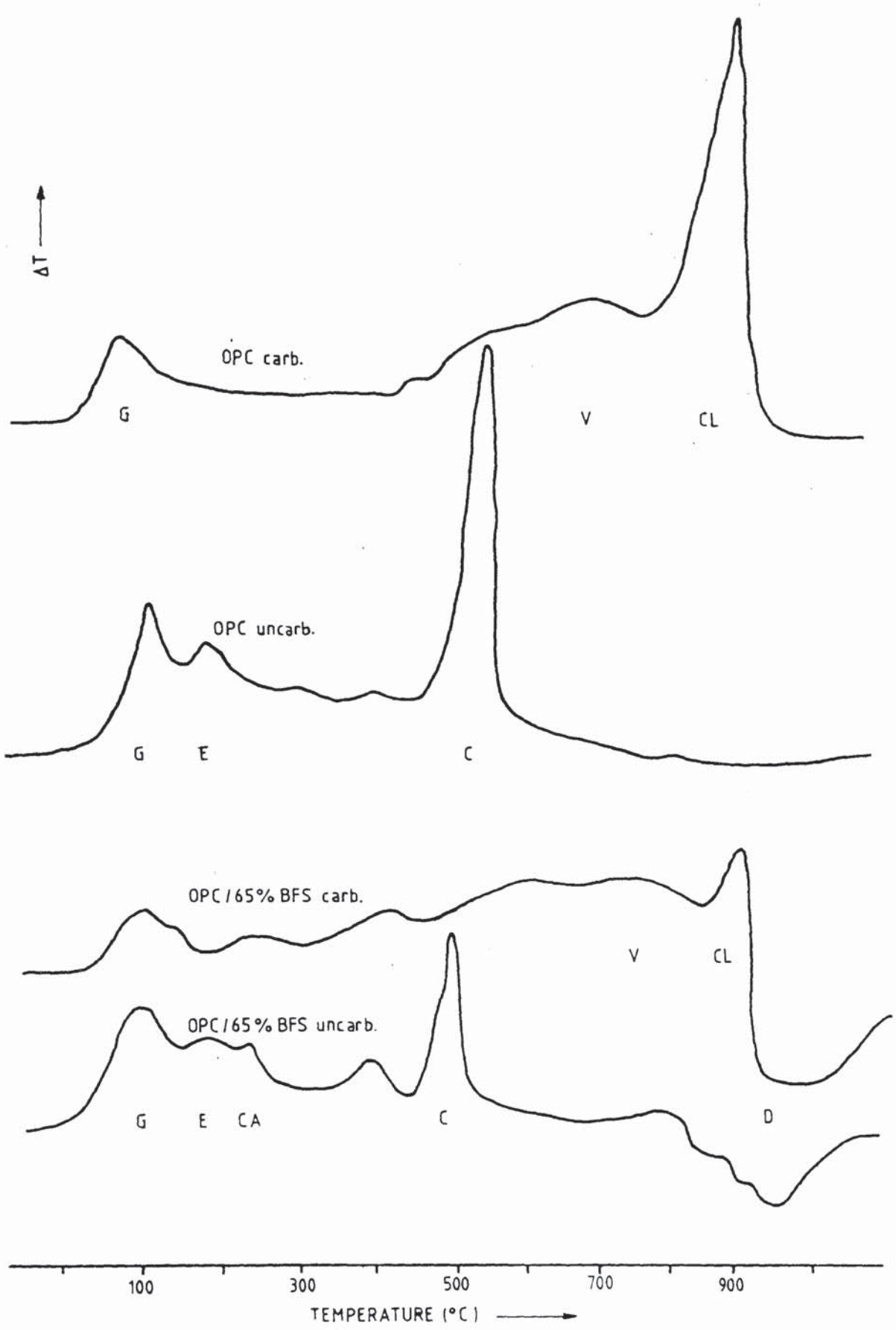

FIGURE 4.10 : DTA thermographs of carbonated and uncarbonated OPC and 65% BFS/ OPC pastes. G = C-S-H gel, E = ettringite, CA = C_4AH_{13}, C = calcium hydroxide, V = vaterite, CL = calcite, D = devitrification of glassy phase.

solution. In chapter 3 it was found that, contrary to the uncarbonated pastes, in the pore solution of carbonated pastes there are high concentrations of calcium, magnesium, and silicate ions. The interactions of these solutes with the diffusing ions may affect the diffusion mechanism.

By comparing the pore size distribution of the carbonated and uncarbonated OPC pastes (fig 4.5) it can be seen that the volume of pores in the uncarbonated paste is much higher than that in the carbonated paste. On the contrary, however, the diffusion coefficients of the carbonated paste are much higher. It would appear from this that in the uncarbonated OPC paste the interactions of the diffusing ions with the surrounding medium dominate and the final result is the retardation of ionic diffusion.

On the other hand, however, by comparing the carbonated OPC paste and the carbonated 65% BFS paste, for which the mechanism of ionic diffusion may be assumed to be similar (similar values of activation energies), it can be seen (fig 4.5) that the paste with the larger volume of pores offers the lesser resistance to ionic diffusion (tables 4.5 and 4.6).

The calculated diffusion coefficients of the pastes used in this chapter are in the decreasing order of $D_{carb.BFS}$, $D_{carb.OPC}$, $D_{unc.OPC}$, $D_{unc.BFS}$ (tables 4.2,4.3,4.5,4.6). The decreasing order of the total porosities of these pastes (fig

4.5), however, is different. This indicates that there is no direct relation between total porosity and ionic diffusion. The characterization of cement pastes according to their resistance to ionic diffusion using the total porosity can therefore be misleading.

Contrary to the results for the uncarbonated pastes, in both the carbonated pastes used in this chapter, sodium ion was found to have the same diffusion coefficient as chloride ion. A factor contributing to this phenomenon is probably the insignificant concentration in carbonated pastes of OH^- ions, which as mentioned in part I, exchange Cl^- ions as they counterdiffuse in the uncarbonated materials.

In part I it was suggested that another factor which is probably associated with the higher diffusion rates of anions, compared to those of cations, in uncarbonated OPC and 65% BFS pastes is the difference in the size of the hydrated ions which enables the smaller chloride ions to move more "easily" in the pores than sodium ions. The fact that in the carbonated pastes Na^+ and Cl^- ions have the same diffusion coefficients and that this does not happen with larger ions (see chapter 5), may indicate that after carbonation the size of the continuous pores increases, so that ions in the size range of hydrated Cl^- and Na^+ ions may have the same "degrees of freedom" in the pores. This may be associated with the increase of the volume of pores greater than 40nm,

after carbonation found in chapter 3.

4.5 CONCLUSIONS

The conclusions obtained from this chapter can be summarized as follows:

(1) The mechanism of ionic diffusion in OPC paste is different from that in 65% BFS blended cement paste or in carbonated OPC and 65% BFS cement pastes.

(2) There is no direct relation between total porosity and ionic diffusion in cement pastes.

(3) Cement pastes with 65% BFS content display high resistance to ionic diffusion, compared to ordinary portland cement pastes of equal w/c.

(4) Carbonation decreases the resistance of cement pastes to ionic diffusion, moreso for 65% BFS blended cement pastes than portland cement pastes.

(5) In carbonated pastes, chloride ions diffuse with the same rate as the co-diffusing sodium ions.

(6) In uncarbonated 65% BFS blended cement paste chloride ions diffuse faster than the co-diffusing sodium ions.

CHAPTER 5: Effect of geometrical characteristics of the pore structure on ionic diffusion.

5.1 INTRODUCTION

The general examination of ionic penetration in hardened cement paste, in chapter 4, has shown that the main way for aggressive ions to enter into hardened cement paste, and thus into concrete, is by diffusion through the pores. From the various types of cement pastes examined it was found that, in general, the most important factors affecting ionic diffusion are the interactions of the diffusing ions with the pore surfaces and the geometry of the continuous pores in which diffusion takes place. Although in the literature there are a number of published studies [122,123,125,126] which examine the effect of surface interactions on ionic diffusion, there is a lack of experimental data concerning the effect of the geometry of pores on ionic diffusion. The aim of this chapter is to present some experimental data which can contribute to the understanding of the relationship between ionic diffusion and the geometry of the pores. The fact that the activation energies for ionic diffusion in the carbonated pastes tested in chapter 4 were found to be, within experimental error, the same (suggesting a similar mechanism of ionic diffusion), together with the fact that in these pastes sodium and chloride ions were found to diffuse with the same, relatively high, speed make the carbonated

pastes a simple system for the examination of this relationship.

The general principle of the method employed was to compare the kinetics of ionic diffusion in carbonated cement pastes, for ions with different radii. The ions needed for the experiment had to satisfy two requirements:

(1) constant shape and charge,

(2) known radii for the hydrated ions.

Examples of such ions are the quaternary ammonium ions (158). By increasing the chain length of the constituent alkyl groups their ionic radius increases without changing their shape or charge. In addition, their large size, symmetrical shape and low charge, enable the calculation of the radii for the hydrated ions from their limiting mobilities, as will be explained in the next paragraph.

5.2 IONIC RADII FOR THE HYDRATED IONS

Because of the polar nature of the water molecule, and hence its potential to interact with dissolved ions, the size of an ion in water can not be considered simply in terms of its crystallographic radius. The kinetic entity which is called ion, may be the bare ion or it may carry with it water molecules sufficiently firmly bound to be regarded as part of the ion.

The most direct method available for the determination of the size of the kinetic unit is based on Stokes' law (159) which is derived from classical hydrodynamics. According to it, the radius of a large spherical ion is given by the following equation:

$$r = \frac{0.820 \mid Z \mid}{\lambda \; n} \qquad \text{(ref. 159)}$$

where: r = the ionic radius (Å)

Z = the valency of the ion

λ = the ionic equivalent conductivity ($cm^2 \Omega^{-1} equiv^{-1}$)

n = the viscosity of the medium (poise).

For small ions, the conditions for the validity of Stokes' law are not fulfilled. Robinson and Stokes (159) have shown that Stokes' law is of the correct form for ions which fall in two categories:

(a) ions which are intrinsically large and of low surface charge, and

(b) ions of sufficiently large surface charge to form firmly hydrated entities.

As they pointed out, however, the numerical constant of the Stokes' equation may be different. To overcome this problem they estimated correction factors to Stokes' law in water (fig. 5.1) which enabled them to calculate ionic radii for any ion with symmetrical shape and Stokes' law radius greater than about 2 Å.

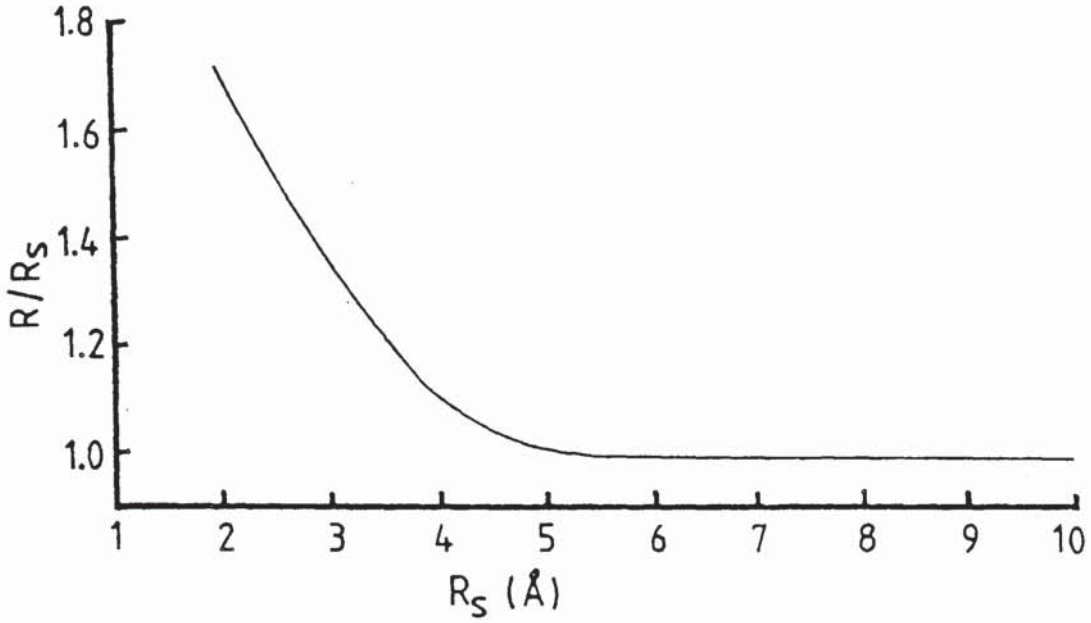

FIGURE 5.1: Correction factors for Stokes' law in water at 25°C (from ref. 159).

R_S = Stokes' law radius, R/R_S = correction factor

Table 5.1: Radii of the hydrated ions (from ref.159).

Ion	R(Å)
$N(C_2H_5)^+_4$	4.00
$N(C_3H_7)^+_4$	4.52
$N(C_4H_9)^+_4$	4.94
$N(C_5H_{11})^+_4$	5.27
Na^+	3.30

The hydrated radii of the ions used in this chapter are tabulated in table 5.1 according to the results of Robinson and Stokes (159).

5.3 EXPERIMENTAL PROCEDURE

The experimental work carried out consisted mainly of diffusion coefficient measurements for six different ions in carbonated OPC and OPC/65%BFS cement pastes. In order to examine the influence of the co-diffusing ion, parallel experiments were carried out for the same ions as bromides and as chlorides.

5.3.1 Specimen preparation

Cylindrical specimens of 0.5 w/c ratio made with 100% OPC and 35%OPC/65%BFS were prepared as decribed in chapter 3 (section 3.3.1). After a curing period of 28 days in a high humidity room at 22^{o}C they were demoulded and their middle sections sliced into 2.3 mm to 2.8 mm discs as described in section 3.3.1. The discs were then lightly ground on 600 grade carbide paper, rinsed with deionized water and finally placed, as described in section 3.3.2, in air tight containers in which the relative humidity was maintained at 65%. At 24 hour intervals, 100% CO_2 gas was passed over the discs and through a water trap for half an hour. The carbonation procedure was terminated 60 days after the complete

carbonation of the discs was detected using phenolphthalein (98).

5.3.2 Experimental set up

The carbonated cement paste discs were fitted between the two compartments of the diffusion cells used in chapter 4 (figure 4.2). Compartment 1 of each cell was filled with 0.1 M of the investigated ionic species, while compartment 2 was filled with a known volume of deionized water. Four cells were set up for each condition tested and were then placed in a water bath of a constant temperature of 25°C. On a regular basis, a certain amount of the solution in compartment 2 was withdrawn and analysed for sodium, chloride or quaternary ammonium ions, by the methods described in chapter 2. The withdrawn solutions, one ml for the case of tetraethylammonium ions and 0.1 ml for the rest of the ions, were not replaced as the effect of the overall reduction in volume on the calculated diffusion coefficients was insignificant. The experiments were terminated before the concentration in compartment 2 had reached 0.01 M, after at least six readings had been recorded. On completion of each set of diffusion measurements, the thicknesses of the discs were determined by means of a micrometer gauge.

Samples of both types of specimens used were dried in an oven at 105°C and subjected to mercury intrusion

porosimenty as described in chapter 2.

5.4 RESULTS

Figure 5.2 represents a typical plot of the rise in concentration of the ions in compartment 2 with time. It can be seen that after a period of time, when diffusion becomes established across the disc, the concentration of both the quaternary ammonium ions and the chloride ions in compartment 2 increases linearly with time.

As in the case of sodium and chloride ions in chapter 4, assuming that conditions of quasi-steady state diffusion are operating across the disc, Fick's first law can be applied. A solution of it (see appendix 12) enables the calculation of the diffusion coefficient from the following equation:

$$D = \frac{S\ V_2\ l}{A\ (C_1 - C_2)}$$

where: D = the diffusion coefficient ($cm^2 sec^{-1}$)

V_2 = the volume of the solution in comp. 2 (cm^3)

A = the cross-sectional area of the disc (cm^2)

l = the thickness of the disc (cm)

C_1, C_2 = the concentrations of the investigated ionic species in comp. 1 and 2 (mole cm^{-3})

S = the gradient of the rectilinear plot of C_2 versus time.

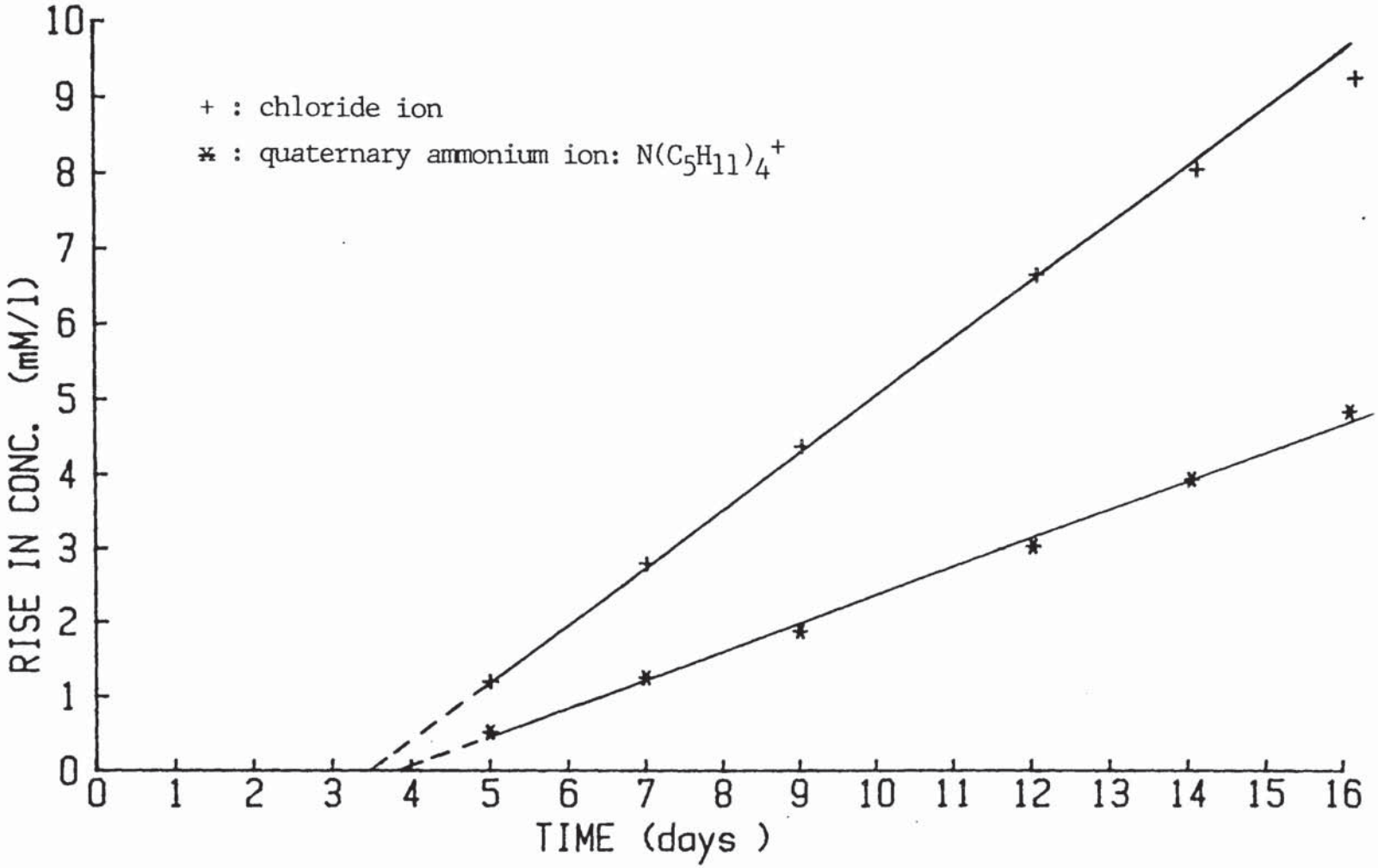

FIGURE 5.2 : Concentration versus time for chloride and quaternary ammonium ions, $N(C_5H_{11})_4^+$, in compartment 2 of the diffusion cell No 4 (OPC carbonated paste).

The calculated values of the diffusion coefficients are tabulated in tables 5.2 to 5.5. Tables 5.2 and 5.3 show the diffusion coefficients for the quaternary ammonium ions as bromides in OPC and 65% BFS carbonated cement pastes respectively. Plots of these data versus the corresponding ionic radii, are presented in figure 5.3. Tables 5.4 and 5.5 show the diffusion coefficients for sodium and quaternary ammonium ions as chlorides, for OPC and 65% BFS carbonated cement pastes respectively. The diffusion coefficients for the co- diffusing chloride ions are also tabulated in the same tables. Figure 5.4 shows the plots of the diffusion coefficients for the sodium and quaternary ammonium ions versus their ionic radii.

Useful information about the mechanism of ionic diffusion can be obtained by comparing the diffusion coefficients in cement pastes (D) with those in infinitely dilute solutions (D_o) in table 5.6, calculated from the limiting equivalent conductivites [159]. Their ratio, Do/D, can be considered as a measure of the retardation of ionic diffusion caused by cement paste. Figures 5.5 and 5.6 show the change of this ratio with the ionic radius of the diffusing ion, in OPC and 65% BFS carbonated cement pastes respectively.

Finally, figure 5.7 shows the pore size distributions of the two types of carbonated cement pastes tested.

Table 5.2: Diffusion coefficients for quaternary ammonium ions as bromides in carbonated OPC paste ($D \times 10^7 cm^2 s^{-1}$).

cell No	$N(C_2H_5)_4^+$	$N(C_3H_7)_4^+$	$N(C_4H_9)_4^+$	$N(C_5H_{11})_4^+$
1	2.2	1.1	0.43	0.59
2	1.3	1.0	0.56	0.45
3	2.2	0.9	0.39	0.40
4	1.7	1.1	0.44	0.52
MEAN	1.8	1.0	0.46	0.49

Table 5.3: Diffusion coefficients for quaternary ammonium ions, as bromides in carbonated 65% BFS cement pastes ($D \times 10^7 cm^2 s^{-1}$).

cell No	$N(C_2H_5)_4^+$	$N(C_3H_9)_4^+$	$N(C_4H_9)_4^+$	$N(C_5H_{11})_4^+$
1	4.5	1.4	1.5	0.91
2	4.9	1.5	1.1	1.06
3	4.9	1.4	1.1	0.99
4	4.0	1.9	1.3	0.98
MEAN	4.6	1.5	1.3	0.99

Table 5.4: Diffusion coefficients for quaternary ammonium ions, as chlorides and for the co-diffusing chloride ions, in carbonated OPC paste ($D \times 10^7$ cm^2s^{-1}).

cell No	$N(C_2H_5)_4^+$	$N(C_4H_9)_4^+$	$N(C_5H_{11})_4^+$	Na^+
1	1.0	0.65	0.80	2.6
2	1.5	0.64	0.65	2.4
3	1.0	0.47	0.25	2.1
4	1.5	0.55	1.05	2.5
MEAN	1.3	0.58	0.69	2.4
Co-diffusing chloride ions				
1	1.6	1.4	1.7	2.5
2	2.2	1.8	1.5	2.3
3	1.6	1.2	1.0	2.0
4	2.1	1.5	2.0	2.3
MEAN	1.9	1.5	1.5	2.3

Table 5.5: Diffusion coefficients for quaternary ammonium ions as chlorides and for the co-diffusing chloride ions, in carbonated 65% BFS cement paste ($D \times 10^7$ cm^2s^{-1}).

cell No	$N(C_2H_5)_4^+$	$N(C_4H_9)_4^+$	$N(C_5H_{11})_4^+$	Na^+
1	2.6	1.6	1.8	5.3
2	2.5	1.8	1.6	6.1
3	3.6	1.7	1.9	5.0
4	4.5	1.7	1.7	5.5
MEAN	3.3	1.7	1.7	5.5
Co-diffusing chloride ions				
1	3.9	3.1	2.9	5.5
2	3.9	3,4	3.1	4.8
3	3.6	3.4	3.0	5.1
4	4.8	3.9	2.9	5.9
MEAN	4.1	3.5	3.0	5.3

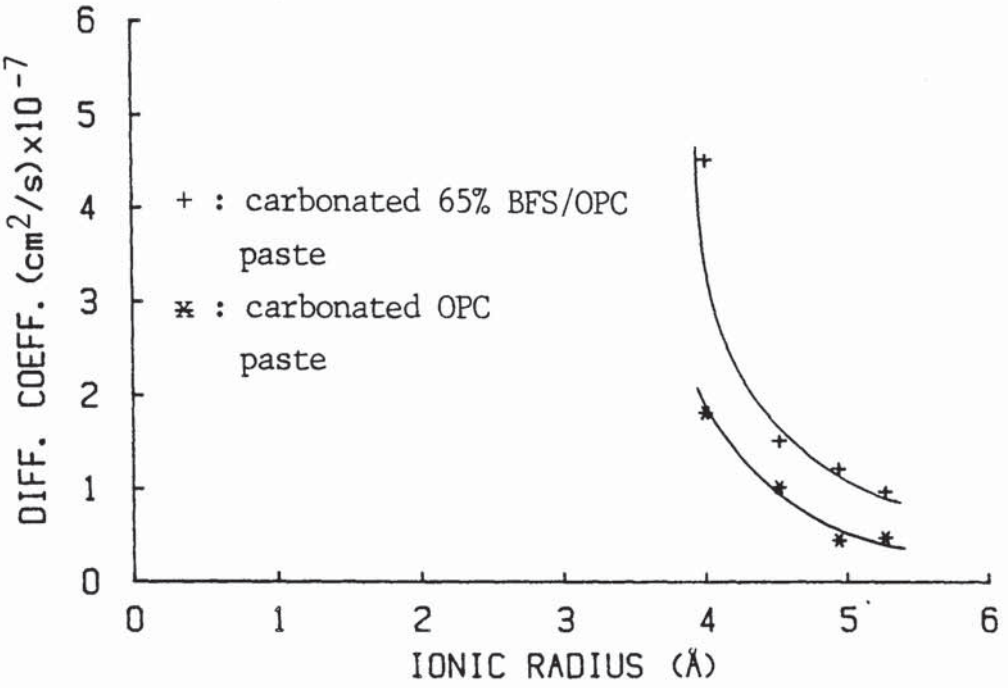

FIGURE 5.3 : Diffusion coefficient versus ionic radius for quaternary ammonium ions as bromides.

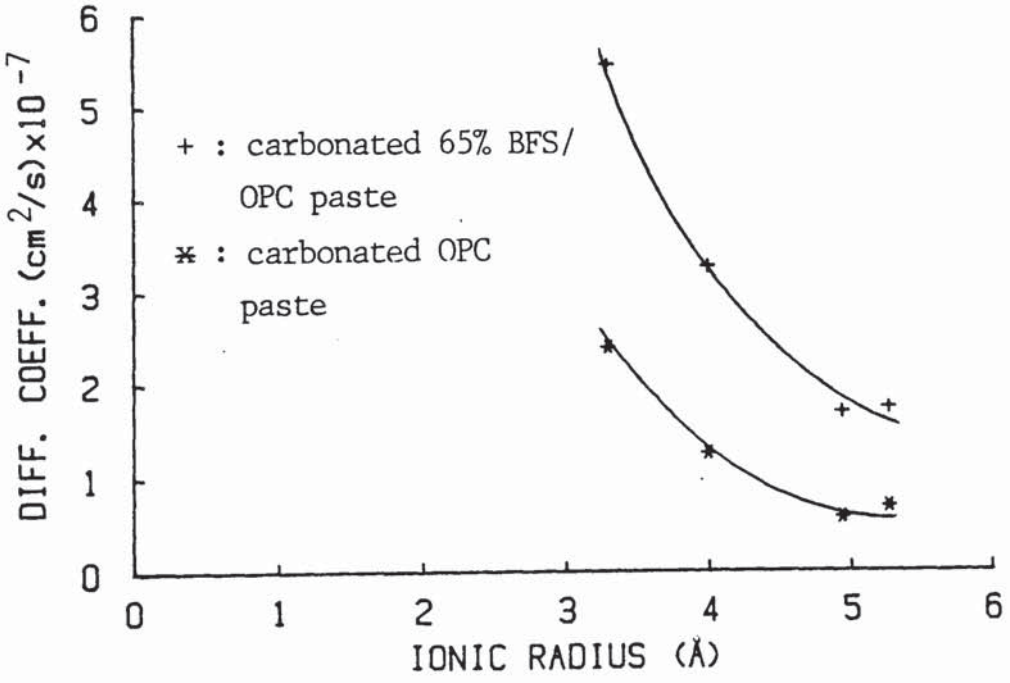

FIGURE 5.4 : Diffusion coefficient versus ionic radius for quaternary ammonium ions and sodium ion as chlorides.

Table 5.6: Ionic diffusion coefficients for the infinitely dilute aqueous solution at 25°C (cm^2s^{-1}).

Ion	D_o
Cl^-	2.03×10^{-5}
Na^+	1.33×10^{-5}
$N(C_2H_5)_4^+$	8.69×10^{-6}
$N(C_3H_7)_4+$	6.23×10^{-6}
$N(C_4H_9)_4^+$	5.18×10^{-6}
$N(C_5H_{11})_4^+$	4.65×10^{-6}

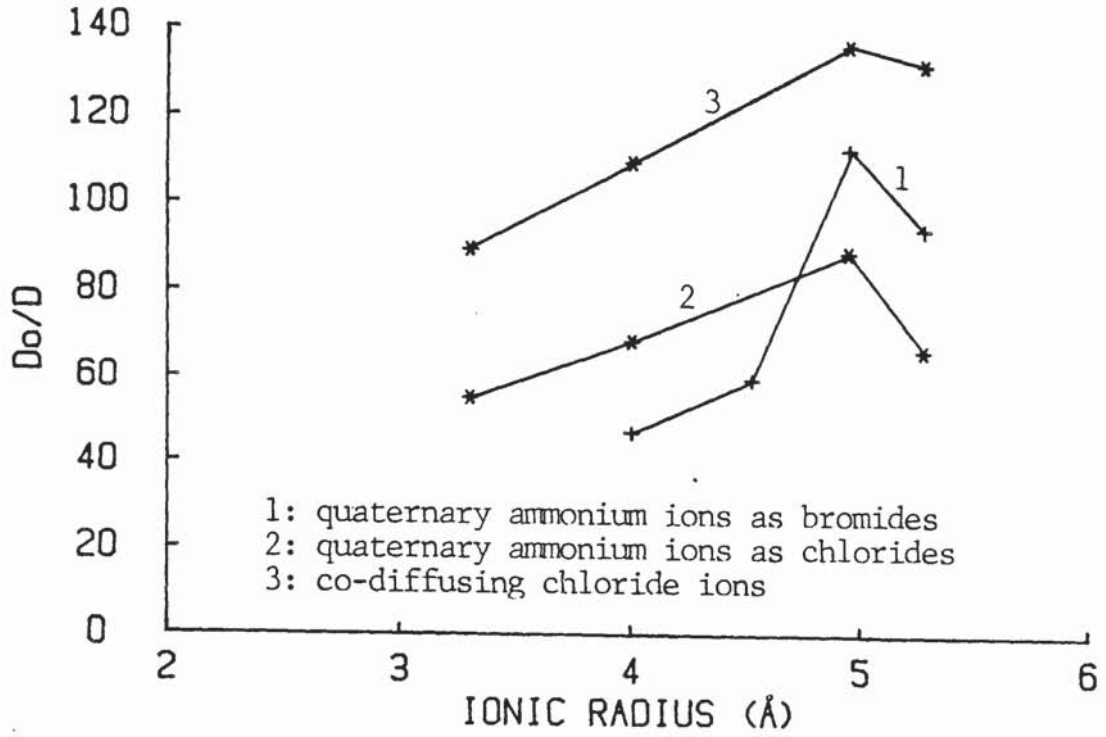

FIGURE 5.5 : The ratio D_o/D versus ionic radius for quaternary ammonium ions diffusing in carbonated OPC paste.

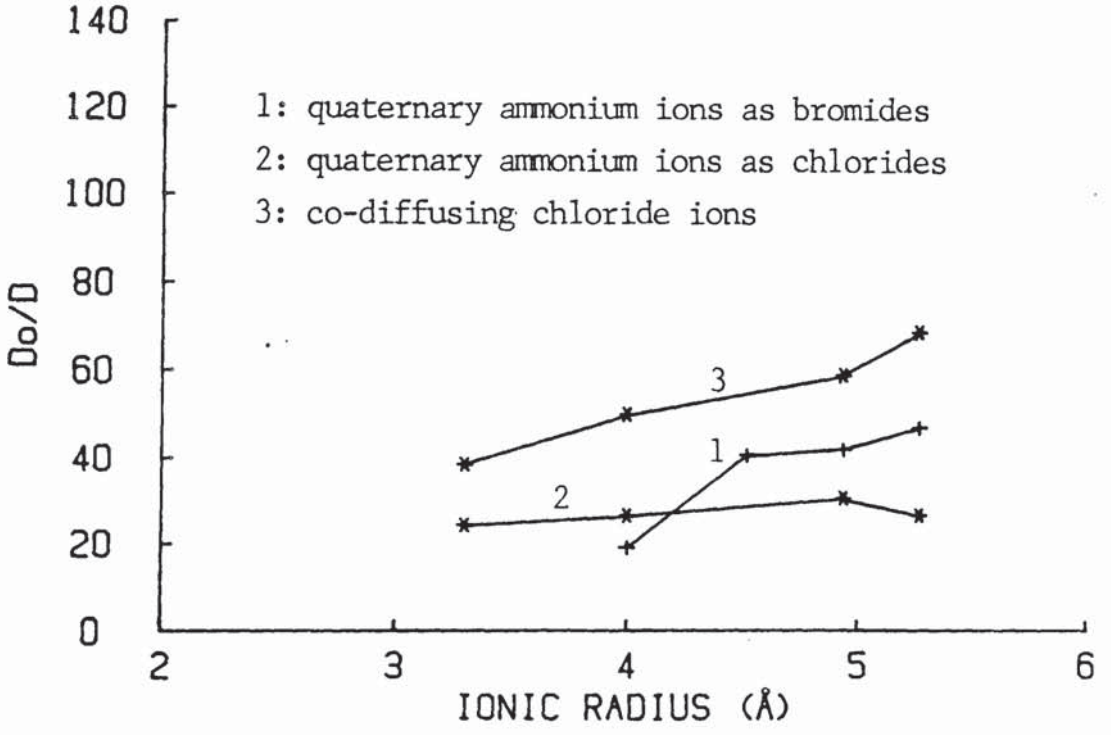

FIGURE 5.6 : The ratio D_o/D versus ionic radius for quaternary ammonium ions diffusing in carbonated 65% BFS/OPC paste.

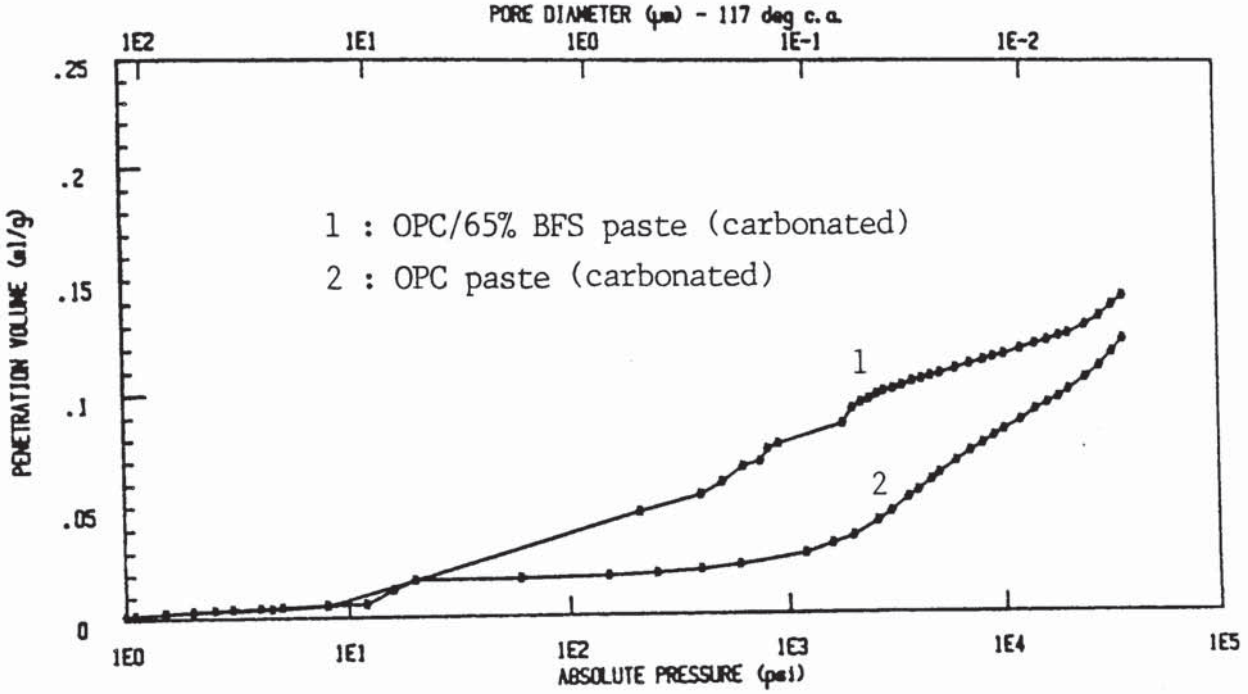

FIGURE 5.7 : Pore size distributions for carbonated OPC and OPC/65% BFS cement pastes.

5.5 DISCUSSION

As can be seen from figure 5.3, the curves obtained by plotting the diffusion coefficients for the quaternary ammonium ions as bromides versus their ionic radii, for the OPC and the 65% BFS carbonated cement pastes, are similar. This supports the suggestion made in chapter 4 that the mechanisms of ionic diffusion in these two types of carbonated cement paste are similar. Further support comes from the fact that the same situation exists in figure 5.4 which represents the equivalent curves for sodium ion and quaternary ammonium ions as chlorides.

The fact that in both figures the diffusion coefficients for the carbonated 65% BFS paste are higher than those of the carbonated OPC paste may be associated with the larger volume of pores of the former (see figure 5.7). Comparing the curves obtained for bromides (fig. 5.3) with those obtained for chlorides (fig. 5.4) it can be seen that they are different. The fact that the only difference between the two situations is the different anions, indicates that the diffusion of cations is affected by the co-diffusing anions. In addition, it is clear that anions are affected by co-diffusing cations because the diffusion coefficient for chloride ion in both the carbonated pastes (tables 5.4 and 5.5) changes with the co-diffusing cation (the other factors affecting ionic diffusion remaining constant). Therefore co-diffusing anions

and cations are mutually influenced.

Figure 5.5 (curves 1 and 2) shows that the ratio D_o/D, which can be considered as a measure of the retardation of ionic diffusion caused by cement pastes, increases with the increase of ionic radius up to 5 Å. For ionic radii larger than that value, however, it appears to decrease. A similar situation exists when the ratio D_o/D for chloride ion is plotted against the radius of the co-diffusing quaternary ammonium ions (curve 3). This indicates, as mentioned earlier, that the diffusion of anions is influenced by the diffusion of the accompanying cations.

The ratio D_o/D for ions larger than 5Å decreases because the numerator (D_o) i.e. the diffusion coefficient in infinitely dilute solution, decreases with the size of the ions (table 5.6), whereas the denomenator (D) remains effectively unchanged for ions larger than a critical size (see tables 5.2 to 5.5). The latter is possibly caused by a decrease of the volume of continuous pores larger than the critical size which causes only small further reduction of the diffusion coefficient, for any increase of ionic radius beyond the critical size.

Figure 5.6 shows the variation of the ratio D_o/D versus the radii of ions diffusing in carbonated 65% BFS cement paste.

By comparing this figure with the equivalent figure for the carbonated OPC paste (fig. 5.5) two conclusions can be obtained :

(1) the slag paste offers a lower resistance to ionic diffusion,

(2) the earlier-mentioned "critical" pore size of the slag paste is larger than that of the OPC paste.

Both these conclusions may be associated with the larger volume of pores of the carbonated slag paste (fig. 5.7).

Useful information on the mechanism of ionic diffusion can be obtained by plotting together the diffusion coefficients of quaternary ammonium ions versus their ionic radii, and the diffusion coefficients of the co-diffusing chloride ions versus the ionic radii of the corresponding quaternary ammonium ions. Figure 5.8 is for the carbonated OPC paste and figure 5.9 is for the carbonated 65% BFS paste. The two curves in each figure meet at the point which corresponds to sodium and chloride ions. Since chloride and sodium ions have, within experimental error, the same diffusion coefficients for carbonated pastes, their points on these plots coincide. As the size of the diffusing cation increases, however, the difference between the diffusion coefficients of chloride ions and the accompanying quaternary ammonium ions increases. The explanation for this phenomenon is probably complicated because ionic diffusion is affected by many factors. The effect of the geometrical characteristics

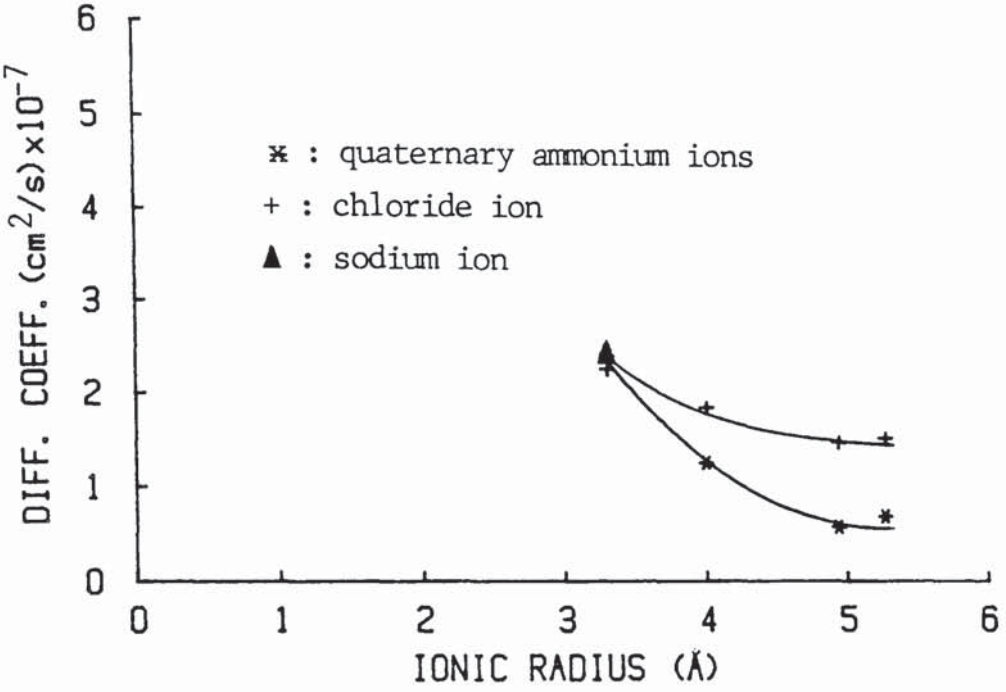

FIGURE 5.8 : Diffusion coefficients of cations and co-diffusing anions versus the radii of the cations for carbonated OPC paste.

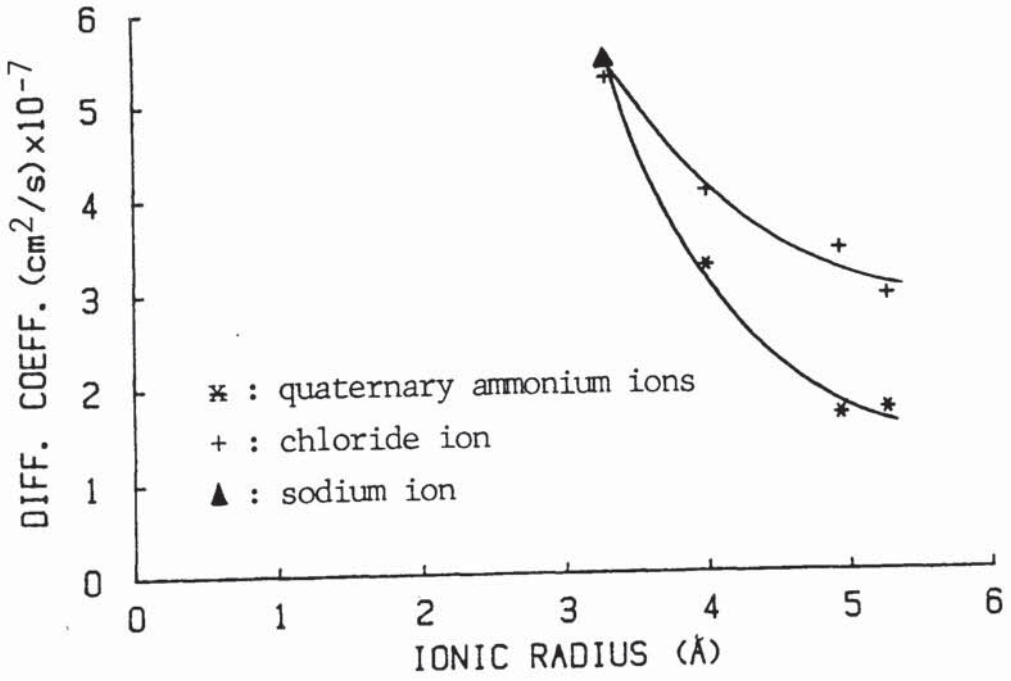

FIGURE 5.9 : Diffusion coefficients of cations and co-diffusing anions versus the radii of the cations for carbonated 65% BFS cement paste.

of the pores on ionic diffusion, however, can be speculated on by taking into account the difference between the size of chloride ion and quaternary ammonium ions. Chloride ion, which is a relatively small ion and more mobile than the quaternary ammonium ions [159], may diffuse more easily through the pores of cement paste. By doing so, it creates on a microscopic scale a charge separation,i.e. a gradient of electric potential. This may tend to increase the speed of the cation and decrease that of the anion. Because of the large size of the quaternary ammonium ions and the constrained space in which they can move, however, it may be assumed that their speed can increase only up to a certain value depending on the size of pores and the size of the ion. Any imbalance in charge resulting from the unequal migration of ions should be restored by the counter diffusion of other ions present in the cement paste. As the size of the cation decreases, however, it moves more easily through the pores and so its speed of migration approaches that of the smaller chloride ion.

In the case of diffusion of NaCl, contrary to the diffusion of quaternary ammonium chlorides, anions and cations were found to diffuse with the same speed probably because of the following reasons:

(1) charge density on the surface of sodium ions is higher than that of the larger quaternary ammonium ions and hence they may be attracted more strongly to the co-diffusing ions

(2) the sizes of sodium and chloride ions may be both relatively small compared with the size of the continuous pores of the carbonated pastes and hence they may have the same diffusional pathways available to them.

For diffusion of NaCl in uncarbonated cement pastes with smaller sizes of continuous pores the difference in size between sodium ion and chloride ion may become significant. This may create a situation similar to that described above, for the diffusion of quaternary ammonium chlorides in carbonated pastes, leading to higher diffusion rates for chloride ion compared to those for the larger sodium ion. An example of such pastes may be the uncarbonated OPC/65% BFS paste which generally has a compact pore system. Although the mechanism of ionic diffusion in this paste appears to be similar to that in the carbonated pastes studied in the present work (see section 4.4.4), the diffusion coefficients for chloride ion were found to be higher than those for sodium ion (table 4.2).

5.6 CONCLUSIONS

(1) The mechanisms of ionic diffusion in carbonated OPC and 65% BFS cement pastes are similar.

(2) The higher diffusion coefficients for carbonated 65% BFS cement paste, compared to those for carbonated OPC paste, are associated with the larger volume of continuous

pores of the former.

(3) The co-diffusing anions and cations are mutually influenced.

(4) Ionic diffusivities in cement paste decrease significantly as the size of the hydrated ions increases. An increase in ionic radius beyond a "critical" size, however, causes only a small further reduction in ionic diffusivities.

CHAPTER 6 : Strength

6.1 INTRODUCTION

In common with that of all brittle materials, the strength of hardened cement paste is primarily affected by its pore structure. Although this relation is generally accepted, there are two different approaches to it. The first considers that the volume porosity is the major determinant of strength. Various equations have been proposed (see section 6.2.2) showing the relation between strength and total porosity. All, however, are empirical, derived from curve fitting. A general theory has not yet been developed. The second approach is based on Griffith's criterion (see section 6.2.3) and indicates that the strength of cement paste is controlled less by the total porosity than by "critical" flaws in the material.

Despite the arguments as to the applicability of Griffith's criterion to hardened cement paste or concrete, some researchers (182,184-186) claimed to have demonstrated that by removing the macro-defects of a few millimetres from cement paste, the strength was increased considerably. For the production of macrodefect free cement paste, however, they used organic polymer admixtures which, as found by others (193,194), affect the structure and properties of the paste. The material used, therefore, was

not pure cement paste but a material similar to it.

A better understanding of the relation between macrodefects and the strength of hardened cement paste can be obtained by using specimens produced with the conventional processes, without any added material. This chapter is concentrated on the production of such specimens and the measurement of their tensile strength. The principle was to use specimens with the smallest possible cross section, so that the probability of a macrodefect existing within them was very small.

Before the description of the experimental procedure, a review is made of the relevant literature.

6.2 LITERATURE REVIEW

6.2.1 Origin of strength in hardened cement paste

The mechanisms by which interatomic and molecular bonding forces in cement paste produce the low tensile and relatively high compressive strength are still controversial. Originally, two different theories were proposed to explain the hardening mechanism of cement [160]. According to the first theory, proposed by Le Chatelier [161] in 1887, the development of strength was due to the interlocking of fibrous or "needle-shaped" crystals. The second theory,

proposed by Michaelis [162] a few years later, considered hardening to be the result of the precipitation of a colloidal gel from a saturated solution. Bernal et al [163] combining these two theories suggested that hardening could be due to the interlocking of the extremely small fibrous crystals of the calcium-silicate-hydrate which are of colloidal dimensions.

According to Powers [164] the strength of hardened cement paste arises from two general kinds of cohesive bonds in the gel; van der Waals' bonds (i.e. physical attraction between solid surfaces) and chemical bonds. As he reported, on converting gel to well organized crystals by curing in steam at about 204°C, cohesion is destroyed, indicating that the physical bonds are the most important in cement gel. This argument, however, is controversial. Wittmann [165] has suggested that the van der Waals' bonds and chemical bonds each contribute about 50% of the total strength, while Krokosky [166] has argued that the system is held together primarily by chemical bonds.

According to Brunauer [167], to cause failure of hardened cement paste in shear or compression, the chemical bonding forces in the gel structure must be overcome, whereas in tension or cleavage only the van der Waals' forces have to be exceeded. As he pointed out, since the latter are of a lower order of magnitude than chemical forces, this could explain

why the tensile strength of cement paste is lower than the compressive.

From the assumption that the strength of the gel is the only source of the strength of hardened cement paste, Powers (164) considered that the strength of a specimen of cement paste is related to the amount of gel within its boundaries. This means that strength is related to the degree to which gel fills the space available to it and therefore to the porosity. He expressed this as a "gel-space ratio" which is the ratio of gel volume to the sum of gel volume, capillary volume and entrained air volume. Gel pores are included in the gel volume. By testing specimens of cement paste of various water to cement ratios and at various stages of hydration, cured at normal temperature, he found a linear relationship between log compressive strength and log of the gel : space ratio. The empirical relationship obtained is of the form:

$$\sigma = A X^n$$

where: σ = the compressive strength

X = the gel-space ratio

n = a constant having a value usually between 2.6 to 3

A = a constant representing the strength of cement paste when $X=1$, i.e. when the gel fills all the available space. It is a characteristic of each cement paste.

The above relationship shows that the strength of hardened cement paste increases with the amount of gel present, i.e. with the reduction in porosity. Odler and Robler [168] showed that at a constant porosity the strength of cement paste increases with the increase of the amount of hydrates in the paste, at the expense of the non-hydrated material. As they found, however, this effect is distinctly less significant than that of porosity.

6.2.2 Strength - porosity relationships

It is generally accepted that porosity has a reducing effect on the strength of a material. To express this, several empirical or semi-empirical equations have been suggested, which are of four basic types [169]. These four equations are as follows:

$$\sigma = \sigma_{ob} (1 - p)^n \qquad \text{(eq.1)}$$

suggested by Balshin for porous brittle polycrystalline materials,

$$\sigma = \sigma_{or} \, e^{-(K_r p)} \qquad \text{(eq.2)}$$

suggested by Ryshkevitch [170] for porous sintered alumina and zirconia,

$$\sigma = K_s \ln (p_o/p) \qquad \text{(eq.3)}$$

suggested by Schiller (171) for gypsum pastes, and

$$\sigma = \sigma_{oh} - K_h p \qquad \text{(eq.4)}$$

suggested by Hasselman [172,173] for polycrystalline

refractory materials. In the above equations, σ_{ob}, σ_{or}, σ_{oh} are strengths at zero porosity, n, K_r, K_s, K_h are constants and p_o is the porosity at zero strength. Schiller (171) showed that equations 2 and 3 deviated slightly at the two extremes of porosity. Equation 2 is accurate at low porosities and equation 3 at high porosities.

Equations of the above four types were employed by several investigators, to represent the effect of porosity on the strength of cement paste or concrete. Fagerland (174) pointed out that Powers's equation (section 6.2.1) is a special case of Balshin's equation (eq.1). Experiments carried out by him showed that for different degrees of maturity, the constant n in Balshin's equation had different values and that for pastes made with the same cement and the same w/c ratio, strength up to 28 days is almost a linear function of porosity. He also observed that at high porosities, better agreement is obtained with Schiller's equation (eq.3).

Experiments by Robler and Odler (169) showed that, out of the four general types of equation mentioned above, Hasselman's linear relation expresses most accurately the relationship existing between strength and porosity of hardened cement paste. As they reported, however, in the range of porosities for which experimental data are available, the strength-porosity plots, as expressed by any of the four equations, are similar (figure 6.1).

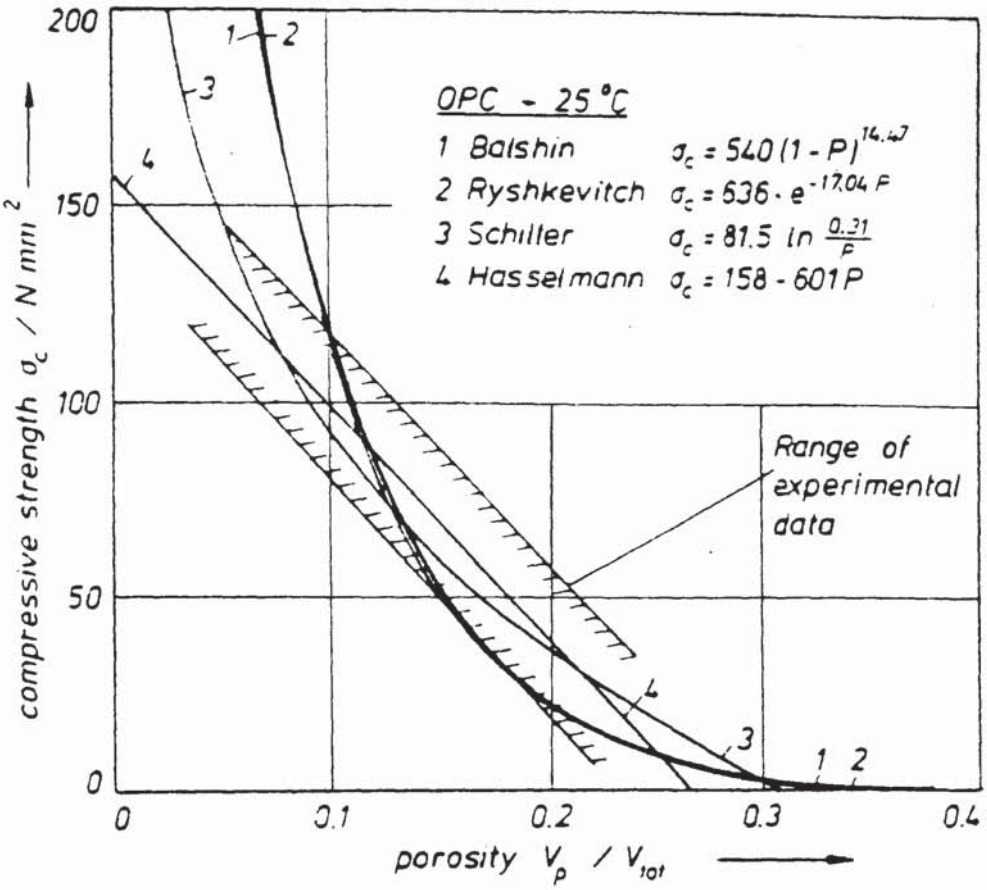

FIGURE 6.1 : Relationship between porosity and strength. Range of experimental data and calculated functions (from ref. 169).

To determine that equation which reflects the existing strength-porosity relation with best accuracy even down to zero porosity, data for pastes with porosities even below 5% would be needed. Pastes with such low porosities, however, could not be experimentally prepared with the conventional mixing processes. Attempts to achieve such low porosities and therefore to approach the theoretical strength of hardened cement paste have been made by several researchers using special techniques.

Odler et al [175] and Yudenfreund et al [176] by using cement powder finer than normal (fineness 600-900 m^2/Kg) and additives as rheological aids, achieved hardened cement paste with low porosity and compressive strength of about 204 MPa at 28 days.

Roy and Gouda [177,178] prepared hardened cement paste with porosity down to 2% and strengths 644 MPa and 63 MPa, compressive and tensile respectively, by using "hot-pressing" techniques. They found a linear correlation between strength and log porosity of the form:

$$P = P_0 \exp(-K S)$$

where: P = the porosity

P_0 = the zero-strength porosity

S = the strength

K = a constant, about 3.7×10^{-5} when S is expressed in psi.

Data for normal pastes, however, do not fit the equation. Reasonable fit is only obtained for hot pressed pastes and for the low porosity pastes prepared by Odler et al [175] and Yudenfreund et al [176].

Brown et al [179] observed that equations of Balshin's or Ryshkewitch's type, which relate strength with volume porosity, disagree with certain experimental data. As they suggested, this disagreement is due to the fact that not only the total porosity but the nature of the pores as well may affect strength. They proposed the following equation which takes pore shape and orientation into account:

$$\sigma = \sigma_{max} \{1-\sum_i [(x_i a_i/v_i) P_i]\}$$

where: σ = the strength

i = the kinds of pores

x_i, a_i, v_i = are constants which depend on the geometrical shape and orientation of the pores

P_i = the contribution made by the pores of the i^{th} kind to total porosity ($P = \sum_i P_i$)

Similarly, Older and Robler [168] examining the effect of the pore size distribution on the strength of hardened cement paste using mercury intrusion techniques, found that pores with different radii have different effects on strength. As they pointed out, the effect of pores with radius $r < 10$ nm is negligible while the effect of pores with radius $r = 10$ nm to $r = 100$ nm and $r > 100$ nm is similar and significantly

greater than that of the pores with r < 10 nm.

Jambor [180] distinguished two categories of pores in cement paste, according to their effect on strength: (a) the hydration micropores (r < 1 μm) whose size distribution and shape depend on the type and volume of the hydration products; (b) the "technological" pores (r > 1μm) comprising air voids and similar large flaws or microcracks. His experiments had shown that the most unfavourable influence on strength is produced by the "technological" pores, especially of larger size. As he pointed out, the size of all pores in cement paste diminishes with proceeding hydration. The rate of the decrease, however, depends on the activity of the cement used, the conditions of curing and the w/c ratio of the paste. He found [181] that the latter affects not only the total porosity but also the rate of cement hydration and the composition and properties of the hydration products formed. Taking all the above factors into consideration he developed the following formula which was confirmed by experimental results:

$$S = K \frac{\sqrt{(P_o - P)}}{(w/c)\ P}$$

where: P = the total porosity at the time of test

P_o = the initial porosity, the value of which is given by the sum of the volumes of mixing water and air voids in a volume unit of the paste immediately after its compaction

K = a coefficient, the value of which depends on the type and activity of cement, on the curing conditions, on the dose of cement in a volume unit of the paste and on the type of test specimens

S = the strength.

6.2.3 Fracture mechanics approach

A number of researchers approached the relationship between strength and pore structure of hardened cement paste from another point of view. Their work was based on fracture mechanics and particularly on Griffith's criterion. The latter states that the tensile strength, σ, of brittle materials is related to an effective critical crack of length 2c according to the equation:

$$\sigma^2 = \frac{2 E \gamma}{\pi c}$$

where E is the Young modulus of elasticity of the material and γ the surface free energy per unit area.

Birchall et al [182] suggested that the pore volume is not the major determinant of cement paste's strength and that the main influence on strength is the presence of macrodefects of a few millimetres. By using water-soluble polymers, high shear mixers, and by removing the trapped air from the cement paste mixture [183] they produced a "macro- defect-

free" (MDF) cement paste. Despite the large total volume of pores remaining in the material, its flexural strength was found to be as high as 70 MPa. They explained the high strengths in terms of the Griffith criterion. By testing in flexure notched samples of "macro-defect-free" cement paste they found that the results fitted the Griffith curve reasonably well (fig.6.2). When notched samples of normal cement pastes were tested, it was found that the results gave reasonable fit to the Griffith curve for notches exceeding 1.1 mm in length. For smaller notches the strengths remained constant, equal to that of the unnotched samples (figure 6.2). They suggested that this deviation from the Griffith curve was caused by large natural flaws in the cement paste.

The above hypothesis was later supported by Alford (184) who demonstrated by experiment that natural pores could be regarded as critical flaws. By plotting the maximum pore size in a number of pastes against flexural strength, he obtained a curve which approximates to the theoretical Griffith curve. Points for pastes without large pores but still with large total porosity, such as MDF pastes and pastes prepared using a polymer admixture, lay on the curve. By plotting the flexural strength against the total porosity of the same pastes, however, he found that although the curve obtained was non-linear, points for pastes without the large pores lay off the fitted curve. This observation led him to

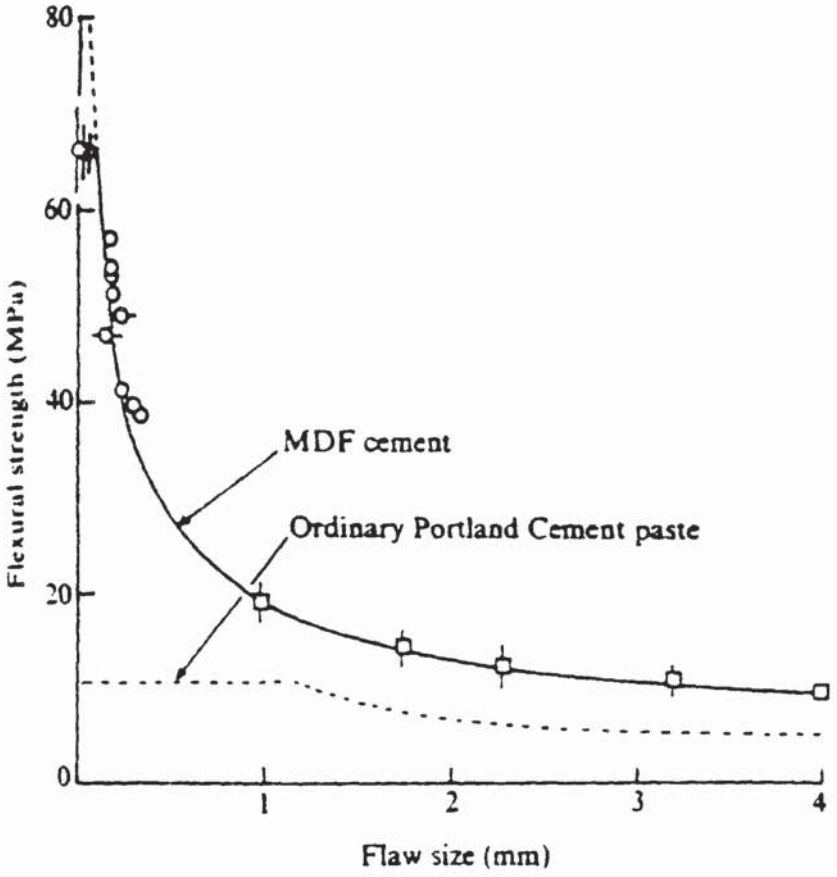

FIGURE 6.2 : Results of flexural tests of notched MDF cement paste (——) compared with ordinary cement paste (----). □,Flaws introduced by diamond saw; o, flaws introduced by air bubbles or glass microballoons. (from ref. 182).

the conclusion that the correlation between total porosity and strength of cement paste is largely fortuitous because the methods used to reduce the total porosity also reduce the critical flaw size.

Similar experiments by Alford et al [185] showed that there is a considerable scatter between the data points for strength and total porosity of ordinary and MDF cement pastes. By measuring the maximum pore size of the MDF pastes, with flexural strengths 60-70 MPa, they found that it lies between 100 and 150 μm. They suggested that this is the size of the flaw consistent with strengths of 60-70 MPa. In some of the pastes, however, they detected much smaller maximum pore sizes, around 20 μm. As they pointed out, this suggests that in these cases some other part of the cement microstructure such as the gel/clinker/portlandite interface is acting as the critical flaw.

Kendal et al [186], in order to connect the volume porosity dependence of strength suggested by some researchers [170-173] and the pore length dependence of strength suggested by others [182-185] proposed a theory which was based on the assumption that in hardened cement paste there are two kinds of pores;

(i) colloidal pores, ~2 nm in size, too small to initiate cracking but of such frequency as to form a substantial fraction of the total volume,

(ii) "crack-like pores", some millimetres in length, long enough to initiate cracks at low stress levels, but contributing only about 10% to the total volume fraction of porosity.

According to their theory, the criterion for crack extension is given by the equation:

$$\sigma^2 = \frac{E_0 R_0 (1-p)^3 \exp(-K\,p)}{\pi\, c}$$

where: σ = the tensile strength

p = the volume of porosity

E_0 = the Young modulus at zero porosity

R_0 = the fracture energy at zero porosity

c = the length of a crack-like pore

K = a constant.

This equation demonstrates that strength is a function of two independent variables; the volume of porosity and the length of a crack-like pore. The length of the crack-like pore, however, is more important as a reduction of the volume of pores from 30% to zero increases the strength by a factor of 2, while a reduction in the length of a crack-like pore from 1 mm to 0.01 mm increases the strength by a factor of 10.

As it can be seen from the above equation the plotting of strength against pore volume is not sensible unless pore length remains constant. Similarly strength cannot be plotted against crack length unless porosity volume is constant.

When porosity volume is kept constant, however, the above equation becomes of the Griffith type.

To test their theory experimentally, Kendall et al (186) plotted the flexural strength against notch length of notched specimens of ordinary and MDF cement pastes. They found that both fitted their equation with the results of the MDF paste lying on a higher Griffith curve. They attributed this to the lower total porosity of the MDF paste. In agreement with Birchall et al (182) and Alford (184,185) they found that for ordinary cement paste the flexural strength was not increased for notches less than 1 mm in length. For the MDF paste the results fitted the curve to smaller notch depths, 0.1 mm. As they pointed out, this was because the large natural pores had been eliminated in the MDF paste and since the largest cement grains were around 0.1 mm in diameter, elastic mismatch or poor grain bonding may have become significant.

Using scanning electron microscopy, Alford et al (185) compared the nature of the microstructure on a finer scale between ordinary and MDF cement pastes, both of low w/c ratio. They found them to be similar with main features of interest, cleavages across residual clinker particles, rims of inner hydration product on some clinker particles and calcium hydroxyde crystals on a fine scale.

Groves [187], by transmission electron microscopy, observed that in MDF cement pastes much of the calcium hydroxide is present in the form of a cluster of platelets around 10 nm thick. The very large calcium hydroxide crystals which can be found in higher w/c ratio pastes and may act as flaws [188] were absent in these pastes.

The relative effects of the various microstructural features on strength of composite materials had been investigated by Hasselman and Fulrath [189]. They considered that in any composite material there are two kinds of structural features. Structural features which can be considered as flaws or defects and structural features which can be considered as micromechanical stress concentrators. Due to the stress concentrations, some regions of the material's body are stressed more than others and so when a flaw is present in such regions the strength and the fracture process of the material are affected. From the above assumption they postulated that the effect of pores, which may act as stress concentrators on strength is governed by the relative size of the Griffith flaw and the volume of material over which the stress concentrations act. On this basis they distinguised three different cases:

(1) The pore size is much larger than the flaw size. Under loading conditions flaws located near pores will be entirely within a stress concentration field. A precipitous decrease in strength would be expected with the introduction of the

first pore into the loaded area.

(2) The size of the pore approaches the flaw size. In this case the flaws will not be entirely located in areas of stress concentration. On introduction of the first pore a smaller decrease in strength would be expected than for case 1, but the decrease would still be precipitous.

(3) The pore size is much smaller than the flaw size. The stress concentration field will no longer be large enough to affect the strength of the material appreciably. Only a monotonic decrease in strength with porosity should be observed with no precipitous drop. The amount of the material available to carry the load will determine the strength in this case.

Williamson [190], referring to the above theory, reported that in cement paste the most important case is that in which the flaw size is of the order of magnitude of the stress concentration zone, so that on the average, only a segment of a flaw is subjected to the stress concentration. Examining the microstructure of cement paste using scanning electron microscopy he concluded that the boundaries between the various microstructural features can be characterized as possible flaws. A list of such flaws includes the boundaries between: (1) unhydrated core and inner hydration product of each cement grain, (2) inner hydration product and outer product columnar zone in each grain, (3) outer product columnar zones of two different

grains, (4) portlandite and outer product columnar zone of cement grains, (5) portlandite crystals (i.e. a grain boundary), and (6) the hydration products of the minor compounds and other features. The cracks caused by shrinkage are another possible flaw, but as he pointed out they follow one or more of the above boundaries. As stress concentrators he considered the pores, the entrapped and/or intentionally entrained air voids and the pseudomorphs or original cement grains particularly when entrapped in portlandite crystals.

The application of the Griffith equation to cement systems has been controversial. Although Birchall et al [182] and others [184-186] claim to have demonstrated that Griffith theory applies adequately to ordinary cement pastes, Wright and Byrne [191] found that concrete was insensitive to notches. Similarly, Higgins and Bailey [192] showed that hardened cement paste is a relatively notch insensitive material whose strength is not great ly reduced by the flaws normally present in it.

Beaudoin and Feldman [193] reported that the fracture energy and Young modulus of cement systems are not constant. They both depend on porosity, w/c ratio, the environment and other matrix properties. So, as they pointed out, the use of Griffith's equation to compare polymer modified cement systems with ordinary cement paste is not correct. They

also noted that it is uncertain whether macropores can be considered as flaws in the Griffith sense. Pores in cement paste, having different pore shapes, do not fit the Griffith definition of a flaw which assumes that the flaws are atomically sharp and their major/minor axis ratio is large. Referring to the work of Birchall et al (182) and others (184-186) they stated that the principal reason why the MDF cement paste is stronger than normal pastes and does not follow the strength - porosity curve for the latter is the stress - modifying characteristics of the polymer. They suggested that the polymer in the MDF pastes modifies the pore shape in regions of high stress (fig 6.3.a) and also bridges the microcracks, resisting crack growth and increasing the tensile strength (fig 6.3.b). Additionally, owing to the very low w/c ratios (0.08-0.2) and the press moulding used, MDF pastes contain large amounts of dense unhydrated cement particles. A small amount of additional hydration, therefore, (although total porosity remains effectively unchanged) is sufficient to "glue" the unhydrated cement particles together, enabling them to contribute more fully to the strength (fig 6.3.c).

6.3 EXPERIMENTAL PROCEDURE

The experimental work carried out in this chapter, as mentioned in the introduction, was concentrated on the production and testing in tension of very small cement paste

FIGURE 6.3 : Schematic illustrations of various stress-modifying mechanisms in MDF cement paste (from ref. 193).

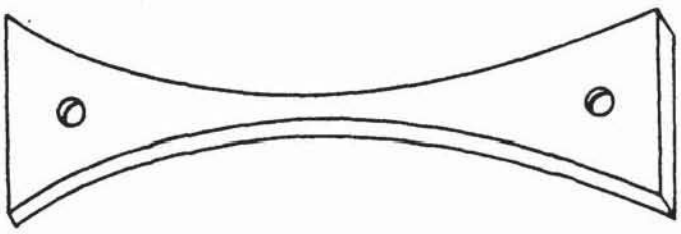

FIGURE 6.4 : The specimen for direct tension test.

specimens prepared by the conventional processes. The average thickness and width of the specimens at the middle regions were 0.95 mm. For comparison, larger specimens were also prepared and tested with the same techniques. The average thickness and width at the middle regions of these specimens were 2.58 mm.

6.3.1 Specimen preparation

The specimens (figure 6.4), were made at 0.3 w/c ratio, by mixing ordinary portland cement with deionized water. Cement powder was first sieved through a 150 μm mesh (in order to produce a consistent fineness of powder) and weighed. The correct amount of deionized water was then added to it, to produce a 0.3 w/c ratio mixture. This was mixed thoroughly by hand for 5 minutes using a glass rod and hand laid in specially designed PTFE moulds (fig. 6.5).

The moulds consisted of a base and two plates which could slide on the base to give the required width of the specimen. The thickness of the specimen was controlled by the thickness of the plates. To avoid any leakage of paste, "Vaseline" petroleum jelly was applied between the base and the plates.

After moulding, in order to produce the two holes for the loading of the specimen (fig.6.4), two small pieces of 3 mm

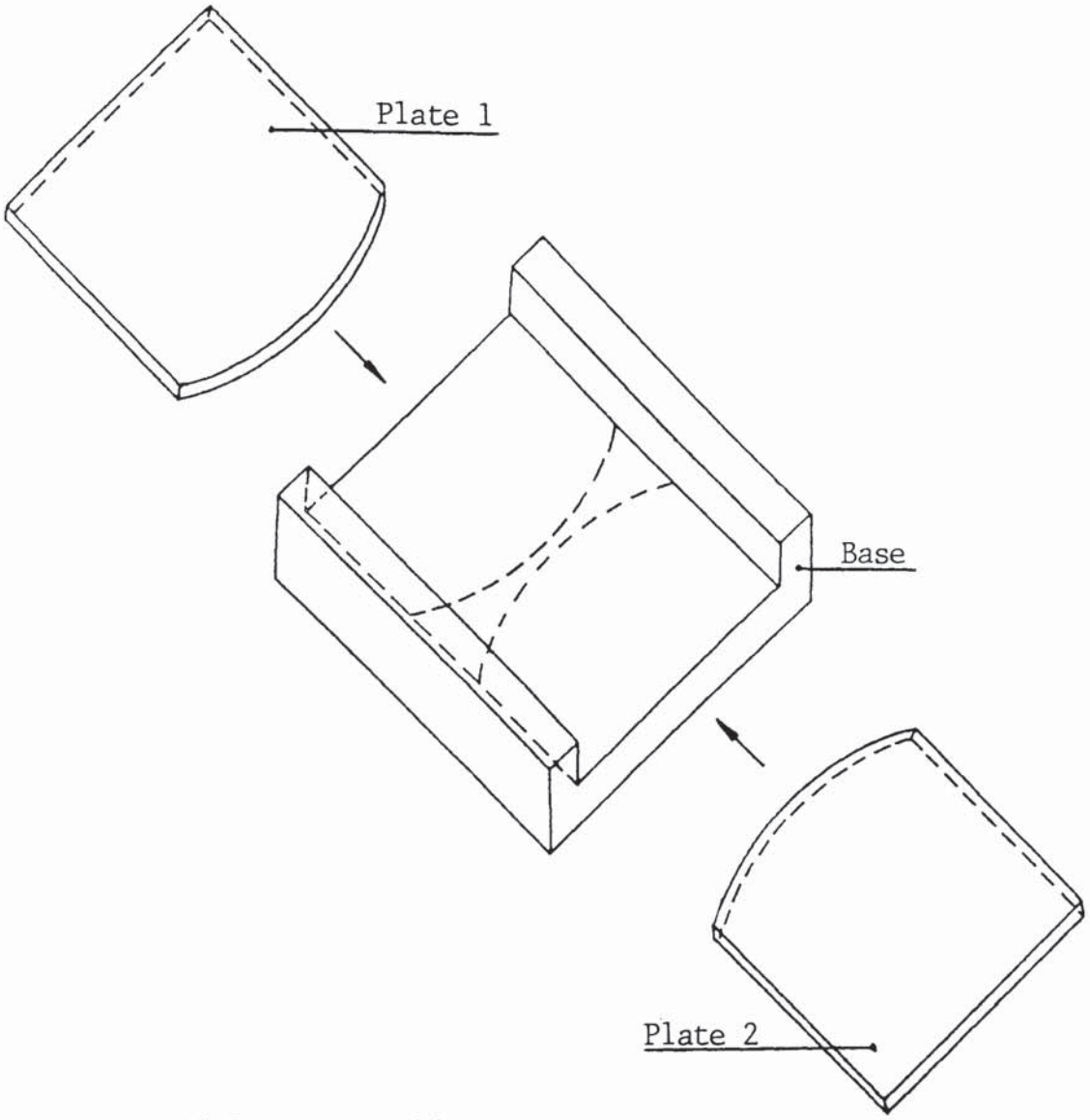

FIGURE 6.5 : The mould.

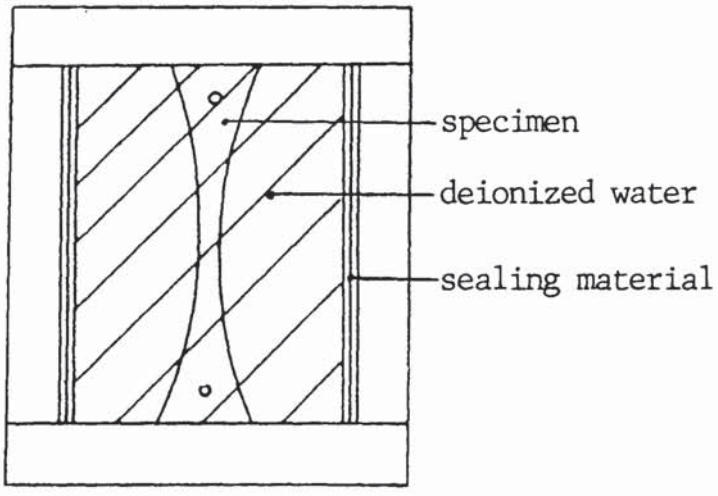

FIGURE 6.6 : The flooded mould.

diameter plastic tube were inserted, with the help of a guide, at certain places near the two ends of each specimen. The moulds were then placed in a high humidity box at room temperature for 20 hours. After these first 20 hours, the small pieces of tube were removed from the specimens and the moulds were flooded with deionized water (fig.6.6). Each specimen remained in this situation for seven days and was then demoulded. For the demoulding the one plate was first removed from the base and then the specimen was pushed by the second plate off the base, on to a third PTFE plate. Using the latter, the specimen was then placed in a small container which was filled with the same water which previously was used in the mould (to minimise any leaching phenomena) and kept there for other 20 days.

Great care was taken to keep the specimens wet at all times during the preparation procedure as well as later during the testing, to avoid any strength reductions associated with drying (195).

6.3.2 Direct tension test

The small thickness of the specimens and therefore the very low load needed for failure did not allow the use of any standard direct tension test such as that prescribed in the 1971 edition of BS 12. For this reason an alternative method was adopted which employs the action of gravity.

Two S-shaped pieces of strong wire were passed through the holes near the two ends of the specimen. Using the first wire the specimen was then hung from a horizontal steel rod and, using the second wire, a PVC container was hung from the specimen, putting it under tension (figure 6.7). Mercury was then poured into the container slowly, until the failure of the specimen occured. At failure, the flow of mercury was stopped immediately using a plastic clip (fig.6.7).

In order to have the same loading rate for all the specimens, the mercury was poured from a reservoir located at a standard level for all the tests.

After each test the container with the used mercury was weighed and then the area at the point of fracture was measured by means of a travelling microscope. Specimens whose fracture point did not coincide with their thinnest point were not taken into account.

6.3.3 Apparent density

A measure of the compactness of the specimens at the "critical" thinnest point is the apparent density at that point. It can be obtained from the ratio of the weight of the dry specimen and its external volume. The specimens used here were of constant cross section, equal to the cross section at

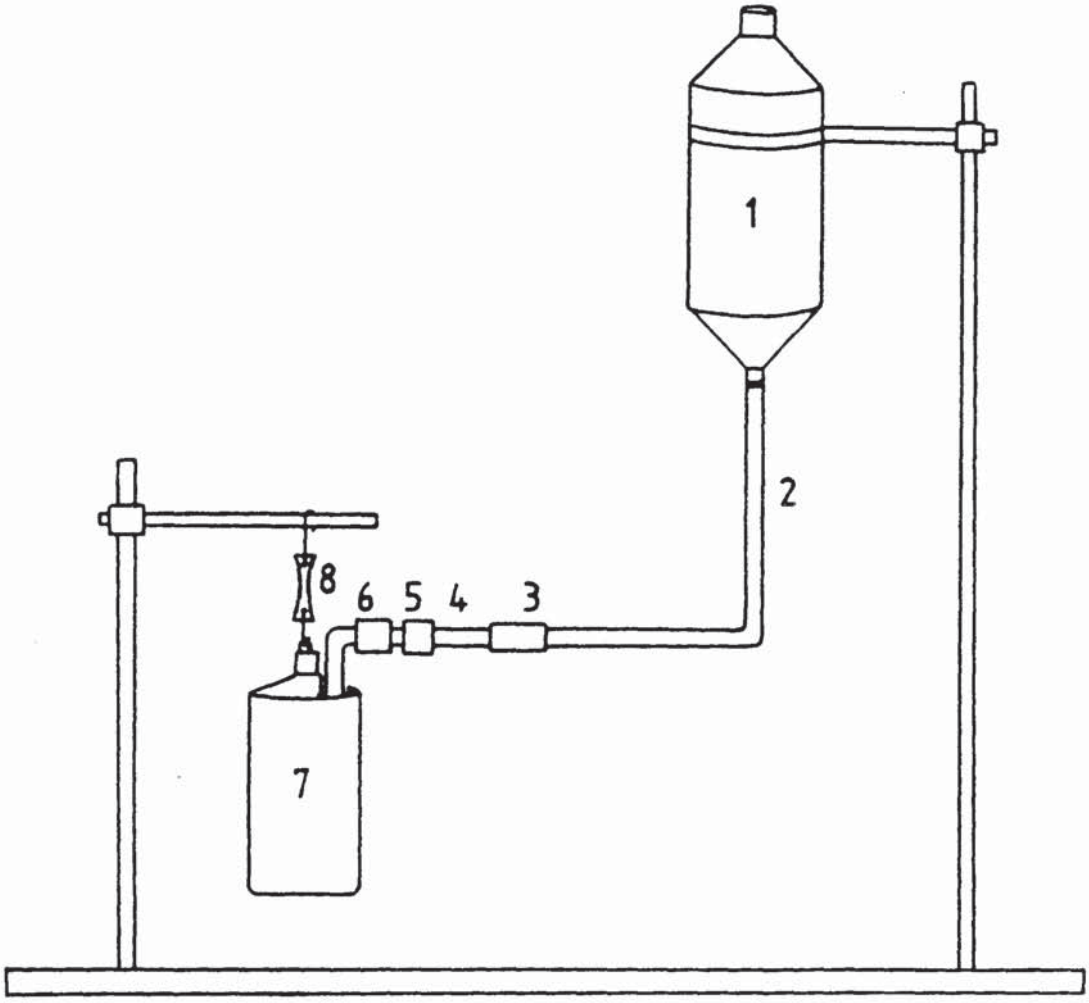

FIGURE 6.7 : Direct tension test.
1: mercury, 2: glass tube,3: joint, 4: plastic tube, 5: clip, 6: flow rate control (adjustment of the cross section of the tube at that point), 7: used mercury, 8: the specimen.

the middle of the specimens used for the direct tension test. Their preparation procedure was that described in section 6.3.1.

After 28 days curing in water (section 6.3.1) the specimens were kept in the oven at 105°C for two days and then their weight was measured. By using a density bottle, their external volume was then calculated from the displacement of mercury which is a non wetting liquid.

6.4 RESULTS

The tensile strength of each specimen in MPa (N/mm^2) is given by the equation:

$$\sigma = g \frac{M}{A}$$

where: M = the mass of the mercury used (Kg)

A = the area at the point of fracture (mm^2)

g = the gravitational field strength ($=9.8\ ms^{-2}$)

The measured strengths for specimens of the two different sizes are tabulated in tables 6.1 and 6.2. Table 6.1 shows the measured areas at the point of fracture and the corresponding strengths of size 1 specimens (average thickness of 0.95 mm), whereas table 6.2 shows those for size 2 specimens (average thickness of 2.58 mm). Fifty specimens were tested for each size. The mean strengths for size 1 and size 2

specimens were found to be statistically significantly different with values 8.73 MPa and 6.32 MPa respectively (the statistical comparison is shown in appendix 15). A graphical representation of the data is shown in figures 6.8 and 6.9. As can be seen the dispersion of the obtained strengths is different between the two sizes. The standard deviation, σ_{n-1}, for the data are 2.94 and 1.88 for size 1 and size 2 specimens respectively.

The apparent densities of the two sizes of specimens used which are shown in table 6.3 were found to be statistically equal. They were calculated using the following equation:

$$d = \frac{13.6\ W_s}{W_m}$$

where: d = the apparent density (g cm^{-3})

W_s = the weight of the dry specimen (g)

W_m = the weight of the displaced mercury (g).

A worked example of calculations is shown in appendix 16.

Table 6.1: Tensile strengths of hardened cement paste specimens of size 1 (average thickness = 0.95 mm).

No	Area mm^2	Weight of mercury, Kg	Strength MPa
1	0.702	0.475	6.65
2	0.632	0.771	11.97
3	0.831	0.579	6.83
4	0.510	0.662	12.71
5	0.236	0.289	12.00
6	0.667	0.524	7.70
7	0.637	0.580	8.92
8	0.645	0.276	4.19
9	0.645	0.409	6.22
10	0.667	0.397	5.83
11	0.494	0.196	3.88
12	0.715	0.725	9.93
13	0.744	0.426	5.60
14	0.610	0.649	10.43
15	0.525	0.453	8.46
16	0.553	0.303	5.37
17	0.643	0.485	7.39
18	0.632	0.475	7.36
19	1.357	0.552	3.99

cont. over

No	Area mm^2	Weight of mercury, Kg	Strength MPa
20	0.605	0.407	6.60
21	0.586	0.610	10.20
22	0.538	0.759	13.83
23	0.567	0.965	16.68
24	0.955	1.078	11.06
25	0.348	0.150	4.22
26	1.627	1.300	7.830
27	0.929	0.502	5.30
28	1.282	1.760	13.45
29	1.896	1.419	7.33
30	1.053	0.521	4.85
31	0.764	1.152	14.78
32	0.677	0.609	8.82
33	1.263	1.413	10.96
34	1.824	2.418	12.99
35	1.733	1.481	8.38
36	0.942	0.709	7.38
37	1.058	0.829	7.68
38	0.622	0.761	11.99
39	0.655	0.591	8.84
40	0.981	0.780	7.79
41	0.716	0.518	7.09

cont. over

No	Area mm^2	Weight of mercury, Kg	Strength MPa
42	0.937	0.888	9.29
43	0.766	0.431	5.51
44	1.753	1.759	9.83
45	1.704	1.740	10.01
46	1.822	1.828	9.83
47	0.780	0.802	10.08
48	0.988	1.261	12.51
49	1.115	0.913	8.03
50	0.889	0.832	9.17
51	1.301	1.020	7.68
52	1.407	1.230	8.57

Table 6.2 : Tensile strengths of hardened cement paste specimens of size 2 (average thickness = 2.58 mm).

No	Area mm^2	Weight of mercury, Kg	Strength MPa
1	6.570	3.000	4.48
2	4.555	2.845	6.14
3	7.094	3.282	4.53
4	4.070	3.545	8.54
5	6.854	3.425	4.90
6	3.488	0.920	2.58
7	7.123	4.675	6.43
8	4.923	2.720	5.42
9	6.347	4.110	6.35
10	7.461	4.880	6.41
11	7.214	6.440	8.75
12	6.975	5.275	7.41
13	7.232	5.290	7.17
14	6.830	4.720	6.77
15	7.187	4.829	6.59
16	7.412	4.910	6.49
17	6.598	6.610	9.82
18	9.894	6.910	6.84

cont. over

No	Area mm^2	Weight of mercury, Kg	Strength MPa
19	6.742	4.215	6.13
20	7.556	4.900	6.36
21	7.434	6.800	8.96
22	7.379	4.670	6.20
23	6.631	6.633	9.80
24	8.258	4.890	5.80
25	8.492	2.170	2.50
26	4.292	3.815	8.71
27	6.841	3.040	4.35
28	6.602	3.835	5.69
29	4.135	1.270	3.01
30	7.032	3.645	5.08
31	6.367	3.000	4.62
32	7.100	4.410	6.09
33	7.607	4.315	5.56
34	6.990	4.070	5.71
35	6.825	3.860	5.54
36	8.016	6.085	7.44
37	6.778	5.920	8.56
38	6.780	7.195	10.40
39	6.315	4.605	7.14
40	7.213	2.444	3.32

cont. over

No	Area mm^2	Weight of mercury, Kg	Strength MPa
41	6.301	4.700	7.31
42	8.531	4.701	5.40
43	6.827	2.236	3.21
44	6.031	2.782	4.52
45	4.121	3.881	9.23
46	5.323	3.992	7.35
47	6.333	3.444	5.33
48	7.540	5.393	7.01
49	6.981	5.186	7.28

Table 6.3: Apparent densities at the thinnest point of the hardened cement paste specimens.

No	size	d_a g/cm^3	Mean d_a
1	1	1.899	
2	1	1.887	1.893
3	2	1.904	
4	2	1.913	1.909

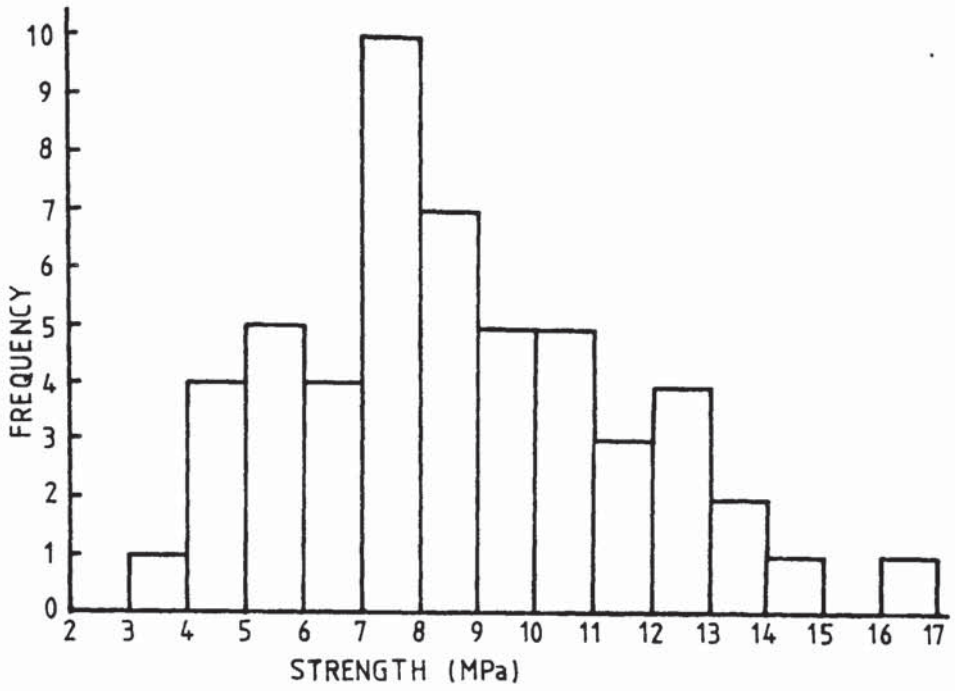

FIGURE 6.8 : The frequency of the tensile strength of 52 specimens of size 1 (average thickness = 0.95 mm).

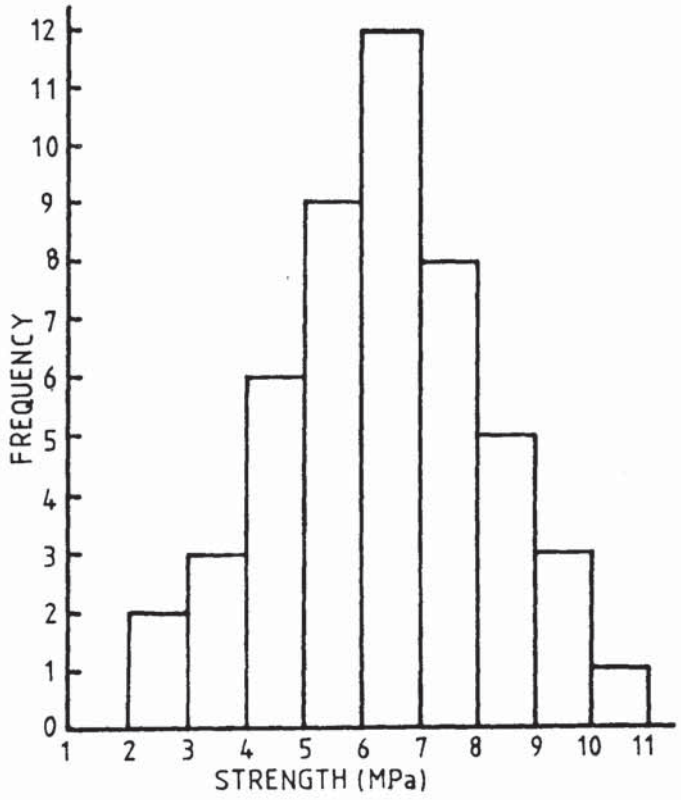

FIGURE 6.9 : The frequency of the tensile strength of 49 specimens of size 2 (average thickness = 2.58 mm).

6.5 DISCUSSION

The results in this chapter show that the tensile strength of hardened cement paste increases as the size of the specimen decreases. Since there is no significant difference between the apparent densities of the two sizes of specimens (table 6.3), the higher tensile strength of the smaller specimen can not be attributed to a better packing of the particles. Similarly, it can not be attributed to a lower porosity because the preparation technique and the w/c ratios were the same for both sizes of specimens.

In the field of fracture mechanics, it is generally known that the strength, especially the tensile strength of brittle materials depends on the volume of the specimens. The results in this chapter show that this behaviour is common to hardened cement paste. Although the specimens used have the same shape and were tested under the same conditions, those with smaller volume showed higher mean tensile strength. This is explained in terms of Griffith's criterion which, as mentioned earlier, states that strength is controlled by flaws of critical length. As the volume decreases, the probability of finding a critical flaw reduces and thus the mean strength increases. This had been shown statistically, for a brittle material, by Weibull [196,197]. By assuming that the material is isotropic and statistically homogeneous, and that failure at the critical flaw leads to

total failure (perfect brittle fracture), he found that the mean tensile strength, $\bar{\sigma}$, of the material is given by the following equation (196):

$$\bar{\sigma} = \frac{\sigma_0}{V^{1/m}} \Gamma(1+1/m)$$

where: $\bar{\sigma}$ = the mean tensile strength

V = the volume

σ_0 = a normalising factor

m = the Weibull modulus which describes the flaw size distribution of the material

$\Gamma(1+ 1/m)$ = the "gamma function" of m.

As the volume of the specimen decreases, the strength increases. A theoretical limit to the decrease of the volume would be of molecular dimensions, incapable of sustaining a flaw. This volume could give an upper limit of the strength, the theoretical strength.

Birchall et al (182) tried to approach the upper limit of flexural strength of hardened cement paste in a different way. Instead of decreasing the probability of existence of a critical flaw by reducing the volume of the specimens, they eliminated the flaws in the material by a special preparation technique involving the use of organic polymers. The flexural strengths obtained were of the order of 70 MPa. In agreement with Birchall et al (182), Alford (184,185), using the same type of cement paste, suggested that the correlation between

total porosity and strength of hardened cement paste is fortuitous and that the main factor influencing strength is the presence of flaws. If this hypothesis is taken into account, it can be predicted that by reducing the volume of cement paste specimens, and therefore the size of the critical flaws in the failure cross section, the strength would increase irrespective of the total porosity. The smallest specimen used in this chapter is probably among the smallest specimens which can be prepared using the conventional preparation process. The highest tensile strength obtained therefore is probably one of the closest approaches to the theoretical strength of ordinary hardened cement paste, prepared by the conventional procedure. The fact that this strength is much lower than that obtained for the MDF paste, may indicate that the high strengths obtained for the latter are caused by the combined result of the removal of the flaws or macropores and the action of the polymer. The polymer probably changes the structure and properties of the paste [193,194] so the obtained material can not be compared directly with ordinary cement paste.

6.6 CONCLUSIONS

(1) The tensile strength of hardened cement paste is influenced by the presence of flaws or macropores with size of the order of one millimetre.

(2) Ordinary cement paste cannot be compared directly with

paste prepared with special techniques using organic polymer admixtures because the structure and properties of the two materials may be different.

(3) Arguments that the correlation between strength and total porosity of hardened cement paste is fortuitous may not be valid because they are based on the comparison of ordinary cement paste with cement paste prepared using organic polymer admixtures.

CHAPTER 7 : General discussion and conclusions

7.1 GENERAL DISCUSSION AND SUGGESTIONS FOR FUTURE WORK

The aim of the present work, as mentioned in the introductory chapter, was to contribute to the understanding of cement paste and its role in reinforced concrete. For this reason three crucial properties of cement paste, which affect the performance of reinforced concrete, were investigated.

Cement paste contributes not only to the strength but also to the durability of reinforced concrete. Thus, apart from strength, which is the most obviously required characteristic for structural use of reinforced concrete, the other two properties investigated, the resistances to carbonation and to ionic penetration, are related to the protection of steel reinforcement from corrosion.

The work carried out was mainly focussed on a common feature of the properties under investigation, viz. their relation with the pore system (pores and pore solution) of cement paste.

7.1.1 Resistance to carbonation

Although the carbonation of cement paste or concrete is well

documented [51-98], uncertainties still exist, as mentioned in section 1.2, in areas such as the theoretical representation of the carbonation process, the characterization of cement pastes according to their resistance to carbonation and the effects of carbonation on the pore system and particularly on the pore solution of cement paste. Work described in this thesis has attempted to fill some of these gaps.

7.1.1.1 Theoretical representation of the carbonation process

It is generally known that the relationship between the carbonation depth, x, and time, t, is parabolic. This was shown both theoretically [7,52,53] and experimentally [69,63]. For the prediction of carbonation depths in concrete structures and for the development of materials of improved resistance to carbonation the most important factor of the relationship is the constant of proportionality, K, which is related to the rate of carbonation.

It was shown theoretically [7], that for the simple unidirectional diffusion of CO_2 in concrete, assuming that there is no variation of the diffusion coefficient with time or depth, the constant K is proportional to $\sqrt{(DC/A)}$, where D is the diffusion coefficient of CO_2, C is the CO_2 content in the atmosphere and A is the amount of carbonatable material present in a unit volume of concrete. Experimentally, the above relationship was verified in chapter 3 by using cement

paste specimens of the form of thin discs. Such specimens enabled fast equilibration of the relative humidity in the pores with that of the external atmosphere, thus minimizing variations of D with depth from the surface of the specimens.

Data from practice, where the diffusion coefficient of CO_2 probably changes with depth due to variations of the R.H. in the pores, may not perfectly fit the above mentioned relationship for the rate of carbonation. In order to assess the effect of possible effective variation of D with depth on the constant K, the work carried out in chapter 3 needs to be continued in the future, by exposing one surface of cylindrical or prismatic specimens (of the same age) to atmospheres of different CO_2 content. Any significant deviations from the linear relationship between the depth of carbonation and the square root of time should be attributed to variations of the diffusion coefficient of CO_2 with the depth from the surface of the specimen.

7.1.1.2 Characterization of cement pastes according to their resistance to carbonation

The experimental verification of the relationship for the constant K shows that the amount of carbonatable material per unit volume of cement paste, A, is directly related to the resistance of the paste to carbonation. Since the greater

part of the CO_2 intake during carbonation is by the CaO bearing phases [37], the amount of CaO present in a unit volume of cement paste represents the carbonatable material present in the paste (see appendix 11 and Fig. 3.16) and thus it can be considered as indicative of the resistance to carbonation. Conversely, however, the porosity of the paste before the beginning of carbonation is not representative of the resistance to carbonation because, as was expected, no direct relation was found between this parameter and the rate of carbonation.

By exposing OPC and 65% BFS cement pastes to three different atmospheres it was found that there is a critical concentration of CO_2 in the atmosphere for which both pastes carbonate at the same rate. As explained in section 3.4.4.1, knowledge of this concentration is essential if carbonation rates of cement pastes measured under accelerated conditions are to be used as guides to the behaviour of the pastes under natural conditions. It is important therefore first to confirm the existence of this critical CO_2 concentration by further experiments using OPC and 65% BFS cement pastes made with different w/c ratios and secondly to establish whether it exists for all types of cement pastes.

Another parameter which may be expected to be indicative of the resistance of cement paste to carbonation is the

diffusion coefficient of CO_2, which probably depends on parameters such as the w/c ratio, the compaction, and the curing conditions of the paste. This is an area where more concentrated research is needed for the determination of diffusion coefficients of CO_2 in cement paste. It would be possible then first to confirm the relation between the diffusion coefficient of CO_2 and the resistance to carbonation and secondly to obtain relationships between the diffusion coefficient and parameters such as the w/c ratio, the temperature and the R.H. of the exposed atmosphere.

7.1.1.3 Effects of carbonation on the pore system of hardened cement paste

The effects of carbonation on the pore structure and phase composition of cement pastes have been the subjects of several published studies [51,52,56,57,89,91]. According to them, the main products of carbonation are calcite and vaterite which are produced in the pores thus altering the pore size distribution. Similar results were obtained in the present investigation where it was shown also that the ratio of vaterite to calcite increases with the increase of the rate of carbonation. The most interesting result obtained, however, was the increase of the volume of pores greater than about 40 nm, after carbonation, despite the decrease of the total porosity. This size range of pores may be associated with the continuous pores [4,126,156] which

affect properties related to mass transport phenomena such as the penetration of aggressive ions, oxygen or moisture into cement paste or concrete.

As mentioned in section 2.9, the results obtained by mercury intrusion porosimetry may not faithfully represent the pore size distribution of cement paste because, inter alia, the application of high pressures may damage the pore structure. Therefore, in order to confirm the apparent increase of the continuous pores after carbonation, there is a need for further work involving the determination of pore size distributions of carbonated pastes by other methods [46].

As far as the effect of carbonation on the pore solution of cement paste is concerned, in chapter 3 it was found that, apart from the obvious reduction of the concentration of OH^- ions, the concentration of the accompanying Na^+ and K^+ ions was also reduced. On the other hand, the breakdown of the chloride containing phases had the effect of increasing the free chloride content in solution. Such a release of chloride, aided by the reduction in pH, reduces the ability of cement paste to protect the steel reinforcement from corrosion. Even where carbonation has not penetrated to the level of the outermost steel bars in a structure, the chlorides released in the carbonated layer may diffuse inwards reaching the steel reinforcement. In this case, although the pH around reinforcement may be higher than that of the surface layer,

localised corrosion may be expected to occur [7].

The most striking result obtained from pore solution analysis of carbonated pastes was the high concentrations of calcium and magnesium ions, accompanied by the presence of silicate ions. Relatively high concentrations of such ions were observed only in the pore solutions of cement pastes carbonated under accelerated conditions, after the pH had dropped below 8. In practice therefore, where carbonation under natural conditions is slow, the concentrations of calcium, magnesium and silicate ions may be low. Despite that, the results obtained are important because they show that carbonation of cement paste and particularly of C-S-H gel is a complex process and that further work is needed in this area in order to understand clearly the carbonation mechanisms. The use of ion chromatography should be continued using other separator columns and reagents in order to provide further quantitative analysis of all ionic species present in the pore solution of carbonated cement pastes (e.g. silicate ions and ionic forms of soluble silica).

7.1.2 Resistance to ionic penetration

As mentioned earlier, ions enter into concrete, which has been made and placed according to specifications [112], usually by diffusing through the pores of the cement matrix [11,111]. Currently, however, there is no clear understanding

of the mechanisms of ionic diffusion and thus any efforts to design concretes or other cementitious materials of improved resistance to ionic penetration are somewhat hampered [136]. The development of a general ionic diffusion theory is therefore important. Part of the work described in this thesis has attempted to widen the knowledge of mechanisms of ionic diffusion in hardened cement paste and hence to contribute to the development of such a theory.

The principle of the method of investigation was to compare kinetic data relating to the diffusion of ions in cement pastes with different pore systems. Results obtained show that there is no direct relation between total porosity and ionic diffusivities. As was suggested, the diffusion of ions in hardened cement paste is affected directly by the interactions of the diffusing ions with the pore surfaces, the size and volume of continuous pores of the paste and the type and concentration of the other ionic species present in the pore solution.

Experimental results in chapters 4 and 5 suggested that the mechanisms of ionic diffusion in carbonated OPC and 65% BFS cement pastes are similar. Ionic diffusivities in the carbonated slag paste, however, were found to be higher than those in the carbonated OPC paste. This difference can be attributed to the larger volume of continuous pores of the former and/or to stronger interactions of the diffusing ions

with the pore surfaces of the latter. This could be investigated by determining diffusion coefficients in carbonated OPC and 65% BFS pastes for neutral molecules of radii similar to those of the ions used in the present work (136). Diffusion coefficients for the neutral molecules similar to those for ions would suggest that the differences between the ionic diffusivities in carbonated OPC and 65% BFS pastes are simply due to physical differences between their pore structures.

The above approach could be also used for uncarbonated BFS-blended pastes in order to investigate whether the significant retardation of ionic diffusion offered by such pastes is mainly a result of their low porosities and discontinuous pore structures or is due to strong pore surface interactions. Measurements of activation energies for ionic diffusion in the pastes studied in the present work showed that the mechanism of surface interactions in the 65% BFS blended cement pastes was different from that in the OPC pastes. This difference, as suggested in section 4.4.2, may be associated with the different type of C-S-H gel in the slag paste.

The size of the hydrated ions was found to have a great influence on ionic diffusivities in carbonated pastes. As the size of the diffusing cation was increased, both the diffusion coefficients of the cation and the co-diffusing anion were

significantly decreased. Beyond a certain radius for each type of cement paste, however, an increase in radius caused only a small further reduction of the diffusion coefficient (fig. 5.3, 5.4). In order to establish more precisely the form of the relationships and hence to calculate the "critical" radius for each type of cement paste, there is a need for further experiments with other ions. Experiments with ions larger than those already used would also permit the extrapolation of the curves to the r-axis and hence the estimation of the maximum size of continuous pores present in the pastes.

In agreement with other studies [117,37], results obtained in the present work suggested that another factor affecting the diffusion of ions in hardened cement paste is the type and concentration of the other ionic species present in the pore solution. This could be investigated by comparing diffusion coefficients for cement paste specimens (discs) which were previously cured for long periods of time either in a reproduction of the pore solution or in high concentration solutions of different ionic species. Differences in ionic diffusivities between the various specimens could then be attributed to the different ionic species present in the pore solutions.

7.1.3 Strength

From the literature review on strength in chapter 6 of this

thesis it is clear that the relationship between strength and pore structure of hardened cement paste may be approached from two different points of view. The first considers that the volume porosity is the major determinant of strength while according to the second, which is based on Griffith's criterion, the strength is governed by the presence of large flaws or macropores.

Based on the second approach, in order to improve the strength of hardened cement paste, some researchers [182,184] prepared "macro-defect-free" cement paste (MDF) by using special preparation techniques and organic polymer admixtures. They suggested that the high strength obtained for this material was a result of the removal of the macrodefects, and that the correlation between total porosity and strength of hardened cement paste is fortuitous because the methods used to reduce the total porosity also reduce the macrodefects.

Results obtained in the present work, however, in which ordinary cement paste was used to investigate the above argument, suggest that although strength of hardened cement paste is influenced by the presence of flaws or macropores, the increase of strength resulting from the removal of macrodefects is much lower than that suggested from results obtained for MDF paste. Therefore, the high strength of this paste is probably a result mainly of the special preparation

techniques involving a polymer which changes the structure and properties of the material (193). Further investigations on the relationships between strength and macrodefects, therefore, should be carried out using ordinary cement paste specimens.

The applicability of Griffith's criterion to hardened cement paste could be tested by plotting the tensile strength of hardened cement paste specimens versus the maximum size of flaws or macropores present in the failure cross section. This could be done by employing optical or other methods to measure the maximum size of macrodefects in the failure cross section. Specimens with various cross sections could be used, prepared and tested as described in the present work.

7.2 GENERAL CONCLUSIONS

Both the strength and durability of hardened cement paste are directly affected by its pore system. Therefore, efforts to improve the performance of concretes or other cementitious materials for practical applications should be based on a clearer understanding of the relationships between the pore system and properties of cement paste.

The experimental work carried out has attempted to fill some of the gaps in current knowledge and to generate areas for

future research. Many of the conclusions, however, are tentative and require confirmation from further studies, particularly from tests carried out under natural conditions. The general conclusions obtained may be summarized as follows:

(1) Cement pastes with high CaO content offer an improved resistance to carbonation. This property of cement paste, however, is also affected by the pore structure and hence by factors such as the w/c ratio, the compaction and the curing conditions of the paste.

(2) There is no direct relation between carbonation resistance of cement paste and the porosity before carbonation. The resistance to carbonation is probably affected by the volume of continuous pores in the paste because it is directly related with the rate of diffusion of CO_2.

(3) Contamination of cement paste with NaCl appears to reduce slightly the resistance to carbonation.

(4) Carbonation modifies the pore size distribution, the pore solution and the phase composition of cement paste and thus affects most of its properties. The extent of the modifications appear to be substantially influenced by the amount of CO_2 in the atmosphere. This must be taken into account if atmospheres with high CO_2 content are to be used for accelerated carbonation tests.

(5) There is a critical concentration of CO_2 in the

atmosphere for which OPC and 65% BFS cement pastes carbonate at the same rate. Knowledge of this concentration is essential if carbonation rates, measured under accelerated conditions, are to be used as guides to the behaviour of the pastes under natural conditions.

(6) Carbonation reduces the resistance of cement paste to ionic penetration. Hence, cementitious materials originally designed for low ionic permeability may lose their resistance when used in conditions which promote high carbonation rates.

(7) There is no direct relation between the total porosity and the resistance of cement paste to ionic diffusion. Cement pastes with a compact pore structure and discontinuous pore system, however, such as the BFS-blended pastes, cause a significant retardation of ionic diffusion.

(8) The mechanism of ionic diffusion in ordinary portland cement paste is different from that in 65% BFS blended cement paste or in carbonated OPC and 65% BFS cement pastes.

(9) The co-diffusing anions and cations are mutually influenced. It also appears that the diffusing ions both influence and are influenced by all the other ionic species present in the pores, so that an ionic charge balance is maintained throughout the pore solution network.

(10) Ionic diffusivities in cement paste decrease significantly as the size of the hydrated ions increases. An increase in ionic radius beyond a "critical" size, however,

causes only a small further reduction in ionic diffusivities. (11) The presence of flaws or macropores in hardened cement paste reduces its tensile strength. Arguments, however, that the correlation between strength and total porosity is fortuitous may not be valid because they are based on the comparison of ordinary cement paste with cement paste prepared using organic polymer admixtures.

REFERENCES

(1) BYE, G. C.

"Portland cement, composition, production, and properties", pub. The institute of ceramics, Pergamon Press, London, 1983.

(2) POWERS, T. C. ; BROWNYARD, T. L.

"Studies of the physical properties of hardened portland cement paste", Portland cement association, Research Bulletin 22, 1947.

(3) FELDMAN, R. F.

"Pore structure, permeability, and diffusivity as related to durability", 8th International congress on the chemistry of cement, Proc., Vol I, principal reports, pp 336-356, Rio de Janeiro, Brazil, 1986.

(4) UCHIKAWA, H.

"Effect of blending component on hydration and structure formation" , Journal of Research of the ONODA cement company, Vol. XXXVIII, No 115, pp 79-155, Tokyo, Japan, 1986.

(5) BOZHINOV, G. ; BAROVSKY, N.

"To the analysis of the pore structure of cement stone" 8th International congress on the chemistry of cement, Proc., Vol. V, pp 22-28, Rio de Janeiro, 1986.

(6) WITTMANN, F. H.

"Properties of hardened cement paste", 7th Intern. congress on the chemistry of cement, Proc., Vol. I,

principal reports, sub-theme VI-2, pp1-14, Septima ed., Paris, 1980.

(7) PAGE, C. L.

"Barriers to the prediction of service life of metallic materials", Masters, L.W., Ed., "Problems in service life prediction of building and construction materials", NATO advanced science Institute series: Applied Sciences, Martinus Nijhoff, E. 95, 1985, pp 59-74.

(8) TUUTTI, K.

"Corrosion of steel in concrete", Swedish cement and concrete research Institute, S-100, 44-CBI Forskning research fo. 4.82, Stockholm, 1982.

(9) MURDOCK, L. J. ; BROOK, K. M.

"Concrete, Materials and Practice", 5th edition, Edward Arnold, Pub. , London, 1979, pp 377-379

(10) CALLEJA, J.

"Durability", 7th Intern. congress on the chemistry of cement, Proc., Vol. I, principal reports, sub-theme VII-2, pp1-48, Septima ed. , Paris, 1980.

(11) SORENSEN, B. ; MAAHN, E.

"Penetration rate of chloride in marine concrete structures", Nordic concrete research, Vol. 1, pp 24.1-24.18, 1982.

(12) RAMACHANDRAN, V. S. ; FELDMAN, R. F. ; BEAUDOIN, J. J.

"Concrete science, treatise on current research", Heyden, Pub., London, 1981, pp 54-59.

(13) DIAMOND, S.

"Cement paste microstructure", Conf. on Hydraulic cement pastes: their structure and properties, Proc., Sheffield 1976, Cem. and Concr. Assoc., Slough, pp 2-30.

(14) DIAMOND, S.

"The microstructures of cement paste in concrete", 8th International congress on the chemistry of cement, Proc, Vol I, principal reports, pp 122-147, Rio de Janeiro, Brazil 1986.

(15) TAYLOR, H. F. W.

"Studies on the chemistry and microstructure of cement pastes", Proc. British Ceramic Society, Vol.35, pp 65-82, 1984.

(16) WITTMANN, F. H.

"The structure of hardened cement paste - a basis for a better understanding of the material's properties", Conf. on Hydraulic cement pastes: their structure and properties, Proc., Sheffield 1976, Cem. and Concr. Assoc., Slough, pp 96-117.

(17) MEHTA, P. K.

"Hardened cement paste - Microstructure and its relationship to properties", 8th Intern. congress on the chemistry of cement, Proc., Vol. I, pp 113-121, Rio de Janeiro, Brazil, 1986.

(18) POWERS, T. C.

"Structure and physical properties of hardened cement

paste", Journal of the American ceramic society, Vol. 41, pp 1-6, 1958.

(19) KONDO, R. ; DAIMON, M.
"Phase composition of hardened cement paste", Proc., of the VI Intern. conf. on the chemistry of cement, Moscow, 1974.

(20) LONGUET, P. ; BURGLEN, L. ; ZELWER, A.
"La phase liquid du ciment hydrate", Revue Materiaux de construction et Travaux Publics, Vol. 676, 1973, pp 35-41.

(21) BARNEYBACK, R. S. Jr. ; DIAMOND, S.
"Expression and analysis of pore fluids from hardened cement pastes and mortars", Cement and Concrete Research, Vol. 11, 1981, pp 279-285.

(22) POWERS, T. C.
"The physical structure of portland cement paste", chapter 10 - The chemistry of cements, H.F.W. Taylor, Ed., Academic Press, Pub., London, 1964, pp 391-416.

(23) HANSEN, T. C.
"Physical structure of hardened cement paste - A classical approach ", Materials and Structures, Vol. 19, No 114, 1986, pp 423-436.

(24) NEVILLE, A. M.
"Properties of concrete", 3rd edition, Pitman, Pub., London, 1981, pp 32-35.

(25) SMOLCZYK, H. G.
"Slag structure and identification of slags", 7th

Intern. congress on the chemistry of cements, Proc. Vol I, principal reports, sub-theme III-1, pp 4-17, Septima ed., Paris 1980.

(26) RAMACHANDRAN, V. S. ; FELDMAN, R. F. ; BEAUDOIN, J. J. "Concrete science, treatise on current research", Heyden, Pub., London, 1981, pp 271-273, 186-189.

(27) SILSBEE, M. ; MALEK, R. I. A. ; ROY, D. M. "Composition of pore fluids extruded from slag cement pastes", 8th Intern. congress on the chemistry of cement, Proc., Vol. IV, theme 3, pp 263-269, Rio de Janeiro, 1986.

(28) VOGEL, A. T. "Vogel's text-book of quantitative inorganic analysis", forth edition, Longmans, Pub., London, 1978, pp 310-311.

(29) ibid. pp 754-755.

(30) ibid. pp 695-697.

(31) CROMPTON, T. R. "Determination of organic substances in water", Vol. 1, Chichester Wiley - Interscience Pub., 1985, pp 247-249.

(32) THOMAS, L. C. ; CHAMBERLIN, G. J. "Colorimetric chemical analytical methods", 9th edition, The Tintometer Ltd Pub., Salisbury England, 1980, pp 24-26.

(33) WEISS, J. "Handbook of ion chromatography", Dionex Pub., 1986,

pp 1-4, 19-20.

(34) LEA, F. M.

"The chemistry of cement and concrete", third edition, Edward Arnold Pub., London, 1970, pp 270-279.

(35) TAYLOR, H. F. W.

"Bound water in cement paste and its significance for pore solution compositions", Mat. Res. Soc. Symp., Proc., Vol 85, pp 47-54, Materials Research Society, 1987.

(36) LAMBERT, P.

"The corrosion and passivation of steel in concrete", PhD thesis, Aston University, 1983.

(37) SERGI, G.

"Corrosion of steel in concrete: cement matrix variables", PhD thesis, Aston University, 1986.

(38) BERMAN, H. A.

"Determination of chloride in hardened portland cement paste, mortar and concrete", Journal of Materials, Vol. 7, 1972, pp 330-335.

(39) BRAGG, L.

"The crystalline state, Vol.1, A general survey", Bell, Pub, 1949.

(40) TAYLOR, H. F. W. (edidor)

"The chemistry of cements", Vol.2, Appendix I, Academic Press, Pub., London, 1964, pp 347-404.

(41) WASHBURN, E. W.

"Porosity I. Purpose of investigation. II. Porosity and

the mechanism of absorption", Journal of the American ceramic Society, Vol. 4, 1921, pp 916-922.

(42) WINSLOW, P. M. ; DIAMOND, S.
"A mercury porosimetry study of the evolution of porosity in Portland cement", Journal of Materials, Vol. 5, (3), 1970, pp 564-585.

(43) HOOTON, R. D.
"Permeability and Pore structure of cement pastes containing Fly Ash, Slag, and Silica fume", Blended Cements, ASTM STP 897, G. Frohnsdorff Ed., ASTM, Philadelphia, 1986, pp 128-143.

(44) FELDMAN, R. F.
"Significance of porosity measurements on blended cement performance", Proc. of the CANMET/ACI first International conference on the use of Fly Ash, Silica Fume, Slag and other mineral by-products in concrete, Montebello, Canada, ACI SP-79, Vol.1, V.M. Malhotra, Ed.,1983, pp 415-434.

(45) FELDMAN, R. F.
"Pore structure damage in blended cements caused by mercury intrusion", Journal of the American Ceramic Society, Vol. 67(1), 1984, pp 30-33.

(46) DAY, R. L. ; MARSH, B. K.
"Measurement of porosity in blended cement pastes" Cement and Concrete Research, Vol.18, pp 63-73, 1988.

(47) BUENFELD, N.

Discussion on the paper: "Permeability of normal and lightweight mortars", by B. K. Nyame, Magazine of Concrete Research, Vol. 38 (134), 1986, pp 51-52.

(48) MARSH, B. K. ; DAY, R. L.

"Some difficulties in the assesment of pore structure of high performance blended cement pastes", Materials Research Society Symp., Proc., "Very High Strength Cement-based Materials", Vol. 42(1), pp 113-122, 1985.

(49) MIDGLEY, H. G. ; ILLSTON, J. M.

"Some comments on the microstructure of hardened cement pastes", Cement and Concrete Research, Vol. 13, (2), pp 197-206, 1983.

(50) SEREDA, P. J. ; FELDMAN, R. F. ; RAMACHANDRAN, V. S.

"Structure formation and development in hardened cement pastes", 7th Intern. Congress on the chemistry of cement, Proc., Vol. I, principal reports, sub-theme VI-1, pp 4-44, ed. Septima, Paris, 1980.

(51) PIHLAJAVAARA, S. E.

"Some results of the effect of carbonation on the porosity and pore size distribution of cement paste". Materiaux et constructions, Vol. 1, No 6 (1968) pp 521-526.

(52) KONDO, R. ; DAIMON, M. ; AKIBA, T.

"Mechanisms and Kinetics on carbonation of hardened cement", 5th Intern. Symp. on the chemistry of cement

Proc., Vol. III, Supplementary paper III-116, pp 402-409, Tokyo 1968.

(53) DAIMON, M. ; AKIBA, T. ; KONDO, R.
"Through pore size distribution and kinetics of the carbonation reaction of portland cement mortars". Journal of the American Ceramic Society , Vol. 54, No 9 (1981), pp 423-428.

(54) Handbook of Chemistry and Physics
52nd edition, The chemical Rubber Co, Cleveland Ohio, 1971-1972.

(55) KLEMM, W. A. ; BERGER, R. L.
"Accelerated curing of cementitous systems by carbon dioxide, Part I: Portland cement". Cement and Concrete Research, Vol. 2, 1972, pp 567-576.

(56) SAUMAN, Z.
"Carbonation of porous concrete and its main binding components", Cement and Concrete Research, Vol. 1, pp 645-662, 1971.

(57) SAUMAN, Z.
"Effect of CO_2 on porous concrete", Cement and Concrete Research, Vol 2, pp 541-549, 1972.

(58) MATOUSEK, M.
"Carbonation of cellular concrete under the conditions in exposed structures", Carbonation of concrete-RILEM Intern. Symp., Cement and Concrete Association, theme 6, paper 4, 1976.

(59) PARROTT, L. J.

"A review of carbonation in reinforced concrete", Cement and Concrete Association, Slough, 1987.

(60) NISCHER, P.

"Influence of concrete quality and environment on carbonation", Proc., RILEM seminar on the durability of concrete structures under normal outdoor exposure, Hannover, 1984, pp 231-238.

(61) BYE, G. C.

"Portland cement, composition, production and properties", Appendix, Pub.: The institute of ceramics, Pergamon press, London, 1983, p.139.

(62) HAMADA, M.

"Principal paper - Neutralization (carbonation) of concrete and corrosion of reinforcing steel", 5th Intern. Symp. of the chem. of cement, Proc., Vol III, part III, Properties of cement and concrete, pp 343-369, Tokyo 1968.

(63) SMOLCZYK, H. G.

"Explorations to the German longtime - study on the rate of carbonation", Carbonation of concrete - RILEM Intern. Symp., Cem. and Concr. Ass., Theme 3, paper 2, 1976.

(64) WIERIG, H. J.

"Longtime studies on the carbonation of concrete under normal outdoor exposure", Proc. , RILEM seminar on the durability of concrete structures under normal

outdoor exposure, Hannover, 1984, pp 239-249.

(65) TREADAWAY, K. W. J., MACMILLAN, G., HAWKINS, P., FONTENAY, C.

"The influence of concrete quality on carbonation in Middle Eastern conditions - A preliminary study", Corrosion of reinforcements in concrete construction, Proc., Soc. of Chem. Industry, London 1983, pp 101-118.

(66) HO, D. W. S., LEWIS, R.K.

"Carbonation of concrete and its prediction", Cement and Concrete Research, Vol. 17, pp 489-504, 1987.

(67) MEYER, A.

"Investigations on the carbonation of Concrete", 5th Intern. Symposium on the chemistry of cement, proc., supplementary paper III - 52, pp 394-401, Tokyo 1968.

(68) AKIBA, T., MINEGISHI, K., SUDOH, G.

"Mechanisms and Kinetics in neutralization of concrete in sea water", 7th Intern. congr. on the chemistry of cement Proc. Vol. III communications, pp VII57-VII62, Paris 1980.

(69) SCHUBERT, P, von BERG W.

"The carbonation behaviour of mortars and concretes containing fly ash", Carbonation of concrete - RILEM Intern. Symp., Cement and Concrete Assosiation, theme 3, paper 4, 1976.

(70) SCHUBERT, P., EFES, Y.

"The carbonation behaviour of mortar and concrete with jet cement", Carbonation of concrete - RILEM Intern. Symp., Cem. and Concr. Ass., theme 3, paper 5, 1976.

(71) ALEKSEEV, S. N., ROZENTAL, N. K.

"The rate of concrete carbonation", Carbonation of concrete - RILEM Int. Symp., Cem. and Concr. Ass., theme 3, paper 6, 1976.

(72) SMOLCZYK, H. G.

"Written discussion - Carbonation of concrete", 5th Intern. Symp. on the chemistry of cement, Proc., Vol. III, part III, pp 369-382, Tokyo 1968.

(73) SMOLCZYK, H. G.

"Oral discussion - Carbonation of concrete", 5th Intern. Symp. on the chemistry of cement, Proc., Vol III, part III, pp 382-383, Tokyo 1968.

(74) SMOLCZYK, H. G.

"Physical and chemical phenomena of carbonation", Carbonation of concrete - RILEM Intern. Symp., Cem. and Concr. Ass., theme 1, paper 1, 1976.

(75) VERBECK, G. J.; HELMUTH, R. H.

"Principal paper - Structures and physical properties of cement paste", 5th Intern. Symp. on the chemistry of cement, Proc. Vol III, part III, pp 1-31, Tokyo 1968.

(76) MILLS, R. H.

"Molecular sieve effect in concrete", 5th Intern. Symp.

of the chemistry of cement, Proc., vol III, supplementary paper III-46, pp 74-85, Tokyo 1968.

(77) SCHOLZ, E.; WIERIG, H. J.
"Carbonation of fly ash concrete", Proc. RILEM seminar on the durability of concrete structures under normal outdoor exposure, Hannover, 1984, pp 258-265.

(78) KRZYWOBLOCKA - LAUROW, R.
"Effect of increased curing temperature upon carbonation of concrete", Carbonation of concrete RILEM Intern. Symp., Cem. and Concr. Ass., theme 1, paper 6, 1976.

(79) SCHIEBL, P.
"Some aspects of corrosion protection of reinforcement embeded in outdoor structural members", Proc. RILEM seminar on the durability of concrete structures under normal outdoor exposure, Hannover, 1984, pp 197-201.

(80) SAUMAN, Z.; LACH, V.
"Longterm carbonization of the phases $3CaO.Al_2O_3.6H_2O$ and $3CaO.Al_2O_3.SiO_2.4H_2O$", Cement and concrete Research, Vol. 2, pp 435-446, 1972.

(81) MAYCOCK, N. J.; SKALNY. J.
"Carbonation of hydrated calcium silicates", Cement and concrete Research, Vol. 4, pp 69-76, 1974.

(82) PIHLAJAVAARA, S. E.; PIHLMAN, E.
"Effect of carbonation on microstructural properties of cement stone", Cement and concrete Research, Vol.

4, pp 149-154, 1974.

(83) POWERS, T.C.

"A hypothesis on carbonation shrinkage", Journal of the portland cement Association, (Research and Development Labs), Vol. 4, No 2, pp 40-50, 1962.

(84) BERGER, R.

"Stabilization of silicate structures by carbonation" Cement and Concrete Research Vol. 9, pp 649-651, 1979.

(85) SAUMAN, Z., LACH, V.

"To the long term carbonation of binding components in cellular concretes", Carbonation of concrete - RILEM Intern. Symp., Cem. and concr. Assoc., theme 6, paper 3, 1976.

(86) ROY, D. M.

"Mechanisms of cement paste degradation due to chemical and physical factors", 8th Intern. Congr. on the chemistry of cement, Vol I, principal reports, pp 362-380, Rio de Janeiro, 1986.

(87) COLE, W. F.; KROONE, B.

"Carbon dioxide in hydrated portland cement", Journal of the American concrete Institute, Proc., Vol. 56, No 64 pp 1275-1295, 1960.

(88) MOOREHEAD, D.R.

"Cementation by the carbonation of hydrated Lime", Cement and Concrete Research , Vol.16, pp 700-708, 1986.

(89) ROZENTAL, N. K., ALEKSEEV, S. N.
"Change in concrete porosity during carbonation", Carbonation of concrete-RILEM Intern. Symp., Cem. and Concr. Assoc., theme 2, paper4, 1976.

(90) YUPING, Z.; DEDONG, L.; GUOKUANG, S.
"Investigation into the carbonation of autoclaved aerated concrete", 8th Intern. Congr. on the chemistry of cement, Proc., Vol. V, theme 4, pp 93-98, Rio de Janeiro, 1986.

(91) PIHLAJAVAARA, S. E.
"Carbonation, engineering properties, and effects of carbonation on concrete structures", Carbonation of concrete - RILEM Intern. Symp., Cem. and Concr. Assoc., theme 4, paper 1 1976.

(92) MANNS, W.,;WESCHE, K.
"Variation in strength of mortars made of different cements due to carbonation", 5th Inter. symp. of the chemistry of cement, Proc., Vol. III, supplementary paper III-16, pp 385-393, Tokyo 1968.

(93) VERBECK, G.
"Carbonation of hydrated portland cement", Second pacific area national meeting : "Cement and Concrete", Los Angeles, 1956, ASTM s.t.p. No 205, pp 17-36, American Society for Testing Materials, 1958.

(94) PARROTT, L. J.
"Increase in creep of hardened cement paste due to carbonation under load", Magazine of concrete

research, Vol. 27, No 92, pp 179-181, 1975.

(95) GONZALEZ, J. A.; ALGABA, S.; ANDRADE, C.
"Corrosion of reinforcing bars in carbonated concrete", British Corrosion Journal, Vol. 15, No 3, pp 135-139, 1980.

(96) GONZALEZ, J. A.; ALONSO, C.; ANDRADE, C.
"Corrosion rate of reinforcements during accelerated carbonation of mortar made with different types of cement", Intern. conference on corrosion of reinforcements in concrete construction, Proc., A. P. Crane Ed., Society of chemical industry, pp 159-174, London, 1983.

(97) TREADAWAY, K. W. J.
"Research into durability of reinforcement in concrete structures under normal exposure conditions", Proc., RILEM seminar on the durability of concrete structures under normal outdoor exposure, Hannover, 1984, pp 202-209.

(98) RILEM Draft Recomendation CPC-18
"Measurement of hardened concrete carbonation depth", Materiaux et construction, Vol. 17, No102, pp 435-440, 1984.

(99) FORRESTER, J. A.
"Measurement of carbonation", Carbonation of concrete-RILEM Intern. Symp., Cem. and Concr. Assoc., theme 2, paper 1, 1976.

(100) KOLTHOFF, I. M., ELVING, P. J.

"Treatise on analytical chemistry", Part II, Vol. 2 pp 114-115 and 132-133, Wiley - Interscience Pub. New York, 1962.

(101) ILER, R.

"The chemistry of silica", Wiley - Interscience Pub., New York, 1979, pp 94-104.

(102) RAMACHANDRAN, V. S.

"Applications of differential thermal analysis in cement chemistry", Pub: Chemical Publishing company, New York, 1969.

(103) LACH, V, SAUMAN, Z.

"The determination of $CaCO_3$ modifications in the carbonated concrete", Carbonation of concrete – RILEM Intern. Symp., Cem. and Concr. Assoc., theme 1, paper 5, 1976.

(104) REGOURD, M. ; HORNAIN, H. ; MORTUREUX, B.

"Microstructure of concrete in aggressive environments", Durability of building materials and components, ASTM STP 691, P. J. Sereda and G. G. Litran, Eds., American Society for Testing and Materials, 1980, pp 253-268.

(105) FTIKOS, Ch. ; PARISSAKIS, G.

"The combined action of Mg^{++} and Cl^- ions in cement pastes", Cement and Concrete Research, Vol. 15, pp 593-599, 1985.

(106) KRISHNAMOORTHY, S.; JAIN, N. K.
"Influence of blending fly ash with portland cement on the pore structure changes of portland cement mortars cured in NaCl solutions", 8th Intern. congr. on the chemistry of cement, Proc., Vol. V, theme 4, pp 67-72, Rio de Janeiro, 1986.

(107) ATKINSON, A.; HEARNE, J. A.; KNIGHTS, O. F.
"Aqueous chemistry and thermodynamic modelling of $CaO-SiO_2-H_2O$ gels", U.K. Atomic energy authority, Harwell, report AERE-R12548, 1987.

(108) PAGE, C. L.; VENNESLAND, O.
"Pore solution composition and chloride binding capacity of silica fume cement pastes", Materiaux et construction, Vol 16, No 91, 1983, pp 19-25.

(109) ROY, D. M.; IDORN, G. M.
"Hydration, structure and properties of blast furnance slag cements, mortars and concretes", Journal of the American concrete Institute, Proc., Vol. 79, No 43, 1982, pp 444-457.

(110) BUTLER, F. G.; MORGAN, S.R.; WALKER, E. J.
"Studies on the rate and extent of reaction between calcium hydroxide and pulverized fuel ash", 5th Intern. Conf. on Alkali-Aggregate Reactions in concrete, Proc., Cape Town 1981, National Building Research Institute, CSIR, Pretoria, 1981 5252/38, pp 1-6.

(111) KAY, E. A.; FOOKES, P. G.; POLLOCK, D.J.
"Deterioration related to chloride ingress", Concrete,

Vol. 15, No 11, 1981, pp 22-28.

(112) British Standard Code of Practice, CP110 part I: 1972 (Ammended, May 1977).

(113) JOST, W.
"Diffusion in solids, liquids, gases", Academic press Inc., New York, 1960, pp 139-143.

(114) ibid. pp 1-3

(115) BUENFELD, N. R.; NEWMAN, J. B.
"Examination of three methods for studying ion diffusion in cement pastes, mortars and concrete", Materials and structures, Vol. 20, 1987, pp 3-10.

(116) PAGE, C. L.; SHORT, N. R.; TARRAS, A. El.
"Diffusion of chloride ions in hardened cement pastes", Cement and Concrete Research, Vol. 11, 1981, pp 395-406.

(117) KONDO, R.; SATAKE, M.; USHIYAMA, H.
"Diffusion of various ions in hardened portland cement", Cement Association of Japan, 28th general meeting, Tokyo 1974, pp 41-43.

(118) GOTO,S.; ROY, D. M.
"Diffusion of ions through hardened cement pastes", Cement and Concrete Research, Vol.11, 1981, pp 751-757.

(119) ATKINSON, A. ; NICKERSON, A. K.
"The diffusion of ions through water saturated cement", Journal of Materials science, Vol. 19, 1984, pp 3068-3078.

(120) ATKINSON, A. ; NICKERSON, A. K.
"Diffusion and sorption of Cs, Sr and I in water saturated cement", U.K. atomic energy authority, Harwell, report AERE R12124, 1986.

(121) PARSONS, R.
"Handbook of electrochemical constants", Pub.: Butterworth, London, 1959.

(122) TAKAGI, T.; GOTO, S.; DAIMON, M.
"Diffusion of I^- ion through hardened cement paste", Review of the 38th general meeting of cement Association of Japan, May 1984, pp 72-75.

(123) GOTO, S.; DAIMON, M.
"Ion diffusion in cement paste", 8th International congress in the chemistry on cement, Proc., Vol. VI, pp 405-409, Rio de Janeiro, 1986.

(124) STEIN, H. N.
"Surface charges on calcium silicates and calcium silicate hydrates", Journal of colloid and interface science, Vol. 28, No 2, 1968, pp 203-213.

(125) UCHIKAWA, H.; UCHIDA, S.; OGAWA, K.
"Diffusion of alkali ions in hardened cement paste containing slag or fly ash", Review of the 38th general meeting of the cement Association of Japan, Vol. 14, 1984, pp 56-59.

(126) UCHIKAWA, H.; UCHIDA, S.; OGAWA, K.
"Influence of character of blending component on the diffusion of Na^+ and Cl^- ions in hardened blended

cement paste", 8th Intern. Congr. on the chemistry of cement, Proc., Vol. IV, theme 3, Rio de Janeiro, 1986, pp 251-256.

(127) BAKKER, R. F. M.

"On the cause of increased resistance of concrete made from blast furnance cement to the alkali-silica reaction and to sulphate corrosion", Doctorial Thesis, Maastricht, The Netherlands, 1980, RWTH, Aachen, FRG.

(128) BAKKER, R. F. M., THOMASSEN, W. J. M.

"The influence of the type of cement on the diffusion of ions", Concrete Research Foundation of the Dutch cement industries, June 1977.

(129) SMOLCZYK, H. G.; RHEINHAUSEN, D.

"State of knowledge on chloride diffusion in concrete", Betonwerk + Fertigteil - Technic, HEFT 12, 1984, pp 837-843.

(130) BRODERSEN, H. A.

"Zur Abhangigkeit der Transportvorgange verschiedener ionen im Beton von Struktur und Zusammensetzung des Zementsteines", Dissertation, RWTH Aachen, 1982, s. a. "Transportvorgange verschiedener ionen in Beton", Beton - Informationen, 23, 1983 H.3.S. 36/38.

(131) KUMAR, A. ; ROY, D. M.

"Retardation of Cs^+ and Cl^- diffusion using blended cement admixtures", Journal of the Americal Ceramic

society, Vol. 69, No 4, 1986, pp 356-360.

(132) KUMAR, A., ROY, D. M.

"Pore structure and ionic diffusion in admixture blended portland cement systems", 8th Intern. congress on the chemistry of cement, Vol. V, communications, theme 4, pp 73-79, Rio de Janeiro, 1986.

(133) KUMAR, A.; ROY, D. M.

"Diffusion and pore structure in portland cement pastes blended with low calcium fly ash", Mat. Res. Soc. Symp. Proc., Vol. 85, 1986, Materials Research, Society.

(134) LI, S. ; ROY, D. M.

"Investigation of relations between porosity, pore structure and Cl^- diffusion of fly ash and blended cement pastes", Cement and Concrete Research, Vol.16, 1986, pp 749-759.

(135) MALEK, R.I.A.; ROY, D. M.; LICASTRO, P.H.

"The diffusion of chloride ions in fly Ash cement pastes and mortars", Mat. Res. Soc. Symp. Proc., Vol. 86, 1987, Materials Research Society, pp 239-250.

(136) PAGE, C. L.

"An overview of current research", 2nd International conference on deterioration and repair of reinforced concrete in the Arabian Gulf, Proceedings, Vol.II, Bahrain, 1987, pp 161-171.

(137) SPINKS, J.W.T.; BALDWIN, H.W.; THORVALDSON, T.
"Tracer studies of diffusion in set portland cement", Canadian Journal of Technology, Vol. 30, 1952, pp 20-28.

(138) COLLEPARDI; M.; MARCIALIS, A.; TURRIZIANI, R.
"The penetration of de-icing agents in cement pastes", Il cemento, 3/1972, pp 143-149.

(139) COLLEPARDI, M.; MARCIALLIS, A.; TURRIZIANI, R.
"The kinetics of penetration of chloride ions into the concrete", Il cemento, 4/1970, pp 157-164.

(140) COLLEPARDI, M.; MARCIALLIS, A.; TURRIZIANI, R.
"Penetration of chloride ions into cement pastes and concretes", Journal of the American Ceramic Society, Vol. 55, 1972, p 534.

(141) GOTO, S. ; TSUNETANI, M. ; YANAGIDA, H. ; KONDO, R.
"Diffusion of chloride ion in hardened cement paste", Journal of Ceramic Society of Japan, Vol. 87, 1979, pp 126-133.

(142) TRAETTEBERG, A.
"The mechanism of chloride penetration in concrete", Report by: Cement and Concrete Research Institute, Trondhein, Norway, STF65, A77070, 1977.

(143) MIDGLEY, H. G.; ILLSTON, J. M.
"Effect of chloride penetration on the properties of hardened cement pastes", 7th Intern. congress on the chemistry of cement, Proc., Vol. III, communications, theme VII, pp 101-103, ed. Septima, Paris, 1980.

(144) MIDGLEY, H. G.; ILLSTON, J. M.

"The penetration of chlorides into hardened cement paste", Cement and Concrete Research, Vol. 14, pp 546-558, 1984.

(145) MEHTA, P. K.

"Effect of cement composition on corrosion of reinforcing steel in concrete", Chloride corrosion of steel in concrete, ASTM STP 629, D. E. Tonini and S. W. Dean, Eds., American Society for testing and Materials, 1977, pp 12-19.

(146) GJORV, O. E.; VENNESLAND, O.

"Diffusion of chloride ions from seawater into concrete", Cement and Concrete Research, Vol 9, pp 229-238, 1979.

(147) OST, B. ; MONFORE, G. E.

"Penetration of chloride into concrete", Journal of the PCA research and development laboratories, Vol. 8(1), 1966, pp 46-52.

(148) BOCKRIS, J. O. M. ; REDDY, A. K. N.

"Modern Electrochemistry", Vol. 1, Macdonald, Pub., London, 1970, pp 340-342, 455-458.

(149) LOW, P. F.

"Influence of adsorbed water on exchangeable ion movement", Clays and Clay Minerals, Vol. 9, ed. A. Swineford, Proc. 9th National conference on clays and Clay Minerals, Lafayette, Indiana, 1960, pp 219-228, Pergamon, Oxford, 1962.

(150) REGOURD, M.

"Structure and behaviour of slag portland cement hydrates", 7th Intern. congress on the chemistry of cement.Proc., Vol. I, principal reports, sub-theme III-2, pp 10-26, Paris 1980.

(151) REGOURD M.

"Slags and slag cements", Concrete Technology and Design, Vol. 3, Cement replacement materials, R. N. Swamy, Ed., Surrey University Press, Blakie, Pub., London, 1986, pp 73-99.

(152) SERSALE, R. ; MARCHESE, B. ; FRIGIONE, G.

"Microstructure and properties of hydrated cements with different slag content", 7th Intern. congr. on the chemistry of cement, Proc., Vol. II, communications, III-63 -III-68, ed. Septima, Paris 1980.

(153) LAMBERT, P. ; PAGE, C. L. ; SHORT, N. R.

"Diffusion of chloride ions in hardened cement pastes containing pure cement minerals", British ceramic society, Proc., The chemistry of chemically related properties of cement, F. P. Glasser ed., No 35, Sept. 1984, pp 267-276.

(154) DAUBE, J. ; BAKKER, R.

"Portland Blast-furnance Slag cement: a review", Blended cement, ASTM STP 897, G. Frohnsdorff, Ed., ASTM, Philadelphia, 1986, pp 5-14.

(155) EFES, Y.

"Effect of cements with varying content of granulated

blast furnance slag on chloride diffusion in concrete", Betenwerk + Fertigteil - Technik, Heft 4, 1980, pp 224-228, 5, pp 302-306, 6, pp 365-368.

(156) BAKKER, R. F. M.

"Permeability of blended cement concretes", Proc. of the CANMET/ACI first Intern. conf. on the use of fly ash, silica fume, slag and other mineral by-products in concrete, Montebello, 1983, M. Malhotra, Ed., ACI Pub., SP-79, Vol.1, pp 589-605.

(157) SHAW, D. J.

"Inroduction to colloid and surface chemistry", 3rd edition, Butterworths Pub., London, 1980, p 149.

(158) GINSBURG, D.

"Concerning Amines, their properties, preparation and reactions", The commonwealth and international library, Pergamon press, 1967, pp 73-75 and 126-132.

(159) ROBINSON, R. A. ; STOKES, R. H.

"Electrolyte solutions", 2nd edition (revised), Butterworths, London, 1970.

(160) NEWMAN, K.

"Concrete systems", chapter 8 - "Composite materials", L. Holiday ed. , Elsevier Pub., 1966, pp 336-446.

(161) LE CHATELIER, H.

Ann. des Mines, Ser. 8, Vol. II, 1887, p 345.

(162) MICHAELIS, W.

Chemikerzeitung, Vol 17, 1893, p 982.

(163) BERNAL, J. D. ; JEFFERY, J. W. ; TAYLOR, H. F. W.
"Crystallographic research on the hydration of Portland cement. A first report on investigations in progress", Magazine of Concrete Research, Vol.4, 1952, pp 49-54.

(164) POWERS, T. C.
"Structure and physical properties of hardened portland cement paste", Journal of the American Ceramic Society, Vol. 41, 1958, pp 1-6.

(165) WITTMANN, F. H. J.
"Interaction of hardened cement paste and water", Journal of the American Ceramic Society, vol. 56, No 8, 1973, pp 409-415.

(166) KROKOSKY, E. M.
"Strength vs structure. A study for hydraulic cement", Materiaux et constructions, Vol. 3, No 17, 1970, pp 313-323.

(167) BRUNAUER, S.
"Tobermorite gel - the heart of concrete", American Scientist, vol. 50, 1962, pp 210-229.

(168) ODLER, I. ; ROBLER, M.
"Investigations on the relationship between porosity structure, and strength of hydrated cement pastes, part II: effect of pore structure and of degree of hydration", Cement and Concrete Research, Vol. 15, 1985, pp 401-410.

(169) ROBLER, M. ; ODLER, I.

"Investigations on the relationship between porosity, structure and strength of hydrated cement pastes, Part I: effect of porosity", Cement and Concrete Research Vol. 15, 1985, pp 320-330.

(170) RYSHKEWITCH, E.

"Compression strength of porous sintered alumina and zirconia", 9th communication to ceramography, Journal of the American Ceramic Society, Vol. 36, 1953, pp 65-68.

(171) SCHILLER, K. K.

"Strength of porous materials", Cement and Concrete Research, Vol. 1, 1971, pp 419-422.

(172) HASSELMANN, D. P. H.

"On the porosity dependence of the elastic moduli of polycrystalline refractory materials", Journal of the American Ceramic Society, Vol 45, 1962, pp 452-453.

(173) HASSELMANN, D. P. H.

"Relation between effects of porosity on strength and on Youngs's modulus of elastisity of polycrystalline materials", Journal of the American Ceramic Society, Vol.46, 1963, pp 564-565.

(174) FAGERLUND, G.

"Strength and porosity of concrete", Proc. RILEM/IUPAC symposium : Pore structure and properties of materials, Academia, Prague, 1974.

(175) ODLER, I. ; YUDENFREUND, M. ; SKALNY, J. ; BRUNAUER, S.
"Hardened cement pastes of low porosity, part III" Cement and Concrete Research, Vol. 2, No 4, 1972, pp 463-480.

(176) YUDENFREUND, M. ; HANNA, K. M. ; SKALNY, J.; ODLER, I. ; BRUNAUER, S.
"Hardened cement pastes of low porosity, part V", Cement and Concrete Research, Vol. 2, No 6, 1972, pp 731-743.

(177) ROY, D. M. ; GOUDA, G. R.
"Porosity - strength relation in cementitious materials with very high strengths", Journal of the American Ceramic Society, Vol 56, 1973, pp 549.

(178) ROY, D. M. ; GOUDA, G. R. ; BOBROWSKY, A.
"Very high strength cement pastes prepared by hot pressing and other high pressure techniques", Cement and Concrete Research, Vol.2, 1972, pp 349-366.

(179) BROWN, S.; BIDDULPH, R. B. ; WILCOX, P. D.
"A strength - porosity relation involving different pore geometry and orientation", Journal of the American Ceramic Society, Vol.47, 1964, pp 320-322.

(180) JAMBOR, J.
"Pore structure and strength of hardened cement pastes", 8th Intern. Congr. on the chemistry of cement, Proc., Vol. III, theme 2, pp 363-368, Rio de Janeiro, 1986.

(181) JAMBOR, J.

"Influence of water - cement ratio on the structure and strength of hardened cement pastes", Conference on Hydraulic cement pastes: their structure and properties, Proc., Sheffield 1976, Cem. and Concr. Ass., Slough, pp 175-188.

(182) BIRCHALL, J. D. ; HOWARD, A. J. ; KENDALL, K.

"Flexural strength and porosity of cements", Nature, Vol. 289, 1981, pp 388-389.

(183) BIRCHALL, J. D.

"Cement in the contex of new materials for an energy - expensive future", Phil., Trans. Royal Soc. London, A310, pp 31-42, 1983.

(184) ALFORD, N., McN.

"A theoretical argument for the existence of high strength cement pastes", Cem. and Concr. Res., Vol. 11, 1981, pp 605-610.

(185) ALFORD, N., McN. ; GROVES, G. W. ; DOUBLE, D. D.

"Physical properties of high strength cement pastes", Cem. and Concr. Res. Vol. 12, 1982, pp 349-358.

(186) KENDALL, K. ; HOWARD, A. J. ; BIRCHALL, J. D.

"The relation between porosity, microstructure and strength and the approach to advanced cement based materials", Phil. Trans. Royal Soc. London, A310, pp 139-153, 1983.

(187) GROVES, G. W.

"Microcrystalline calcium hydroxide in portland

cement pastes of low w/c ratio", Cem. and Concr. Res., Vol. 11, 1981, pp 713-718.

(188) DALGLEISH, B. J. ; PRATT, P. L. ; MOSS, R. I.
"Preparation techniques and the microscopical examination of portland cement paste and C_3S", Cement and Concrete Research, Vol 10, 1980, pp 665-676.

(189) HASSELMAN, D. P. H. ; FULRATH, R. M.
"Micromechanical stress concentrations in two -phase brittle matrix ceramic composites", Journal of the American Ceramic Soc., vol 50, 1967, pp 399-404.

(190) WILLIAMSON, R. B.
"Solidification of portland cement", Progress in materials science, Vol. 15, No 3, 1972, pp 269-281.

(191) WRIGHT, W. ; BYRNE, J. G.
"Stress concentration in concrete", Nature, Vol. 203, 1964, pp 1374-1375.

(192) HIGGINS, D. D. ; BAILEY, J. E.
"Fracture measurements on cement paste", Journal of Materials science, Vol. 11, 1976, pp 1995-2003.

(193) BEAUDOIN, J. J. ; FELDMAN, R. F.
"High strength cement pastes, a critical appraisal", Cem. and Concr. Res., Vol. 15, 1985, pp 105-116.

(194) SWAMY, R. N.
"Polymer reinforcement of cement systems", Journal of Materials Science, Vol. 14, 1979, pp 1521-1553.

(195) ALEXANDER, K. M.
"Errors caused by partial drying of hardened portland cement during testing", Nature, Vol. 183, 1959, pp 885-886.

(196) JAYATILAKA, A. de S.
"Fracture of engineering brittle materials", Applied science publishers, London, 1979, pp 122-126.

(197) LIEBOWITZ, H. (edidor)
"Fracture, an advanced treatise", Vol. VII, Academic Press, New York. 1972, pp 256-258.

(198) CHATFIELD, C.
"Statistics for technology", third edition, pub: Chapman and Hall, London, 1983, pp 166-199.

(199) ibid. pp 134-146.

(200) ibid. p 336.

APPENDIX 1 : Determination of carbonates and bicarbonates present in the pore solution of carbonated cement pastes.

When titrating a carbonate solution with acid, two inflections are established at around pH 9 and pH 4 which coinside respectively to the conversion to bicarbonate and to the complete neutralization (see section 2.3.3). In all the titrations carried out in the present work, no such clear inflections were observed (fig. 3.5, 3.6). It was assumed that the amount of acid needed to drop the pH of each solution down to 4, was that needed to neutralize the total amount of carbonates and bicarbonates which were in the solution. Although the results may not be totaly representative, they show the possible maximum concentrations of carbonates and bicarbonates in the extracted pore solutions.

Example calculation for the pore solution of OPC/65%BFS cement paste, carbonated in 100% CO_2.

To titrate six millilitre of pore solution down to pH 4 it required 11.8 ml of 1mM nitric acid (figure 3.5).

For bicarbonates we have:

$$HCO_3^- + H^+ \longrightarrow H_2CO_3$$

$$m = \frac{m' V'}{V}$$

where : m = molarity of solution (HCO_3^-)

V = volume of solution

m' = molarity of acid

V' = volume of acid.

$$m = \frac{1 \times 11.8}{6} = 1.97 \text{ mmol/l } HCO_3^-$$

For carbonates we have :

$$CO_3^{--} + 2H^+ \longrightarrow 2HCO_3^-$$

$$2HCO_3^- + 2H^+ \longrightarrow 2H_2CO_3$$

i.e. two lots of acid are required to titrate CO_3^{--}.

Primary ionization constant: $\frac{[H^+]\,[CO_3^{--}]}{[HCO_3^-]} = 5 \cdot 10^{-11}$

at pH 7.57 (pH of the pore solution ; table 3.2) :

$$[H^+] = 2.69 \cdot 10^{-8} \quad , \quad (pH = -\text{Log}_{10}[H^+])$$

$$\frac{[CO_3^{--}]}{[HCO_3^-]} = \frac{5 \cdot 10^{-11}}{2.69 \cdot 10^{-8}} = 1.86 \cdot 10^{-3}$$

If $y = [CO_3^{--}]$ and $x = [HCO_3^-]$, then

$$y = 1.86 \cdot 10^{-3} x \qquad \text{(eq.1)}$$

As twice as much acid is required for CO_3^{--}, we also have:

$$x + 2y = 1.97 \text{ mmol/l} \qquad \text{(eq. 2)}$$

Sub. eq. 1 into eq. 2 : $x = [HCO_3^-] = 1.96$ mmol/l

From eq. 1 : $y = [CO_3^{--}] = 3.65 \cdot 10^{-3}$ mmol/l

APPENDIX 2 : Chloride calibration curves.

Absorption values (ABS) at 460 nm wavelength as read-off the spectrophotometer were translated into Cl^- concentrations from the following calibration curves constructed from standard chloride solutions.

a. "High" concentrations :

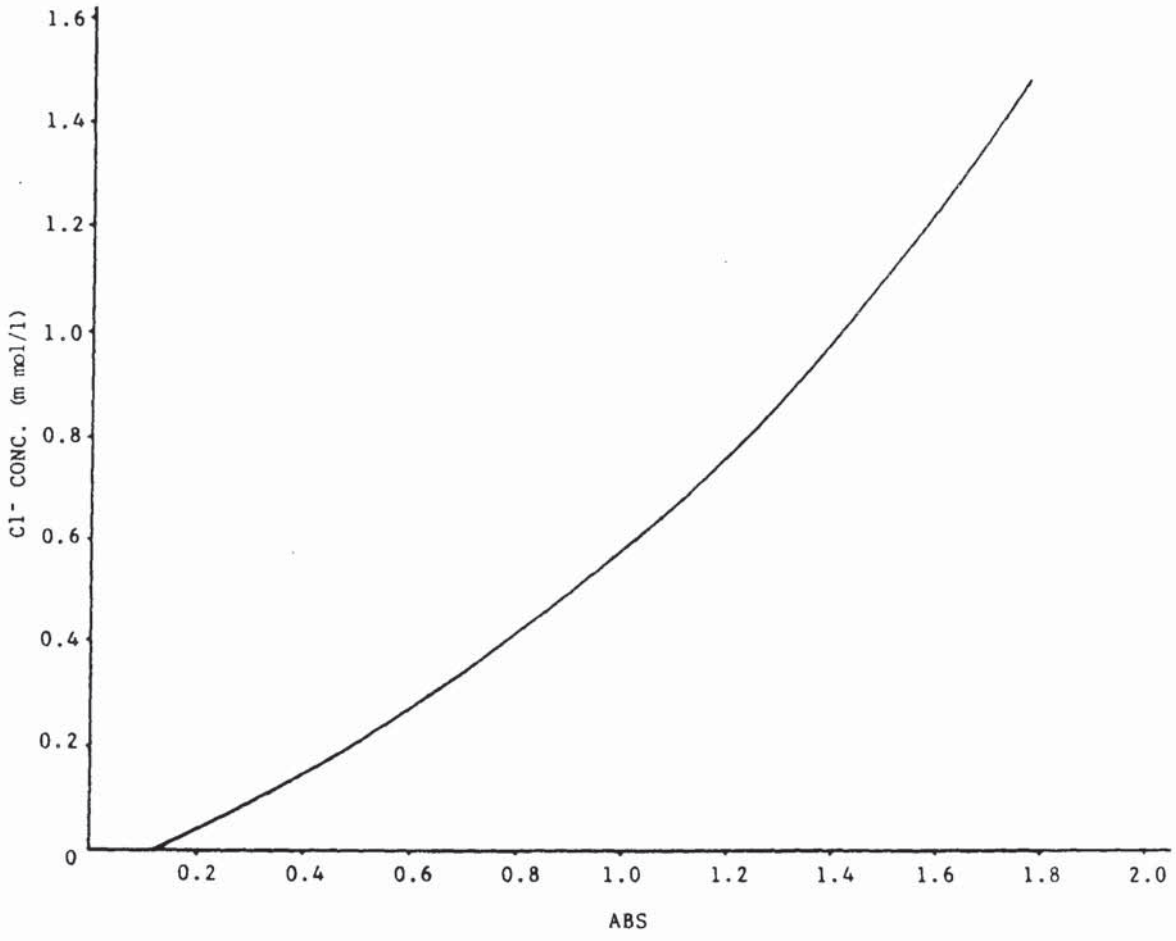

b."Low" concentrations :

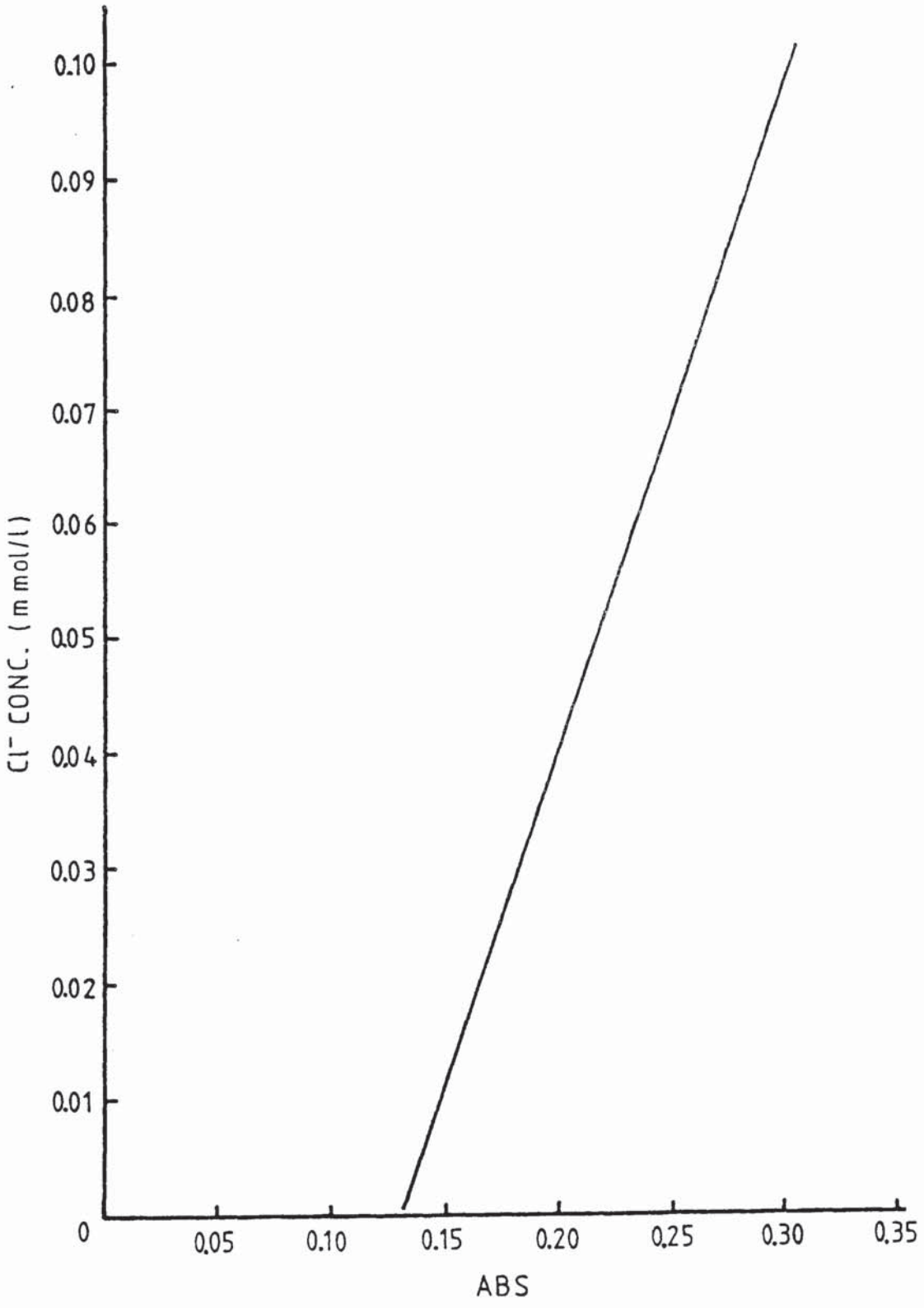

APPENDIX 3 : Calibration curves for quaternary ammonium ions.

By plotting the concentrations of standard quaternary ammonium ion solutions against absorption values (ABS) obtained from the spectrophotometer, at 415 nm wavelength, the following calibration curves were constructed.

a. $(C_2H_5)_4N^+$ calibration curve :

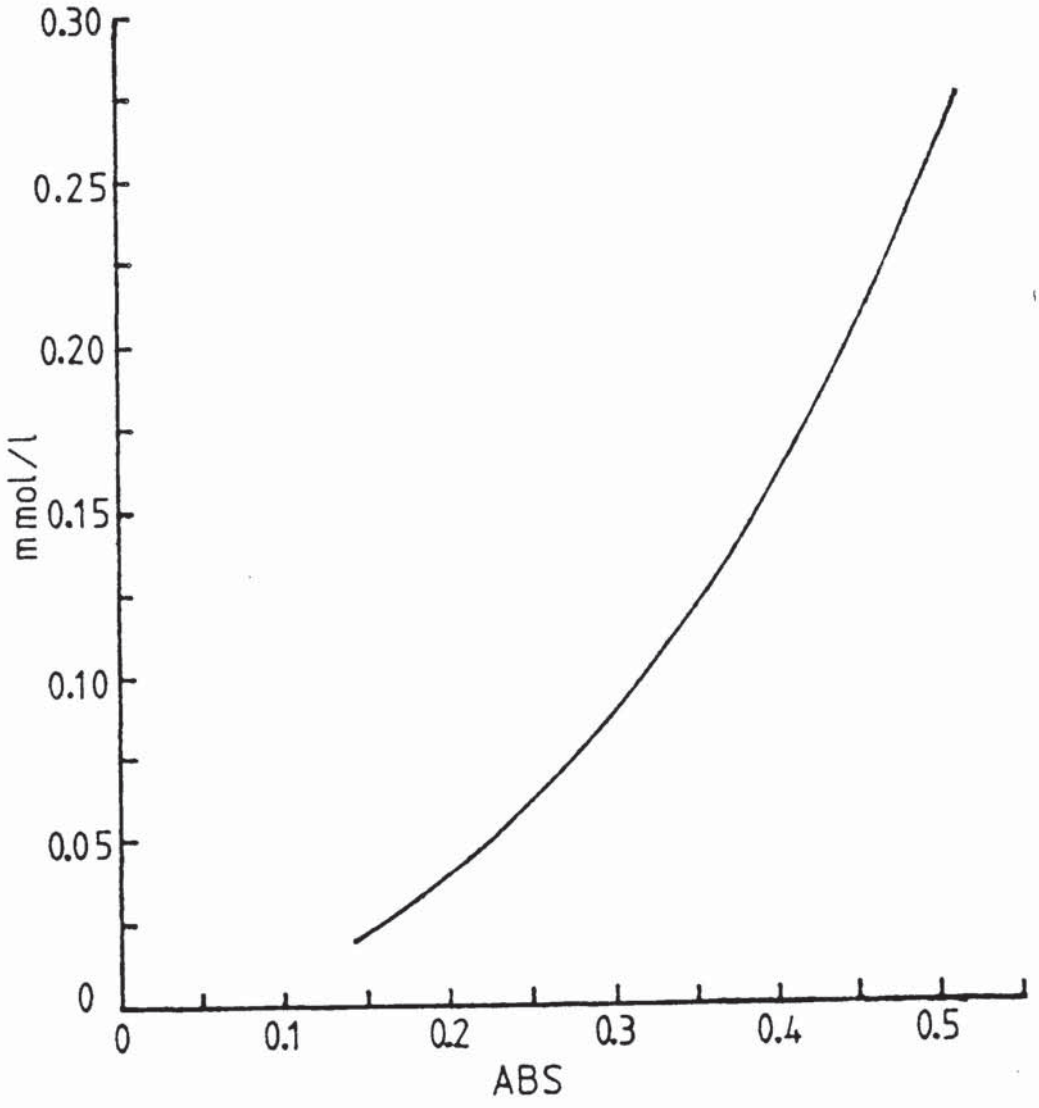

b. $(C_3H_7)_4N^+$ calibration curve :

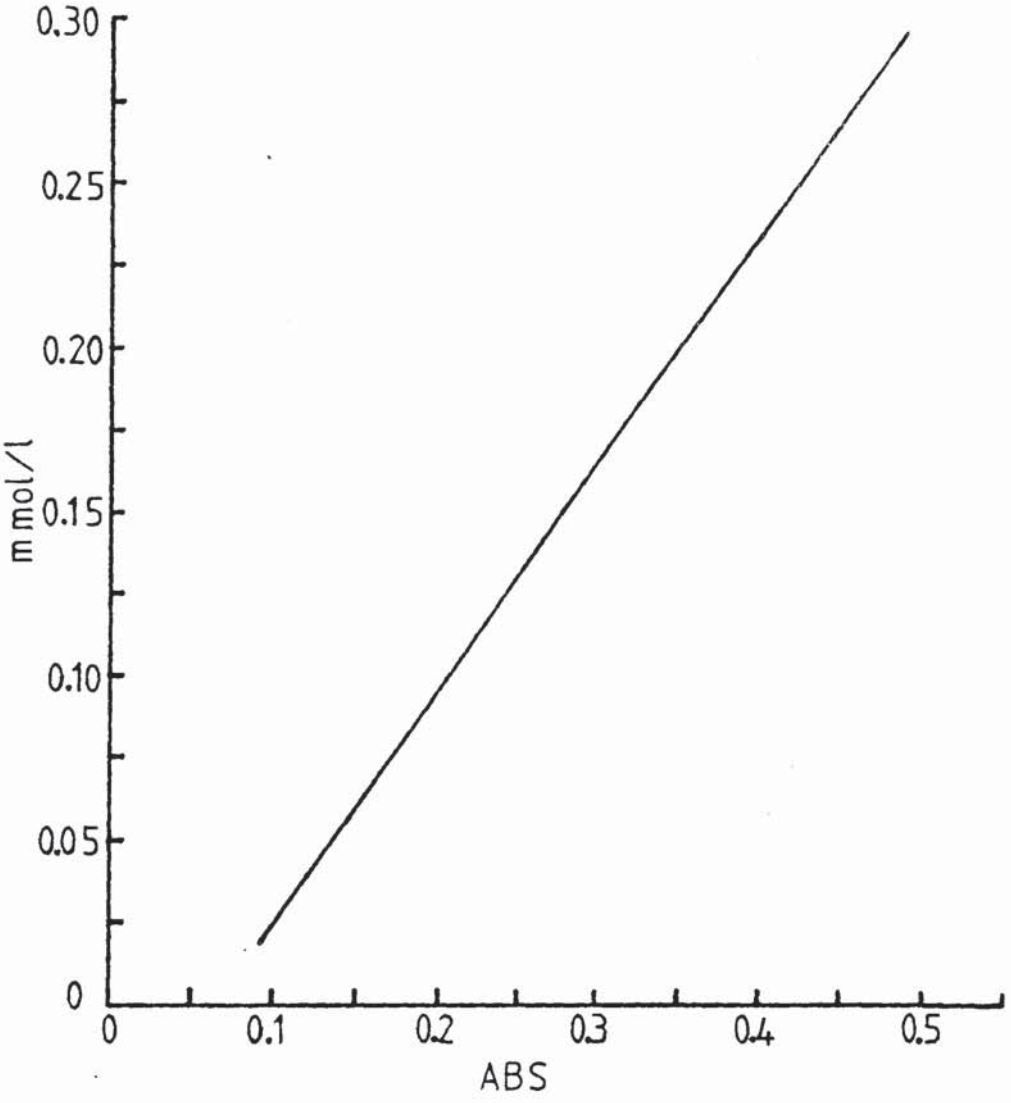

c. $(C_4H_9)_4N^+$ calibration curve :

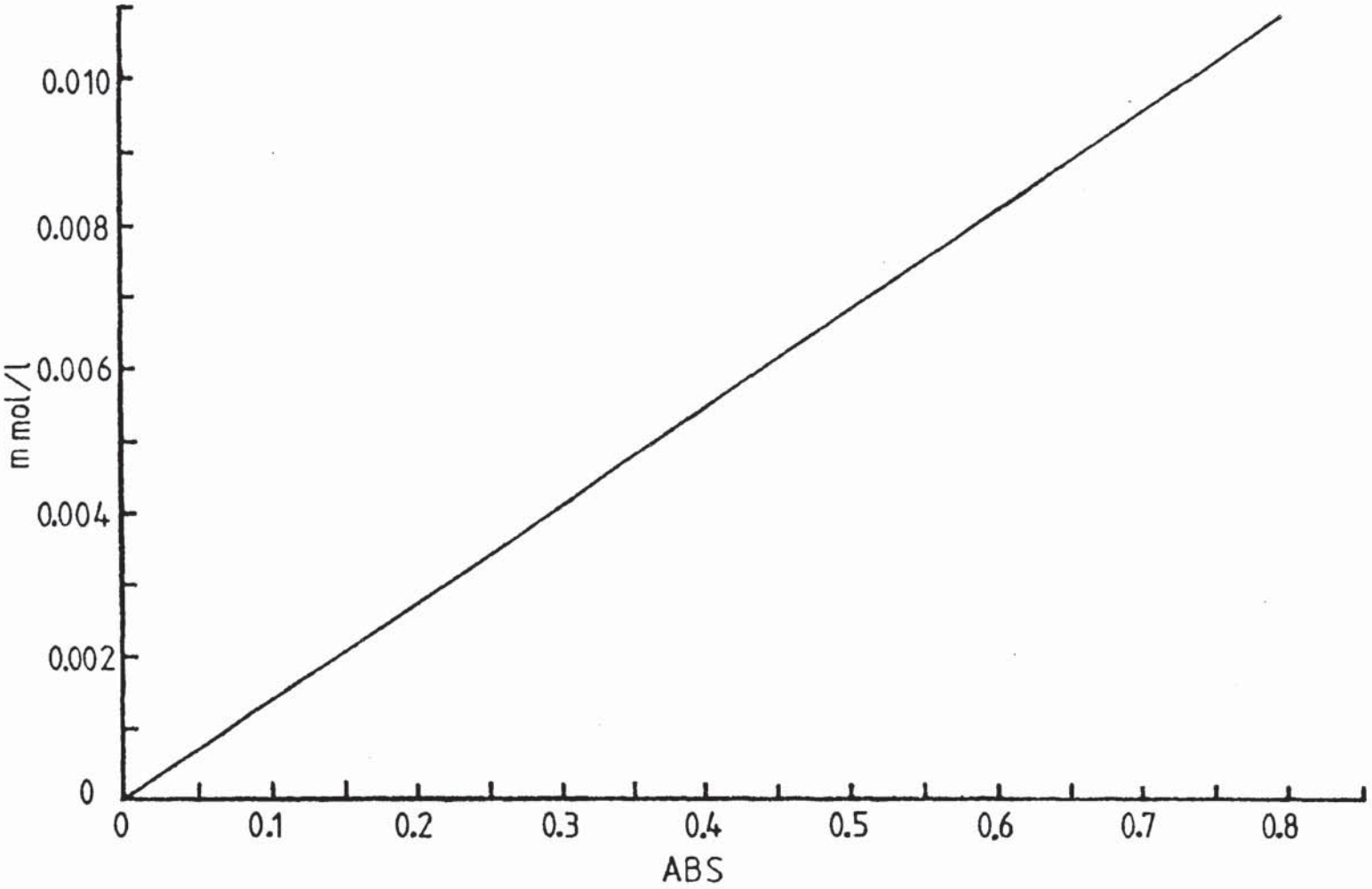

d. $(C_5H_{11})_4N^+$ calibration curve :

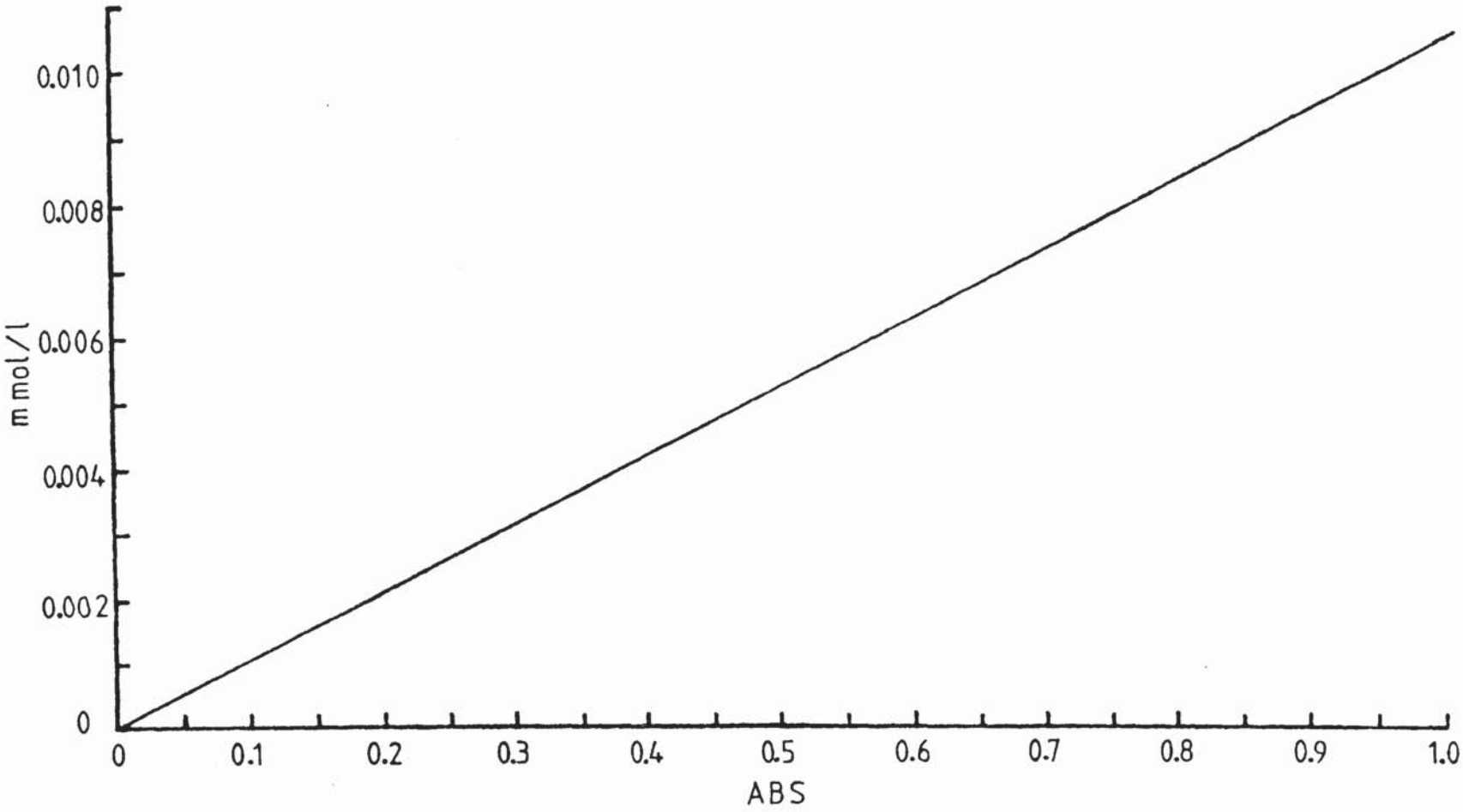

APPENDIX 4 : Ion chromatographic analysis; a worked example.

Sample : Pore solution of carbonated 65% BFS cement paste, diluted by 1000 in deionized water.

Standard solution : 0.0375 mmol/l Na^+, 0.016 mmol/l K^+, 0.100 mmol/l Mg^{++}, 0.310 mmol/l Ca^{++}.

Column : HPIC - CS3

Eluant : 27.5 mM HCl, 2.25 mM DAP, 2.25 mM L - histidine monohydrochloride monohydrate (table 2.2)

Eluant flow rate : 1 ml/min

Regenerant : 70 mM TMAOH (table 2.2)

Regenerant flow rate : 5 ml/min

Detector sensitivity : 30 μS

Chart speed : 20 cm/h

The chromatographs of the sample and standard solution are shown in figures A 4.a (fig 3.7a) and A 4.b respectively.

The concentration of each ionic species can be calculated from the following equation:

$$C_X = h_X C_S / h_S$$

where: C_X = the unknown concentration

h_X = peak height of sample's chromatograph

C_S = concentraion of standard solution

h_S = peak height of standard solution's chromatograph

The measured values of h_x and h_s, together with the calculated ionic concentrations of the sample (C_x) are tabulated in the following table:

Ion	C_s (mmol/l)	h_s (mm)	h_x (mm)	C_x (mmol/l)
Na^+	0.0375	31.5	20.0	0.0238
K^+	0.0160	13.0	9.0	0.0111
Mg^{++}	0.1000	45.0	37.0	0.0822
Ca^{++}	0.3100	65.0	43.0	0.2050

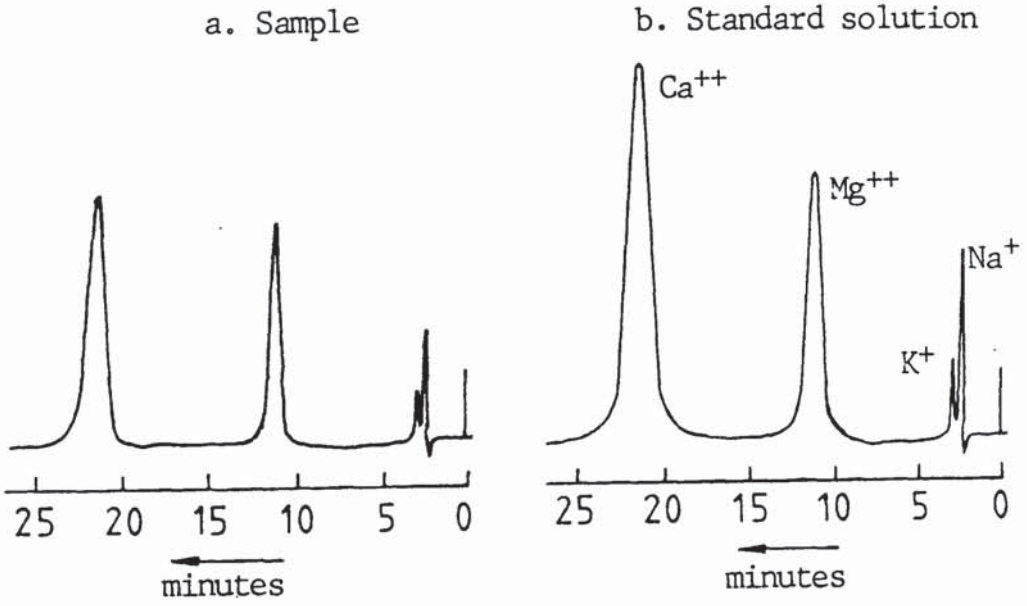

FIGURE A 4 : Ion chromatographs of sample and standard solutions.

APPENDIX 5 : Determination of evaporable and non-evaporable water content in cement pastes.

(i) Derivation of equations used (from ref. 36).

The mass of the cement paste before and after heating to 105°C and 950°C may be defined as follows:

$$W_o = W_c + W_e + W_n + W_a \quad \text{(eq.1)}$$

$$W_{105} = W_c + W_n + W_a \quad \text{(eq.2)}$$

$$W_{950} = W_c\,(100 - i)/100 + W_a \quad \text{(eq.3)}$$

where : W_o = original mass of cement (g)

W_{105} = mass of cement at 105°C (g)

W_{950} = mass of cement at 950°C (g)

W_c = mass of unhydrated cement (g)

W_e = mass of evaporable water (g)

W_n = mass of non-evaporable water (g)

W_a = mass of admixtures (g)

i = loss-on-ignition (% g/g of unhydrated cement)

From the above equations expressions for evaporable and non-evaporable water contents may be developed:

(eq.1) - (eq. 2) : $W_e = W_o - W_{105}$ (eq.4)

If $W_a = a\,W_c\,/100$ (eq.5)

where: a = admixture content (% g/g of unhydrated cem.),

then from eq.3 :

$$W_{950} = [W_c (100 - i) + a W_c]/100$$

$$W_{950} = W_c (100 - i + a) /100 \qquad \text{(eq.6)}$$

$$W_c = 100 \; W_{950}/(100 - i + a) \qquad \text{(eq.7)}$$

Evaporable water (E.W.) (%g/g unhydrated cement) $= 100 \; \frac{W_e}{W_c}$

Sub. W_e from eq. 4 :

$$E.W.(\%) = 100 \; \frac{(W_o - W_{105})}{W_c}$$

Sub. W_c from eq. 7 :

$$E.W.(\%) = \frac{(W_o - W_{105})\,(100 - i + a)}{W_{950}} \qquad \text{(eq.8)}$$

Non - evaporable water (%g/g unhydrated cem.) $= 100 \; \frac{W_n}{W_c}$

From eq. 2 : $W_n = W_{105} - W_c - W_a$

Sub. W_a from eq. 5 :

$$W_n = W_{105} - W_c - a W_c /100$$

$$W_n = W_{105} - W_c (1 + a/100)$$

Sub. W_c from eq. 7 :

$$W_n = W_{105} - 100 \; W_{950} \frac{(1 + a/100)}{(100 - i + a)}$$

$$W_n = \frac{W_{105}\,(100 - i + a) - (100 + a) W_{950}}{(100 - i + a)}$$

Divide by W_c from eq. 7 and multiply by 100 to give the non -

evaporable water (%) :

$$N.E.W.(\%) = \frac{[W_{105}(100-i+a) - (100+a)\,W_{950}]\,[100-i+a]}{100\,(100-i+a)\,W_{950}} \cdot 100$$

$$N.E.W.(\%) = [W_{105}(100-i+a) - W_{950}\,(100+a)]\,/W_{950} \qquad \text{(eq.9)}$$

or $$W_{950} = W_{105}\,(100-i+a) \,/\, [N.E.W.(\%)+100+a] \qquad \text{(eq.10)}$$

(ii) Worked example

Example for carbonated OPC paste (table 3.5) :

Weight of crusible : 4.2566 g

Weight of crusible + sample : 4.6777 g

Weight of crusible + sample at 105°C : 4.6341 g

Bound hydrogen in sample : 0.45%

Weight of sample (hydrated cement) : W_o = 0.4211 g

Weight of sample at 105°C : W_{105} = 0.3775 g

Water lost from the sample at 105°C : $W_o - W_{105}$ = 0.0436 g

Water lost from 1 g of hydrated cement at 105°C :

$$\frac{W_o - W_{105}}{W_o} = \frac{0.0436}{0.4211} = 0.1035 \text{ g}$$

Bound hydrogen in 1 g of hydrated cement : 4.5×10^{-3} g

Bound water in 1 g of hydrated cement :

$$\frac{4.5 \times 10^{-3} \times 18}{2} = 0.0405 \text{ g}$$

Total water in 1 g of hydrated cement :

$$0.1035 + 0.0405 = 0.144 \text{ g}$$

So, 1 - 0.144 = 0.856 g of unhydrated cement contains 0.0405 g of bound water.

Non - evaporable water (N.E.W.) =

$$= \frac{0.0405}{0.8560} = 0.0473 \text{ g/g unh. cem.} = 4.73\%$$

From eq. 10 :

$$\text{Weight at } 950^{o}C = \frac{0.3775 \cdot 100}{4.73 + 100} = 0.3605 \text{ g}$$

From eq. 8 :

$$\text{Evaporable water (E.W.)} = \frac{0.0436}{0.3605} 100 = 12.09\%$$

$$= 0.1209 \text{ g/g unh.cem.}$$

APPENDIX 6 : Total and free chloride determination

Worked example of calculation for carbonated (in 100% CO_2) OPC paste (table 3.4)

Weight of sample at 105°C = 0.8854 g

Need to correct to weight at 950°C :

from appendix 5,

W_{105} = 0.3775 g gives W_{950} = 0.3605 g

W_{105} = 0.8854 g gives W_{950} = 0.8455 g

$$\text{Total chloride (mmol/g)} = \frac{\text{Conc. of sol. (mmol/l) x Dilution}}{W_{950} \times 1000}$$

$$= \frac{0.7 \times 13}{0.8455 \times 1000}$$

TOTAL Cl^- = 0.011 mmol/g cem.

$$\text{Free chloride (mmol/g)} = \frac{\text{Conc. of sol. (mmol/l) x E.W.(g/g)}}{1000}$$

$$= \frac{9.00 \times 0.1209}{1000}$$

FREE Cl^- = 0.001 mmol/g cem.

APPENDIX 7 : DTA identification peaks

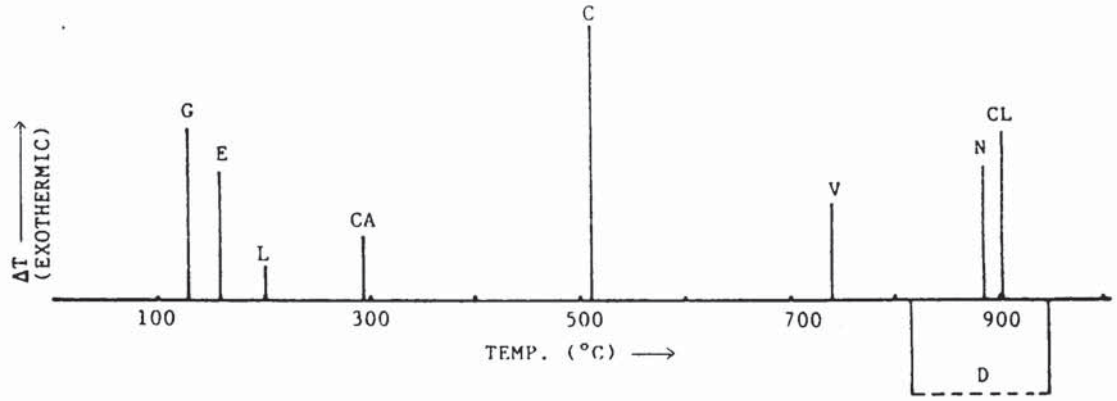

	From ref.		From ref.
G = C-S-H gel	102	V = vaterite	103
E = ettringite	102	N = sodium chloride	102
L = calcium chloroaluminate	102	CL = calcite	103
CA = C_4AH_{13}	102	D = devitrification of glassy phase	102
C = calcium hydroxide	102		

APPENDIX 8 : Example of identification of XRD trace

The values for 2θ, d-spacing ($d = \lambda / 2\sin\theta$; λ = 1.542Å for Cu, K_α radiation) and relative intensity I which are shown in the following table were determined from the x-ray diffractometer trace of the carbonated OPC paste (0% BFS; figure 3.10). The values of d and I were compared to standard data, as shown in the table, to identify the phases.

			Standard Data (ref.40)		
2θ	d(Å)	I	Calcite	Vaterite	Ettringite
15.8	5.61	23			5.61(vs)
18.0	4.93	22			
19.9	4.46	22			
24.4	3.65	15			3.67(w)
24.9	3.58	24		3.58(s)	
27.0	3.30	31		3.30(s)	3.27(vw)
29.4	3.04	63	3.035(vvs)		
32.7	2.74	33		2.73(s)	
33.9	2.64	22			
36.0	2.50	11	2.495(m)		
39.3	2.29	15	2.285(s)		
43.0	2.10	14	2.095(s)		
43.8	2.07	19		2.059(s)	

cont. over

2θ	d(Å)	I	Calcite	Vaterite	Ettringite
47.2	1.93	18	1.927(w)		
48.4	1.88	14	1.875(ms)		
49.9	1.83	18		1.825(s)	

Key to table: scale of decreasing relative intensities : vvs, vs, s, ms, m, mw, w, vw, vvw.

APPENDIX 9 : Pore size distribution calculation example.

Example for OPC paste (fig.3.12).

Weight of sample dried at 105°C (W_s) = 5.6579 g

Cell factor = 0.000778 cc/count

A = Applied pressure (psi)

B = Penetraion counter

C = Corrected counter indication = B - Result of blank run

D = Pore diameter (117° contact angle) = 124.9 ÷ A (μm)

E = Volume of pores of indicated diameter and larger =

= C x (cell factor ÷ W_s) (ml/g)

The above values are determined for increasing applied pressures and tabulated as follows :

A	B	C	D	E
1.3	25	25	96.1	0.00344
2.1	33	33	59.5	0.00454
3.5	35	35	35.7	0.00481
6.0	38	38	20.8	0.00523
11.0	43	43	11.4	0.00591
115.0	112	112	1.09	0.0154
250	126	126	0.500	0.0173

cont. over

A	B	C	D	E
350	140	140	0.357	0.0193
530	157	157	0.236	0.0216
635	169	169	0.197	0.0232
700	177	177	0.178	0.0243
820	185	185	0.152	0.0254
900	194	194	0.139	0.0267
1900	305	305	0.0657	0.0419
2100	395	394	0.0595	0.0542
2600	620	619	0.0480	0.0851
2900	706	705	0.0431	0.0969
3100	756	755	0.0403	0.104
3400	803	802	0.0367	0.110
3800	877	876	0.0329	0.121
4200	930	929	0.0297	0.128
4600	975	974	0.0272	0.134
5100	1027	1026	0.0245	0.141
6100	1131	1129	0.0205	0.155
7100	1215	1213	0.0160	0.167
8000	1292	1289	0.0156	0.177
9000	1369	1365	0.0139	0.188
10000	1428	1423	0.0125	0.196
12000	1514	1508	0.0104	0.207
14000	1571	1563	0.00892	0.215
16000	1610	1596	0.00781	0.219

cont. over

A	B	C	D	E
18000	1638	1621	0.00694	0.223
20200	1661	1641	0.00618	0.226
24000	1692	1665	0.00520	0.229
28000	1719	1684	0.00446	0.232
32000	1740	1701	0.00390	0.234
36200	1760	1711	0.00345	0.235
40200	1774	1715	0.00311	0.236
44000	1790	1724	0.00284	0.237

A plot of E v's A and/or D produces a pore-size distribution curve as shown in figure 3.12.

APPENDIX 10 : Increase in carbonation depths with time of BFS blended cement pastes, with or without a 1% Cl^- addition (as NaCl), exposed to various atmospheres.

(i) BFS blended pastes exposed to 100% CO_2 (65%R.H.)

Time (day)	Depth (μm)			
	0% BFS		25% BFS	
	with NaCl	without NaCl	with NaCl	without NaCl
4	185	103	185	90
5	395	255	285	130
6	470	485	365	160
7	570	600	462	200
10	915	870	600	310
12			850	450
13	1200	1100		
16	1480	1300	1150	600
17			1450	920
18		1490		
22				1480

Time (day)	Depth (μm)			
	45% BFS		65% BFS	
	with NaCl	without NaCl	with NaCl	without NaCl
3			170	90
4	200	70		
5			730	150
6	640	245		
7			1500	350
8	1100	380		430
9				530
10	1480	520		800
11				1100
12		1000		1450
14		1480		

(ii) 65% BFS cement pastes exposed to 5% CO_2 and Air

Time (day)	Depth (μm)			
	5% CO_2		Air	
	with NaCl	without NaCl	with NaCl	without NaCl
18	180	45		
27	440	260		
33	560	280		
39	820	475		
46	1070	600		
50	1500	780		
60		914		
64		1110	85	60
75		1500	140	100
102			340	300
110			450	400
130			550	530
139			630	570
148			680	600
160			810	680
175			870	750
202			990	860
231			1095	950
259			1195	1098
312			1351	1248

APPENDIX 11: Calculation of the parameter "A" which represents the variation of the carbonatable material with the variation of the OPC content of cement paste.

The greater part of the CO_2 intake during carbonation of cement paste is by the CaO bearing phases [37]. The amount of the CaO present in a cement paste therefore is representative of the amount of carbonatable material of the paste. The value "A" is the amount of CaO present in 100 gr of the cementitious material used in each type of cement paste.

CaO content of the materials used (from table 2.1) :

a) OPC = 64.5%

b) BFS = 39.4%

CaO content per 100 gr of the cementitious material used in each type of cement paste (value "A") :

a) 100% OPC = 64.5 x 1 = 64.5 gr

b) 75% OPC + 25% BFS = 64.5 x 0.75 +39.4 x 0.25 = 58.2 gr

c) 55% OPC + 45% BFS = 64.5 x 0.55 + 39.4 x 0.45 = 53.2 gr

d) 35% OPC + 65% BFS = 64.5 x 0.35 + 39.4 x 0.65 = 48.2 gr.

APPENDIX 12 : Solution to Fick's first law of diffusion.

For one-dimentional, steady-state diffusion the simple linear law known as Fick's 1st law is applicable.

$$J = - D \frac{dC}{dx} \qquad \text{(eq.1)}$$

where : J = Flux or diffusion current density - the amount of material diffusing in a unit time per unit area perpendicular to the x-axis.

D = Diffusion coefficient

C = Volume concentration

x = Distance along direction of diffusion.

Under steady-state conditions, the above equation can be integrated to :

$$J = -D \frac{(C_2 - C_1)}{\Delta x} \qquad \text{(eq. 2)}$$

where C_1 and C_2 are concentrations at the ends of the diffusional length Δx.

For a thin disc of thickness l, we have :

$$J = D \frac{(C_1 - C_2)}{l} \qquad \text{(eq. 3)}$$

For a diffusion cell as in figure 4.2 the flux of ions entering the "low" compartment is given by:

$$J = \frac{V}{A} \frac{dC_2}{dt} \qquad \text{(eq.4)}$$

where: V = the volume of the solution in the compartment

A = the cross sectional area of the disc.

From equations 3 and 4 we have

$$\frac{D(C_1-C_2)}{l} = \frac{V}{A}\frac{dC_2}{dt}$$

Assume C_1 is constant :

$$\int_{C_2=k}^{C_2=C_2} \frac{-d(C_1-C_2)}{(C_1-C_2)} = \frac{DA}{Vl}\int_{t=t_o}^{t=t} dt$$

$$[-\log_e (C_1-C_2)]_k^{C_2} = \frac{DA}{Vl}(t\text{-}to)$$

$$\log_e [(C_1-k)/(C_1-C_2)] = DA\,(t-t_o)/Vl$$

$$\log_e [1+(C_2-k)/(C_1-C_2)] = DA\,(t-t_o)/Vl$$

For $t > t_o$, $C_2 - k << C_1-C_2$

i.e. $C_2 << (C_1+k)/2$

and $(C_2 - k)(C_1-C_2) = DA\,(t-t_o)/Vl$

if, $S = \frac{C_2 - k}{t-t_o}$

then $D = \frac{SVl}{A(C_1-C_2)}$

APPENDIX 13 : Calculation of ionic diffusion coefficient D.

Example calculation for chloride ion in carbonated OPC paste.

Figure 4.7 shows the rise in concentraion of chloride ions in compartment 2 of the diffusion cell No 1 at 25°C.

S(slope of the graph) = 5.93×10^{-5} mmol $l^{-1}s^{-1}$

V(volume of solution in comp. 2) = 82.5 ml

l(thickness of the disc) = 0.275 cm

A(cross sectional area of the disc) = 9.079 cm^2

C_1(conc. of solution in comp. 1) = 1×10^3 mmol/l

C_2(conc. of solution in comp. 2) = 0 mmol/l

From appendix 12 :

$$D = \frac{S\ V\ l}{A(C_1 - C_2)}$$

$$D = \frac{5.93\ \ 10^{-5}\ \ 82.5\ \ 0.275}{9.079\ \ 10^3} = 14.81\ .\ 10^{-8}\ cm^2\ s^{-1}$$

APPENDIX 14 : Calculation of activation energy for ionic diffusion in cement paste.

Example calculation for chloride diffusion in carbonated OPC paste.

Using the values of table 4.5 and taking x as 1/T in $^{o}K^{-1}$ and y as $\log_{10}D$, values of Σx, Σy, Σx^2, Σy^2, Σxy and n can be calculated.

These are as follows:

$\Sigma x = 83.965 \cdot 10^{-3}$ $\quad\quad$ $\Sigma x^2 = 282.430 \cdot 10^{-6}$

$\Sigma y = -170.664$ $\quad\quad$ $\Sigma y^2 = 1166.027$

$\Sigma xy = -0.5738$ $\quad\quad$ $n = 25$

Need to determine values a and b of the best fit equation (ref.198) :

$$y = a + bx$$

where, $$b = \frac{n\Sigma xy - \Sigma x \Sigma y}{n\Sigma x^2 - (\Sigma x)^2} = -1338.718$$

and $$a = \frac{\Sigma y - b\Sigma x}{n} = -2.330$$

best fit equation is:

$$y = -2.330 - 1338.718\ x$$

Activation energy, U

$$D = D_o\ e^{-(U/RT)} \qquad \text{(ref. 149)}$$

where: D = diffusion coefficient

U = activation energy

R = molar gas constant

T = absolute temperature

D_o = constant which depends on the effective porosity, the path tortuosity and the entropy of activation.

$$\log_e D = \log_e D_o - (U/R\,T)$$

$$\log_{10} D = \log_{10} D_o - (U/2.303\,R\,T)$$

The slope of the equation (fig. 4.8) is : $b = -U/2.303\,R$

$$-U = 2.303 \times R \times b$$

$$-U = 2.303 \times 8.314 \times (-1338.718)$$

$$U = 25632.62 \text{ J/mole}$$

$$U = 25.63 \text{ KJ/mole}$$

Correlation coefficient

$$r = \frac{n\Sigma xy - \Sigma x \Sigma y}{\sqrt{[(n\Sigma x^2 - (\Sigma x)^2)\,(n\Sigma y^2 - (\Sigma y)^2)]}} \qquad \text{(ref.198)}$$

$$r = -0.882$$

95% confidence intervals:

$$S^2_{y/x} = (\Sigma y^2 - a\Sigma y - b\Sigma xy)/(n-2) \qquad \text{(ref.198)}$$

$S_{y/x} = 0.099$

$$b \pm t_{0.5\ a,\ n-2} \frac{S_{y/x}}{\sqrt{[\Sigma x^2 - (\Sigma x)^2 n^{-1}]}}$$

where $a = 0.025$

$b \pm 2.069 \times 151.832$

$U = 25.63 \pm 6.01$ KJ/mole

APPENDIX 15: Statistical comparison between the strengths of size 1 and size 2 cement paste specimens.

Test null hypothesis, $H_o : \mu_1 = \mu_2$, against the alternative hypothesis, $H_1 : \mu_1 > \mu_2$, where $\mu_1 = \bar{X}_1$ and $\mu_2 = \bar{X}_2$ (ref. 199).

size 1 specimens: $\bar{X}_1 = 8.73$

$\Sigma x_1 = 453.98$

$\Sigma x_1^2 = 4403.24$

$n_1 = 52$

size 2 specimens : $\bar{X}_2 = 6.32$

$\Sigma x_2 = 309.23$

$\Sigma x_2^2 = 2120.73$

$n_2 = 49$

Sum of squares for 1 = $\Sigma x_1^2 - (\Sigma x_1)^2 n_1^{-1} = 439.820$

Sum of squares for 2 = $\Sigma x_2^2 - (\Sigma x_2)^2 n_2^{-1} = 169.237$

$$S_p^2 = \frac{\text{Sum of squares 1 + Sum of squares 2}}{(n_1 + n_2) - 2} = 6.152$$

$$t = \frac{(\bar{X}_1 - \bar{X}_2) - \Delta_o}{\sqrt{[S_p^2 (n_1^{-1} + n_2^{-1})]}} = \frac{(8.73 - 6.32) - 0}{\sqrt{(6.152 \times 0.0396)}} = 4.480$$

For a one-tailed test :

$t_{0.001,99} = 3.185$ (from tables ; ref. 200) < 4.880

Therefore the hypothesis H_1 is true, i.e. $\bar{X}_1$ is significantly larger than $\bar{X}_2$.

APPENDIX 16 : Apparent density determination for cement paste specimens.

$$\text{Apparent density (d)} = \frac{\text{Weight of the dry specimen } (W_s)}{\text{External volume of the specimen } (V)}$$

External volume of the specimen (V_e) = Volume of displaced mercury (V_m)

$$V_m = \frac{\text{Weight of the displaced mercury } (W_m)}{\text{Density of mercury } (d_m)}$$

$$d_m = 13.6 \text{ gcm}^{-3}$$

$$d \text{ (g cm}^{-3}) = \frac{W_s \text{ (g)} \times 13.6 \text{ (g cm}^{-3})}{W_m \text{ (g)}}$$

Specimen : OPC paste (w/c ratio 0.3) - table 6.3

Thickness = 0.91 mm (size 1)

Weight of specimen at 105°C (W_s) = 0.1703 g

Weight of displaced mercury (W_m) = 1.2194 g

$$\text{Apparent density (d)} = \frac{0.1703 \times 13.6}{1.2194} = 1.899 \text{ g cm}^{-3}$$